NOTICE

The quality of this microform is heavily dependent upon the quality of the original thesis submitted for microfilming. Every effort has been made to ensure the highest quality of reproduction possible.

If pages are missing, contact the university which granted the degree.

Some pages may have indistinct print especially if the original pages were typed with a poor typewriter ribbon or if the university sent us an inferior photocopy.

Reproduction in full or in part of this microform is governed by the Canadian Copyright Act, R.S.C. 1970, c. C-30, and subsequent amendments.

AVIS

La qualité de cette microforme dépend grandement de la qualité de la thèse soumise au microfilmage. Nous avons tout fait pour assurer une qualité supérieure de reproduction.

S'il manque des pages, veuillez communiquer avec l'université qui a conféré le grade.

La qualité d'impression de certaines pages peut laisser à désirer, surtout si les pages originales ont été dactylographiées à l'aide d'un ruban usé ou si l'université nous a fait parvenir une photocopie de qualité inférieure.

La reproduction, même partielle, de cette microforme est soumise à la Loi canadienne sur le droit d'auteur, SRC 1970, c. C-30, et ses amendements subséquents.

UNIVERSITY OF ALBERTA

Solvent Extraction Using Rapid Stirring and a Porous Membrane Phase Separator: Thermodynamic and Kinetic Studies

by

Lawrence N. Amankwa

A Thesis

Submitted To The Faculty Of Graduate Studies And Research

In Partial Fulfilment Of The Requirements For The Degree

Of Doctor Of Philosophy

Department of Chemistry

Edmonton, Alberta

Spring, 1990

NOTICE

The quality of this microform is heavily dependent upon the quality of the original thesis submitted for microfilming. Every effort has been made to ensure the highest quality of reproduction possible.

If pages are missing, contact the university which granted the degree.

Some pages may have indistinct print especially if the original pages were typed with a poor typewriter ribbon or if the university sent us an inferior photocopy.

Reproduction in full or in part of this microform is governed by the Canadian Copyright Act, R.S.C. 1970, c. C-30, and subsequent amendments.

AVIS

La qualité de cette microforme dépend grandement de la qualité de la thèse soumise au microfilmage. Nous avons tout fait pour assurer une qualité supérieure de reproduction.

S'il manque des pages, veuillez communiquer avec l'université qui a conféré le grade.

La qualité d'impression de certaines pages peut laisser à désirer, surtout si les pages originales ont été dactylographiées à l'aide d'un ruban usé ou si l'université nous a fait parvenir une photocopie de qualité inférieure.

La reproduction, même partielle, de cette microforme est soumise à la Loi canadienne sur le droit d'auteur, SRC 1970, c. C-30, et ses amendements subséquents.

ISBN 0-315-60163-9

This work is dedicated to my parents.

ABSTRACT

An improved rotating stir apparatus is described for performing liquid-liquid extraction rate studies in which instrument band broadening effects are reduced. The extraction cell incorporates a remote sample injector and a porous membrane phase separator. Although band broadening is reduced, nevertheless, it is shown that the resulting absorbance versus time extraction profile experiences severe distortions due to residual instrument band broadening and that this distortion can be mathematically eliminated via deconvolution in order to obtain the mass transfer coefficient, β_{mt}. Studies on the extraction of *o*-nitroaniline from the dispersed aqueous phase into chloroform and on the extraction of *o*-nitrophenolate from the continuous chloroform phase into the dispersed aqueous phase show that β_{mt} is about the same for both processes ($\beta_{mt} \approx 2 \times 10^{-3}$ cm/s).

The apparatus has been used to study the rate of the homogeneous oxidation of iodide ion by ferric ion in the aqueous phase, by monitoring the extraction of the product, iodine, into chloroform. The measured absorbance versus time extraction profile includes contributions from the chemical reaction itself, from the mass transfer of iodine and from instrument band broadening. Mathematical deconvolution of the measured absorbance versus time profile with an impulse response function obtained by injecting triiodide makes it possible to obtain the profile for the chemical reaction. (Pseudo) first order rate constants were measured as a function of $[I^-]^2$ to obtain the third order chemical reaction rate constant, which agrees with literature values. (Pseudo) first order rate constants as high as 0.4 s^{-1} were measured, and it is estimated that reducing instrument band broadening would permit the measurement of first order rate constants as high as 2 s^{-1} (i.e. $t_{1/2} \approx 0.4$ s).

It is possible with this apparatus to study the interfacial adsorption of surfactants at the liquid-liquid interface. Ion-pairs of both tetrahexyl ammonium picrate, (QP), and tetrahexyl ammonium bromothymol blue, (QHB), adsorb strongly at the chloroform/water interface. At the interface QP undergoes a dissociative reaction to give the ions Q^+ and P^-.

The former ion, because it is surface active, stays adsorbed at the interface. However, because P^- is not surface active, it desorbs into the aqueous phase, and therefore the dissociation reaction at the interface is inhibited by the presence of excess NaP in the aqueous phase. In consequence, the extent of adsorption of QP at the interface decreases with increasing concentration of NaP in the aqueous phase. The interfacial ion-pair formation constant, K_{IP}, is calculated to be 1.4×10^5 L mole^{-1}.

The behaviour of the ion-pair QHB at the interface differs from that of QP. Since both the constituent ions Q^+ and HB^- are adsorbed at the interface, dissociation of QHB is not detected in these experiments. However, when excess HB^- is present, both HB^- and QHB are simultaneously adsorbed. The competitive adsorption between the strongly adsorbed HB^- and the weakly adsorbed QHB has been quantified in this work.

Owing to the interfacial activity of both QP and QHB, the first order rate constants for the extraction of of these species from water into chloroform vary with the concentration of ion-pair reagents in the aqueous phase. The dependence of the extraction rate constant on reagent concentration does not, however, imply that the rate of extraction is chemical reaction controlled. The observed dependence of the extraction rate constant on reagent concentration can be explained in terms of additional resistance to mass transfer associated with desorption of solute from the interface into the chloroform phase.

ACKNOWLEDGEMENT

I wish to express my sincere gratitude to Professor F. F. Cantwell, for the counselling, and encouragement he provided me throughout this work. I also thank him for his help in writing this manuscript.

I wish to thank Dr. A. C. Lucy for providing the computer programs used in this work.

I also acknowledge the financial assistance given to me under the auspicies of Graduate Research Assistantship and/or Graduate Teaching Assistantship by the Department of Chemistry, University of Alberta.

Finally, I extent my thanks to the staff of the General Office, the Machine Shop, the Glass Blowing Shop and the Stores for their help and for making working in Chemistry an enjoyable experience.

Table of Contents

LIST OF TABLES

LIST OF FIGURES

LIST OF SYMBOLS

A	Absorbance
A	Interfacial area (cm^2)
a	Activity (Equation 1.1)
a	(subscript) aqueous phase
b	(subscript) bulk liquid phase
C	concentration (mole/L)
c	(subscript) continuous phase
D	Liquid-Liquid distrubution ratio (see equation 1.3)
D	Diffusion coefficient (cm^2/s)
d	(subscript) dispersed phase
d_p	Mean drop size
E	Turbulent convection diffusivity (cm^2/s)
F	Constant (Equation 7.2)
F	Faraday constant
F	Correction factor (Equation 8.1)
F	Flow rate (Equation 4.6)
f_ϕ	Constant (Equation 2.23)
g	Acceleration due to gravity
J	Flux (mole/cm^2 s)
I	(subscript) instrument
i	(subscript) interface
K_D	Liquid-liquid distribution constant (C_o/C_a)
K_{IP}	Ion-pair formation constant (L/mole)
K_{ext}	Ion-pair extraction constant (L/mole)
K_{ads}	Interface/liquid phase distribution constant for ion-pair ($[QP]_i/C_o$)

K'_{ads}	Interface/liquid phase distribution constant (species-independent) (n_{ads}/AC_o)
k_{ads}	Adsorption rate constant (s^{-1})
k_{des}	Desorption rate constant (s^{-1})
K	Equilibrium adsorption constant (L/mole) (Equation 7.9)
k	Boltzman's constant
k_r	First order chemical reaction rate constant (s^{-1})
k_{mt}	Pseudo order order extraction rate constant (s^{-1})
L	Length of surface (Equations 4.4 and 4.5)
L	Impeller dimension (cm)
L	Tube length (Equation 4.6)
M	(subscript) mass transfer process
m	Mass (g)
N	Impeller rotation speed (rpm, rps)
N_{Re}	Impeller Reynold's number
N_{Sc}	Schmidt number
N_{Sh}	Sherwood number
N_{We}	Weber number
N_A	Avogadro's number
n_{ads}	Moles of solute adsorbed at the interface (species-independent)
ns	(subscript) non-stirring
o	(subscript) organic phase
o	(subscript) overall
P	Stirrer power number (Equation 2.24)
R	Resistance (s/cm)
R	(subscript) reaction
s	(subscript) stirring
T	Temperature

t	Time (s)
V	Volume
W	Rotation speed of diffusion cell (Equation 2.14)
γ	Activity coefficient (Equation 1.1)
γ	Interfacial tension (dyne/cm)
ρ	Density
μ	Viscosity
v_{max}	Maximum flow velocity (Equation 2.3)
υ	Kinematic viscosity (μ/ρ)
δ	Thickness of the stagnant Nernst film
d	Thickness of adsorbed layer
σ	Charge density (Equation 7.21)
σ^2	Variance (second statistical moments)
σ^*	Area occupied per molecule
β	Mass transfer coefficient (cm/s)
Z_D	Thickness of stagnant Nernst film (equation 2.14)
Z	Ionic charge

CHAPTER 1

1.0 INTRODUCTION

Solvent extraction (SE), also known as liquid-liquid extraction or liquid-liquid distribution, is a process for separating components in solution by their distribution between two *immiscible* liquid *phases*. A quantitative understanding of liquid-liquid distribution was first introduced empirically in 1872 by Berthelot and Jungfleisch [1], and later elucidated thermodynamically in 1891 by Nernst [2] in a distribution law which states that; " When a material is distributed between two mutually immiscible liquid phases, the concentration ratio in the two phases at a given temperature is independent of the total amount " [3, 4]. Depending on the equilibrium distribution constant, transfer from one phase to another can be quantitative. The principle of SE is based on this quantitative transfer of solute from one phase across the *interface* (which is the boundary surface between the phases) into the other phase[4]. In general there are two distinct types of solvent extraction processes. The first type involves only mass transfer while, in the second, either a homogeneous or a heterogeneous chemical reaction accompanies the mass transfer.

1.1 APPLICATIONS OF SOLVENT EXTRACTION

Although solvent extraction techniques were used by many early chemists, it was not until in the early 1940's that the technique achieved recognition as a powerful separation technique. Presently SE is being applied in many fields [3, 5] such as nuclear engineering, hydrometallurgy, biotechnology, chemical engineering, manufacturing industries, food and pharmaceutical industries, and analytical chemistry.

Solvent extraction is extensively used in the recovery of uranium and plutonium from irradiated nuclear fuels and for the extraction of uranium from uranium ore [6 - 8]. Solvent extraction has been in most cases the process of choice for the extraction of metals from their respective ores, and also for the treatment of industrial waste effluents [7, 9-12].

In the petrochemical industry solvent extraction has been used for the separation of mixtures of aromatic and aliphatic hydrocabons. In addition solvent extraction is used in the manufacture of several important petrochemicals (such as caprolactams) and petrochemical based products (for example, terylene, nylon and acrylic etc.) [13, 14] .The most important applications of solvent extraction in the food and the pharmaceutical industries are the in the manufacture of penicillins [15-17] and in the isolation of flavors and aromas. Solvent extraction is also used as a synthetic tool for manufacturing of drugs through the use of phase transfer catalysis [17, 18]. Solvent extraction is also used for the removal of undesirable constituents from a raw material. The most obvious example of this application of solvent extraction is the decaffeination of "instant" coffee [19-21]. In analytical chemistry, SE provides a simple and effective means for improvment of analytical methods and enhancement of sensitivity (by preconcentration) and selectivity (by interference removal) [7, 22-27].

1.2 EQUILIBRIUM ASPECTS OF SOLVENT EXTRACTION

Phase distribution equilibria refers to the distribution of a sample component between phases that are of different composition than the component of interest. At steady state the distribution is measured in terms of the thermodynamic distribution constant, K_D^o , which is defined as the ratio of the activity of the component in one phase to that in the second phase.

$$K_D^o = \frac{a_2}{a_1} = \frac{C_2 \gamma_2}{C_1 \gamma_1} \qquad (1.1)$$

where "a", C and γ are, respectively,the activity, concentration and activity coefficient of the component. The subscripts "1" and "2" refers to the two phases. The concentration distribution constant, K_D , which is the parameter generally used in analytical chemistry, is

defined as the ratio of the concentration of the component in phase 2 to that in phase 1. Hence we have,

$$K_D = \frac{C_2}{C_1} = K_D^{\circ} \frac{\gamma_1}{\gamma_2} \qquad (1.2)$$

At very low (infinite dilution) sample concentrations the ratio γ_1/γ_2 is unity so that $K_D = K_D^{\circ}$. In this thesis phase 1 is water and phase 2 is chloroform.

When the sample component exists in more than one chemical form in one of the phases the distribution is characterized by the distribution ratio, D, defined as follows [3].

$$D = \frac{(\text{formal concentration})_2}{(\text{formal concentration})_1} \qquad (1.3)$$

where the formal concentration means the total concentration of all chemical forms. The value of D varies with experimental conditions such as pH, whereas at low concentrations the value of K_D is invariant for a system at a particular temperature.

1.3 KINETICS AND MECHANISM OF SOLVENT EXTRACTION

Ideally, one would like a solvent extraction process to proceed rapidly to distribution equilibrium. Vigorous shaking and adjustment of the chemical variables such as pH, ionic strength or addition of extractants are often used to increase the rate of the extraction. Prior to the work by Honaker and Freiser [28] on the extraction kinetics of zinc dithizonate, very few extraction studies had been done under non-equilibrium conditions [28-30]. Their work addressed some questions of both fundamental and practical interest, such as the role of the liquid-liquid interface in the extraction process and the mechanism of the extraction process. Now, solvent extraction kinetics has become an increasingly important subject and it is being studied in many fields not only to help

understand the phenomenon of liquid-liquid interfacial mass transfer, but also as a tool for studying the kinetics of inherently fast chemical reactions [31-34].

To understand the mechanism of an extraction process it is necessary that one looks at an extraction system in both a macroscopic and a microscopic sense. The macroscopic problem deals with the reactor design in relation to fluid dynamics within the reactor cell while the microscopic aspect of extraction deals with the local rate of transfer of reactants and/or products between the two phases as governed by the local bulk-phase conditions of concentration and temperature. Hydrodynamically, the *bulk* liquid phases far from the interface experience vigorous convective mixing. As the interface is approached from the bulk solution the vigor of the convection gradually decreases until it is zero immediately adjacent to the interface. This is predicted from "boundary-layer theory" [35]. Solute is moved through the liquid phases either toward or away from the interface by a contribution of convection and diffusion, with convection playing a greater role away from the interface and diffusion playing a greater role near the interface. In order to simplify calculations involving this convective/diffusive mass transfer of solute the situation near the interface is approximated by various models such as the two-film model, the penetration and surface-renewal model and the boundary-layer model. These models will be discussed in Chapter 2. In this thesis extraction rates are interpreted in terms of the two-film model.

When no other rate limiting processes are occuring except convective/diffusion mass transfer the extraction process is said to be in the "mass transfer" or "diffusional" regime [36]. In this regime the rate of extraction increases often linearly, with the degree of stirring in the extraction system [36]. On the other hand, when mass transfer processes can be considered to be practically instantaneous with respect to other processes, such as a chemical reaction, the extraction process is considered to be in the "chemical kinetic" or "kinetic" regime and the rate of extraction is independent of stirring rate. When an extraction occurs at a rate that is controlled by both mass transfer and a chemical reaction it is said to be in the "mixed" regime.

The rate of mass transfer depends on three factors: the area of contact, the effective driving force, and the mass transfer coefficient. In SE the area of contact is the total liquid-liquid interfacial area accessible for mass transfer. The driving force is usually dictated by concentration gradient and the equilibrium partition ratio of the solute between the two phases. The mass transfer coefficient is a constant and is related to the solute diffusion coefficient and the system hydrodynamics. In general mass transfer across the whole interfacial region is greatly affected by factors such as fluid viscosity, interfacial tension, interfacial area, cleanliness of the interface and solute parameters such as concentration and diffusion coefficient.

For the past two decades several researchers have proposed numerous measurement techniques and models for studying liquid-liquid interfacial kinetics [36, 37, 38]. Because of distinct differences among the techniques and models there is no consensus on the theory of interfacial chemical reaction mechanism and on reported mass transfer kinetic data.

1.4 GOALS OF RESEARCH

The goals of the research include the design, characterization and use of a rapid-stir solvent extraction system incorporating a porous membrane phase separator for studying mass transfer kinetics and homogeneous chemical reaction kinetics as well as adsorption equilibria at the chloroform/water interface. The research will also focus on developing a method involving the use of Fast Fourier Transform (FFT) deconvolution for eliminating the distortion caused by instrument band broadening on mass transfer rate data.

In Chapter Two, a theoretical discussion of the models used to describe mass transfer in SE will be presented. The contribution of mass transfer rate and chemical reaction rate to the observed extraction rate are also discussed. A review of the techniques available today for studying solvent extraction kinetics will also be presented in terms of their capabilities and limitations.

In Chapter Three the contribution of instrumental components to the spreading (band broadening) of experimentally acquired extraction data will be discussed. Instrument band broadening will be treated in terms of variance as measured by the second statistical moment. The concept of Fast Fourier Transform deconvolution for eliminating contributions of instrument band broadening to extraction data will also be introduced in this chapter.

In Chapter Four a discussion of the design and characterization of the rapid stir solvent extraction apparatus will be presented. The characterization will include studies of the effects of changes in instrumental and experimental parameters on the mass transfer rate.

In Chapter Five the results of mass transfer rate data for the extraction of *o*-nitroaniline from an aqueous buffer into chloroform, and of a sodium salt of *o*-nitrophenol from chloroform into an aqueous phase using the apparatus discussed in Chapter Four will be presented and interpreted in terms of the two-film theory.

In Chapter Six the capabilities and limitations of the apparatus for studying fast chemical reaction rates will be discussed. The rate of the homogeneous oxidation of I^- by Fe^{3+} will be studied as a model system.

In Chapter Seven, the use of the apparatus for interfacial concentration measurements in the investigation of interfacial adsorption equilibria of tetrahexyl ammonium salts of picrate and bromothymol blue at the chloroform/water interface will be presented.

In Chapter Eight, the effects of interfacial adsorption of ion-pair reagents and products on ion-pair extraction rates of tetrahexyl ammonium picrate and bromothymol blue will be presented. Finally in Chapter Nine, a brief proposal of future extension of the research work presented in this thesis will be discussed.

CHAPTER 2

KINETIC MODELS AND METHODS FOR MASS TRANSFER STUDIES

2.1 INTRODUCTION

Kinetic aspects of solvent extraction have been extensively investigated and numerous reviews and books pertaining to the subject have been published [36, 39, 40]. In extraction kinetics, one faces two types of problems,which have been classified by Tarasov and Yagodin [40] as direct and inverse. The former consists of a description of the kinetics, given concrete well-known phenomena. The later, which is of most interest to chemists, involves the identification of definite phenomena and the ascertainment of their mechanisms from experimental data on the mass transfer rate.

Mass transfer is effected by molecular diffussion and solution convection (either laminar or turbulent). Among these extractive processes, molecular diffusion is the most prevalent, and occurs even in instances when conditions such as stirring require that convection should be operative. Various models [35, 41-47] have been propossed to explain the phenomenon of mass transfer in terms of the structure of the interfacial region through which mass transfer occurs, but only three are in common use [48].

2.2 THE FILM THEORY

Among the models, the "film" theory postulated by Nernst [41] and Whitman [46, 47] gives the simplest description of the interface. This theory idealizes the interfacial region as a hypothetical thin film of unstirred(stagnant) layer. Mass transfer therefore involves diffusion across this film and is usually confined to the direction normal to the surface. When a solute at high dilution is diffusing across this film, the steady-state flux can be written in terms of the mass transfer coefficient using Fick's first law as;

$$J_1 = \beta (C_{1i} - C_1) \qquad (2.1)$$

where J_1 is the flux of component 1 relative to the surface (e.g. mol/cm^{2}s), β is the mass transfer coefficient (e.g. cm/s), and C_{1i} and C_1 are the surface (interfacial) and bulk concentrations in the fluid into which the transfer is taking place. Equation 2.1 can also be expressed in terms of the solute diffusion coefficient, D, from which it can be shown [48] that the mass transfer coefficient is defined mathematically as;

$$\beta = \frac{D}{\delta} \qquad (2.2)$$

where δ is the hypothetical thickness of the stagnant Nernst film.

This model is not only applicable to transfer across liquid-liquid interfaces but can be applied effectively to transfer across liquid/solid and liquid/gas interfaces [39]. It is also particularly useful in work on membrane transport and in the study of electrode kinetics [48]. In membrane studies the membrane is regarded as a stagnant phase and transport within it is treated, in most instances, as due to molecular-diffusion processes.

Where two liquid phases are in contact, it is necessary to modify the model to include two stagnant films, one on each side of the interface. In such a case, the total resistance to mass transfer is given by the sum of the two stagnant-film resistances, which act in series. Figure 2.1 is a schematic representation of the interfacial region in an extraction system according to the Whitman "two-film" model [36]. It is composed of bulk phases of the two immiscible fluids and an interfacial region between them. The interfacial region is composed of two hypothetical thin films on each side if the interface itself. These two films are called the Nernst diffusion films. Within each of the two bulk phases there is significant convective mixing which can be caused by either one or a combination of these processes; mechanical agitation, stirring and thermal gradient. In consequence, a sample placed in a bulk is instantaneously distributed within that phase. The fluids within the two Nernst

diffusion films are considered to be free from mixing by convection and are regarded as being stagnant. The thickness of the Nernst diffusion film is dependent upon the hydrodynamic condition occuring inside the entire extraction system. Empirically, the boundary of the diffusion film from the interface is defined as the point at which the fluid flow velocity is about 37% that of the mean flow velocity.

Using the Whitman two-film model of the interface it is possible to describe the processes which must occur in order to transport a solute molecule from one bulk phase into another bulk phase. Basically, a solute molecule leaves one bulk phase by purely convective and instantaneous mass transfer and enters the Nernst diffusion film on the same side of the interface. Mass transfer then occurs by diffusion towards the interface. Normally, though not always, transfer across the interface itself is instantaneous so that the ratio of concentrations of solute in the liquid regions immediately adjacent to the two sides of the interface is given by the equilibrium distribution ceofficient. When a film of adsorbed material is present at the interface there is an additional finite resistance to mass transfer across the interface itself [39]. Once on the other side of the interface solute diffuses through the second Nernst diffusion film toward the second bulk liquid phase. In the absence of interfacial resistance the rate of extraction of a solute is related inversly to the thickness of the two Nernst diffusion films and directly to the net diffusion coefficients of the solute within the two films[39, 45].

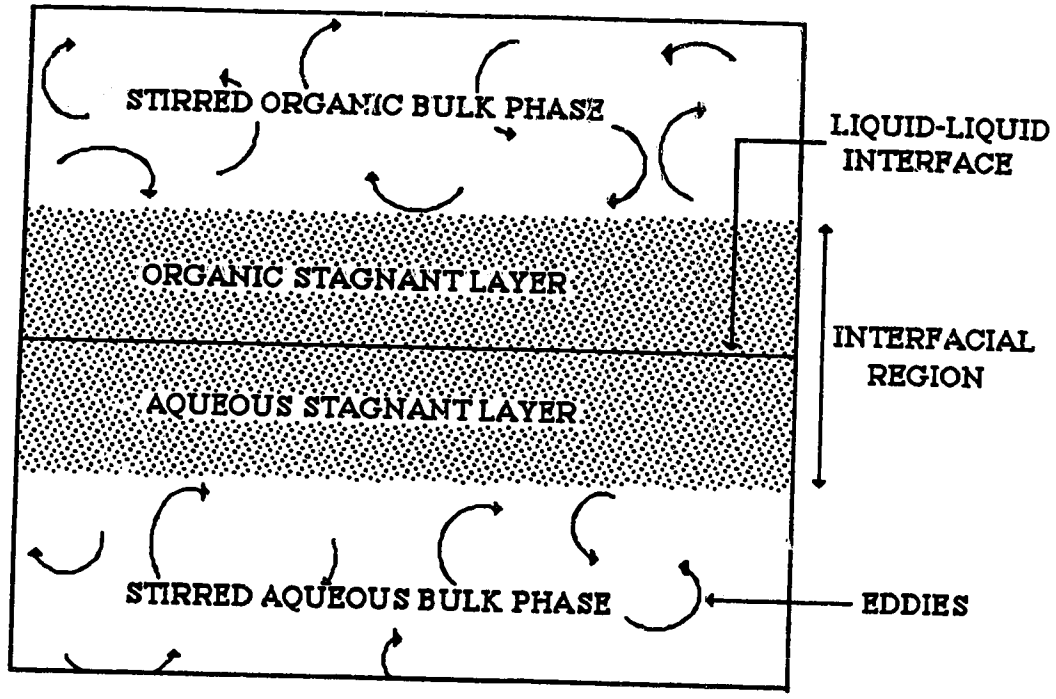

Figure 2.1 Diagram of an interfacial region between two immiscible liquid phases.

2.3 PENETRATION AND SURFACE-RENEWAL MODELS [43-45, 48]

These models provide a better physical picture of mass transfer than the thin film theory. Whereas the film theory applies under steady-state mass transfer, the penetration and the surface renewal models deal with transient conditions. The penetration model [43] assumes the interfacial region to be a very thick film continuously generated by flow, and mass transfer involves diffusion into this film. The model also assumes that mass transfer in the direction normal to the film is dominated by diffusion while convection is more important for mass transfer in the direction of fliud flow. The mathematical treatment of this model leads to a new definition of the mass transfer coefficient as follows [45];

$$\beta = 2\sqrt{\frac{Dv_{max}}{\pi L}} \qquad (2.3)$$

where L is the length of surface and v_{max} is the maximum flow velocity. The quantity L/v_{max} , often called the "contact time", has the same significance as the film thickness in the thin film model and it is also usually not known a priori. With this model, doubling the diffusion coefficient increases the mass transfer coefficient by a factor of the square root of 2.

The surface-renewal [44] model on the other hand regards the interfacial region as composed of two zones, a large well-mixed region and a surface region that is renewed so fast by fluid flow that it behaves as a thick film. Within this film mass transfer is described by the penetration theory. The mathematical description of this model depends on the length of time that a small fluid element spends in this region. From a combination of probability treatment [45] with flux, the mass transfer coefficient is derived as;

$$\beta = \sqrt{\frac{D}{\tau}} \qquad (2.4)$$

where τ is the surface renewal time. With this model also, doubling the diffusion coefficient increases the mass transfer coefficient by a factor of the square root of 2.

2.4 THE TURBULENT-BOUNDARY-LAYER MODEL [35, 45, 48]

A much more sophisticated theory is the "boundary layer" concept which assumes that fluid flow varies as a power series from the bulk towards the interface. When the velocity and its gradient in shearing flow near an interface are large enough for the momentum forces to exceed the viscous forces the flow pattern becomes irregular and turbulent. The region where the flow experiences disruption and the interface is called the "boundary layer" and it is usually defined as the locus of distance over which 99% of the disruptive effect occurs. Within the "boundary-layer" turbulence is damped so that the flow pattern becomes laminar and eventually the flow velocity is zero at the interface. Mass transfer across the interface generates concentration gradients in the "boundary-layer" between the surface and the fully turbulent regions in the bulk. Within the "boundary-layer" mass transfer in the stationary layer nearer to the surface is by molecular diffusion while in the intermediate layer both turbulent convection and molecular diffusions contribute to mass transfer. The flux, J, of solute across the interface is hence given as [48];

$$J = -(D + E)\frac{dC}{dX} \qquad (2.5)$$

where D is the solute diffusivity, E is the turbulent convection diffusivity, C the solute concentration in the bulk phase and X is the thickness of the boundary-layer. Although the "boundary-layer" model gives a more complete description of mass transfer, it is mathematically more complex to handle.

2.5 MEASUREMENT OF EXTRACTION RATES

Using the "two-film" theory, it is clear that the overall rate of mass transfer is controlled by the degree of diffusive resistance to mass transfer. The overall resistance is the sum of resistances in each of the two liquid phases and that at the interface itself [39].

$$R_o = R_1 + R_i + R_2 \qquad (2.6)$$

where R_1 and R_2 are the diffusional resistances within the "Nernst films" on the phase 1 and 2 sides of the interface respectively. For a very clean interface, the interfacial resistance, R_i , is relatively small and therefore negligible. As a result, the overall resistance, R_o , encountered during solute transfer is given by the expression:

$$R_o = R_1 + R_2 \qquad (2.7)$$

These diffusional resistances are related to the individual mass transfer coefficients by the expressions:

$$R_1 = \frac{1}{\beta_{mt,1}} = \frac{1}{\beta_1} + \frac{1}{K_D\beta_2} \qquad (2.8)$$

and

$$R_2 = \frac{1}{\beta_{mt,2}} = \frac{1}{\beta_2} + \frac{K_D}{\beta_1} \qquad (2.9)$$

where $\beta_{mt,1}$ and $\beta_{mt,2}$ are the overall mass transfer coefficients, while β_1 and β_2 are the specific mass transfer coefficients in the phases 1 and 2 respectively. K_D is the distribution coefficient (the ratio of concentration in phase 2 to that of phase 1) of the solute between the two phases. When the distribution coefficient is large the overall

resistance to mass transfer is that associated with phase 1. The resistance associated with phase 2 becomes significant for smaller values of K_D. The overall measured mass transfer coefficient, β_{mt} , is $(1/\beta_{mt,1} + 1/\beta_{mt,2})^{-1}$ and varies between β_1 and β_2. Normally, conditions are adjusted to produce quantitative extraction at equilibrium and hence the rate of extraction is controlled only by the resistance to mass transfer in the raffinate phase, therefore, ($\beta_{mt} = \beta_{mt,1}$).

From the "two-film" model and equations analogous to Fick's first law, the steady state flux, J, of solute into the receiving phase is given by the expression:

$$J_2 = \beta_{mt}\left(C_1 - \frac{C_2}{K_D}\right) \qquad (2.10)$$

where C is the bulk concentration of solute. Integration of Equation 2.10 gives:

$$\mathrm{Ln}\left(\frac{C_{2,\,eq}}{C_{2,\,eq} - C_2}\right) = \beta_{mt}\frac{A}{V_1}\ t \qquad (2.11)$$

where $C_{2,\,eq}$ is the equilibrium concentration of solute in the receiving phase, C_2 is the concentration at time t, A is the total interfacial area and V_1 is the volume of the raffinate phase. A plot of the left hand side of Equation 2.11 against time should give a straight line with a slope corresponding to the observed (pseudo) first order extraction rate constant, k_{mt} , which is defined as follows;

$$k_{mt} = \beta_{mt}\frac{A}{V_1} \qquad (2.12)$$

In many of the solvent extraction systems that are important in analytical, synthetic and hydrometallurgical applications, a chemical reaction accompanies the transfer of solute from one bulk liquid phase to the other. In consequence, the rate of solvent extraction in

such systems are, usually, governed by the rate of the chemical reaction, by the rate of mass transfer between the phases, or by some combination of both chemical and mass transfer rates [36].

For example, when a chemical reaction with a rate constant, k_r , accompanies the mass transfer the observed extraction rate constant is designated as k_{obs} , and is related to the chemical reaction rate and the mass transfer rate constant by:

$$\frac{1}{k_{obs}} = \frac{1}{k_r} + \frac{1}{k_{mt}} \qquad (2.13)$$

Provided that the chemical reaction does not involve a reactant that is adsorbed at the liquid-liquid interface, k_r is independent of both the surface area, A, and β_{mt}. If a reactant is interfacially adsorbed then k_r in Equation 2.13 is still independent of β_{mt} but it is dependent on A and is related to the true chemical reaction rate constant by the factor A/V_1 [49]. If the rate of the chemical reaction which is associated with an extraction process is much larger than the mass transfer rate then, as predicted by Equation 2.13, the experimentally measured extraction rate k_{obs} is equal to the mass transfer rate constant k_{mt}. On the other hand if the mass transfer rate constant is much larger than the chemical reaction rate constant then k_{obs} becomes equal to the chemical reaction rate constant, k_r. Thus, in order to measure the rate of a chemical reaction accompanying an extraction process, it is necessary to perform the experiment under conditions where mass transfer is faster than the chemical reaction (i.e. in the "chemical kinetic" regime where k_{mt} is relatively large so that mass transfer control of the rate is effectively eliminated) [49].

2.6 INSTRUMENTAL TECHNIQUES FOR MEASURING MASS TRANSFER RATES

Several experimental techniques have been reported for studying interfacial mass transfer kinetics [36, 37]. Typically, most of the techniques and the apparatus have been designed to operate either in a kinetically limited regime, or to allow calculation of the contribution of the diffusional component to the overall extraction rate. The techniques that are in common use today can be classified into the following groups: the stirred-cell techniques, the single drop techniques, the rotating diffusion cell, the liquid-jet recycle reactor, the liquid-liquid segmented flow method, the electrochemical methods, the capillary method, the falling-film reactor, and the " in-liquid ejection " contactor. Among these the rotating diffusion cell, the rapid stir-cell, the single drop and liquid-liquid segmented flow are the only methods that can produce large enough values of k_{mt} to permit the measurement of relatively fast chemical reactions by solvent extraction.

2.6.1 STIRRED CELL TECHNIQUE

The stirred cell techniques are subdivided into two categories [37]: those of the Lewis cell [50] type on one hand, and the highly agitated contactor (rapid-stir cell) on the other. The Lewis cell, illustrated in Figure 2.2, and its various modifications [51-55] provide direct liquid-liquid contact with a well defined interfacial area, and stirring of both phases without breakup of the interface. The interfacial area available for mass transfer is defined by the cell geometry and agitation is caused by two impellers, one for each phase. The modified designs of this device also provide for continuous monitoring of the extent of extraction with time by either radiometric, electrochemical or spectroscopic techniques. In this way difficulties associated with volume variation caused by intermittent sampling are eliminated. Some of the newer designs [51, 52] even allow for operations at relatively high Reynolds numbers without disturbing the interfacial area. It is therefore possible with these devices to obtain rate versus stirring speed curves at different chemical compositions. These make it possible to recognize when the rate of extraction is diffusionally or

kinetically controlled. The main disadvantage with their use is that experimental values of k_{mt} are small because the factor A/V_1 is small so that it not possible to use these devices for studying fast chemical reactions in the "kinetic" regime.

The highly agitated contactors comprise all those devices in which the two phases are so highly agitated that droplets of one phase are dispersed in a continuum of the second phase. The dispersion is characterized by an equilibrium distribution of drop diameters which is maintained by some combination of the opposing processes of drop break-up and coalescence [56-60]. With these devices it is possible to reduce the thickness of the diffusion layer, δ, to 10-30 μm and more importantly, to increase A/V_1 so that k_{mt} is quite large. The most reputable designs include the AKUFVE apparatus [61] designed for measuring distribution coefficients, and the rapid stir solvent extraction apparatus shown in Figure 2.3 which was invented by Carter and Freiser [62] for interfacial kinetic measurements. The latter apparatus consists of a Morton flask with inlets for the stirrer shaft, sample introduction and intermittent sampling probe. This design has since been modified by Watarai et. al. [63] to incorporate components for continuous monitoring of the rate of extraction and an instantaneous data analysis. Continuous monitoring is accomplished by the introduction of a microporous membrane phase separator which is capable of selectively filtering water-immiscible solvents from an intimate admixture with an aqueous phase. An on-line minicomputer provides data analysis.

The main limitation of the rapid-stir techniques is the poorly defined hydrodynamics [37]. The diffusion layer thickness, δ, and A/V_1 cannot be accurately predicted from hydrodynamics. However, theory does allow approximate prediction of A/V_1, β_{mt}, and k_{mt} and a recent approach by Aprahamian et.al. [64] has shown that it is possible to estimate drop size and interfacial area in a rapid-stir system using experimental data.

Rapid-stir apparatus are suitable for studying solvent extraction rates in the " kinetic" regime which can be achieved for slow to moderately fast reactions. The chemical reactions that can be studied can occur either in the bulk phase (homogeneous) or at the liquid-liquid interface (heterogeneous). Danesi et. al [65] have reported the rate constant and proposed mechanisms for the reaction of cupric and ferric ions with β-hydroxy oximes using the AKUFVE apparatus. Numerous other reports [62, 66-69] on the extraction kinetics of metal chelates using the Morton flask have been published. The rates of extraction in all cases were in the "kinetic" regime where the metal-ligand formation reaction was slow compared to diffusion through the Nernst film. Higuchi et. al. [32] have used the Lewis cell to measure the extraction rates of bromide ion-pairs of an organic ammonuim ion from water into chloroform and concluded that the rate was governed by diffusional mass transfer. Cantwell et al. [70] have measured the mass transfer rate constant for the extraction of tetrabutyl ammonium picrate from an aqueous solution into chloroform and concluded that the rate of mass transfer was controlled by the rate of diffusion through the Nernst layer on the aqueous side of the interface.

Figure 2.2 has been removed due to the unavailability of copyright permission.

Figure 2.2 Original contacting cell developed by Lewis [50].

Figure 2.3 has been removed due to the unavailability of copyright permission.

Figure 2.3 Rapid stir extraction apparatus [62]. (A) High speed motor; (B) Stir shaft; (C) Nitrogen inlet; (D) Sample outlet; (E) Morton flask.

2.6.2 SINGLE-DROP TECHNIQUE

The principle of the single drop technique [36, 37, 71] consists of producing drops of an organic or aqueous phase near one end of a vertical column which has been filled with a second immiscible liquid phase. Depending on the density difference between the two fluids the drops travel either downwards or upwards along the column and during this time extraction takes place across the drop interface. The relative motion of the fluids creates convective mixing within the drop to enhance the rate of mass transfer. From the time of travel, the drop size and its volume it is possible to determine the rate of extraction. Extraction may take place either from the dispersed drops into the continuous phase or in the reverse direction.

Theoretical analysis of data by the single drop technique is based on the following assumptions:

The change in concentration of the feed phase must be negligible.

The drops must be spherical and uniform in size.

The circulation pattern within the drops can be analyzed.

Negligible mass transfer occurs during drop formation and in the pool of coalesced drops at the end of the column.

In practice however, only the first assumption is generally satisfied. When the extraction rate is very rapid, much of the extraction takes place during the drop formation [39]. On the other hand when the extraction is very slow, very long columns are required to ensure enough residence time. Finally, the hydrodynamics within the drops are difficult to accurately predict, especially when the drops are small or when surfactants are present [72-75]. The true extraction regime is therefore difficult to establish and this makes the interpretation of the extraction data very difficult [76-79]. The advantages of this technique are that only very small sample volumes are required and also there is the possibility of getting information on very slow chemical reactions. In spite of these facts

numerous reports on extraction kinetics by single drop techniques have been published. Jansson et.al. [78] have measured the extraction rate constant for alkylammonium picrate ion-pairs to and from chloroform and found the extraction constants were in good agreement with extraction constants obtained under equilibrium conditions. Nordgren et. al. [77, 80-83] have used the single drop technique to obtain ion-pair extraction rate constants. Whewell et. al. [71] have used this technique to study the extraction kinetics of copper with LIX reagents, and reported the possibility of identifying an interfacial chemical reaction.

2.6.3 ROTATING DIFFUSION CELL

The rotating diffusion cell (RDC) technique for extraction [37, 84, 85] is based on the same principle as the rotating disc electrode and therefore several detailed accounts on rotating disc hydrodynamics and diffusion patterns are already available [86]. The basic design of the rotating diffusion cell consists of a thin membrane attached to the end of a rotatable hollow cylinder which when rotating creates well defined hydrodynamics on both sides of the filter (membrane). A schematic diagram of a rotating diffusion-cell designed by Albery et. al. [85] is given in Figure 2.4. Mass transfer occurs from the inner chamber through the membrane into the outer chamber. Depending on the design of the cell, the overall mass transfer can encounter up to five resistances in series. Normally there are two diffusive boundary layers, one on each side of the membrane, and two interfacial transfer resistances. Also there is an additional resistance due to solute diffusion through the liquid held in the membrane. When the inner and outer solutions are identical, the diffusive boundary layer contributions on each side of the membrane are the same. Therefore the exact mathematical formulation for the resistances depends on the system being studied. The overall mass transfer coefficient is also dependent on the effective area and the thickness of the membrane, hence, these membrane thickness must be well characterized.

The main advantage of the rotating diffusion cell is that the hydrodynamics near the membrane surface are well characterized.

The thickness of the "stagnant" diffusional layer in solution is defined mathematically as follows:

$$Z_D = 0.643\, W^{-1/2} D^{1/3} \upsilon^{1/6} \qquad (2.14)$$

The above equation is referred to as the Levich equation [86], where Z_D is the diffusive boundary layer thickness, W is the rotational speed(in Hz) of the membrane, u is the kinematic viscosity (cm^2/s), and D is the diffusion coefficient of the solute (cm^2/s). It is possible using Equation 2.14 to predict the mass transfer contributions from the diffusion layer in solution and to separate them from an overall measured extraction rate constant. One of the main problems with the use of the rotating diffusion cell for solvent extraction kinetic studies is that, while Z_D can be made very small by rapid rotation, the membrane thickness has a lower practical limit which imposes an upper limit to the achievable mass transfer rate. In most instances also, membrane pore sizes are not accurately known and this also introduces error in the estimation of the mass transfer rates. Although RDC techniques can be used to study the extraction rate in the "kinetic" regime, until recently, all the processes investigated with the RDC could be classified as purely diffusive. Guy and Fleming [87] have used the RDC for estimating diffusion coefficients of various esters of nicotinic acid in different kinds of organic barriers. Others [85, 88] have also used the RDC to determine aqueous-lipid partition coefficients for solute transfer across phospholipid/aqueous interfaces. Various thermodynamic variables associated with the transfer process have also been measured using the RDC [88-92]. It was observed that, for the transfer of methyl and ethyl nicotinates across a water/isopropyl myristate interface, the activation energy barrier is enthalpic because there appears to be a large entropy for

transfer into the interfacial region. Recently, it has been shown that it is possible to study interfacial chemical chelation reaction rates with the RDC [93-94].

Figure 2.4 has been removed due to the unavailability of copyright permission.

Figure 2.4 Rotating Diffusion Cell [85]; (M) millipore filter separating inner and outer solutions; (B) stationary cylindrical baffle; (C) rotating Perspex cylinder; (P) Pulley system driven by a velodyne motor/generator; (S) hollow stainless steel shaft.

2.6.4 LIQUID JET RECYCLE REACTOR

The Liquid Jet Recycle Reactor (LJRR) [37, 38, 95] which features a jet stream of one phase in an outer cocurrent flow of an immiscible second phase was proposed as a superior technique for studying interfacial reactions in liquid-liquid systems. The LJRR is designed to provide continous recycle of the outer phase and for its concentration to be monitored. The details of the jet chamber are illustrated in Figure 2.5. The principle of the LJRR is based on several assumptions and requirements about fluid physical properties, hydrodynamics, temperature and the types of interfacial process that can occur. Under normal experimental conditions, however, most of these requirments are difficult to maintain and as a consequence, the jet velocity profile does not remain constant with distance down the jet as required. In addition to the problem of not maintaining a fully relaxed jet, the apparatus is difficult to operate due to the sensitive nature of the jet. Presence of surface active agents also causes instabilities in the jet. Aside from all these difficulties with the LJRR, it has not yet been fully tested for the measurements of fast chemical reaction kinetics. So far, the LJRR has only been used successful in measuring diffusivities of solutes in liquids [95]. Attempts to use this device to study the interfacial reaction mechanism for the extraction of copper have not been complete [96].

2.6.5 LIQUID-LIQUID SEGMENTED FLOW

Solvent extraction flow injection analysis (SE/FIA) [97, 98] is a technique which employs segmented flow to automate solvent extraction and to increase the speed of SE. SE/FIA has since been found to have potential as a technique for studying liquid-liquid interfacial mass transfer processes [99-101]. A schematic diagram of an SE-FIA apparatus is shown in Figure 2.6. The technique involves the cocurrent flow of two immiscible liquids through a narrow tube (<0.8 mm i.d.) at a constant rate. The liquids are introduced

into the flow tube in a manner such that the two phases move along the tube as discrete segments in alternation. Owing to the viscous drag along the walls of the tubing a circulatory (bolus) flow [102, 103] is created within the segments, and as a result, mass transfer of solute across the liquid-liquid interface is enhanced. Nord [99] and later Lucy [100] have studied the factors that control the rate of mass transfer in a SE/FIA device, and found that the extraction rate depends upon the following; ratio of tubing cross sectional area to segment volume, segment length, the linear velocity of the flow, and the type of tubing (coiled or straight). The advantage of the technique is that the hydrodynamics of the flow has been well characterized with experimental parameters, and values of k_{mt} can be acheived which are about as large as those obtained with the rapid-stir cell [100]. Disadvantages of the technique are: (i) values of A/V_l are about an order of magnitude smaller than those obtained with the rapid-stir cell; (ii) it is much less convenient for extracting large volumes of sample because of the time required to pump a large volume of solution through a small-bore tube.

Figure 2.5 has been removed due to the unavailability of copyright permission.

Figure 2.5 Detail of the LJRR jet chamber, nozzel and receiver [95].

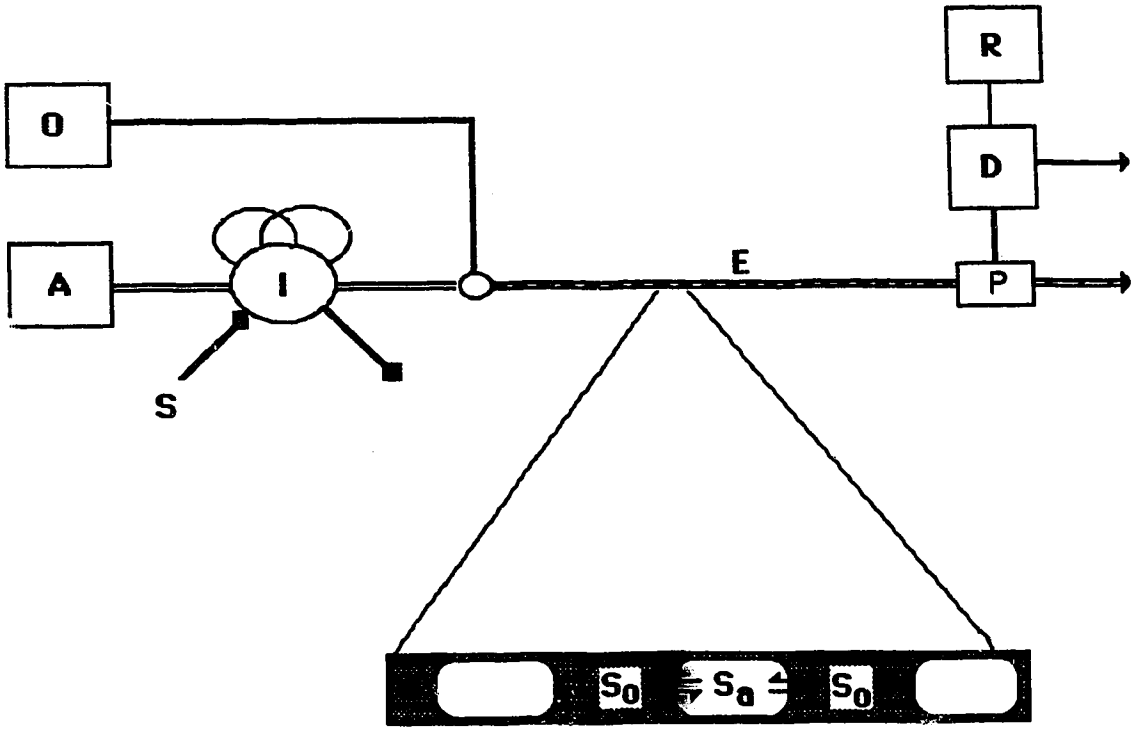

Figure 2.6 Block diagram of a solvent extraction / FIA system showing an expanded section of the segmented flow. (O) is the organic phase; (A) is the aqueous phase; (S) is the sample; (I) is the injection valve; (E) is the extraction tube; (P) is the phase separator; (D) is the detector; and (R) is the recorder.

2.6.6 ELECTROCHEMICAL METHODS

Various electrochemical techniques [37, 104-109] have also been used for studying solute transfer across the interface between two immiscible liquid phases. The application of electrochemical techniques to direct interfacial kinetic measurements is, however, limited by how close the electrodes can be brought to the interface.

2.6.7 CAPILLARY METHOD

Guy and coworkers [90] reported a method based on the capillary-tube procedure for self-diffusion for studying extraction kinetics. The technique involves the immersion of a glass capillary which is filled with a solution of a radiolabelled solute into a large well-stirred volume of the second phase. By measuring the concentration of the solute in the second phase the rate of mass transfer across the liquid-liquid interface can be estimated. The mass transfer rate constant for the transfer of salicylic acid and methyl nicotinate across a water/isopropyl myristate interface determined by this method agrees well with constants determined by the rotating diffusion cell.

2.6.8 OTHER TECHNIQUES

The falling-film [110] and the "in-liquid ejection" [111] contactors are mostly adequate for studies which involve only diffusional mass transfer measurement because of the significant contribution of diffusion to the rate of mass transfer.

Summarized in Table 2.1 are the characteristics of those of the above techniques that have or could easily be used to measure rates of chemical reactions accompanying solvent extraction. It is only those with a combination of large A/V_1 and large β_{mt} and, hence, large k_{mt} that have the ability to measure chemical reaction rates for relatively fast reactions.

Table 2.1 Summaries of the limitations and capabilities of solvent extraction systems

SYSTEM	DESCRIPTION	COMMENTS
Agitated contactors	Rapid-stir cell	- Hydrodynamics ill defined. - A/V_1 only approximate - $A/V_1 \leq 500\ cm^{-1}$ - $\beta_{mt} \leq 2 \times 10^{-3}$ cm/s [13]
Lewis-cell	Fluids layered in cell Each layer stirred separately.	- Hydrodynamics ill defined. - A/V_1 accurately known - $A/V_1 \leq 1\ cm^{-1}$ - $\beta_{mt} \leq 1 \times 10^{-3}$ cm/s [17]
Single drop	Drop falls (rises) in liquid	- Hydrodynamics ill defined - A/V_1 accurately known - $A/V_1 \leq 12\ cm^{-1}$ - $\beta_{mt} \leq 5.7 \times 10^{-2}$ cm/s
Liquid-Jet Recycle Reactor	Liquid jet with cocurrent flow of second phase	- Hydrodynamics well defined - A/V_1 accurately known - $A/V_1 \leq 20\ cm^{-1}$ - $\beta_{mt} \leq 12 \times 10^{-4}\ cm^3/s$ [62]
Rotating Diffusion Cell	Fluids partitioned by rotating membrane	- Hydrodynamics accurately known -A/V_1 reasonably well known - $A/V_1 \leq 1.5 \times 10^{-2}\ cm^{-1}$ - $\beta_{mt} \leq 1 \times 10^{-3}$ cm/s [56]
Liquid-Liquid Segmented Flow		-Hydrodynamics reasonably well known -A/V_1 reasonably well known - $40 \leq A/V_1 \leq 133\ cm^{-1}$ [68] - $4 \times 10^{-3} \leq \beta_{mt} \leq 1 \times 10^{-2}$ cm/s

2.7 PROPERTIES OF LIQUID-LIQUID DISPERSIONS

The rate of mass transfer in turbulent liquid-liquid dispersions has been found to depend upon the physical properties of the dispersion, the drop hydrodynamics, the geometry of the extraction equipment, and the presence of surface active agents. The physical properties that are important in estimating mass transfer rates include the interfacial area, A, the mean drop size, d_p , and the volume of the dispersed phase, V_d. These parameters are interrelated as follows [59];

$$d_p = \frac{\sum_1^n nd^3}{\sum_1^n nd^2} = \frac{6\,V_d}{A} \qquad (2.15)$$

where n is the number of drops having a diameter d in the dispersion. The term d_p is also commonly referred to as the Sauter mean, or surface volume mean diameter.

2.7.1 MEASUREMENT OF DROP SIZE OF A DISPERSION

The most relevant of the various mean drop size definitions for dispersions is the Sauter mean drop diameter defined by Equation 2.15. It may be evaluated from measurements of the interfacial area and the volume of the dispersed phase. Experimental methods for drop size measurement include direct observation by photomicrography [59], scattering of light beams [112], and techniques devised for freezing droplets by polymerization [113]. Another technique [114] based on the difference between the velocities of transmission of acoustic waves in two immiscible liquids has been reported for the measurements of drop size and volume of dispersed phase in liquid-liquid dispersions. It was claimed that measurements could be made continuously without delay and therefore, the technique could be well adapted to process control. The transducer head is sufficiently

small to allow effective point measurements necessary for drop size distribution characterization.

The mean drop size of dispersions has also been determined from theoretical correlations based on the theory of local isotropic turbulence [60]. The correlations often used are given by Equation 2.16 [115-118] and Equation 2.17 [119].

$$\frac{d_p}{L} = 0.06\, f_{\phi}\, N_{we}^{-0.6} \qquad (2.16)$$

Here N_{we} is the impeller Weber number, f_{ϕ} is a function of the phase ratio ϕ (its magnitude is dependent on whether drop breakage or drop coalesence is controlling the dispersion), and L is the diameter of the impeller.

$$d_p \approx \left(\frac{8\gamma}{\pi \rho_c}\right)^{3/5} \frac{L^{2/5}}{(v)^{6/5}} \qquad (2.17)$$

In Equation 2.17, γ is the interfacial tension between chloroform and the aqueous phase, ρ_c is the density of the chloroform continuous phase and v is the mean linear flow velocity. The term v is related to the stirring speed, N, as follows [120];

$$v = \pi N L \qquad (2.18)$$

It will be shown in Chapter 4 that both Equations 2.16 and 2.17 give comparable values for d_p.

2.7.2 MEASUREMENT OF INTERFACIAL AREA OF DISPERSIONS

The methods for measuring interfacial area of liquid-liquid dispersions can be classified either as direct or indirect [59]. The direct methods include experimental measurements of drop size distribution, or the application of theoretical correlations for estimating the interfacial area [59]. The latter, however, do not yield accurate results since these correlations do not apply to all systems.

The indirect methods involve measurements of a chemical reaction rate, measurements of the light-scattering properties of dispersions, and interfacial concentration measurements. The chemical rate method was first suggested by Nanda and Sharma [33, 121]. It involves measuring the rate of diffusion of a species, X, from a dispersed phase into a continuous phase, where it undergoes an irreversible first or pseudo-first order reaction with another reagent, Y. When the reaction is fast enough to keep the concentration of the diffusing species in the bulk of the continuous phase zero at all times, it was shown that under certain conditions the rate of extraction per unit area, R, is given by Equation 2.19 [122];

$$RA = A X_s \left(DkY_b + \beta^2 \right)^{1/2} \qquad (2.19)$$

where D is the diffusion coefficient of the species in the continuous phase, k is the chemical reaction rate constant, β is the continuous phase mass transfer coefficient, X_s is the concentration of X at the interface, and Y_b is the concentration of Y in the bulk continuous phase. If RA is measured for different values of kY_b, while the hydrodynamic condition is maintained constant, a plot of $(RA)^2$ against kY_b gives a straight line with intercept $(\beta A X_s)^2$ and slope $(AX_s)^2 D$. The effective interfacial area, A, can therefore be obtained from these parameters and the physiochemical properties of the system. Although this

method provides data under conditions which normally occur in extraction systems, it is subject to errors since it is highly sensitive to changes in the interfacial tension.

A typical optical method for interfacial area measurement is the light-transmittance method [118, 123] which is based on the ability of a dispersion to scatter incident light. The amount of light that is transmitted is found to be related to the interfacial area by the expression.

$$\mathrm{Ln}\left(\frac{I_o}{I}\right) = \frac{A\,L}{V_d 4} \qquad (2.20)$$

where I_o is the radiant power of incident light, I is the radiant power of transmitted light, and L is the length of the optical path. Although this method can only be applied to transparent dispersions it has an advantage over the chemical reaction method in that the measurements are not influenced by changes in interfacial tension.

Recently Aprahamian et. al. [64] described a technique involving the use of a microporous membrane phase separator for measuring the moles of surfactant adsorbed at the interface in a highly agitated two phase liquid-liquid mixture. By combining moles adsorbed with interfacial excess values which have been independently obtained from interfacial tension measurement, it was possible to calculate the interafacial area and the mean drop size of the dispersion. The interfacial excess, Γ, (mol/cm^2) and the concentration of the surfactant in the bulk liquid phase are related by the equation;

$$\Gamma A = (C_{ns} - C_s)\,V \qquad (2.21)$$

where C_{ns} is the concentration of surfactant in one of the phases comprising the dispersion under conditions of minimum interfacial area (non-stirring), while C_s is the concentration in the same phase under conditions of a large interfacial area (rapid stirring). V is the

volume of the phase being monitored and concentrations are often measured from the optical absorbance of the solution. This method is practical and can be used under conditions which normally occur in solvent extraction sytstems.

2.8 CORRELATIONS OF MASS TRANSFER COEFFICIENTS IN LIQUID-LIQUID DISPERSIONS

Quantitative methods for predicting mass transfer rates between phases in liquid-liquid dispersions are essential in the design of extraction equipments. To this end, a number of approaches for evaluating mass transfer coefficients inside and outside liquid droplets have been reported. So far the subject appears to be well understood for cases where the drops are spherical in shape, and also where no oscillation or interfacial turbulance is exhibited [124]. Generally, the transfer between a single drop and the surrounding fluid may be divided into two categories [124], transfer outside the drop and transfer within the drop. When transfer occurs outside the drop the overall mass transfer rate is dominated by the continuous phase mass transfer coefficient, while for transfer within the drop the overall rate is dominated by the dispersed phase mass transfer coefficient [124].

The magnitude of the mass transfer coefficient is found to be dependent upon conditions such as boundary layer separation, formation and shielding of wakes, and internal circulation. Other interfacial effects such as spontaneous emulsification, Marangoni instability, and interaction between drops (drop breakage and coalescence) which occur in multi-drop systems are also significant in determining the magnitude of the coefficients.

By convention, the rate of mass transfer is expressed in terms of the mass transfer coefficient. These coefficients are often expressed, not as individual numbers, but as correlations of dimensionless quantities. All the common mass transfer correlations that have been reported consist of the same general form. They typically consist of a Sherwood number, N_{Sh}, which contains the mass transfer coefficient, the Schmidt number, N_{Sc},

which is a characteristic of diffusion and the Reynolds number, N_{Re}, which defines the operating flow regime, as shown by the following general Equation [45, 59].

$$N_{Sh} \propto (N_{Re})^{x} (N_{Sc})^{y} \qquad (2.22)$$

The magitude of the indices x and y vary for the different types of mixing devices.

Some of the common continuous phase mass transfer correlations that have been reported for turbulent flow in rapid-stir contactors are given by the equations below [59, 118].

$$(\beta_{mt,\,c})\frac{A}{V} = \frac{72CN^{1.8}\,L\,D^{0.5}\,\emptyset}{(\gamma/\rho')^{0.6}\,(\mu/\rho)^{0.1}\,f_{\emptyset}} \qquad (2.23)$$

$$\beta_{mt,\,c} = 0.13\left(\frac{P}{V}\right)^{1/4} \rho^{-1/4}\,\upsilon^{-5/12}\,D^{2/3} \qquad (2.24)$$

In Equation 2.23, C and $f_{\emptyset}$ are empirical constants and in Equation 2.24, P is the power of the stirrer, υ is the kinematic viscosity and V is the volume of the dispersion. All the other terms have already been defined. Equation 2.23 applies for systems with very small dispersed phase fractions, $\emptyset$, where the degree of drop coalescence is minimal, while Equation 2.24 applies to systems for which the drops behave as rigid spheres with no internal circulation. A similar correlation for the dispersed phase mass transfer coefficient is given by Equation 2.25 [118].

$$\beta_{mt,\,d}\frac{A}{V} = \frac{4\pi^2\,D}{d_p^{\,2}} \qquad (2.25)$$

Cussler [45] has warned, however, that the uncertainty of these correlations is typically 10% or more. Therefore, great caution is required in their application to experimental data.

CHAPTER 3

INSTRUMENT CONTRIBUTION TO BAND BROADENING IN SOLVENT EXTRACTION SYSTEMS

3.1 INTRODUCTION

The rate of mass transfer is measured by extracting a solute from a donor phase into an acceptor immiscible phase while monitoring the change in absorbance (i.e. concentration of the solute) in either one of the phases with time. The rate constant for the extraction process is then evaluated from the observed absorbance vs time profile. In most instances, however, the type of equipment used for the extraction and monitoring of the extraction profile greatly distorts the true shape of the mass transfer profile, making it appear to be more spread out along the time axis. Hence kinetic data obtained from such a profile will not be a true representation of the mass transfer process itself. In this chapter, these adverse instrumental effects on measured extraction rate data will be addressed. First, a technique involving statistical moment analysis for estimating the extent of distortion (spreading) of rate data by the extraction apparatus will be given. Second, a technique involving Fourier Transform deconvolution will be described for eliminating the effects of instrumental distortion of extraction rate data.

3.2 EVALUATION OF BAND BROADENING (SPREADING)

The manner in which an instrument or a measuring device distorts an input signal can be explained in terms of the principles of convolution [125]. Mathematically, convolution can be expressed as:

$$Con_{AB}(\tau) = \lim_{T\to\infty} \frac{1}{2T}\int_{-T}^{+T} A(t)\ B(-t \pm \tau)\,dt \qquad (3.1)$$

where $Con_{AB}(\tau)$ is the convolution function between the two signals A(t) and B(t), and τ is their relative displacement. The minus sign in front of the t of the function B signifies that the function B(t) has to be reversed (from left to right) on the time axis before it is multiplied by A(t). The signals can be a function of essentially any variable, e.g., wavelength, retardation, frequency, accelerating voltage, time, etc. Thus, if A and B are functions of time, the convolution function Con_{AB} will be related to and plotted against the relative time delay between the two signals.

The practical significance of Equation 3.1 can be made clearer by considering what effect a recording device having a relatively long time constant, represented here as B(t), will have on an input signal, for example a step function, represented here as A(t). According to Equation 3.1, the recorded signal, $Con_{AB}(\tau)$, will not be identical to the original input signal but will reflect the response time of the recorder by distorting the original signal. Assuming that the recorder time constant B(t) is an exponential function, Figure 3.1 illustrates the extent of distortion that will occur when the step function is recorded by the recorder. By comparing the original input and the output signals, it is clear that the output signal is more spread out along the time axis than the original input step function. This kind of signal distortion occurs in virtually all measurements and results in such effects as poor resolution in spectroscopic data and excessive band broadening in data obtained with various flow devices.

The principles used in measuring the extent of spreading (band broadening) in chromatography [126, 127], and solvent extraction flow injection analysis [128] is applied here for the measurement of broadening of solvent extraction mass transfer profiles. The contributions to band broadening by various instruments in tandem are normally considered to act independently, and hence broadening from each of the individual instrument components can be added linearly to give the overall broadening (variance) due to the entire instrument, σ^2_I. With solvent extraction equipment

incorporating continuous monitoring devices, such as the one used in this work (see Figure 4.1), the overall instrument variance is given by the expression;

$$\sigma^2_I = \sigma^2_{injection/mixing} + \sigma^2_{membrane} + \sigma^2_{tubing} + \sigma^2_{detector/computer} \quad (3.2)$$

where $\sigma^2_{injection/mixing}$ is the variance associated with injection and mixing processes, $\sigma^2_{membrane}$ the variance associated with transport of the solute through the pores of the membrane, σ^2_{tubing} the variance associated with the non-uniform flow profile within the tubing connecting the extraction cell to the detector, and $\sigma^2_{detector/computer}$ is the variance associated with broadening of the solute zone within the detector flow cell and with the detector and computer response time constants.

In a typical extraction experiment the absorbance due to solute in the organic phase is monotored as a function of time. When the extraction process involves a chemical reaction, the observed absorbance vs time profile reflects three independent processes: the chemical reaction rate, the solute mass transfer rate, and the instrument band broadening. In terms of variances (i.e. second statistical moments, σ^2) the overall variance, σ^2_O, for an extraction involving a chemical reaction and mass transfer, therefore, equals the sum of contributions due to chemical reaction, σ^2_R, mass transfer, σ^2_M, and instrument band broadening, σ^2_I. Hence,

$$\sigma^2_O = \sigma^2_R + \sigma^2_M + \sigma^2_I \quad (3.3)$$

Stastistical Moment Analysis

Normally the broadening of a peak is characterized by a series of statistical moments [126, 129-131], where the normalized n^{th} moment of a peak is defined by the expression;

$$m_n = \frac{\int_0^\infty f(t)t^n dt}{\int_0^\infty f(t)dt} \qquad (3.4)$$

where f(t) is the peak profile and t is the time (volume or distance) coordinate. The zeroth moment of an unnormalized peak is its area. The first moment gives the coordinate of the center of gravity of the peak and thus is equal to, for example, the retention time (or migration distance) of a chromatographic peak. Generally it is convenient to take all moments higher than the first around the center of gravity of the peak, that is, around the t coordinate of the first moment. These higher moments are usually referred to as central statistical moments, and are used to describe the shape of a peak. They are defined by the expression;

$$m_n = \frac{\int_0^\infty f(t)(t - m_1)^n dt}{\int_0^\infty f(t)dt} \qquad \text{for } n>1 \qquad (3.5)$$

The second moment (first central statistical moment) is a measure of the peak variance, σ^2, of the peak profile about the center of gravity. The third moment gives the magnitude as well as the deviation of the peak's horizontal asymmetry, while the fourth moment is the measure of the peak flatness as well as the peak width. All higher odd moments are related to peak asymmetry while the higher even moments measure peak characteristics similar to the fourth moment. The skew and the excess are two moment-related quantities which are useful because they measure directly the deviation of the peak from a perfect Gaussian profile. The skewness, S, is defined from the third moment as:

$$S = \frac{m_3}{\sigma^3} \qquad (3.6)$$

A positive value of skewness indicates a tailing peak, and the magnitude of the skewness reflects the degree of the tailing. The excess, E, is a measure of the flatness of a peak, and it is defined from the fourth moment as follows:

$$E = \frac{m_4}{\sigma^4} - 3 \qquad (3.7)$$

Peak profiles which are more "peaked" than a Gaussian peak have positive values of excess.

Although there are other methods [132] of measuring peak variance, such as the width at half height and the tangent methods, the statistical moment approach gives more accurate results since it makes no prior assumptions about the peak shape. The precision of the calculations are, however, strongly dependent upon factors such as noise [130, 133, 134], baseline drift or error [130, 135], premature termination of data collection [133, 136, 137], and too few data points [133]. For comparison of variances calculated using different moment analysis techniques see Table 3.1 [100].

Solvent extraction kinetic data are usually obtained in the form of a sigmoidal profile. Therefore, in order to apply the concept of spreading or band broadening of a population distribution to such data, we need to somehow convert the extraction data into a peak profile. The conversion of a sigmoidal profile to a peak shaped profile can be done by simply taking the first derivative of the sigmoidal profile. The resulting peak shaped function is then subjected to statistical moment analysis. The magnitude of the second statistical moment (variance) provides us with an estimate of the extent of spreading of the original extraction profile along the time axis.

In this work, the second statistical moments were calculated from digitized absorbance data, f(t), while, dt, the time interval between successive points, corresponds to the data acquisition rate (0.1 s). Moment analysis and data acquisition programs (see Appendices B and C respectively) were written by C. Lucy [100] in ASYST Scientific System (MacMilllan Co. NY). Data digitization, acquisition and analysis were done on an IBM-XT microcomputer interfaced to the detector via a LAB MASTER ADC interface board. The sigmoidal profile was first normalized by dividing all absorbances by the equilibrium absorbance, and then converted to a peak by taking the first derivative. The baseline was determined using linear regression of the data points outside of the integration limits, in order to avoid errors due to drift. In each case peaks were defined by more than 100 data points to ensure adequate precision in the moment calculations. A typical A vs t extraction profile is shown in Figure 3.2, while the first derivative of the data in this Figure is shown in Figure 3.3 along with the values of its statistical moments.

Table 3.1 Comparison of Variances calculated for Snythetic Peaks using Various Measurement Techniquies [100]

Table 3.1 has been removed due to the unavailability of copyright permission.

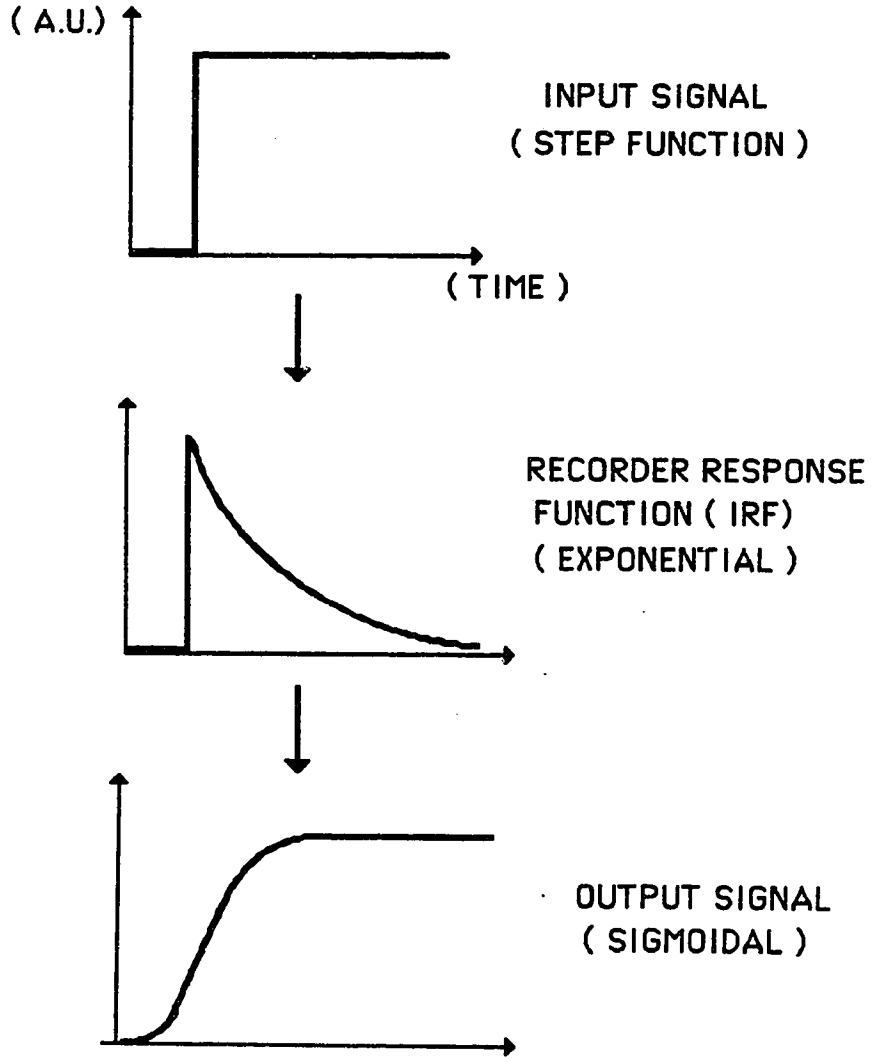

Figure 3.1 Diagram showing the effect of instrument response (band broadening) on an input signal.

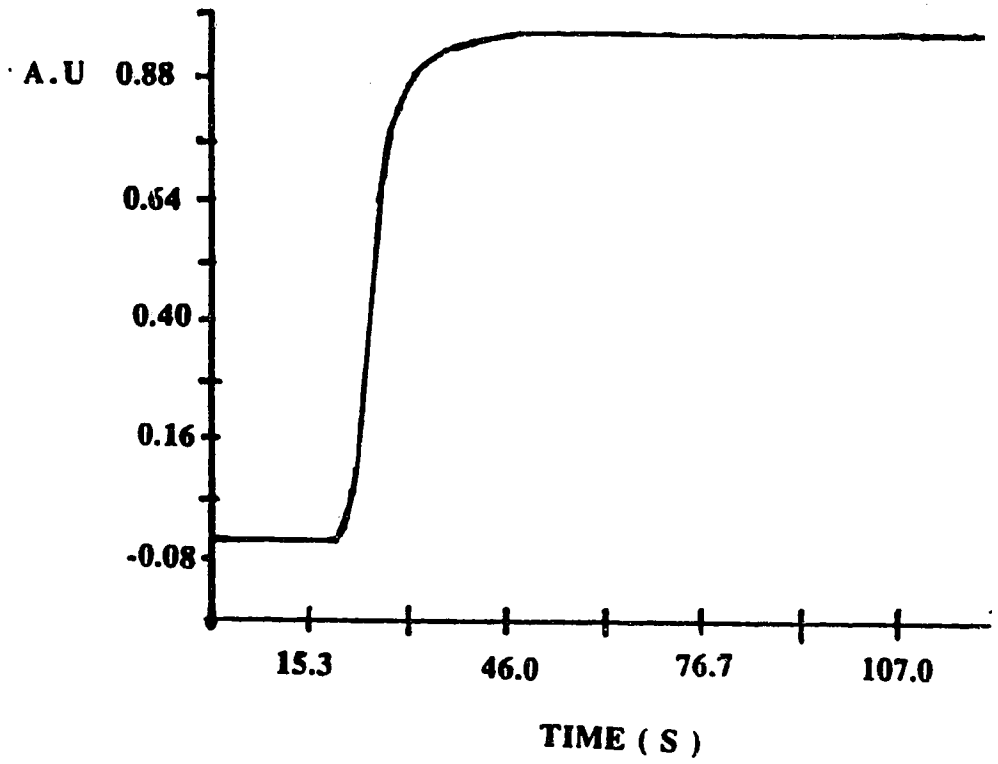

Figure 3.2 Typical extraction Absorbance *vs* Time Profile.

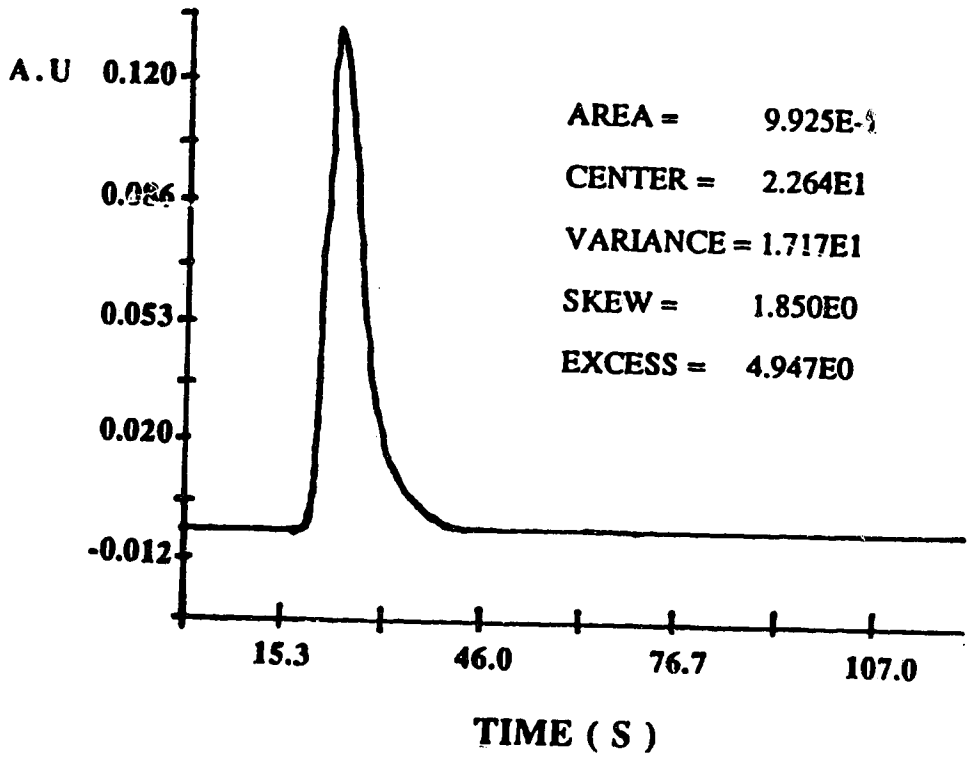

Figure 3.3 Typical first derivative plot of the extraction Absorbance *vs* Time Profile. Calculation of Peak Moments were performed by the Moment Analysis Program (see Appendix B)

3.3 REMOVAL OF INSTRUMENTAL EFFECTS ON MASS TRANSFER KINETIC DATA BY DECONVOLUTION

As discussed in Section 3.2 the distortion of an input signal by a measuring device can be considered as a convolution process. Because this process is a mathematical operation, it is therefore possible for the process to be reversed. The procedures for reversing a convolution operation are generally referred to as deconvolution [125]. Presently, the most commonly used technique for deconvolution is Fourier transformation (FT) [125, 128, 138, 139]. The Fourier transform of a function may be stated as,

$$A(t) = \int_{-\infty}^{+\infty} A(f)\, e^{2\pi i t f}\, df \qquad (3.8)$$

and the inverse transform is

$$A(f) = \int_{-\infty}^{+\infty} A(t)\, e^{-2\pi i t f}\, dt \qquad (3.9)$$

The functions A(t) and A(f) constitute a Fourier transform pair in which A(t) is the time varying property (signal) and A(f) is its frequency composition, which is normally expressed in units of s^{-1} or Hz.

A Fourier transform approach of convolving two functions A(t) and B(t) according to Equation 3.1 is shown schematically in Figure 3.4. Convolution of two functions is equivalent to the multiplication of their Fourier transforms followed by the inverse Fourier transformation of the product. Consider for example, data obtained for an extraction involving a chemical reaction, mass transfer and instrument band broadening, the convolution theorem defines the overall measured response, R_O , by the expression;

$$R_O(t) = R_R(t) * R_M(t) * R_I(t) \qquad (3.10)$$

where $R_O(t)$ is the overall response function (absorbance) with respect to time, and $R_R(t)$, $R_M(t)$ and $R_I(t)$ are the response functions due to chemical reaction, mass transfer and instrument respectively. The symbol " * " denotes the convolution operator. Application of Fourier transformation to Equation 3.1 transforms it to:

$$R_O(f) = R_R(f) \times R_M(f) \times R_I(f) \qquad (3.11)$$

Deconvolution is the opposite of convolution. If the goal is to extract only the response due to chemical reaction, $R_R(t)$, from the overall observed $R_O(t)$, this can be achieved by dividing (deconvolving) the Fourier transform of the overall response by those of mass transfer and instrument, followed by Inverse Fourier transformation (IFT) to yield the expected chemical reaction response in the time domain as shown by Equations 3.12 and 3.13.

$$R_R(f) = \frac{R_O(f)}{R_M(f) \times R_I(f)} \qquad (3.12)$$

$$IFT\left[\frac{R_o(f)}{R_M(f) \times R_I(f)}\right] = R_R(t) \qquad (3.13)$$

Generally, to perform deconvolution, one would require an "instrument" response function and an overall "sample" output response function. An instrument response (also referred to as impulse response function , IRF) is unique for a particular apparatus, and can be broadly defined as the output signal obtained when an impulse is applied to the input of the apparatus. The nature of the impulse response also depends on the type of measurement

that is being sought. As shown by Equation 3.13, if an extraction process involves a chemical reaction and the aim is to extract only chemical reaction data, the appropriate instrument response function to use for deconvolution is the output signal, $R_M(t) * R_I(t)$, obtained when an extraction involving no chemical reaction is performed with the same apparatus and under the same extraction conditions. On the other hand, if the extraction process involves only mass transfer ($R_R(t) = 0$), and the goal is to measure the mass transfer rate, then the appropriate IRF would be $R_I(t)$. The Fourier transform algorithm used in this work is called Fast Fourier Transform (FFT) [140]. It is much more suitable for handling a large number of data points and it is also has a much faster computation time than discrete FT [125, 138]. It can, however, only be applied to data arrays that are a power of 2 in length. The inverse algorithm is called Inverse Fast Fourier Transform (IFFT). It should be emphasized that deconvolution can only be performed with sample and instrument response functions that are significantly different from one another, since the operation by its nature leads to the enhancement of noise levels in the deconvolved signal. In the present work all A vs t profiles exhibited a distorted sigmoidal shape, as shown in Figure 3.2. Depending on the type of extraction process being studied, deconvolutions were performed both to obtain mass transfer rate constants k_{mt} and to obtain chemical reaction rate constants k_r. Regardless of the purpose of the deconvolution, the approach taken was the same and a schematic representation is shown if Figure 3.5 . Once again all the calculations were done on an IBM-XT microcomputer. The calculations were not automated since different extraction profiles may require different special data treatment prior to deconvolution. The overall extraction profile for the sample was mathematically differentiated and smoothed to obtain a peak. This operation significantly reduces the deleterious effect of signal noise on the final result. Next, to obtain the "instrument response function" (IRF), the time delay required for a change occuring in the extraction cell to reach the detector in the absence of band broadening was first subtracted and then the profile was inverted about the horizontal axis as previously described [70].

The resulting profile depicts the output expected when a unit impulse is applied to the input of the extraction apparatus. FFT's were taken of the peak-shaped sample function and of the IRF, the former was divided by the latter, and an inverse Fourier transform was performed to yield the peak-shaped derivative of the desired result. Integration of the peak then yielded the desired extraction profile (A vs t).

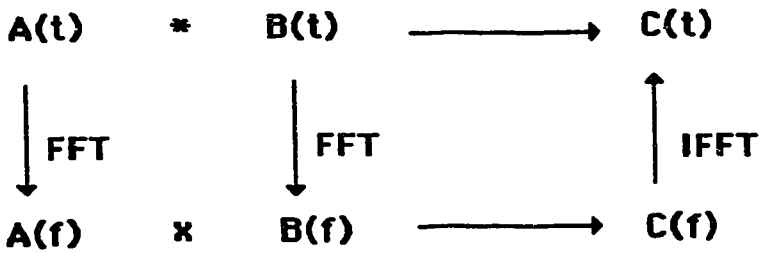

Figure 3.4 Schematic diagram showing the mathematical approach of Fast Fourier transform convolution. FFT; Fast Fourier transformation, IFFT; Inverse fast Fourier transformation.

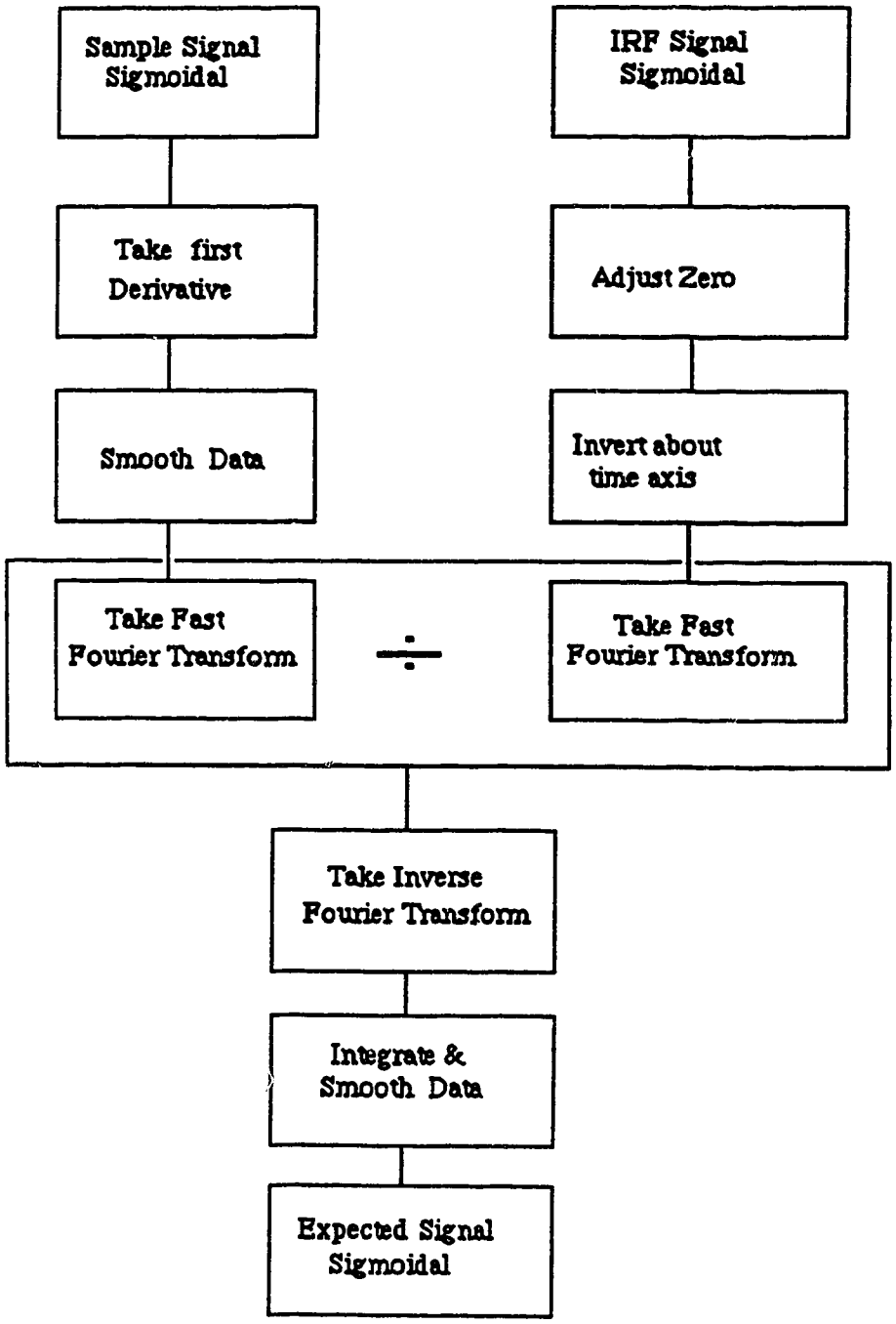

Figure 3.5 Schematic representation of the approach used for deconvolving experimental extraction data.

CHAPTER 4

DESIGN AND CHARACTERIZATION OF THE EXTRACTION APPARATUS

4.1 INTRODUCTION

In this chapter, a rapid stir solvent extraction apparatus employing remote sample injection and a porous membrane phase separator for continuous sampling and monitoring of the extraction rate and instantaneous data analysis is described. The apparatus is designed to be used for studying rates of fast mass transfer and chemical reactions.

The performance characteristics of the system such as extraction variances and rate constants are evaluated with respect to dimensions of various components of the system, and instrumental parameters such as flow rate, stirring speed and detector electronic time constant. The contribution of each instrument component to the overall observed variance of the extraction profile is studied and quantified. Hydrodynamic parameters such as mean drop size and interfacial area at optimum operating conditions are also discussed.

4.2 EXPERIMENTAL

4.2.1 CHEMICALS AND SOLVENTS

o - Nitroaniline (Laboratory Reagent) was used as received from The British Drug House Ltd., Poole. England.

Chloroform was reagent grade (Caldon Laboratory Ltd.) and was freshly washed with distilled water before use to remove impurities and preservatives.

Methanol was analytical grade (Anachemia. Montreal) and was used as received.

Distilled water was made by distilling stock laboratory distilled water from alkaline potassium permanganate in an all glass still. The first 20% of the distillate was discarded

and the middle fraction was collected. This water was used to prepare all aqueous solutions used in this work.

Sodium monohydrogen phosphate and sodium dihydrogen phosphate were analytical reagent grade (Matheson Coleman and Bell, and J.T. Baker Chemical Co.)

Reagent buffer. Sodium phosphate buffer pH 6.5 at an ionic strength of 0.05 M was prepared by mixing 241.0 mL of 0.10 M sodium dihydrogen phosphate with 86.0 mL of 0.10 M sodium hydrogen phosphate and diluting to 1.0 L with distilled water.

Commercial buffers. (Fisher Scientific Co.) of pH = 4.00 ± 0.01, pH = 7.00 ± 0.01 and pH = 10.00 ± 0.01 and were used for calibration of the pH meter (Fisher ACCUMET Model 525 pH/ION Meter) used.

4.2.2 APPARATUS

An overall schematic diagram of the extraction equipment is shown in Figure 4.1, and an enlarged view of the extraction cell is shown in Figure 4.2. The main components are the extraction cell (E), a variable wavelength photometer detector (D) with an 8 μL flow cell (UV 50 , Varian Assoc.) , a strip chart recorder (R) (Recordall 500, Fisher Scientific), an IBM-XT minicomputer (C) interfaced to the detector via a Lab Master ADC Interface Board (TM-40-P6L, Tecmar, Cleveland, OH), and a variable speed peristaltic pump (P) (Minipuls 2, Gilson, Ville-le-Belle, France).

The stainless steel extraction cell (E) has an internal diameter of 7.0 cm and a volume of 270 mL. There are four 8 mm wide removable baffles (H), also made of stainless steel and designed for easy mounting in the extraction cell. The stirring device consists of a high speed stirring motor (1/8 hp) with rotational speed feedback control (M) (Model HST 20N No. 447401 G.K. Heller Corp., Foral Park, NY) and a 3 cm diameter Teflon impeller (I). The stainless steel impeller shaft passes through a combination of Rulon (No. 9127 Johnston Industrial Plastics) and Teflon bearings, (W), in the lid which, purposely, are

not made air-tight in order to allow pressure equalization between the extraction cell and the aluminum cylinder (A) (see Figure 4.1) which surrounds the entire extraction cell.

Inside the aluminum cylinder the extraction cell is immersed in water which is held at 20 ± 0.1°C by means of copper coils (not shown) that pass through the cylinder walls via bulkhead fittings and connect with a circulating constant temperature water bath (B) (Fisher Scientific , Haake G. D3) . The lid of the aluminum pressure cylinder has ports to allow passage of all necessary steel and Teflon connecting tubings. The impeller shaft passes through air-tight Rulon and Teflon seals in this lid.

Prior to an experiment, the inside of the aluminum cylinder, and therefore also the extraction cell, are pressurized at 20 psig with nitrogen from a tank (T1). The organic wetting phase is forced, due to the increased pressure, to pass through the "filter probe" and through a 54 cm long by 0.3 mm i.d. Teflon tube to the flow cell of the photometric detector and then through a similar Teflon tube from the detector cell to an Acidflex peristaltic pump tube (12 cm long by 0.9 mm i.d.) (Technicon Corp., Tarrytown, NY). Depending on the position of the three-port valve V2 (LDC No. CAV3031), the flow is either directed to waste or returned to the extraction cell via a 70 cm long by 0.5 mm i.d. Teflon tubing. Flow to waste was used when extraction times were under 1 min, since the volume of the organic phase lost changes the organic to aqueous phase ratio by only 1%. Flow return to the extraction cell was used when longer extraction times were involved. Injection of sample into the extraction cell is made pneumatically by electrically actuating the solenoid valve V1 (Skinner V520V2100, Honeywell Ltd. Scarborough, Ontario). This causes nitrogen pressure (80 psig) from tank T2 to drive down the Teflon plunger in the injection capsule, thereby forcing the small Teflon plug at the bottom of the capsule to pop out and expel the sample solution from the capsule into the extraction cell. Valve V1 is held open through the duration of the extraction and during this time the higher nitrogen pressure holds down the plunger over the 0.4 cm hole at the bottom of the capsule as a seal so that it does not act on the liquids in the extraction cell.

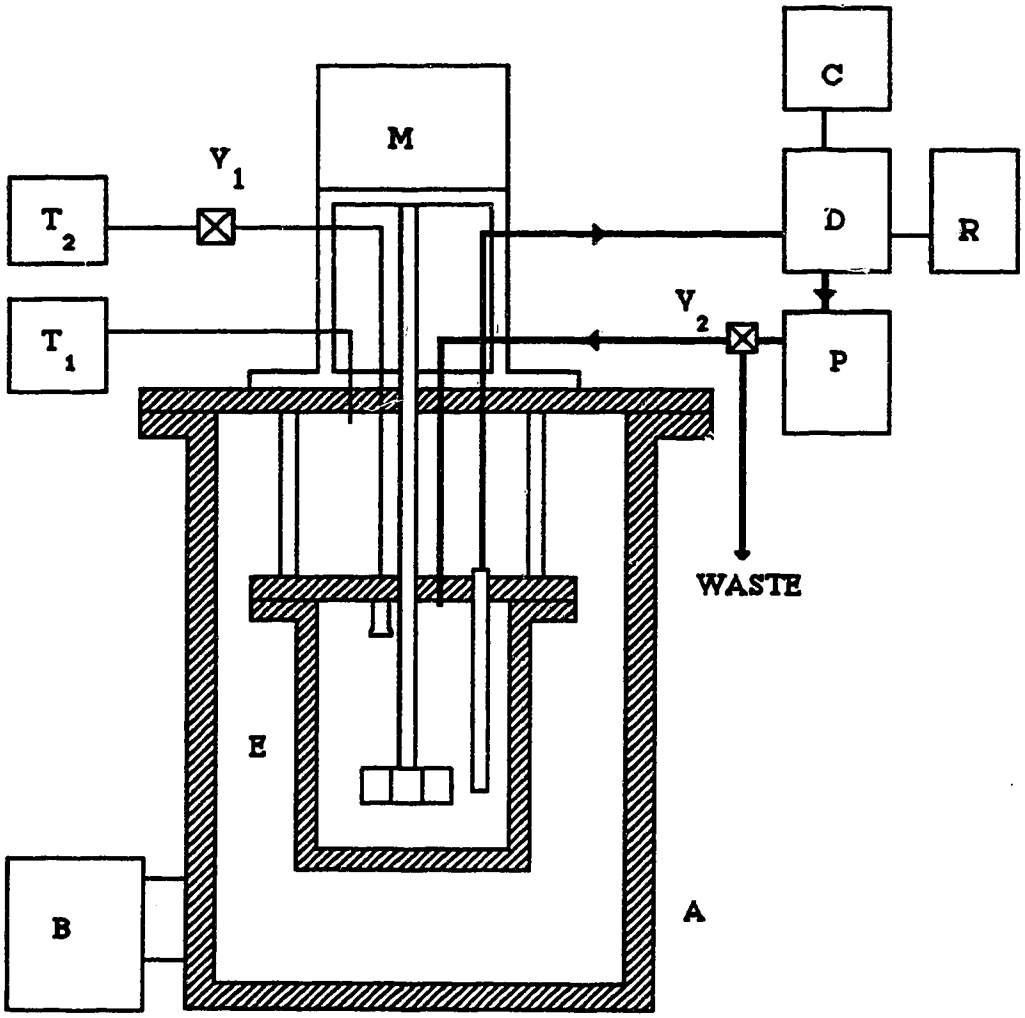

Figure 4.1. Diagram of the extraction apparatus: A, aluminum pressure cylinder; E, stainless steel extraction cell; M, high-speed stirring motor; B, circulating constant temperature bath; T_1 and T_2, tanks of pressurized nitrogen; D, spectrophotometer detector; C, microcomputer; R, strip chart recorder; P, peristaltic pump; V_1, solenoid valve; V_2, manual valve

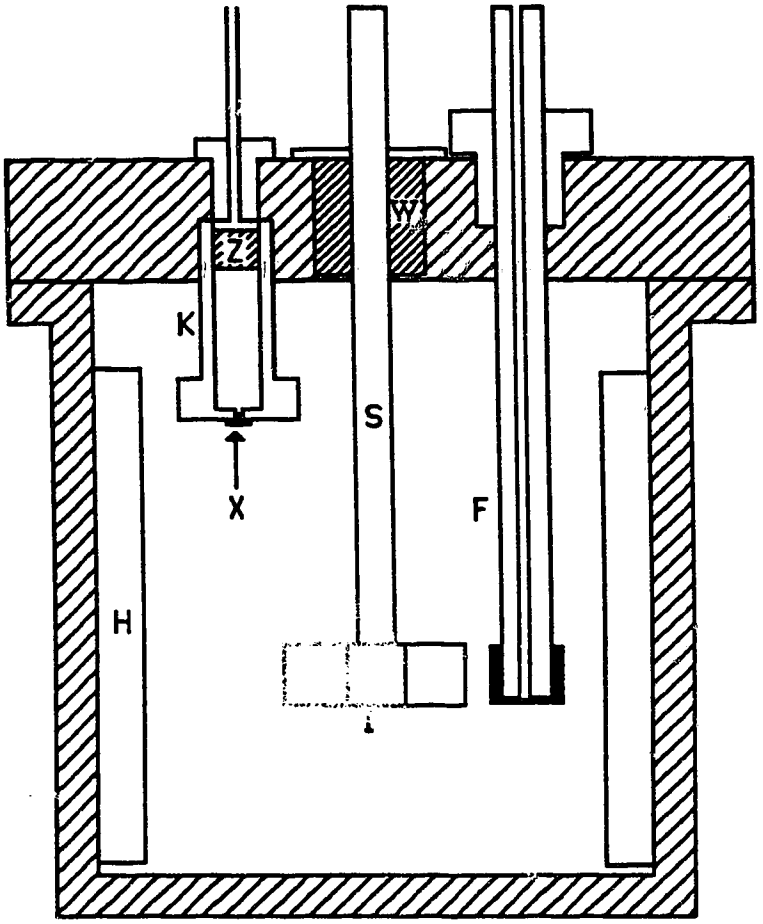

Figure 4.2. Diagram of the stainless steel rapid-stir extraction cell: S, stirrer shaft; F, filter probe; I, impeller; K, injection capsule; H, baffle; W, Teflon and Rulon bearings; X, Teflon plug; Z, Teflon plunger.

4.2.3 INJECTION CAPSULE

An enlarged schematic diagram of the injection capsule showing the before-injection and after-injection configuration of the capsule is illustrated in Figure 4.3. The capsule is essentially a 1.0 cm i.d. by 2.7 cm deep stainless steel cup designed screwed into the lid of the extraction cell as shown in Figure 4.2. Fitted inside the capsule is a 1.0 cm long piston-like Teflon plunger (Z). Also at the bottom of the capsule is a 0.4 cm hole which is normally stoppered with a small force-fit Teflon plug (X). When loading with the solution to be injected, (S), the capsule is held up-side-down and filled through the 0.4 cm hole at the bottom. The hole is then tightly stoppered with the Teflon plug before screwing the capsule into the lid of the extraction cell.

The injection capsule was calibrated for reproducibility in delivering sample into the extraction cell. This was done by injecting 0.25 mL chloroform solution of 1.0×10^{-1} M o-nitroaniline into 100.0 mL of chloroform in the extraction cell and measuring the change in equilibrium absorbance of the resulting solution. The relative deviation for five replicate injections was 1.6 %, which indicates that the injector is capable of performing adquately reproducible injections.

4.2.4 FILTER-PROBE

Figure 4.4 shows two schematic designs of the " filter-probe " used in this work. It is made of a 12 cm long by 0.25 in. o.d. by 0.5 mm i.d. stainless steel tube (F) with either of two sizes of porous Teflon membrane phase separators (M) fitted on the end. In the case of the small probe (Figure 4.4 B), with a membrane area of 0.28 cm^2, two layers of 0.0075 inch. thick, 2-5 μm pore size Zitex porous Teflon (No. E6060223, Chemplast Inc., Wayne, NJ) was stretched over coarse Teflon mesh (S) (LDC) and was held in place with a Teflon sleeve (R), as shown in Figure 4.4. In the large probe (Figure 4.4 A) with a membrane area of 1.32 cm^2, the membrane was stretched over a 1.3 cm diameter piece of Teflon (T) that was force-fit onto the end of the steel tube. The membrane was

either one layer of 0.0075 inch. thick 2-5 μm pore size Zitex, for use in the mass transfer rate studies, or two layers of 0.0055 inch. thick, 5-10 μm pore size Zitex (No. E606-122), for use in the chemical reaction rate and the ion-pair extraction kinetics studies. In all studies in which the aqueous phase was the liquid phase being monitored, one layer of Whatman No. 2 filter paper was used as membrane phase separator.

4.2.5 EFFECT OF CELL PRESSURE ON FLOW RATE

Initially, 200 mL of freshly washed chloroform was placed in the extraction cell and stirred at 1000 rpm (16.6 rps). The peristaltic pump was removed from the system before this study. Nitrogen gas pressure from Tank T_1 was applied to cause pumping of the liquid through the filter probe, the connecting tubing and detector flow cell to an adapted buret via valve V_2. (Note: the membrane phase separator used in this experiment was an early version which consisted of 1 layer of 10-20 μm pore size, 0.0045 inch. thick Teflon with a back-up of 1 layer of 30-60 μm pore size, 0.0075 inch. thick Teflon membrane. The surface area the membrane was 0.126 cm^2).The flow rate of the liquid was determined by measuring the average time required for 1 mL of chloroform to flow into the buret. The experiment was repeated at various nitrogen pressures ranging from 2.5 to 20.0 psig. In another set of experiments, also without the peristaltic pump, the solution in the extraction cell consisted of 100 mL of chloroform and 100.0 mL of buffer.

The ability of the peristaltic pump placed after the detector to control the flow rate was also determined. This was done by maintaining a constant nitrogen pressure in the extraction cell and varying the peristaltic pump rotation speed.

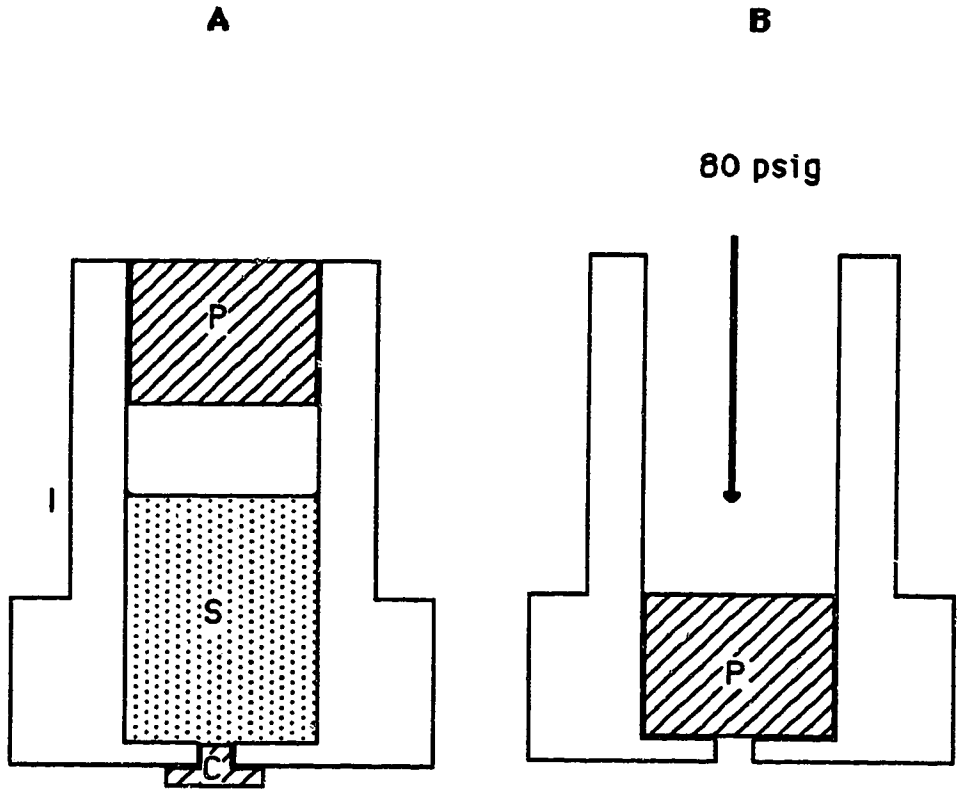

Figure 4.3. Diagram of the sample injection capsule. A; Configuration prior to injection. B; Configuration after injection. P; Teflon plunger S; sample solution, C; Teflon plug.

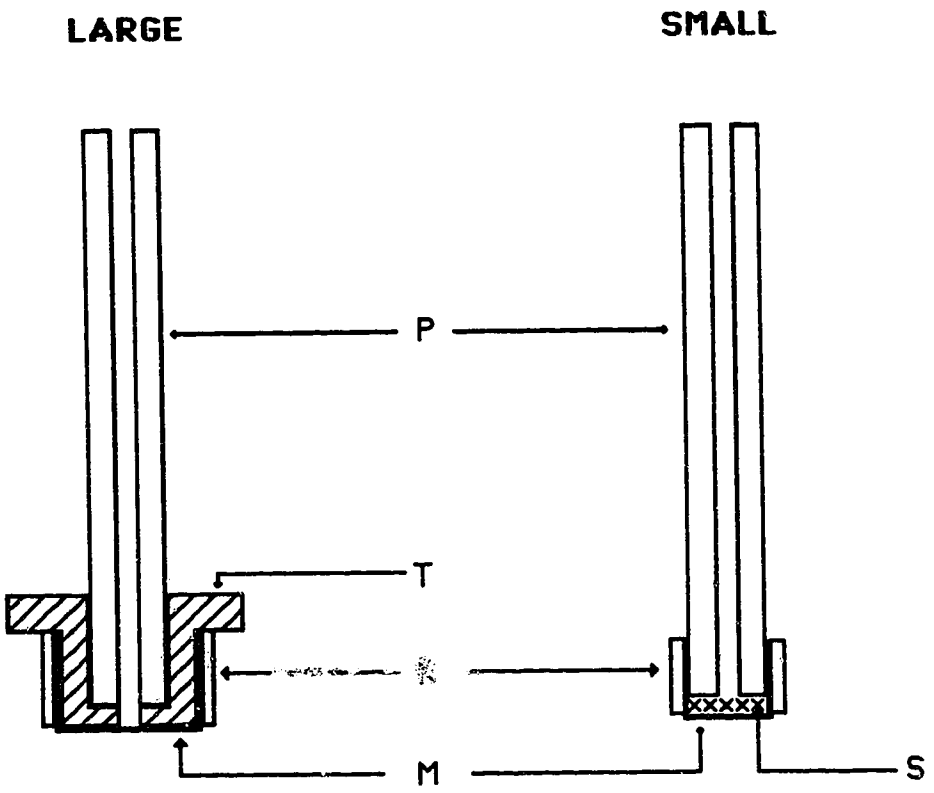

Figure 4.4. Diagram of the filter probe: P, stainless steel tube; T, Teflon adaptor; R, Teflon ring; M, porous Teflon membrane; S, coarse Teflon mesh.

4.2.6 EXTRACTION OF *o*-NITROANILINE FROM WATER

Initially, 100.0 mL of chloroform and 99.0 mL of phosphate buffer pH = 6.5 were placed in the extraction cell and 1.0 mL of 10^{-2} M *o* -nitroaniline in aqueous buffer was pipetted into the injection capsule and the whole extraction system assembled as shown in Figure 4.1. Stirring was initiated and the flow of chloroform phase through the detector was begun at a rate of 1.0 mL/min with the valve V2 switched to direct the flow to waste. Both the small and the large membrane phase separators were employed alternately in this experiment to study the effect of probe size on the extraction rate. The change in the absorbance of chloroform was monitored at 396 nm, and after a steady baseline was established the *o*-nitroaniline was injected to initiate the experiment. The absorbance vs time profile was acquired digitally with an IBM-XT microcomputer.

The experiment was repeated at stirring rates between 13.3 r/s (800 r/min) and 38.3 r/s (2300 r/min) in increments of 3.3 r/s. In addition, the whole series of experiments at the various stirring rates were repeated in a modified form in which 99.0 mL of chloroform and 100.0 mL of aqueous buffer were initially in the extraction cell and 1.0 mL of 1.0 x 10^{-2} M *o*-nitroaniline in chlorofom was the injected sample. The extraction profiles of these latter experiments were used to generate the IRF required for deconvolution of the data from the former experiments, in which o-nitroaniline was extracted from water. Between each run the extraction cell, connecting tubing and detector flow cell were cleaned with distilled water, methanol and finally with chloroform.

4.2.7 CONTRIBUTION OF INSTRUMENTAL COMPONENTS TO BAND BROADENING

A set of experiments was performed at a chloroform flow rate of 1.0 mL/min in order to determine the relative contributions to σ^2_I by the various instrument components. In all these studies it was the small membrane phase separator and a stirring rate of 38.3 r/s that were used.

That part of the instrument variance associated with the membrane and support, probe tube, connecting tubing, detector and computer, σ^2_1, was measured by initially shutting off the pump while stirring at 38.3 r/s. After allowing enough time for mixing to be complete the experiment was initiated by turning on the pump.

In the same manner the part of the instrument variance associated with the probe tubing, connecting tube, detector and computer, σ^2_2, was measured in the same way as σ^2_1 except that the only liquid in the extraction cell was a 1.0×10^{-4} M solution of *o*-nitroaniline in chloroform and also the porous membrane and support were removed from the end of the filter probe.

Finally, the instrument variance associated with the detector and computer, σ^2_3, was measured by placing a slider-type sample injection valve V_3 (part No. CSV-2, LDC) in the Teflon tubing line immediately before the detector. During this measurement the extraction cell served merely as a chloroform solvent reservoir with no aqueous phase or stirring involved. In three series of experiments the chloroform flow rate was 0.66, 1.0 and1.5 mL/min, respectively. In each series five different sliders were used in the injection valve to inject 1.0, 2.0, 5.0, 10.0, and 20.0 μL of a chloroform solution of *o*-nitroaniline. In Figure 4.5 is shown a schematic diagram of the instrument used to measure the detector variance, while in Figure 4.6 is shown the subdivision of the entire equipment into components and the designation of variances associated with the various parts.

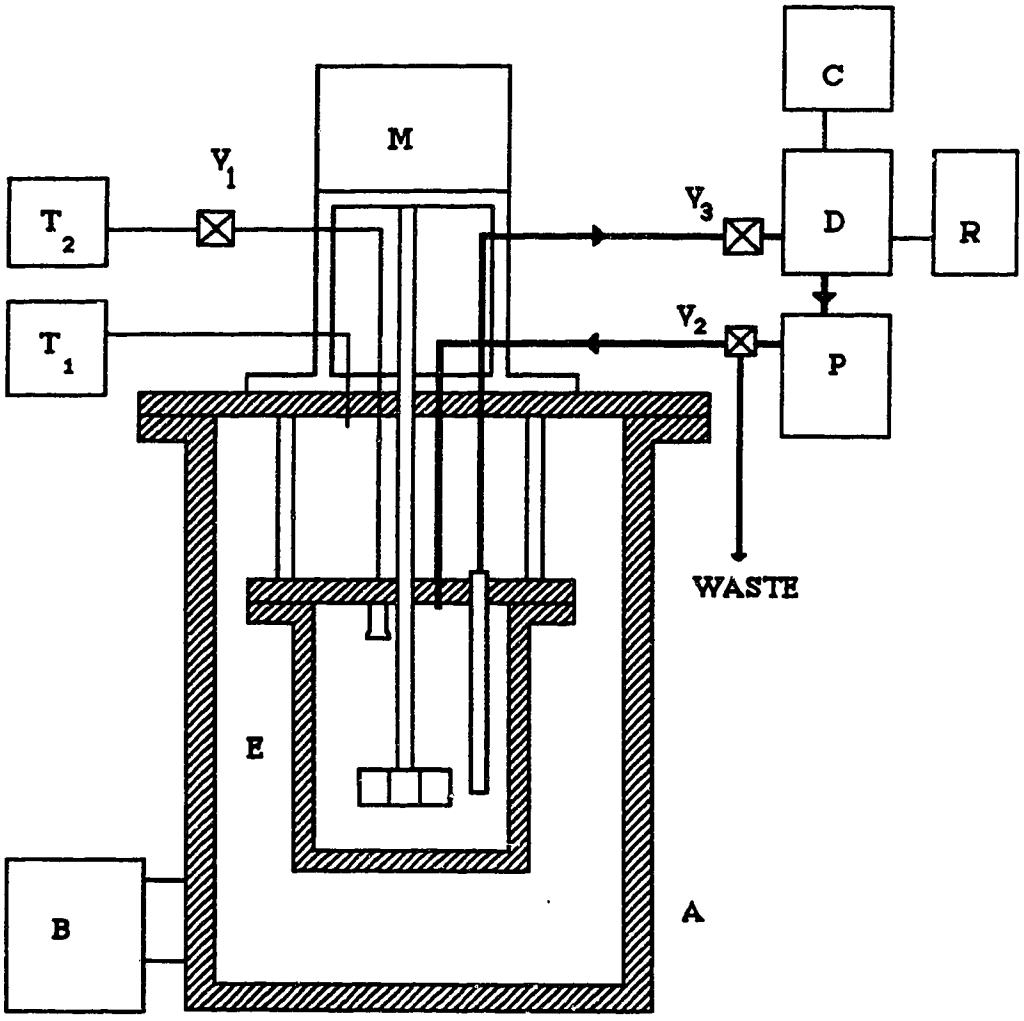

Figure 4.5. Diagram of the extraction apparatus used for measuring detector variance. V_3 is a slider type manual valve for injecting samples directly into the UV detector. The other components are as defined in Figure 4.1

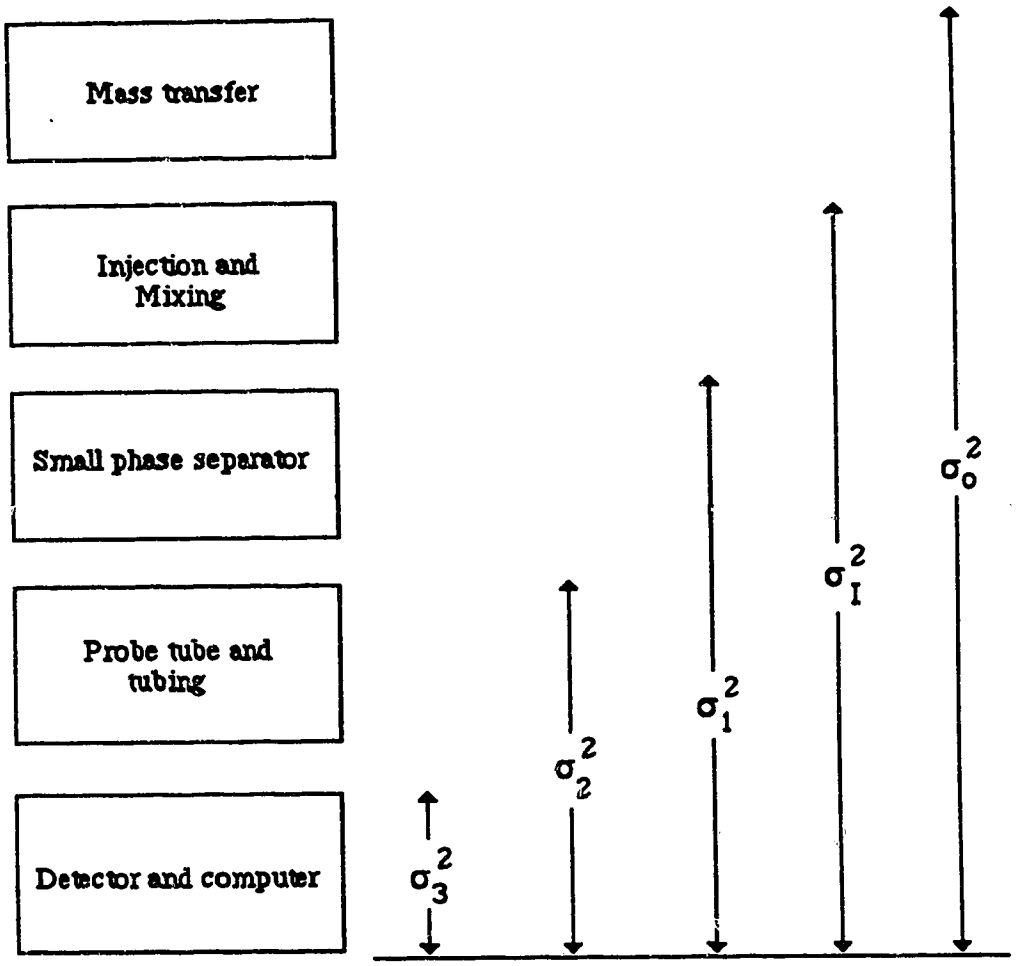

Figure 4.6. Schematic diagram showing the cumulative variance associated with various parts of the extraction apparatus. Mass transfer involves the extraction of *o*-nitroaniline from water into chloroform.

4.3 RESULTS AND DISCUSSION

The apparatus shown in Figure 4.1 was designed to acheive fast mass transfer rates with minimum band broadening arising from its components. The design incorporates a remote sample injection device and a porous membrane phase separator. The duration of injection (i.e. plunger travel time) is of the order of 0.1 s. The internal diameter of the filter probe tube and the connecting tubing were small and an 8 μL flow cell was used for the same reason. The combined volume of the small membrane phase separator, filter probe tube and connecting tubing is 0.066 mL, while that for the larger area probe is 0.076 mL. The photometric detector time constant was 1.0 s and the microcomputer, which was used to acquire all data, had a negligibly small time constant (~ $3x10^{-5}$ s).

The inside of the aluminum cylinder is pressurized at 20 psig with nitrogen from tank T1. The purpose of this pressurized outer vessel is to create a constant pressure pumping device which causes chloroform to flow out of the extraction cell through the membrane phase separator. This avoids placing a pump between the extraction cell and the detector, thereby reducing instrument band broadening. Attempts to produce low dead volume pumping by sealing the bearings in the lid of the extraction cell itself and pressurizing it failed because the liquid in the cell which splashed on the bearings was forced out around the stirrer shaft. Also, attempts to eliminate pressurization entirely and to use the peristaltic pump downstream of the detector to pump the chloroform phase failed because, with flow through the small bore tubing employed to reduced dead volume, the pressure drop in the chloroform was large and caused the formation of gas bubbles in the detector cell as a result of outgassing of air disssolved in the chloroform. The flow rate of the liquid being pumped varies linearly with the nitrogen pressure in the aluminium cylinder as shown in Figures 4.7 and 4.8. The non zero intercept in these plots is due to the fact that the extraction cell was placed slightly higher than the detector and therefore there is flow caused by siphoning. The agitation of the fluid in the extraction cell also causes an induced fluid pressure on the membrane surface and therefore siphoning of liquid occurs. During an

experiment the pumping speed of the peristaltic pump was adjusted so as to give a slower flow rate than would be produced by the 20 psig nitrogen pressure in the extraction cell. This was to provide a slight back-pressure on the flowing organic solvent to prevent gas bubble formation in the detector flow cell.

The overall characteristics of the apparatus were studied using *o* -nitroaniline as a sample component. It has a basicity constant of 12.2 [141] and a distribution coefficient of 135 between chloroform and water [[142]. In sodium phosphate buffer pH = 6.5, it exists essentially as the free base. Thus in a mixture of chloroform and buffer it is quantitatively extracted into the chloroform phase.

4.3.1 FLUID HYDRODYNAMICS IN THE EXTRACTION CELL

The extraction cell consists of a cylindrical stainless steel vessel 7 cm deep and 7 cm in diameter equipped with 4 vertical baffles mounted against the vessel wall and at right angles to it. The impeller was a one piece paddle consisting of four flat rectangular blades 1.7 cm wide and 3 cm tip-tip diameter. The impeller was mounted centrally about 0.5 cm from the bottom of the extraction vessel. This possition of the impeller provides maximum stream velocity [143] at the bottom of the vessel where maximum lifting velocity is required. Furthermore, the discharge is radial, sweeping the vessel bottom, but changes to a vertical flow at the vessel walls. There is also rotary motion of fluid between the impeller and the vessel wall which ensures complete mixing of the two phases even when they have different densities. Presented in Figure 4.9 is the flow parttern observed when a glass, instead of stainless steel, extraction cell was used.

The flow regime in highly agitated mixing vessels is defined in terms of the impeller Reynolds number (R_e) [56, 144,]. This number can be viewed as the ratio of inertial force to the viscous force on the fluid. A low value ($R_e \leq 10$) means that the viscous forces dominate and the flow is well ordered. Under this condition the flow is said to be laminar. On the other hand large values ($R_e \geq 10{,}000$) means that inertial forces dominate,

overcoming the viscous drag and leading to turbulence. The region where $10 \leq R_e \leq 10{,}000$ is refered to as the transition region [56]. Flow pattern within this region is position dependent. The flow is turbulent near the impeller while it is considered to be laminar at remote parts of the mixing vessel. The correlation for Reynolds number for impeller induced agaitation is given as [56];

$$R_e = \frac{L^2 N \rho'}{\mu'} \qquad (4.1)$$

where L is the diameter of the impeller, N is the rotation speed of the impeller (units rps), μ' is the effective mean viscosity of the dispersion defined by the expression;

$$\mu' = \frac{\mu_c}{\phi_c}\left[1 + \frac{1.5\phi_d \mu_d}{\mu_c + \mu_d}\right] \qquad (4.2)$$

and the average density of a dispersion ρ' is defined as;

$$\rho' = \phi_c \rho_c + \phi_d \rho_d \qquad (4.3)$$

Here ϕ is the phase fraction and subscripts c and d refer to continuous and dispersed phases.

Using average values of density ($\rho' = 1.24\ gcm^{-3}$) and viscosity ($\mu' = 0.017$ Poise) for a 1:1 chloroform:water mixture the impeller Reynolds number R_e is 2.5×10^4 at the optimum stirring rate of $38.3\ rs^{-1}$. At such a high R_e, the chloroform-water mixture can be considered hydrodynamically as a "homogeneous isotropic turbulent" dispersion [64]. Drop break-up and coalescence both occur frequently and the steady state drop diameter of the dispersed phase is controlled by drop break-up.

In all of the extraction processes studied in this work, the aqueous phase was the dispersed (droplet) phase and chloroform was the continuous phase. This was shown in two ways. The first was by direct visual observation of the manner in which the dispersion settles after agitation is stopped [145]. A settling dispersion has the appearance of a three-phase system consisting of relatively clear bulk solutions above and below the band of uncoalesced emulsion. At one of the interfaces the rate of travel towards the eventual interface takes place due to settling alone, hence no coalescnce is observed. At the other interface the droplets grow rapidly in size by coalescing with one another and with the adjacent clear bulk phase. This clear bulk phase is the dispersed phase. A diagram of a settling emulsion is shown schematically in Figure 4.10.

The other test performed to distinguish between dispersed and continuous phases involved withdrawing a small volume of the rapidly stirred emulsion and squirting it into either chloroform or water [146]. In chloroform, droplets of aqueous phase persisted, while in water coalescence was rapid and no droplet persisted, indicating that the aqueous phase was the dispersed phase. The fact that both of these tests indicate that the aqueous phase was the dispersed phase agrees with the finding that within the limits in which either phase can be dispersed, the phase in which the impeller is immersed when at rest will normally be the continuous phase [147].

Using the drop size correlation in Equation 2.16 , where $f_\phi = (1 + 3.75\phi)$ for the 4-blade paddle and with $\gamma = 32.8$ cms^{-2}, $\rho_C = 1.48$ gcm^{-3} , L = 3.0 cm, and $\phi = 0.5$, the predicted average drop size d_p is 0.011 cm. Using the alternative correlation for d_p (i.e. Equation 2.17), the predicted average drop size is 0.015. As both correlations give a similar value for d_p the value obtained by Equation 2.16 was chosen arbitarily to be used for estimation of the total liquid-liquid interfacial area. From Equation 2.15 the total liquid-liquid interfacial area created is 5.4×10^4 cm^2.

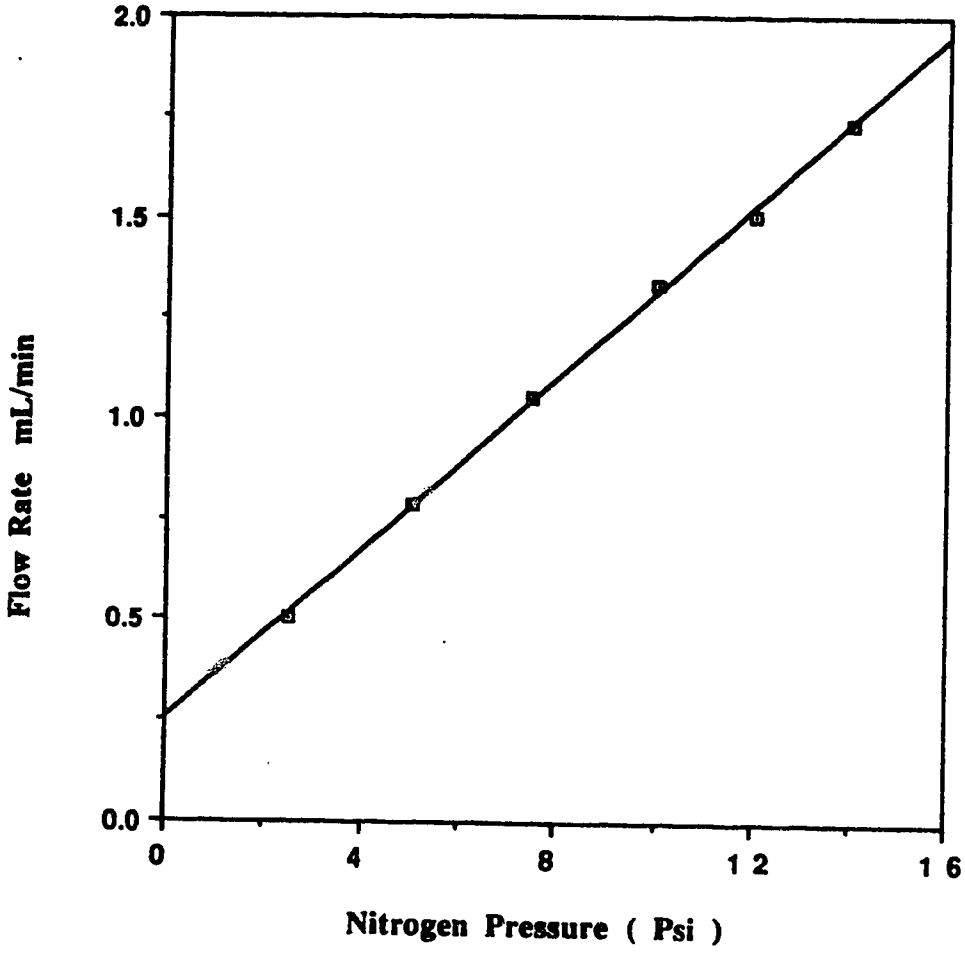

Figure 4.7 Plot of chloroform flow rate vs nitrogen pressure in the extraction cell when the cell contains only chloroform. Measurement was made while stirring the chloroform phase at 16.6 r/s.

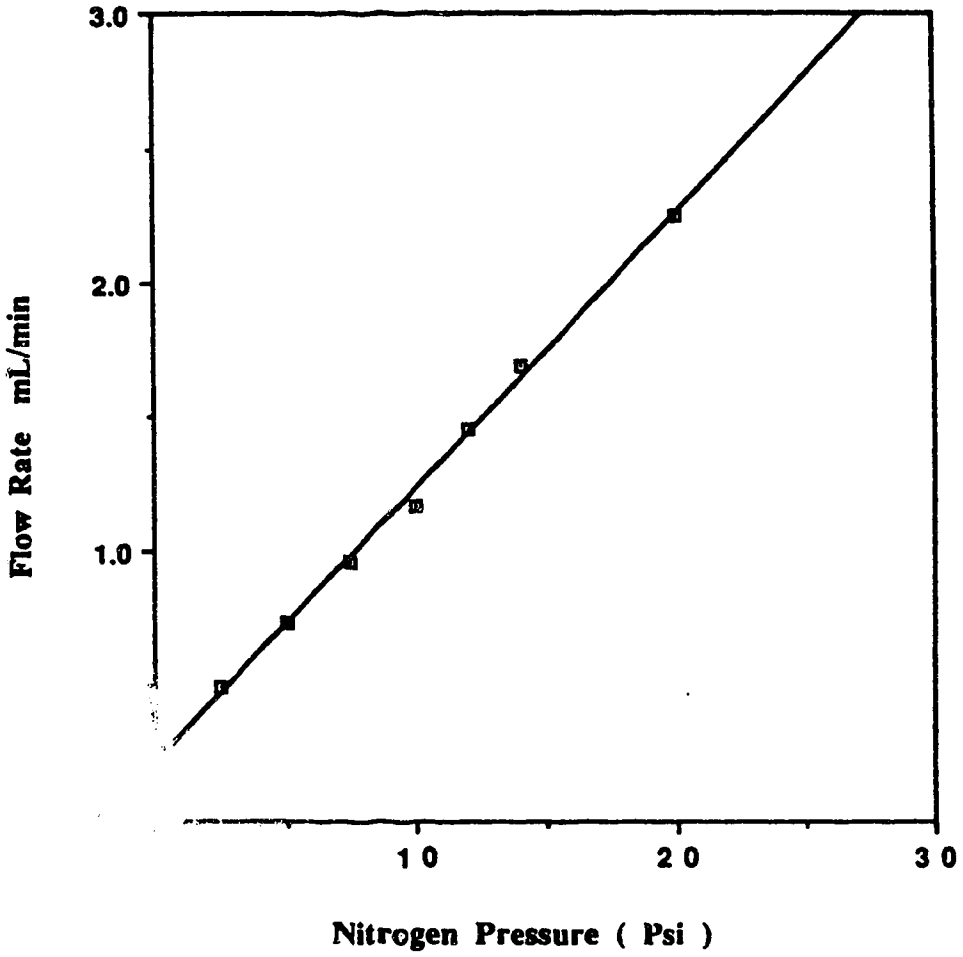

4.8 Plot of chloroform flow rate vs nitrogen pressure in the extraction cell when the cell contains a stirring mixture of equal volumes of chloroform and aqueous buffer. Measurement was made while stirring the mixture at 16.6 r/s.

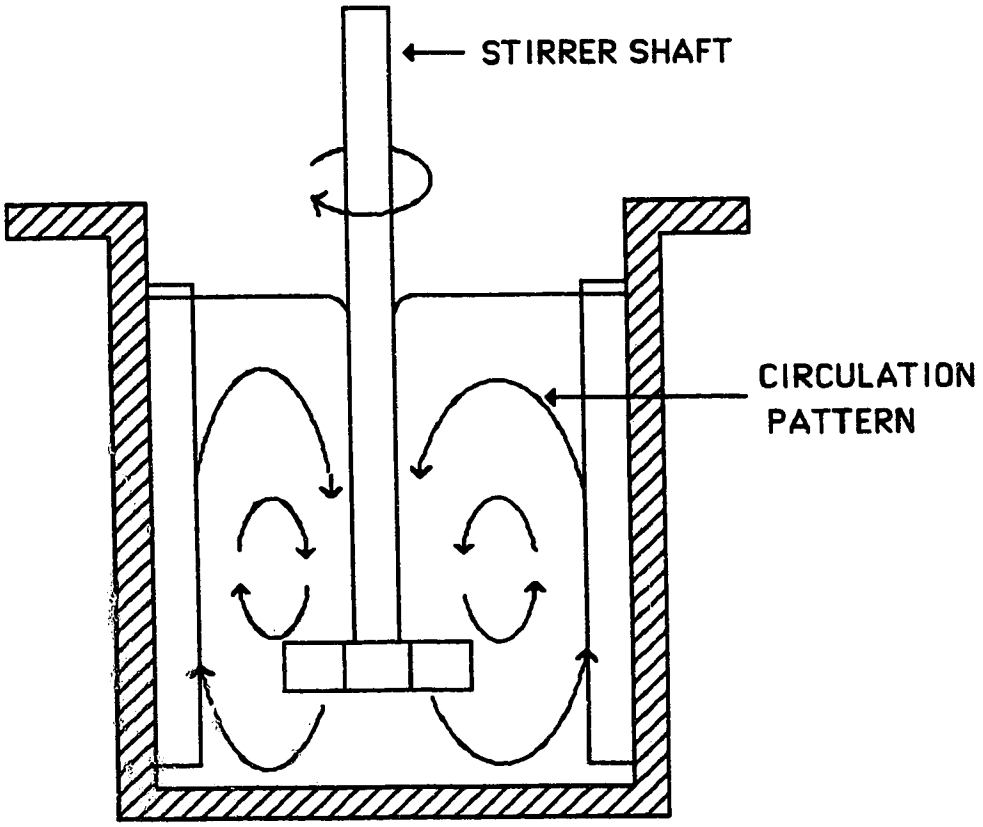

Figure 4.9. Diagram of the flow profile in the extraction cell during rapid stirring. This parttern was observed while stirring 200.0 mL of chloroform at 38.3 r/s in a glass extraction cell.

Figure 4.10 has been removed due to the unavailability of copyright permission.

Figure 4.10. Diagram of a settling emulsion [145]. O/W means oil droplets dispersed in a continuous water phase, and W/O means water droplets dispersed in a continuous oil phase.

4.3.2 THE FILTER PROBE

Micorporous membranes are extensively used as inductors for coalescence and phase separation for liquid-liquid dispersions [63, 146]. In order for a membrane to perform these functions it has to be made of a material that is wetted by only one of the liquid phases constituting the dispersion. It also has to be porous to allow passage of liquid through its pores. Owing to the wetting properties of the membrane when it is placed in a liquid-liquid dispersion the pores are instantly filled with the liquid that wets it to form a wetting-layer on the surface of the membrane. As a consequence contact between the membrane surface and the non-wetting phase is completely prevented. Therefore when a suction action (pump or presure drop) is applied only the wetting phase flows through the membrane. The ability of a microporous membrane to separate one liquid phase from a dispersion of two liquids does not depend on which phase was dispersed. The liquid that wets the membrane is the phase that is separated, so that the choice of which liquid is separated depends on the choice of membrane material. The material commonly used as membranes for separating nonpolar (organic liquid) from an aqueous liquid is fibrous Teflon [63, 148], while paper membrane is commonly used for separating an aqueous liquid. The efficiency of the membrane when used as a phase separator depends not only on the physical properties of the membrane but also on the experimental parameters such as the rotational speed of the impeller and the flow rate of the separated phase through the membrane.

When placed in an impeller-induced dispersion the surface of the membrane experiences a high degree of collision with droplets of the wetting phase. The colliding droplets coalesce with the wetting-layer of liquid on the surface of the membrane. At the same time the shear force created by the tangential flow of the bulk dispersion across the surface of the membrane sweeps the adhered wetting-layer liquid along in the direction of flow until, at the down-stream edge of the membrane surface, it is detached and again

redispersed into droplets. At equilibrium the rates of droplet collision with the adhered boundary-layer and the redispersion of the adhered liquid become equal so that there is always a pool of the wetting liquid adhered to the surface and within the pores of the membrane. The net volume of the adhered wetting-layer that is present at the membrane surface under this condition depends on the degree of stirring (which is proportional to the rotational speed of the impeller), and the length of the membrane along the direction of flow [146].

Assuming that the volume of the adhered wetting-layer liquid is proportional to the thickness of the hydrodynamic boundary-layer, then Equations 4.4 and 4.5 give rough estimates of the volume of the wetting-layer liquid pool when the flow is laminar or turbulent respectively [135].

$$\frac{\delta}{L} = 5\sqrt{\frac{\upsilon}{v\,L}} = \frac{5}{\sqrt{R_{e,L}}} \qquad (4.4)$$

$$\frac{\delta}{L} = 0.37\left(\frac{v\,L}{\upsilon}\right)^{-1/5} = 0.37\left(R_{e,L}\right)^{-1/5} \qquad (4.5)$$

where δ denotes the thickness of the boundary-layer, L the length of the membrane along the direction of flow, v is the flow velocity, υ the kinematic viscosity, and $R_{e,L}$ is the length-Reynolds number. Both equations indicate that δ increases with L but decreases with $R_{e,L}$. Thus, the volume of the wetting-layer increases with increasing diameter of the membrane but decreases at higher stirring rates.

Another experimental parameter that affects the ability of the membrane to separate only the wetting liquid is the rate at which the separated liquid is drawn through the pores of the membrane. If the liquid is drawn at a rate that is larger than the rate of replenishment of the wetting-layer by droplet coalescence, breakthrough of the non-wetting liquid through

the membrane will occur. Escape (degassing) of desolved gases from the liquid also occurs when too large a pressure drop is applied to induce pumping of liquid through the membrane.

An interesting aspect of membrane-induced phase separation is that the liquid passing through the pores comes only from the bulk of the wetting-layer. In consequence, any interfacially adsorbed solute is quantitatively stripped during the separation. A detailed explanation of the mechanism of exclusion of interfacially adsorbed solute during membrane induced phase separation has been given by Persaud et. al. [146]. The stripped solute remains at the interface of the wetting-layer and is swept off the membrane at its downstream end.

4.3.3 CONTRIBUTION OF INSTRUMENTAL COMPONENTS TO BAND BROADENING

The overall variance, σ^2_O, is calculated from the extraction profile obtained when the injection is made under conditions where solute extracts from one phase to the other such as happens when aqueous *o*-nitroaniline is injected. The instrument variance, σ^2_I, on the other hand, can be obtained by injecting a chloroform solution of the solute. In the present work all extraction A vs T profiles exhibited a distorted sigmoidal shape (see Figure 4.11). The contributions of the various instrument components described above to the observed instrument variance were measured using various modifications of the main apparatus shown in Figure 4.1.

Variance due to injection and mixing: Although sample injection is accomplished in about 0.1 s there is a finite time for the injected sample to mix completely with the bulk of the phase from which extraction occurs. The combined injection and mixing times contribute to the spreading of the observed extraction profile. The variance associated with injection and mixing is the difference between σ^2_I and σ^2_1 as shown in Figure 4.6 . The injection and mixing variance is calculated to be $0.36 \pm 0.09\ s^2$, which constitutes about 10 % of the overall variance for an extraction involving mass transfer.

Variance due to the small membrane phase separator: The microporous membrane also contributes significantly to the broadening of the sample band as it passes through the pores of the membrane. The spreading is due to the fibrous nature of the membrane. The pores within the membrane are not uniform in size and flow through them experiences different degrees of obstruction. Fluid flow pattern within the membrane therefore exhibits variations in local flow velocity resulting in a non-uniform flow and consequently a sample band will unavoidably experience some band broadening. The extent of broadening will depend on the porosity and the thickness of the membrane. The combined variance associated with the small membrane phase separator and support used in this work was measured as the difference between σ^2_1 and σ^2_2 and found to be 0.41 ± 0.26 s^2, which constitutes about 12 % of the overall extraction variance.

Variance due to probe tube and connecting Teflon tubing: The 12 cm long, 0.5 mm i.d. stainless steel probe tube and the 54 cm long, 0.3 mm i.d. Teflon tube connecting the membrame to the detector also contribute significantly to the overall instrumental variance. As the sample band flows through these tubes it experiences band broadening resulting from the non-uniformity of the flow pattern. The extent of band broadening in tubes resulting from non-uniform flow profile through tubes has been extensively studied and characterized by the Golay equation [126].

$$\sigma^2_{tube} = \frac{\pi r^4 L}{24 D F} \qquad (4.6)$$

where r is the radius of the tube, L is the tube length, D is the diffusion coefficient of solute and F is the volumetric flow rate. Unfortunately Equation 4.6 applies only for laminar flow through long, straight tubes and therefore it cannot be applied to our system since the the tubes are too short and also they incorporate numerous joints. The variance associated with the probe tube and connecting tubing was therefore estimated

experimentally as the difference between σ^2_2 and σ^2_3 and found to be $1.02 \pm 0.24\ s^2$ which corresponds to about 29 % of the overall extraction variance. For the estimation of σ^2_3 see below.

Variance due to detector and computer: The variance associated with the detector and computer, is given by the following expression;

$$\sigma^2_3 = V_3^2 + V_D^2 + (\tau F)^2 \qquad (4.7)$$

where V_3 is the volume of the injection valve, V_D is the volume of the detector flow cell, τ is the detector electronic time constant (the computer has a negligible time constant), and F is the flow rate of the chloroform phase through the flow cell. The derivation of Equation 4.7 is based on the assumption that both the injection valve and the detector flow cell act as perfect "mixing chamber" [126].

The detector used in this work has three adjustable electronic time constants of 0.5, 1.0 and 2.0 s corresponding to the classifications Fast, Normal and Slow respectively. Shown in Table 4.3 are the results of the detector variance measured at the Fast and Normal time constant settings of the detector, along with the measured instrument variances, σ^2_I, and the relative contribution of the detector and computer variance, σ^2_3, to the overall instrument variance, obtained when a chloroform solution of the sample was injected. It is evident that the detector time constant has a significant effect on the measured detector variance. However, the measured overall instrument variances, σ^2_I, are statistically similar to one another in magnitude when measured at the Fast and Normal settings. This similarity is also reflected in the values of the relative contributions of σ^2_3 to σ^2_2. In consequence a time constant of 1.0 s (the "Normal" setting) was used in all measurements.

The experimental value for the detector and computer variance was determined by injecting smaller and smaller volumes of sample directly into the detector via a 5 cm long, 0.3 mm i.d. Teflon tubing with a slider valve and measuring the variance of the resulting peaks. A plot of peak variance against sample injection volume is presented in Figure 4.12. The plots show two distinct regions. In the first region, peak variance is independent of sample volume, and extends until sample volumes of 2 μL. Beyond sample volumes of 2 μL peak variance increases with sample volume. The shapes of the plots can be explained as follows [149]. For sufficiently small sample volumes (i.e. ≤ 2 μL) laminar flow of the sample zone and the mixing chamber effects in the detector cell are large enough to affect the whole concentration profile over the entire sample zone, resulting in the peaks being more or less Gaussian like in shape so that the variances of the peaks remain more or less constant, independent of injection volume. With large samples (i.e. ≥ 2μL), however, laminar flow and mixing chamber effects affect only the leading and tailing edges of the sample zone but not the central portion. The sample concentration profile along the central portion of the sample zone exhibits a flat "peak" whose height is independent of sample volume and whose width (variance) is dependent on sample volume. The plots also indicate that the measured detector variance is dependent on flow rate, therefore the detector/computer variance was also measured as a function of flow rate of the chloroform carrier stream and a plot of the variance against flow rate was made according to the Equation 4.7.

The detector variance shows a linear dependence on flow rate for the flow rates investigated (0.66, 1.0 and 1.5 mL/min) as shown in Figure 4.13, which is a plot of σ^2_3 vs F^2. The intercept on the variance axis corresponds to the sum of the inherent variances due to the detector flow cell and the slider valve. At sample volumes less than 2 μL, V_3^2 is negligible compared to V_D^2 so that the intercept equals to V_D^2. The manufacturers specification of the detector flow cell used in this work indicates a cell volume of 8 μL. However, measurement indicates that the cell has a volume of 10.8 μL and hence its

inherent variance should be 116.6 μL^2,which agree satisfactorily with the average value of 107.2 μL^2 obtained from Equation 4.7 when 1 and 2 μL samples were injected.

The slope of the plots should correspond to the square of the detector electronic time constant. The plots for the 1 and 2 μL injection valves have slopes of 1.104 and 0.988 s^2 respectively. These values correspond to an average time constant of 1.02 s, which agrees well with the electronic time constant of the detector, 1.0 s. It is clear that the effect of sample becomes significant when sample volumes greater than 2 μL are used. For injector sample volumes ≥ 2 μL, the slopes of the plots are greater than the value of the detector electronic time constant. This is probably because the assumption of a perfect mixing chamber is no longer valid.

Shown in Table 4.1 are the variances for the various sections of the entire extraction apparatus, while the results obtained for the contributions of the individual components to the instrument variance σ^2_I are presented in Table 4.2, along with the variance associated with mass transfer. Also presented are the percentage contributions of each reported variance to the total ($\sigma^2_M + \sigma^2_I$). The percent relative error in these measeurments is less than 15%. For the extraction process studied $\sigma^2_R = 0$. It is evident that the probe tube, connecting tubing and the detector are the major contributors to σ^2_I. The variance associated with these components can be decreased either by decreasing their dimensions or by using a faster chloroform flow rate. The detector electronic time constant of 1 s corresponds to a variance of 1 s^2 which means that 0.45 s^2, or about 30% of σ^2_3, arises from convective/diffusive band broadening in the flow cell. It is also evident that mass transfer represents only about 9% of the total variance, while instrument band broadening is responsible for the remaining 91%. When the goal of using this system is to measure the rate of a fast chemical reaction, efforts need to be concentrated on decreasing instrument band broadening, rather than on speeding up mass transfer. The percent relative error in these measurements is less than 15%.

4.3.4 EFFECT OF FLOW RATE ON BAND BROADENING

The time-based variances σ^2_R and σ^2_M are independent of the flow rate at which the chloroform phase is pumped. Also, the contributions to instrument variance from injection, mixing and detector response time are independent of thechloroform flow rate. However, the components through which chloroform is pumped (i.e. porous membrane and support, probe tube connecting tubing and detector flow cell) all exhibit time-based variances that depend on flow rate. To a first approximation, these devices have volume-based variances (units of cm^6) that are either independent of flow rate or directly proportional to flow rate [49]. Time-based variances are related to volume-based variances by,

$$\sigma^2(\text{time}) = \frac{\sigma^2(\text{volume})}{F^2} \qquad (4.8)$$

Thus, to the extent that σ^2_I has significant contributions from the phase separator, tubing or detector flow cell, the use of higher flow rates will decrease σ^2_I. Unfortunately, an upper limit on flow rate is imposed by the onset of breakthrough of the aqueous phase in the porous membrane phase separator due to the reasons given under Section 4.3.2. Under the present experimental conditions water breakthrough occurs at flow rates of 1.5 mL/min for the small filter probe, and at 3.5 mL/min for the large filter probe. Because the small probe was used for most of the characterization work, a flow rate of 1 mL/min was chosen as the working flow rate.

4.3.5 EFFECT OF STIRRING SPEED

The extraction of *o* -nitroaniline from water into chloroform is not accompanied by a chemical reaction ($\sigma^2_R = 0$) when desolvation and resolvation processes are considered

to be intantaneous. Therefore σ^2_M can be calculated by subtracting the experimental value of σ^2_I from that of σ^2_o. Figure 4.14 is a plot of σ^2_M versus stirring rate (N). It can be seen that σ^2_M decreases exponentially with stirring rate to a value of $0.22 \pm 0.10\ s^2$ at a stirring rate of 38.3 r/s. Beyond stirring rates of 38.8 r/s it becomes difficult to measure σ^2_M accurately. The exponential retlationship between σ^2_M and stirring rate is confirmed by the linearity of the plot in Figure 4.15. During stirring droplets of one phase are dispersed in the second phase. The drop diameter of the dispersed phase is a decreasing function of the stirring rate [36, 118].

This proportionality between drop size and stirring rate holds only until a certain critical value of the stirring rate is reached. Beyond this critical point, because of the slip effect, the drop size remains relatively constant in spite of further increases in the stirring rate [36]. The magnitude of this critical value of stirring rate depends on the cell and stirrer geometries as well as on the physical properties of the two fluids. As the drop size is decreased the liquid-liquid interfacial area across which mass transfer occurs increases and as a result σ^2_M decreases. The decrease in σ^2_M can also result from the decreasing thickness of the Nernst diffusion layer. Hence the rate of mass transfer by molecular diffusion increases and as a result σ^2_M decreases. In consequence, the rate of extraction in stirred systems also exhibit a proportionality with stirring rate. The mass transfer variance, σ^2_M, which can be regarded as being inveresly proportional to the time required for mass transfer to occur, will also decrease with increasing stirring rate and reach a limiting value. Since one of the goals of this work is to detemine the optimum conditions for extractions, all subsequent extraction using this cell were performed at a stirring rate of 38.3 r/s.

Table 4.1. Variances Associated with Various Sections of the Extraction Apparatus.

Segments	Variances (s^2)
σ_o^2	3.56 ± 0.49
σ_I^2	3.24 ± 0.40
σ_1^2	2.88 ± 0.49
σ_2^2	2.47 ± 0.23
σ_3^2	1.45 ± 0.07

Table 4.2. Variances Associated with Instrument Components and Mass Transfer for the Extraction of o-nitroaniline from Water into Chloroform

Component or Process	σ^2 (s^2)	Percent of Overall
Injection and Mixing	0.36 ± 0.09	10
Membrane and Support	0.41 ± 0.26	12
Probe tube and Tubing	1.02 ± 0.24	29
Detector and Computer[a]	1.45 ± 0.07	40
Mass Transfer	0.31 ± 0.10	9
Overall	3.56 ± 0.49	100

a Computer contributes negligibly to the detector and computer variance.

Table 4.3. Effects of Detector Electronic Time Constant on the Detector and Computer Variance.

Time constant τ (s)	Peak Area	σ_3^2	σ_I^2	σ_3^2 / σ_I^2
1.0	3625 ± 39	2.69 ± 0.2	4.58 ± 0.16	56%
0.5	3673 ± 63	1.84 ± 0.17	4.16 ± 0.29	44%

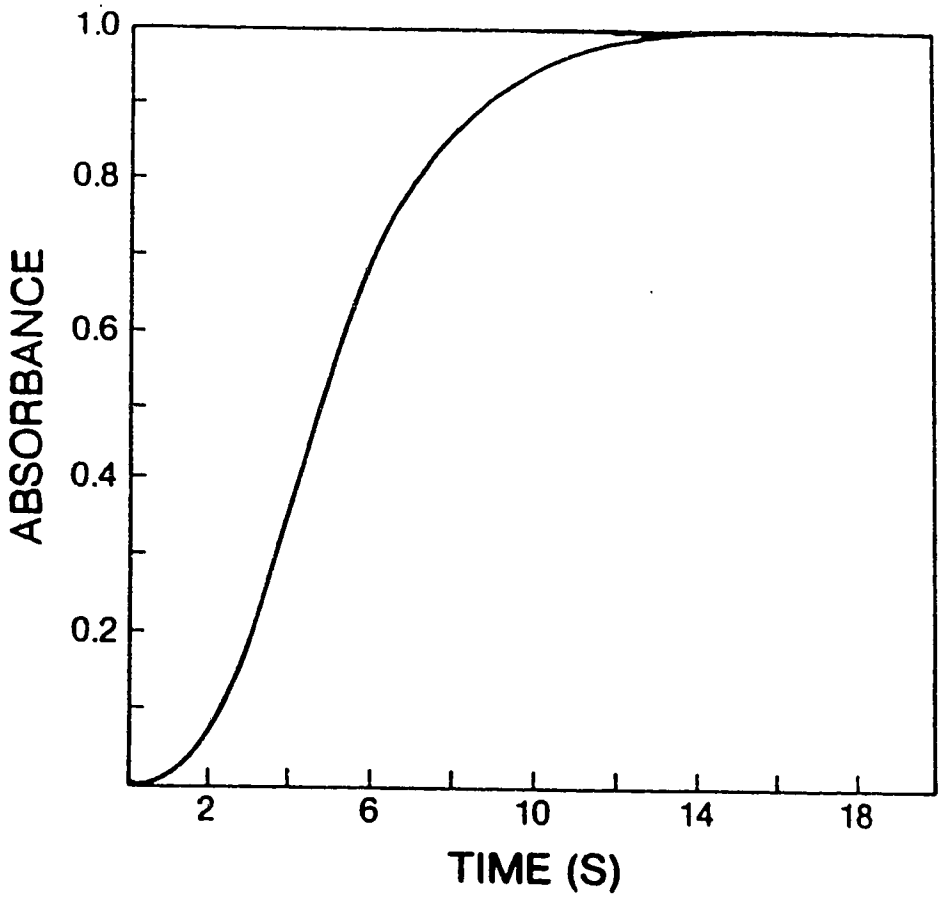

Figure 4.11 Chloroform absorbance vs time profile for the extraction of *o*-nitroaniline from aqueous buffer into chloroform. Flow rate of the chloroform phase was 1 mL/min.

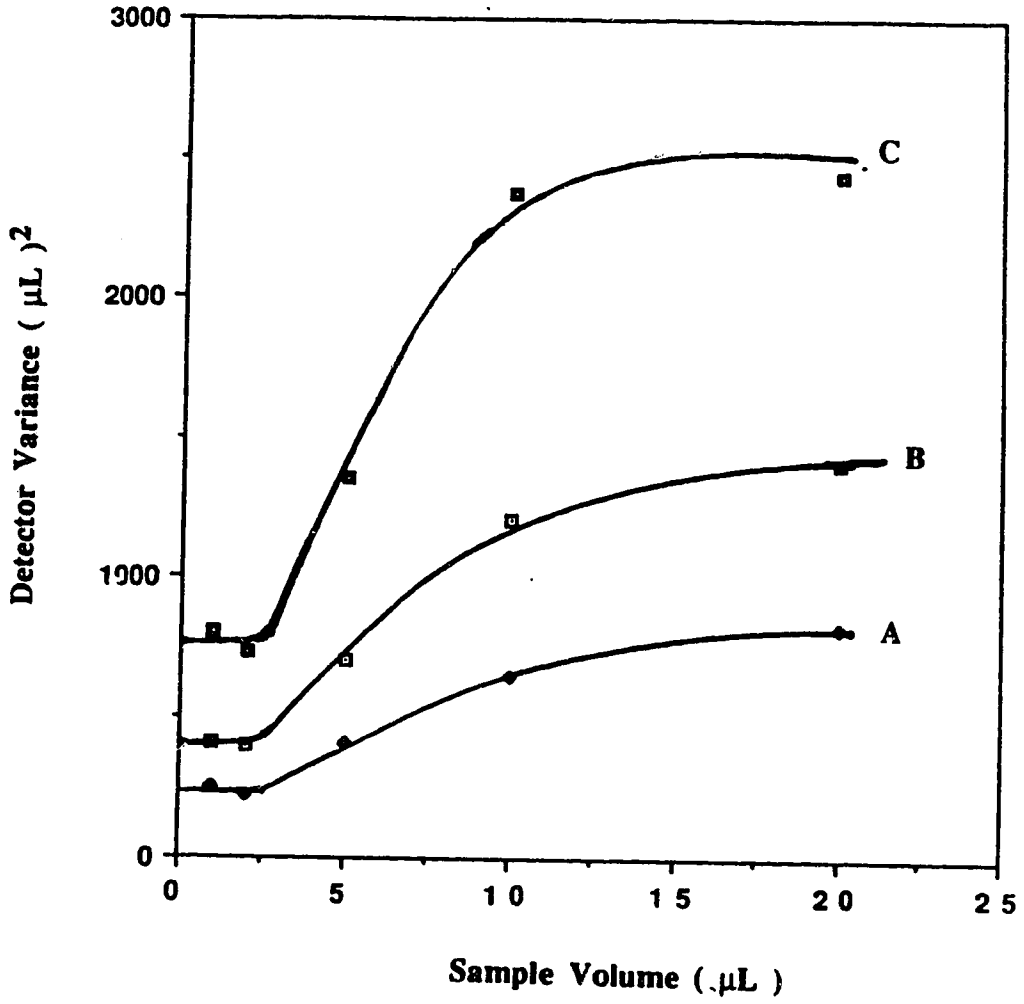

Figure 4.12 Plots of measured detector variance for the UV-50 spectrophotometer vs sample volume (capacity of valve V_3). Flow rate: A; 0.66 mL/min: B; 1.00 mL/min: C; 1.5 mL/min.

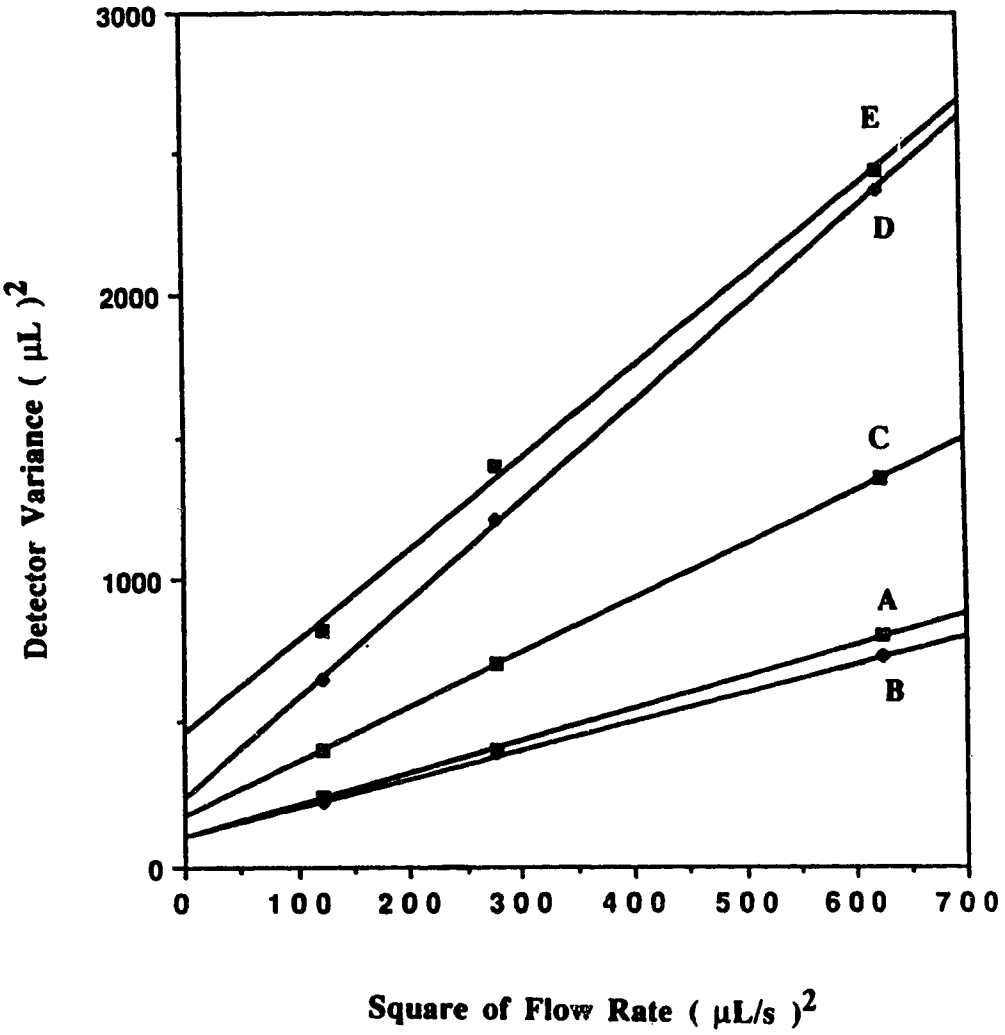

Figure 4.13 Plots of measured detector variance for the UV-50 spectrophotometer vs the square of flow rate. Sample volume (capacity of valve V_3): A, 1.0 μL: B; 2.0 μL: C; 5.0 μL: D; 10.0 μL: E; 20.0 μL. (see Equation 4.7).

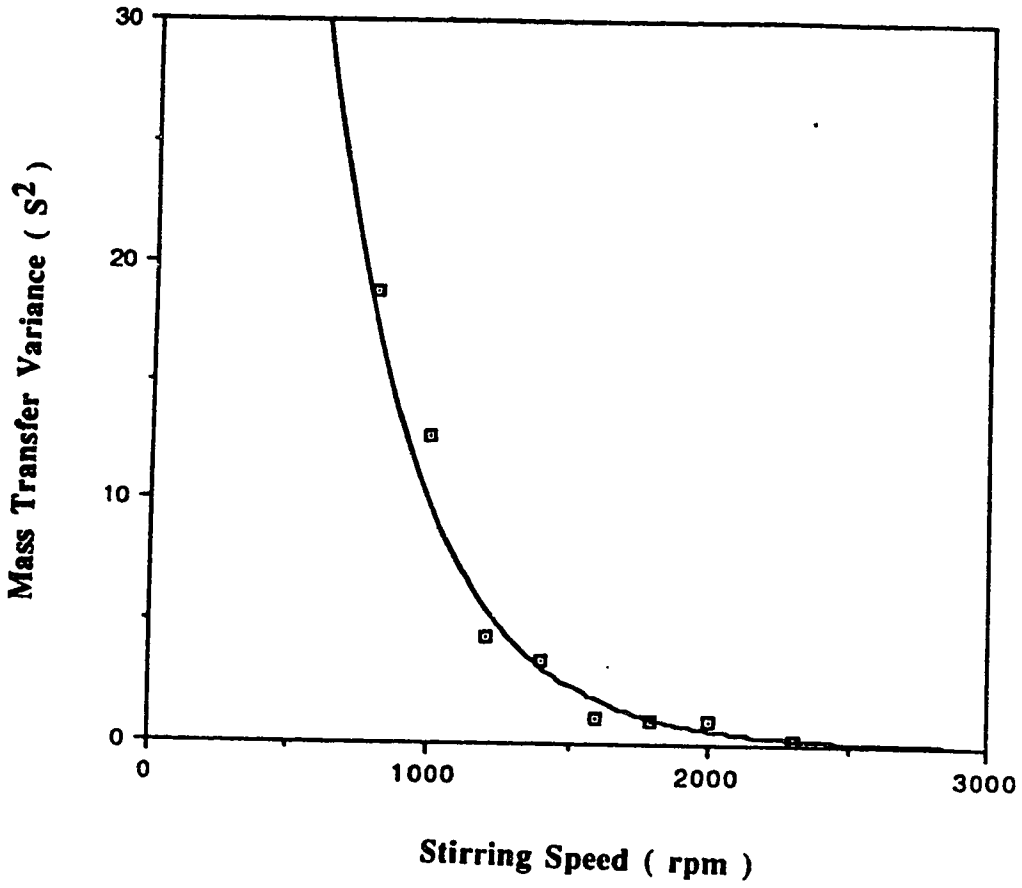

Figure 4.14 Plot of the variance associated with mass transfer vs stirring speed for the extraction of *o*-nitroaniline from aqueous buffer into chloroform. Flow rate of the chloroform phase through the UV-50 detector flow cell was 1 mL/min.

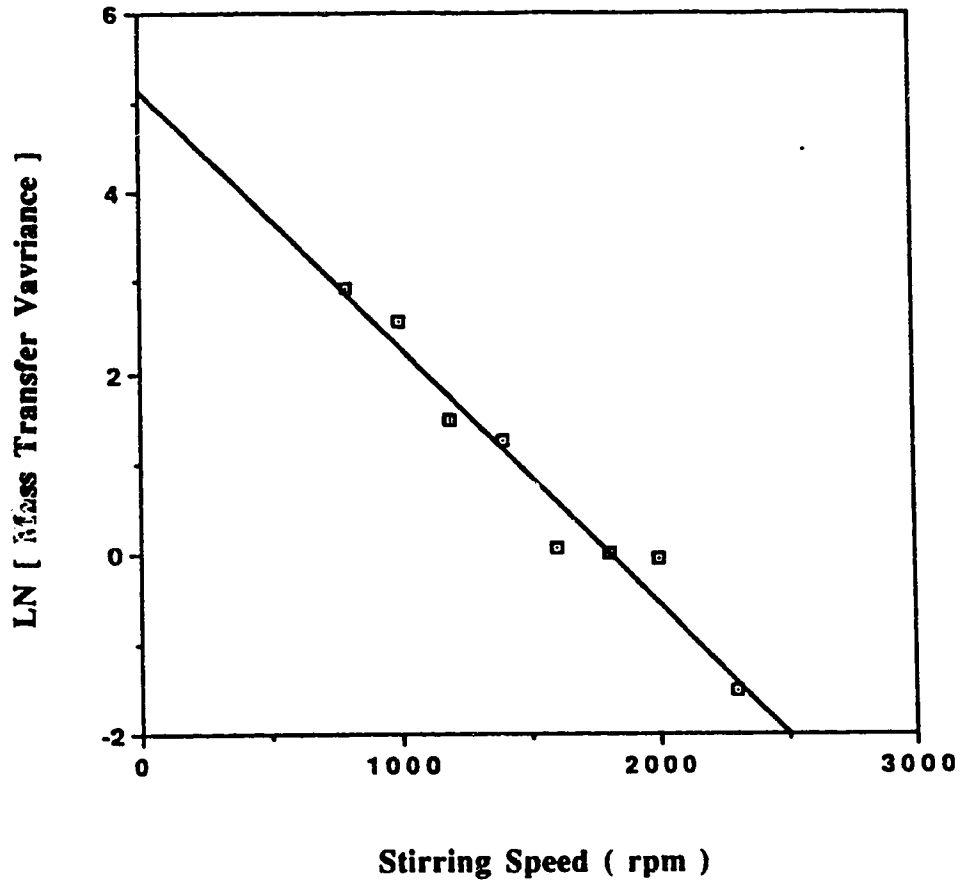

Figure 4.15 Plot of the natural log of the variance associated with mass transfer *vs* stirring speed for the data shown in Figure 4.14.

CHAPTER 5

MEASUREMENT OF MASS TRANSFER COEFFICIENTS UNDER TURBULENT CONDITIONS IN A RAPID-STIR APPARATUS

5.1 INTRODUCTION

The properties that a solvent extraction apparatus must have in order for it to be used successfully for studies of the kinetics of chemical reactions are: ability to produce a large and constant interfacial area, and to achieve high mass transfer coefficients for the transfer of solute from one phase to the other. Among the devices commonly used for mass transfer studies, the rotating diffusion cell, the segmented flow, the single drop and the rapid-stir systems are theoretically capable of acheiving mass transfer coefficients on the order of 1.0 x 10^{-3} to 5.0 x 10^{-2} cm/s [37, 49, 100]. As discussed in Chapter 4, experimentally measured solvent extraction kinetic data are distorted as a result of instrument band broadening. In consequence, unless corrections are made for band broadening, mass transfer coefficients obtained experimentally will be lower than those corresponding solely to mass transfer between the two liquid phases.

In this chapter, the mathematical deconvolution technique discussed in Chapter 3 will be used to eliminate the effects of instrument band broadening in order to gain access to the true mass transfer rate data. The systems that will be studied involve the extraction of *o*-nitroaniline from the dispersed aqueous phase into chloroform, and the extraction of *o*-nitrophenolate from the continuous chloroform phase into the dispersed phase. The processes involved in these extractions are purely mass-transfer controlled. The experimentally measured mass transfer coefficients will be compared with the values obtained from theoretical correlations.

5.2 EXPERIMENTAL

5.2.1 CHEMICALS AND SOLVENTS

o-nitroaniline, chloroform, methanol, distilled water and aqueous buffer were as discussed in Chapter 4.

o-nitrophenol was analytical grade (Aldrich Chemical Co. Inc.) and was used as received.

5.2.2 APPARATUS

The apparatus used for the studies in this chapter is the one already discussed in Chapter 4 and shown in Figure 4.1. The system was operated under optimum conditions with the following instrumental parameters: flow rate of 1.0 mL/min, stirring speed of 38.3 r/s, pumping pressure of 20 psig, and injection pressure of 80 psig. Mass transfer coefficient measurements were done for extractions using both the small and the large porous membrane phase separators.

5.2.3 EXTRACTION OF *o*-NITROANILINE FROM WATER

The experimental procedure used for this extraction has been described in Chapter 4. Each extraction profile consists of 512 data points acquired at 100 ms intervals.

5.2.4 EXTRACTION OF *o*-NITROPHENOL FROM CHLOROFORM

Initially, 100.0 mL of a 1.0×10^{-4} M solution of *o*-nitrophenol in chloroform and 99.0 mL of aqueous buffer pH = 6.5 were placed in the extraction cell. 1.0 mL of 4.0 M sodium hydroxide was charged into the injection capsule. The mixture was stirred and the chloroform phase was pumped with valve V_2 switched to direct the flow to waste. Absorbance of the chloroform phase was monitored at 354 nm, and after a steady baseline was established the sodium hydroxide was injected to initiate the extraction. An extraction

profile consists of 512 data points with 100 ms between ponits. In other runs the concentrations of the sodium hydroxide injected were changed to 0.4, 1.0, and 6.0 M.

In another set of experiments, the extraction cell contained 99.0 mL of chloform and 100.0 mL of aqueous buffer pH = 6.5 into which 1.0 mL of 1.0 x 10^{-2} M solution of *o*-nitorphenol in chloroform was injected to start the experiment. Data from this latter experiment were used to generate the IRF required for deconvolution. The effect of the size of the phase separator on the extraction rate was studied by using both the small and the large membrane phase separators.

5.3 RESULTS AND DISCUSSION

Although only typical extraction profiles are presented in the figures at least three replicate extractions were performed. As discussed in Chapter 3, the overall variance, σ_0^2, of an A vs t curve for an extraction in which a chemical reaction accompanies mass transfer is the sum of the contributions due to chemical reaction (σ_R^2), mass transfer (σ_M^2) and instrument band broadening (σ_I^2) as expressed by Equation 3.3. The shape of an experimental extraction profile is therefore influenced by the effects of all these band broadening processes. For a system in which broadening due to chemical reaction does not exist ($\sigma_R^2 = 0$), either because no reaction is involved or the rate of the reaction is so fast that it is assumed to occur instantaneously, σ_I^2 has been found to contribute about 91% to the overall variance σ_0^2 (see Table 4.2), while only 9% of the overall variance is due to the mass transfer process itself. The use of the observed, uncorrected extraction profile for the calculation of mass transfer coefficients will thus be greatly in error since the extraction profile is controlled to a large degree by processes other than mass transfer. It is important, prior to calculation of extraction rates, to correct the observed extraction profile. Correction of extraction profiles can be made by mathematical deconvolution to remove the undesired instrument band broadening.

5.3.1 EXTRACTION OF *o*-NITROANILINE FROM WATER INTO CHLOROFORM

The extraction of *o*-nitroaniline from aqueous buffer into chloroform involves no chemical reaction. The shape of the measured extraction profile is therefore influenced only by mass transfer and the instrumental band broadening processes discussed in Chapter 3. A representative extraction profile is shown by curve A in Figure 5.1. On the other hand, when a chloroform solution of *o*-nitroaniline is injected the solute remains quantitatively in the bulk of the chloroform phase and hence, no mass transfer process is involved. The A vs t extraction profile observed is therefore only distorted by instrumental band broadening and as a result it is less spread-out along the time axis than that observed when an aqueous solution is injected. This is shown by curve B in Figure 5.1. Deconvolution of the curve A with the IRF generated from curve B yields curve C in Figure 5.1, which is the correct A vs t extraction curve attributed solely to the mass transfer process. A plot of ln [$A_{O,\infty}$ /($A_{O,\infty}$ - A_O)] for the data in curve C is shown by curve A in Figure 5.2. The non-linear, non-steady state portion of the curve (lag time) covers the first 2.9 s, corresponding to the first 55% of the extraction. The linear, steady state portion includes the rest of the curve up to 5.4 s or 97% extraction. Above this point the corrected profile becomes too noisy as a result of deconvolving two profiles that differ only slightly from one another.

The lag time arises as follows [49, 70]. When an aqueous solution of a solute is injected (t = 0 s) the solute is present in the bulk aqueous phase but is absent in the bulk organic and in both the aqueous and organic Nernst films. In the early stages of mass transfer, solute is diffusing through the aqueous Nernst film toward the interface but no solute is diffusing away from the interface in the organic Nernst film. The rate of diffusion of the solute from the bulk aqueous phase to the interface is therefore different from the rate of diffusion away from the interface into the bulk of the organic phase. Hence, the overall mass transfer process can be described as a non-steady state process. During this early non-steady state, a plot of A vs t is concave upward [100]. After some time the rate of diffusion to the interface and away from the interface become equal and a steady state

equilibrium is achieved. The A vs t plot then exhibits the exponential concave downward shape typical of a first-order process. As a result, the integrated first-order plot will not be linear for data in the early stages of extraction. The slope of the linear portion of curve A in Figure 5.2 is the (first-order) mass transfer rate constant k_{mt}. Values of k_{mt} are reported in Table 5.1 for extractions performed using both the small and the large membrane phase separators. As it should be, k_{mt} is found to be independent of membrane size. There is about a 100% increase in the value of the rate constant when it is, correctly, calculated from the deconvolved curve than when it is, incorrectly, calculated from the undeconvolved observed extraction profile. Since the extraction is essentially quantitative at equilibrium the resistance to mass transfer is associated solely with the resistance in Nernst film in the dispersed aqueous phase. Using Equation 2.12 an experimental value of the mass transfer coefficient, β_{mt} , is found to be 1.81×10^{-3} cm s^{-1}, taking $A = 5.4 \times 10^{4}$ cm^2 and V_d = 100 mL. From this value of the mass transfer coefficient, the thickness of the Nernst diffusion film, δ_{aq}, on the aqueous side of the interface, as described by the Whitman two-film model [46] and defined by Equation 2.2, is estimated to be 0.0028 cm, assuming a nominal value of 5.0×10^{-6} $cm^2 s^{-1}$ for the diffusion coefficient.

In an attempt to correlate experimental data with theory, numerous empirical models for mass transfer have been proposed [59, 124, 150]. The assumptions of these models range from mass transfer from drops which act as rigid spheres, to those that exhibit surface circulation, to those that exhibit complete internal mixing. One of the most generally applied expressions relating the fraction extracted, E, with time t, during mass transfer in liquid-liquid dispersions is given by Equation 5.1 [150]:

$$E^2 = 1 - \exp\left(- \frac{4\pi^2 RDt}{d_p^2} \right) \qquad (5.1)$$

where D is the diffusion coefficient of the solute in the dispersed phase and R is a correlation factor which is the product of the phase ratio and a modified Reynolds number R_e'. The value of R depends on the degree of surface circulation and internal mixing experienced by drops during the extraction which, in turn, depend on the relative drop velocity, drop diameter and viscosity and density of the fluids in the vicinity of the interface. For rigid spheres the value of R is unity, while for drops experiencing a higher degree of surface circulation and internal mixing R >> 1. According to Equation 5.1, the observed first order rate constant for an extraction process is given by:

$$\beta_{mt} \frac{A}{V_d} = \frac{4\pi^2 RD}{d_p^2} \qquad (5.2)$$

Taking R = 1, d_p = 0.011 cm and D = 5.0 x 10^{-6} cm^2s^{-1}, the theoretical value of the mass transfer coefficient , β_{mt} = 2.9 x 10^{-3} cms^{-1}. Comparison of the experimental value of β_{mt} (1.8 x 10^{-3} cms^{-1}) with this theoretical value indicates agreement within experimental error. The similarity of the experimental value to the theoretical value when R = 1 suggests that the dispersed aqueous drops appear to behave like rigid spheres with little internal mixing and surface circulation. When there is the presence of surface active impurities, interfacial circulation can be significantly suppressed [36]. Although the reagents and solvents used in this work were of analytical grade, traces of surface active impurities could be present. It is generally found that very small drops moving through a continuous phase show little or no circulation [58].

5.3.2 EXTRACTION OF *o*-NITROPHENOL FROM CHLOROFORM INTO WATER

The pK_a of *o*-nitrophenol is 7.2 [151], and the distribution coefficient of the neutral species between chloroform and water is 350 [152]. Initially, in the mixture of chloroform and aqueous buffer at pH 6.5, *o*-nitrophenol is present quantitatively in the chloroform

phase as the neutral species. When NaOH is injected to initiate the extraction, the pH of the aqueous phase increases rapidly to pH > 11, so that at the final equilibrium *o*-nitrophenol is present essentially in the aqueous phase in the form of its anionic conjugate base. Mass transfer from the chloroform to the aqueous phase is accompanied by the chemical reaction of deprotonation. The deprotonation reaction is, however, very fast so that the shape of the A vs t extraction profile observed when aqueous NaOH is injected is governed only by mass transfer and instrument band broadening. This is verified experimentally, as discussed below. Because mass transfer is from the chloroform phase, the measured absorbance decreases with time as *o*-nitrophenol disappears from the chloroform phase. Thus, prior to deconvolution, the A vs t curve was inverted to produce curve A as shown in Figure 5.3, in order to avoid working with negative values. The appropriate IRF was obtained by inversion of the profile obtained when a chloroform solution of *o*-nitrophenol was injected into a mixture of chloroform and aqueous buffer. A plot of this profile is shown by curve B in Figure 5.3. The extraction profile due solely to mass transfer of *o*-nitrophenol from the chloroform continuous phase into aqueous drops is obtained by deconvolution. A typical deconvolved profile is shown by curve C in Figure 5.3.

A plot of $\ln [A_{0,\infty} / (A_{0,\infty} - A_0)]$ for the data in curve C is shown by B in Figure 5.2. In this extraction steady state is achieved after about 2.0 s, corresponding to 30% extraction. The linear, steady state portion includes the rest of the curve up to about 4.7 s, or 95% extraction. From the slope of the linear portion of the curve B in Figure 5.2 the observed (first order) rate constant k_{mt} for the mass transfer of *o* -nitrophenol from the chloroform continuous phase into aqueous drops was obtained. Again, as shown in Table 5.1, the values are independent of membrane size. Using the average value of $k_{mt} = 1.1 \pm 0.04\ s^{-1}$ and the estimated value of $A = 5.4 \times 10^4\ cm^2$ and $V_d = 100$ mL, an overall experimental value of the mass transfer coefficient $\beta_{mt} = 2.1 \times 10^{-3}\ cms^{-1}$ is obtained. After deprotonation at the liquid-liquid interface, partitioning of *o*-nitrophenolate into the aqueous phase is strongly favoured. Therefore, the overall mass transfer coefficient for the

transfer from chloroform into the aqueous phase is dominated by the mass transfer coefficient in the continuous chloroform phase.

In order to prove that the rate is governed by mass transfer of *o*-nitrophenol in the continuous chloroform phase rather than by mass transfer of NaOH in the dispersed aqueous phase, the experiment was repeated with different concentrations of NaOH. The idea is that NaOH immediately adjacent to the interface is neutralized by the entering *o*-nitrophenol, and if the transfer of more NaOH toward the interface were rate limiting, then k_{mt} would increase with increasing concentration of NaOH in the aqueous phase. Comparison of the third, fourth, sixth, and seventh entries in Table 5.1 show that k_{mt} is independent of NaOH concentration and the mass transfer is, indeed, controlled by the resistance to mass transfer in the Nernst film in the chloroform phase.

Using the value of $\beta_{mt} = 2.1 \times 10^{-3}$ cm s^{-1}, the thickness of the Nernst diffusion film on the chloroform side of the interface, δ_{org}, is estimated to be 0.0024 cm. This value is similar to the thickness of the Nernst film on the aqueous side of the interface, which was calculated above to be 0.0028 cm. This suggests that, although the two liquid phases have different physiochemical properties, the thickness of the Nernst film is controlled mainly by the degree of stirring in the extraction cell. Theoretical estimation of the continuous phase mass transfer coefficient by Equation 2.24 using the relevant experimental parameters gives a value of 10.8×10^{-3} cms^{-1}.

Table 5.1 Mass Transfer Rate Constants for Extraction of *o*-Nitroaniline from Water into Chloroform and for Extraction of *o*-Nitrophenol from Chloroform into Water

Solute	[NaOH] injected, M	extraction	Phase separator	k_{mt}, s^{-1}
o-nitroaniline		aq → org	small	0.99 ± 0.07
o-nitroaniline		aq → org	large	0.95 ± 0.02
o-nitrophenol	0.4	org → aq	small	1.12 ± 0.04
o-nitrophenol	1.0	org → aq	large	1.05 ± 0.08
o-nitrophenol	4.0	org → aq	small	1.25 ± 0.11
o-nitrophenol	4.0	org → aq	large	1.11 ± 0.09
o-nitrophenol	6.0	org → aq	large	1.12 ± 0.00

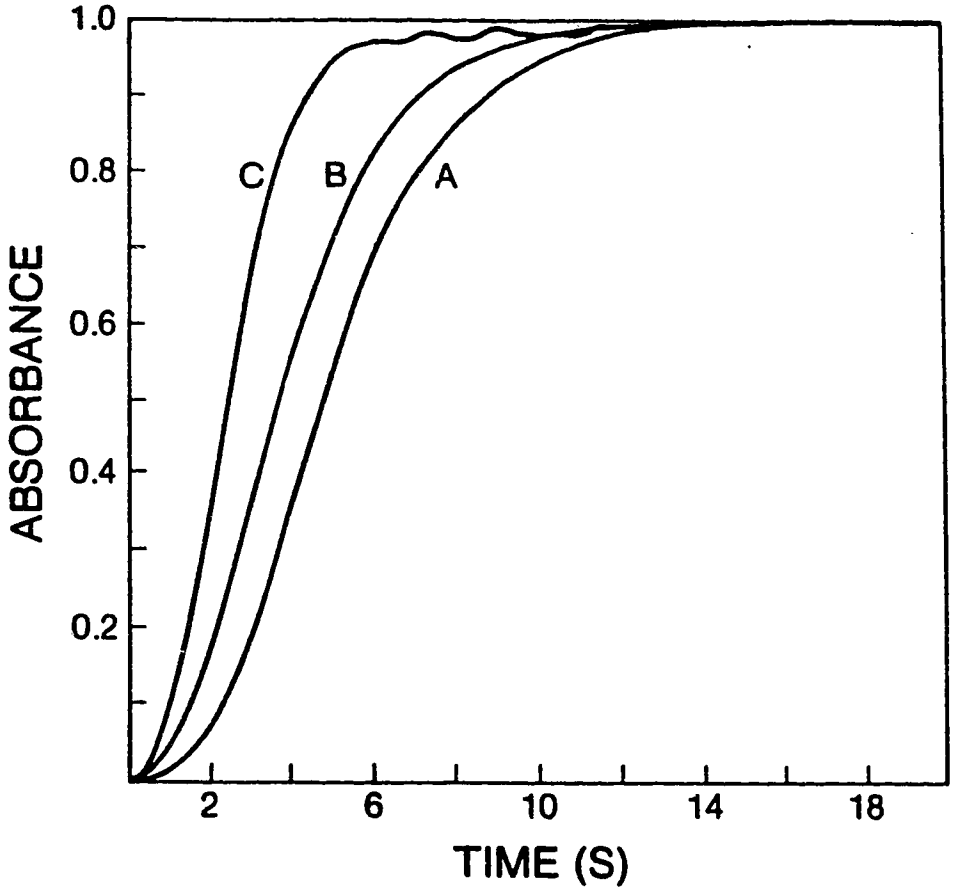

Figure 5.1 Chloroform absormance vs time profile using the UV-50 detector. (A) for the injection of *o*-nitroaniline in water (includes extraction from water into chloroform); (B) for the injection of *o*-nitroaniline already in chloroform; (C) after deconvolution of curve A with the IRF from curve B.

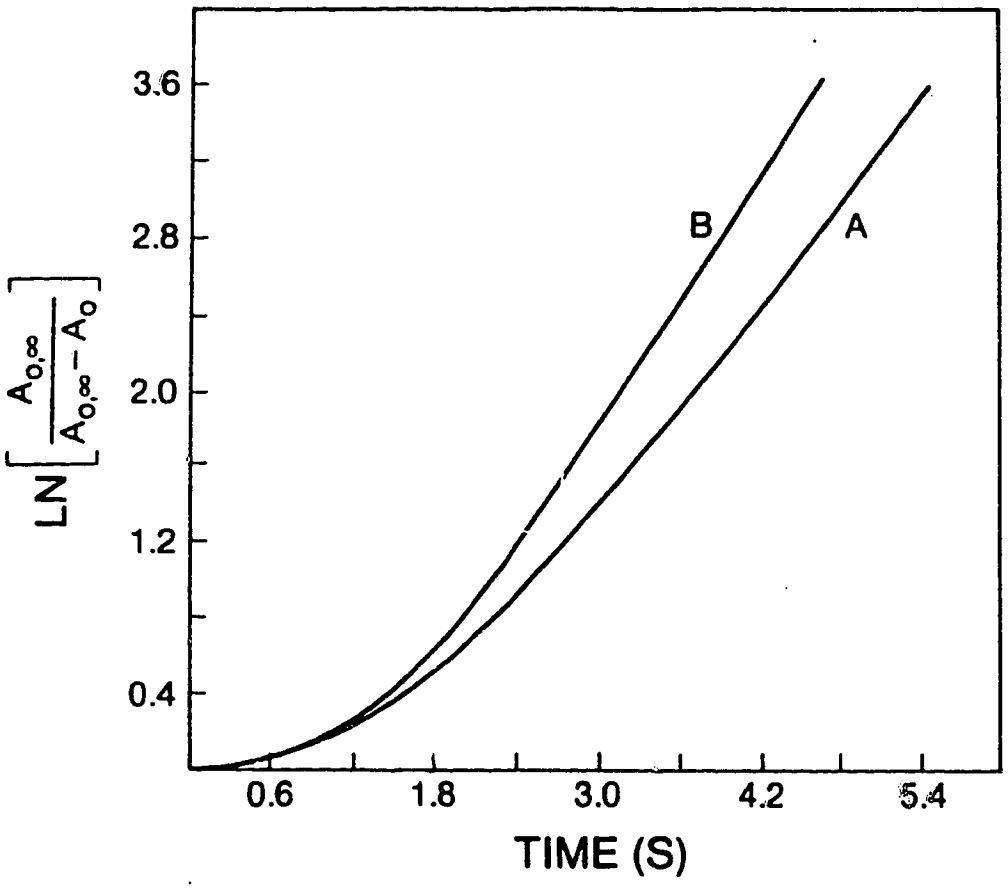

Figure 5.2 First order plots of the deconvolved extraction profiles. (A) for the extraction of *o*-nitroaniline from water into chloroform; (B) for the extraction of *o*-nitrophenol from chloroform into water.

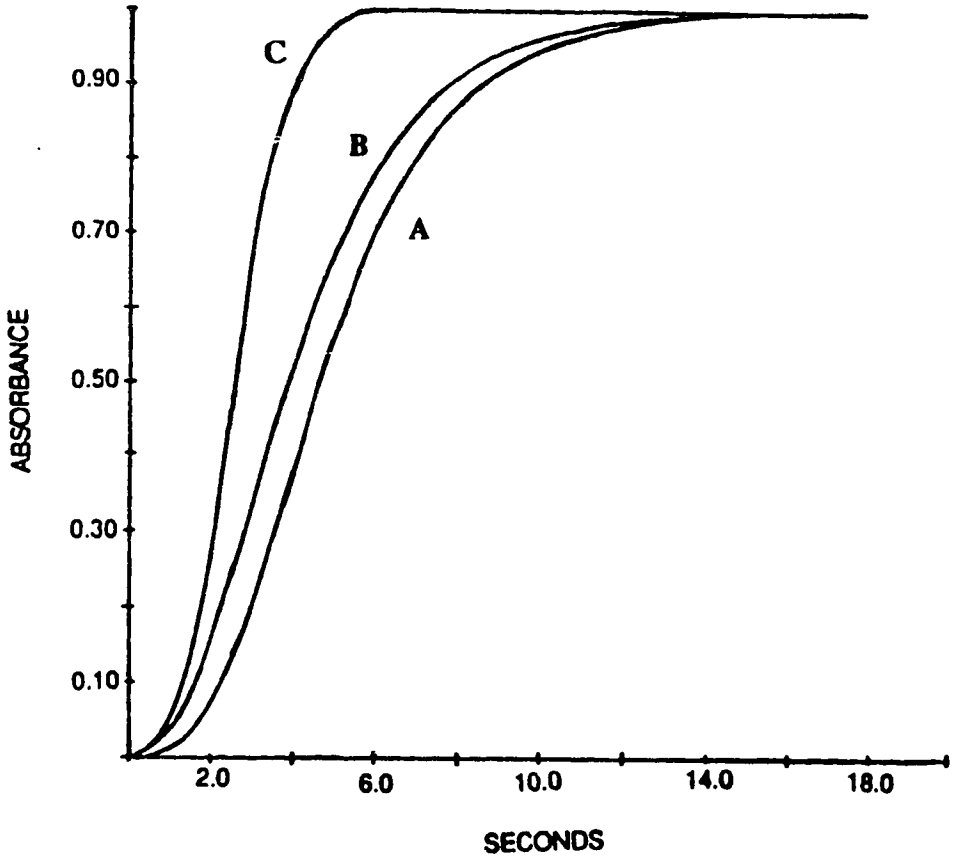

Figure 5.3 Chloroform absorbance vs time profiles. (A) for the injection of NaOH (includes the extraction of *o*-nitrophenol from chloroform into water); (B) for the injection of *o*-nitrophenol already in chloroform into a mixture of chloroform and water; (C) after deconvolution of curve A with the IRF obtained from curve B. Curve A has been inverted about the time axis.

CHAPTER 6

MEASUREMENT OF FAST CHEMICAL REACTION RATES BY SOLVENT EXTRACTION

6.1 INTRODUCTION

In all of the important applications of solvent extraction a chemical reaction accompanies the mass transfer of solute from one liquid phase to the other [36, 18]. The chemical reaction can be homogeneous, if it occurs in one of the bulk phases, or it can be heterogeneous, if it occurs at the liquid-liquid interface and involves at least one interfacially adsorbed reactant. In order to be able to improve the design of industrial extractors and to improve the overall extraction efficiency, it is important to be able to measure the rate of the chemical reaction in all of these systems.

As discussed in Chapter 3, the observed A vs t profile is the sum of three independent processes and defined by Equation 3.3 as:

$$\sigma_O^2 = \sigma_R^2 + \sigma_M^2 + \sigma_I^2$$

where σ_O^2 is the variance of the overall extraction process, σ_R^2 is the variance due to the chemical reaction, σ_M^2 is due to the mass transfer and σ_I^2 is due to instrument bandbroadening. Thus, in order to directly measure the rate of the chemical reaction it is necessary to have σ_R^2 much greater than $\sigma_M^2 + \sigma_I^2$. If σ_R^2 is only slightly greater, equal to or even smaller than $\sigma_M^2 + \sigma_I^2$ then it is necessary to use mathematical deconvolution in order to separate the chemical reaction contribution from the contributions of mass transfer and instrument bandbroadening.

The rapid-stir experiment in which one phase is dispersed in the other under turbulent conditions is particularly an attractive technique to measure the rates of relatively fast homogeneous chemical reactions because the mass transfer rate can be made quite high

[64, 70]. In fact, as shown in Chapter 4, in a well designed rapid-stir device with a small hold-up volume, σ_M^2 can be made an order of magnitude smaller than σ_I^2 so that instrumental bandbroadening, rather than mass transfer, imposes the upper limit on the chemical reaction rate that can be accurately measured.

In this chapter the rapid-stir apparatus described in Chapter 4 is used to study the rate of the homogeneous oxidation of I^- by Fe^{3+} in the aqueous phase, by monitoring the rate of appearance of iodine, I_2, in the chloroform phase. The rate of the reaction was varied by varying the concentrations of reagents to discover the upper limit of reaction rate that can be measured by this apparatus.

6.2 EXPERIMENTAL

6.2.1 REAGENTS AND SOLVENTS

Potassium Nitrate (BDH Chemicals, Toronto) was of analytical grade and was used as received.

Potassium Iodide (Fisher Scientific Co.) was ACS certified and was used as received.

Ferric Nitrate , $Fe(NO_3)_3 .9H_2O$, (Fisher Scientific Co.) was ACS certified and was used as received.

Iodine (BDH Chemicals) was ACS certified and was used as received.

All water was demineralized, distilled and finally distilled over alkaline potassium permanganate. All other chemicals and solvents were reagent grade. Chloroform (Caldon Laboratory Ltd.) was washed with distilled water prior to use. A 1.00 M potassium iodide stock solution was prepared in water that had been purged with nitrogen. Solutions of 1.00 M potassium nitrate, 0.100 M ferric nitrate, and 0.200 M nitric acid were prepared in water. A solution of 0.0166 M potassium triiodide, used to measure the IRF required for the deconvolution operation, was prepared by combining 5.00 mL of 0.100 M ferric nitrate, 5.00 mL of 1.00 M potassium iodide, 2.00 mL of 0.20 M nitric acid and 3.00 mL of water.

6.2.2 APPARATUS

The rapid-stir apparatus used in this work was the same as that described in Chapter 4 except that the porous Teflon membrane phase separator consisted of two layers of 0.0055 inch thick, 5 to 10 μm pore size Zitex (No. E606122, Chemplast, Wayne, NJ). The cell was thermostated at 20.0 ± 0.1 ° C. The variable wavelength photometer detector (UV 50, Varian Assoc.) was set at 520 nm to monitor the absorbance of the chloroform phase flowing through it. The detector signal was acquired digitally on an IBM-XT microcomputer which was interfaced to the detector via a Lab Master ADC Interface Board (TM-40-PCL, Tecmar, Cleveland, OH) as described in Chapter 3.

6.2.3 REACTION AND EXTRACTION PROCEDURE

First, 100.0 mL of chloroform was placed in the extraction cell. Then aqueous stock solutions of KI, KNO_3 and HNO_3 were pipetted into the cell along with water to give a final aqueous phase of 99.0 mL of 0.050 M HNO_3 that had an ionic strength of 0.300 M and contained either 0.020, 0.050, 0.080, 0.100, 0.150 or 0.200 M KI. While stirring at 2300 rpm and pumping the chloroform phase at 1.00 $mLmin^{-1}$ a volume of 1.00 mL of aqueous 0.100 mL $Fe(NO_3)_3$ solution was injected to initiate the reaction. The change in absorbance of the chloroform phase with time was monitored.

In another experiment the initial aqueous and organic phases in the extraction cell were as described above, but the injected solution was 1.00 mL of aqueous 0.0166 M KI_3. Data from this experiment were used to generate the instrument response functions (IRF) required for deconvolving the sample profiles.

6.2.4 DISTRIBUTION COEFFICIENT MEASUREMENT

The distribution coefficient for the distribution of iodine between chloroform and aqueous potassium nitrate was measured as follows: 100.0 mL of 5.00×10^{-4} M

chloroform solution of iodine was added to 100.0 mL of aqueous solution prepared by combining 50.0 mL water and 25.0 mL each of 1.00 M KNO_3 and 0.20 M HNO_3 in a separatory funnel and shaking for 2 min. The phases were separated and the absorbance of the aqueous phase was measured at 460 nm. The concentration of iodine in the aqueous phase was calculated using a molar absorptivity of 746 [153] for iodine in water. The concentration of iodine in the chloroform phase at equilibrium was determined by difference, and the distribution coefficient, K_D, was calculated by the equation:

$$K_D = \frac{[I_2]_{org}}{[I_2]_{aq}} \qquad (6.1)$$

6.2.5 DECONVOLUTION

All observed A vs t extraction profiles exhibited a distorted sigmoidal shape (e.g. Figure 6.1). Deconvolution was performed to obtained the A vs t profile associated with only the chemical reaction between I^- and Fe^{3+}, free of the contribution from both mass transfer of I_2 and instrument bandbroadening. The deconvolution procedure was similar to that described in Chapter 3.

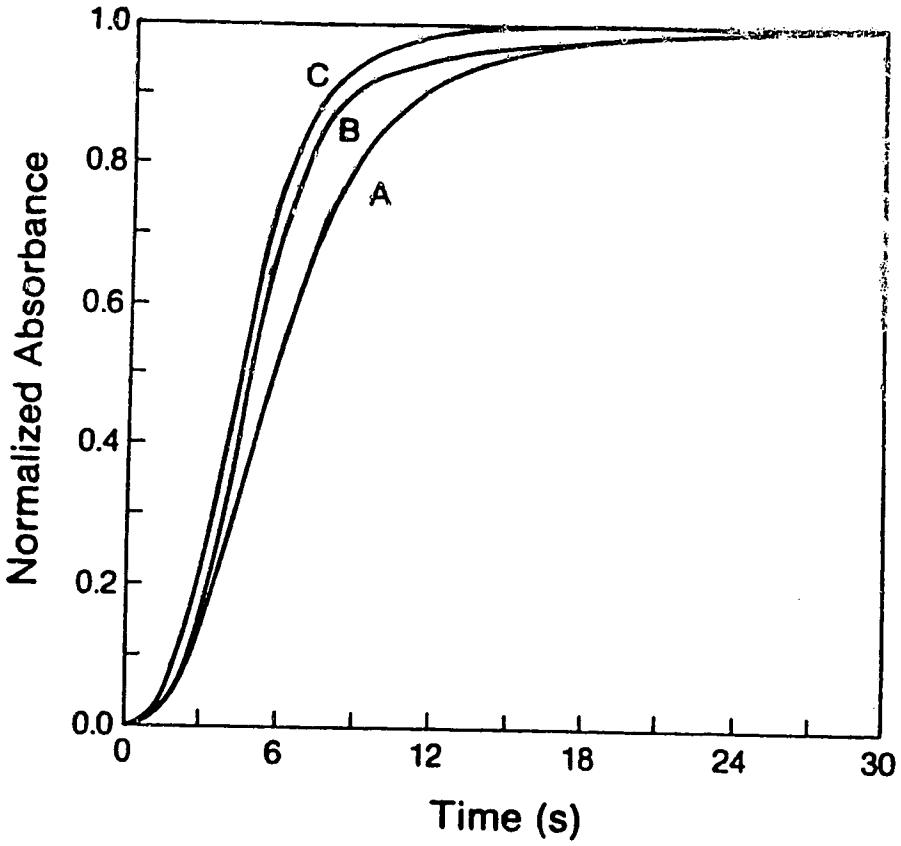

Figure 6.1 Absorbance of the chloroform phase *vs* time. (A) for the injection of $Fe(NO_3)_3$ into aqueous KI (includes chemical reaction and extraction of iodine into chloroform). (C) for the injection of KI_3 into aqueous KI (includes only extraction of iodine into chloroform). (B) after deconvolution of curve A with the IRF from Curve C.

6.3 RESULTS AND DISCUSSION

The oxidation of I^- by Fe^{3+} was chosen for study for several reasons: (i) it has a complex reaction mechanism exhibiting a third order rate law and a retardation effect but, nevertheless, can be made (pseudo) first order under suitable experimental conditions; (ii) one product (I_2) can be extracted into chloroform: (iii) the pseudo first order rate constant can be varied over a range of values.

6.3.1 OXIDATION OF I^- BY Fe^{3+}

The redox reaction between ferric and iodide ions is described stoichiometrically as;

$$Fe^{3+} + I^- \rightleftharpoons Fe^{2+} + 1/2\, I_2 \qquad (6.2)$$

However, the reaction mechanism has been found to involve the intermediates FeI^{2+} and I_2^- according to the following sequence of steps [154, 155].

$$Fe^{3+} + I^- \rightleftharpoons FeI^{2+} \qquad (6.3)$$

$$FeI^{2+} + I^- \rightleftharpoons Fe^{2+} + I_2^- \qquad (6.4)$$

$$Fe^{3+} + I_2^- \rightleftharpoons Fe^{2+} + I_2 \qquad (6.5)$$

From the dependences of the rates of the reaction on the various concentrations of reagents, an overall law can be derived [154, 155].

Let the forward reaction rate constants for reactions 6.3, 6.4 and 6.5 be k'_1, k'_3 and k'_5 respectively, and let those for the rewerse reactions be k'_2, k'_4 and k'_6 respectively. Upon application of the steady-state assumption to the intermediate species FeI^{2+} and I_2^-, the rate law for the formation of I_2 is derived as;

$$\frac{d[I_2]}{dt} = \frac{\frac{k'_1 k'_3 [Fe^{3+}][I^-]^2}{k'_2} - \frac{k'_4 k'_6 [Fe^{2+}]^2 [I_2]}{k'_5 [Fe^{3+}]}}{1 + \frac{k'_4 [Fe^{2+}]}{k'_5 [Fe^{3+}]} + \frac{k'_3 [I^-]}{k'_2}} \qquad (6.6a)$$

The second term in the numerator arises from the reverse of the reaction in Equation 6.5. If it is assumed that k'_4 and k'_6 are small and that k'_5 is large, then these factors combined with the fact that $[Fe^{2+}]^2$ would be small until the reaction has progressed quite far, means that the second term in the numerator of Equation 6.6a can be neglected. This is equivalent to assuming that Equation 6.5 is irreversible. Hence,

$$\frac{d[I_2]}{dt} = \frac{\frac{k'_1 k'_3 [Fe^{3+}][I^-]^2}{k'_2}}{1 + \frac{k'_4 [Fe^{2+}]}{k'_5 [Fe^{3+}]} + \frac{k'_3 [I^-]}{k'_2}} \qquad (6.6b)$$

It has also been shown that $k'_3[I^-] << k'_2$ [154, 155]. Therefore,

$$\frac{d[I_2]}{dt} = \frac{\frac{k'_1 k'_3 [Fe^{3+}][I^-]^2}{k'_2}}{1 + \frac{k'_4 [Fe^{2+}]}{k'_5 [Fe^{3+}]}} \qquad (6.6c)$$

Combining constants gives the following expression;

$$\frac{d[I_2]}{dt} = \frac{k_1 [Fe^{3+}][I^-]^2}{1 + k_2 \left(\frac{[Fe^{2+}]}{[Fe^{3+}]} \right)} \qquad (6.6d)$$

where k_1 and k_2 are constants.

From Equation 6.6d, the third order rate constant for the reaction is;

$$\frac{k_1}{1 + k_2 \dfrac{[Fe^{2+}]}{[Fe^{3+}]}} = \frac{k_1}{1 + R} \qquad (6.7)$$

The second term in the denominator of Equation 6.7 is referred to as the retardation term, R. It arises from the retardation effect of Fe^{2+} on the reaction rate via its competition with Fe^{3+} ions for reaction with I_2^- (Equation 6.4, reverse, vs Equation 6.5, forward). Although it is not implied by the rate law (Equation 6.6d) it has been found experimentally that k_2 decreases with increasing $[I^-]$ [154, 155]. It has been suggested [154] that this may be due to a parallel reaction to that in Equation 6.5 in which the Fe^{3+} complex, FeI^{2+}, also reacts with I_2^- to form I_2. If FeI^{2+} reacts more rapidly than does Fe^{3+} then k'_5 would be larger at higher $[I^-]$, for which $[FeI^{2+}]/[Fe^{3+}]$ is larger. Thus, R depends on $[I^-]$ as well as on $[Fe^{2+}]/[Fe^{3+}]$. The rate of the oxidation reaction, Equation 6.3, also depends on the ionic strength, pH and presence of complexing anions and the concentrations of Fe^{2+}, Fe^{3+} and I^-. However, at $[H^+]$ above 0.02 M the rate is independent of pH [154-157].

The thermodynamic equilibrium constant for the redox reaction (Equation 6.2) at zero ionic strength is 3.8×10^2 at 25 ° C [156]. This corresponds to a concentration equilibrium constant at ionic strength 0.3 of 1.0×10^2 at 20° C. In calculating the concentration constant the activity coefficients under the experimental conditions were calculated by the Davies activity equation [158]. At the excess concentration of I^- used in this work the redox reaction can be considered to be quantitative at equilibrium so that only the forward reaction rate needs to be considered.

In the present work the reaction product, I_2, is extracted into chloroform during the course of the reaction;

$$I_{2,aq} \rightleftharpoons I_{2,org} \qquad (6.8)$$

However, because there is always an excess of I^- ions in the aqueous phase, the I_2 in the aqueous phase is rapidly converted to triiodide ion:

$$I_2 + I^- \rightleftharpoons I_3^- \qquad (6.9)$$

The second order forward rate constant for reaction 6.9 is large ($k_f \sim 10^{10}$ L mol^{-1}s^{-1}) [155], so that it does not effect the overall rate of the redox reaction.
The distribution of iodine in the zero oxidation state when the system has reached equilibrium is therefore controlled by an overall equilibrium between Equations 6.8 and 6.9. It can be shown by coupling the distribution coefficient (Equation 6.1) and the formation constant for Equation 6.9 that:

$$\frac{1}{A_{t=\infty}} = \frac{1 + K_D}{K_D A_{max}} + \frac{K_f [I^-]_{t=\infty}}{K_D A_{max}} \qquad (6.10)$$

Where K_f is the formation constant for triiodide in the aqueous phase(i.e., for Equation 6.9), A_{max} is the absorbance that would be obtained if all of the I^o formed at equilibrium were present as I_2 in the chloroform phase, and $A_{t=\infty}$ is the absorbance of the chloform phase at equilibrium. Similarly, $[I^-]_{t=\infty}$ is the concentration of iodide ion at equilibrium. Equation 6.10 suggests that a plot of $1/A_{t=\infty}$ vs $[I^-]_{t=\infty}$ will be linear. The measured values of $A_{t=\infty}$ are presented in column 6 of Table 6.1. It is evident from Figure 6.2 that

such a plot is indeed linear with a slope of 19.0 ± 0.9 and an intercept of 2.0 ± 0.1. The ratio of the slope to the intercept of the plot is the quantity $K_f / (1 + K_D)$.

The value of K_D, measured in a separate experiment under the same conditions, was 75 ± 2. Combining this value of K_D with the value of 9.5 for the ratio of slope/intercept gives an equilibrium constant for the formation of triiodide of $(7.2 \pm 0.7) \times 10^2$. This is in agreement with the literature value of 7.4×10^2 at 20° C [159].

Table 6.1 Data and Results for the Measurement of Pseudo First Order Rate Constant for the Reaction between Iodide and Ferric Ions

$[I^-]_{t=0}$ (M)	$[I^-]_{t=\infty}$ (M)	$[I^-]_{t=d}$ (M)	$\alpha_{Fe^{3+}}$	F_{Io}	$A_{t=\infty}$	% Reaction at t=d	Pseudo First Order Rate Constant (s^{-1})
0.020	0.019	0.0199	0.84	0.84	0.40	10	0.0057 ± 0.0002
0.050	0.049	0.0497	0.85	0.67	0.35	26	0.0299 ± 0.0016
0.080	0.079	0.0795	0.87	0.56	0.29	46	0.0695 ± 0.0023
0.10	0.099	0.0995	0.88	0.51	0.27	54	0.133 ± 0.001
0.15	0.149	0.1492	0.90	0.41	0.21	76	0.259 ± 0.001
0.20	0.199	0.1991	0.93	0.34	0.17	90	0.423 ± 0.037

[Fe[illegible]] [illegible] 10^{-3} M for all experiments.

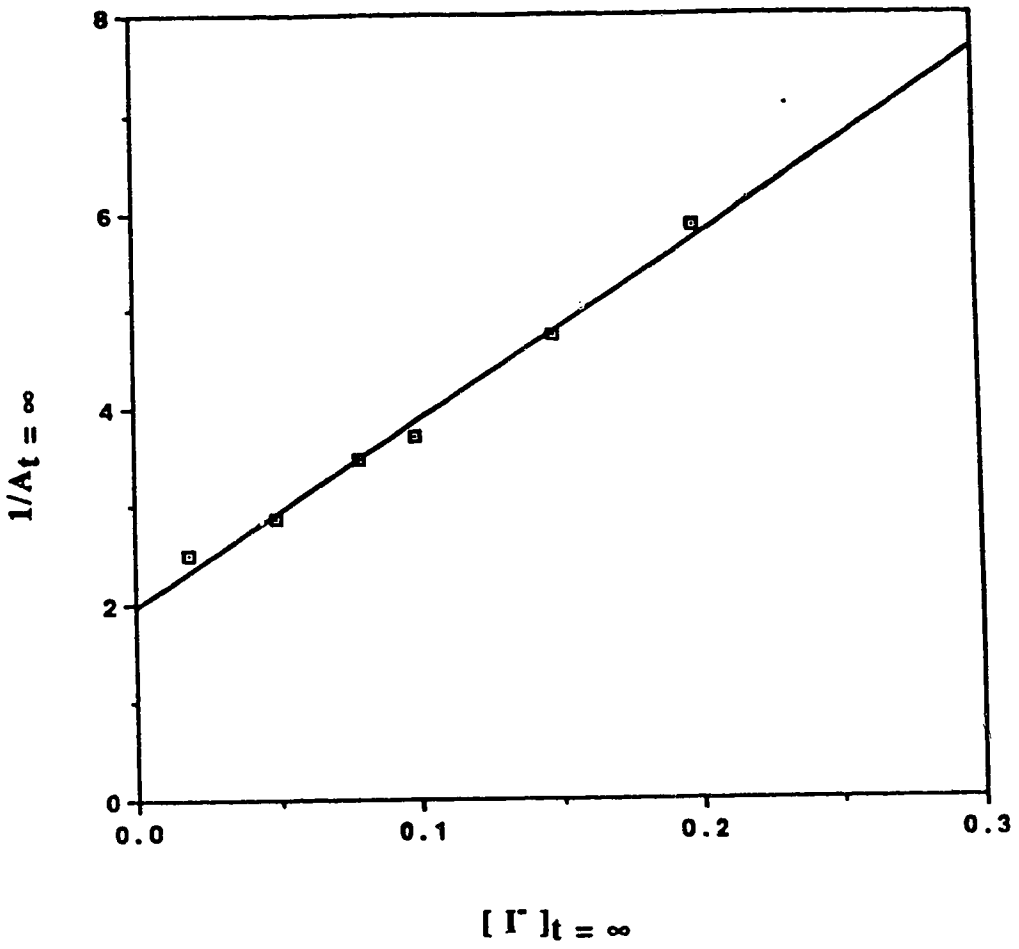

Figure 6.2 Plot of $1/A_{t=\infty}$ vs $[I^-]_{t=\infty}$ (see Equation 6.10). $A_{t=\infty}$ is the absorbance of the chloroform phase after the extraction has reached equilibrium, and $[I^-]_{t=\infty}$ is the concentration of iodide in the aqueous phase at equilibrium.

If the rate of the oxidation reaction is measured by monitoring the rate of formation of iodine, I_2, then it can be shown, by rearranging Equation 6.6d and employing the stoichiometric relationship in Equation 6.2, that

$$\frac{d[I^o]}{dt} = \frac{k_1}{1+R}[I^-]^2\left([I^o]_{t=\infty} - [I^o]\right) = k_{obs}\left([I^o]_{t=\infty} - [I^o]\right) \qquad (6.11)$$

where $[I^o]_{t=\infty}$ is the concentration of all species of iodine in the zero oxidation state formed upon complete reaction and k_{obs} is the pseudo first order rate constans. Since R depends on $[I^-]$ as well as on $[Fe^{2+}]/[Fe^{3+}]$, as described above, kinetic studies of this reaction are usually done by measuring its "initial rate", which is always found strictly to follow a third order rate law because $R << 1$ at the beginning of the reaction.

Since the rate of the triiodide formation reaction, which occurs after iodine is produced by the oxidation reaction, is fast it has no effect on the overall reaction rate. Also the rate of extraction of I_2, once formed, is what constitutes the mass transfer in the system and is not part of the chemical reaction rate.

In the experiments discussed above the initial concentration of Fe^{3+} is always 1.00×10^{-3} M, while the initial concentration of I^- is varied from 0.020 M to 0.200 M as shown in Table 6.1. Although the chemical reaction takes place homogeneously in the aqueous phase, its rate is measured by photometrically monitoring the concentration of I_2 in the chloroform phase. Because of the reaction in Equation 6.9 only a fraction of I_2 formed by the oxidation reaction appears in the chloroform phase to be monitored. The fraction of iodine formed which is extracted, F_{Io}, is given by;

$$F_{I^o} = \frac{K_D}{1 + K_D + K_f[I^-]} = \frac{75}{1 + 75 + 7.2 \times 10^2[I^-]} \qquad (6.12)$$

The quantity F_{I^-} varies from 0.84 to 0.34 for [I^-] between 0.020 M to 0.200 M, respectively, as shown in column 5 of Table 6.1. For the purpose of measuring the rate of the oxidation reaction it does not matter what fraction of iodine extracts, but it is important that the fraction extracted remains constant during the course of a given reaction. Because I^- is always present in excess, this condition is met. For example, in the worst case, with the lowest initial concentration of I^-, the fraction extracted varies from the value of 0.84 by less than 1% relative over the course of the reaction.

There is a further consequence of the fact that [I^-] remains constant during the course of the reaction. When R << 1 Equation 6.6d has the form of a pseudo first order rate law with the rate constant $k_1[I^-]^2$. The largest relative change of the rate constant that would occur as a result of variations in the value of $[I^-]^2$ is only about 4% over all the concentration range studied, therefore any variations of the magnitude of the reaction rate observed will not be due to variations in the rate constant.

6.3.2 EXTRACTION RATE

If the rate of mass transfer of I_2 were instantaneous (which it is not) then the rate of change of I_2 concentration in the chloroform, $d[I_2]_o/dt$, would be the same as the rate of change of I^o in the whole system, $d[I^o]/dt$. Since I_2 is the only light-absorbing species in the chloroform the rate of change of absorbance, A, in the chloroform phase is also a measure of the rate of the oxidation reaction, and dA/dt can be substituted for $d[I^o]/dt$. The purpose of deconvolution is to remove the effect of the time required for mass transfer of iodine and the effect of instrument bandbroadening. Thus, dA/dt for the deconvolved A vs t data is a measure of only the rate of the chemical reaction in Equation 6.2. Curve B in Figure 6.1 shows the deconvolved A vs t extraction profile associated with the chemical reaction carried out in the presence of 0.200 M I^-. In Figure 6.3, the curves A through F are the deconvolved A vs t extraction profiles for the chemical reaction carried out in the

presence of various iodide concentrations. Each curve in Figure 6.3 has been normalized by dividing each absorbance value by its equilibrium absorbance ($A_{t=\infty}$).

The upward concave shape seen during the first couple of seconds in these profiles probably arises, at least in part, as an artifact of smoothing the observed curve before taking its derivative and deconvolving it. Smoothing was necessary since noise has a deliterous effect on deconvolution. The upward concave curvature might also arise in part from an uncompensated lag time associated with diffusion through the Nernst diffusion layer as follows: the extraction is occuring in a "mixed regime" in which the extraction rate is controlled to a significant extent by both the chemical reaction and the mass transfer rate. When Fe^{3+} is injected it mixes rapidly by convection and coalescence/re-dispersion with the bulk liquid in the dispersed aqueous phase drops. There it begins both to react with I^- in the bulk phase and to diffuse into the stagnant Nernst film, where it also reacts with I^-. Thus iodine is produced not only in the bulk aqueous phase but also in the Nernst film. In the presence of excess I^- the value of the (pseudo) first order rate constant does not depend on the local $[Fe^{3+}]$, so that the overall rate of production of I_2 in the aqueous droplets is independent of how much of the reaction occurs in the bulk phase and how much occurs in the Nernst film. However, deconvolution employs an IRF corresponding to extraction of I_2 which was injected in the form of KI_3. This IRF should compensate for the time required for I_2 produced in the bulk aqueous phase to diffuse across the Nernst film under both steady state and non-steady state (i.e. lag time) conditions, but might not correctly compensate for I_2 produced in the Nernst film. The net effect could be an additional uncompensated lag time. Whatever its origin, the upward concavity in the early part of the deconvolved A vs t extraction profile precludes the use of data from the very early part of the reaction.

In Figure 6.4, Curves A through F are plots of $Ln[A_{t=\infty} / (A_{t=\infty} - A)]$ vs t for the corresponding data in Figure 6.3. For a first order chemical reaction such a plot would be linear. The curves in Figure 6.4 are characterized by three sections. The initial upwardly

concave section in the first few seconds arises for the reasons discussed above in connection with Figure 6.3 and does not contain readily usable information. The second section, occuring at longer times, is linear and corresponds to the (pseudo) first order conditions for the oxidation reaction when R << 1. The slopes of these linear portions correspond to values of the (pseudo) first order rate constants for various [I⁻] and are as represented in column 8 of Table 6.1.

The third section of the curves in Figure 6.4 which is observed at still longer times is characterized by a downward curvature. In columns 1, 2 and 3 of Table 6.1 are presented the values of $[I^-]_{t=0}$, $[I^-]_{t=\infty}$ and $[I^-]_{t=d}$ which correspond, respectively, to the initial concentration, concentration when the reaction is completed, and the concentration at time d, above which the curves in Figure 6.4 exhibit significant downward curvature. Comparison of the squares of these iodide concentrations, as required by equation 6.11, shows that the deviation from pseudo first order behaviour occurs where $[I^-]^2_{t=d}$ is, at most, only one percent smaller than $[I^-]^2_{t=0}$. Thus, the deviation from linearity is not due to the decrease in [I⁻] in the pseudo first order rate constant, $k_1[I^-]^2$. Rather, it is due to the fact that R has increased and its no longer much smaller than 1. This, in turn, is due to the increase in $[Fe^{2+}]/[Fe^{3+}]$ (see Equation 6.7). During the course of the reaction, k_2 in Equation 6.2 remains constant because [I⁻] remains essentially constant. The value of k_2 has been shown to be smaller at higher iodide concentrations [154, 155]. Thus, for the reactions carried out with a higher [I⁻] the value of R at any percent reaction is smaller, so that (pseudo) first order conditions are expected to prevail over a greater percentage of the reaction. This is confirmed by the entries in column 7 of Table 6.1, which show that the curves in Figure 6.4 are linear to higher percent reaction in the presence of higher [I⁻].

When these pseudo first order rate constants are plotted vs $[I^-]^2$, a straight line with zero intercept (0.009 ± 0.008) results, as predicted from Equation 6.7 when R << 1 (see Figure 6.5). The slope of this line, which corresponds to the third order rate constant k_1,

is $10.6 \pm 0.4\ L^2/mol^2$ s. This value of k_1 obtained at $\mu = 0.30$ and temperature = 20° C is close to values reported in the literature for the third order rate constant (see Table 6.2).

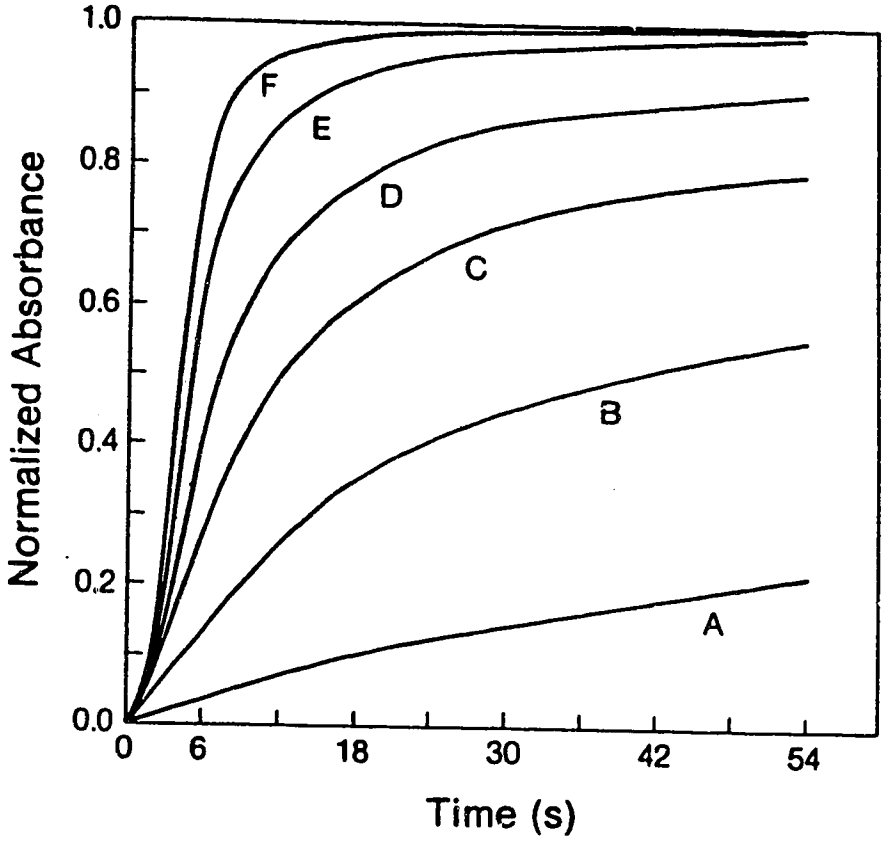

Figure 6.3 Deconvolved extraction profiles for the reaction between 0.001 M ferric and different concentrations of iodide ions. Concentration of iodide is (A) 0.020 M; (B) 0.050 M; (C) 0.080 M; (D) 0.100 M; (E) 0.150 M, (E) 0.200 M.

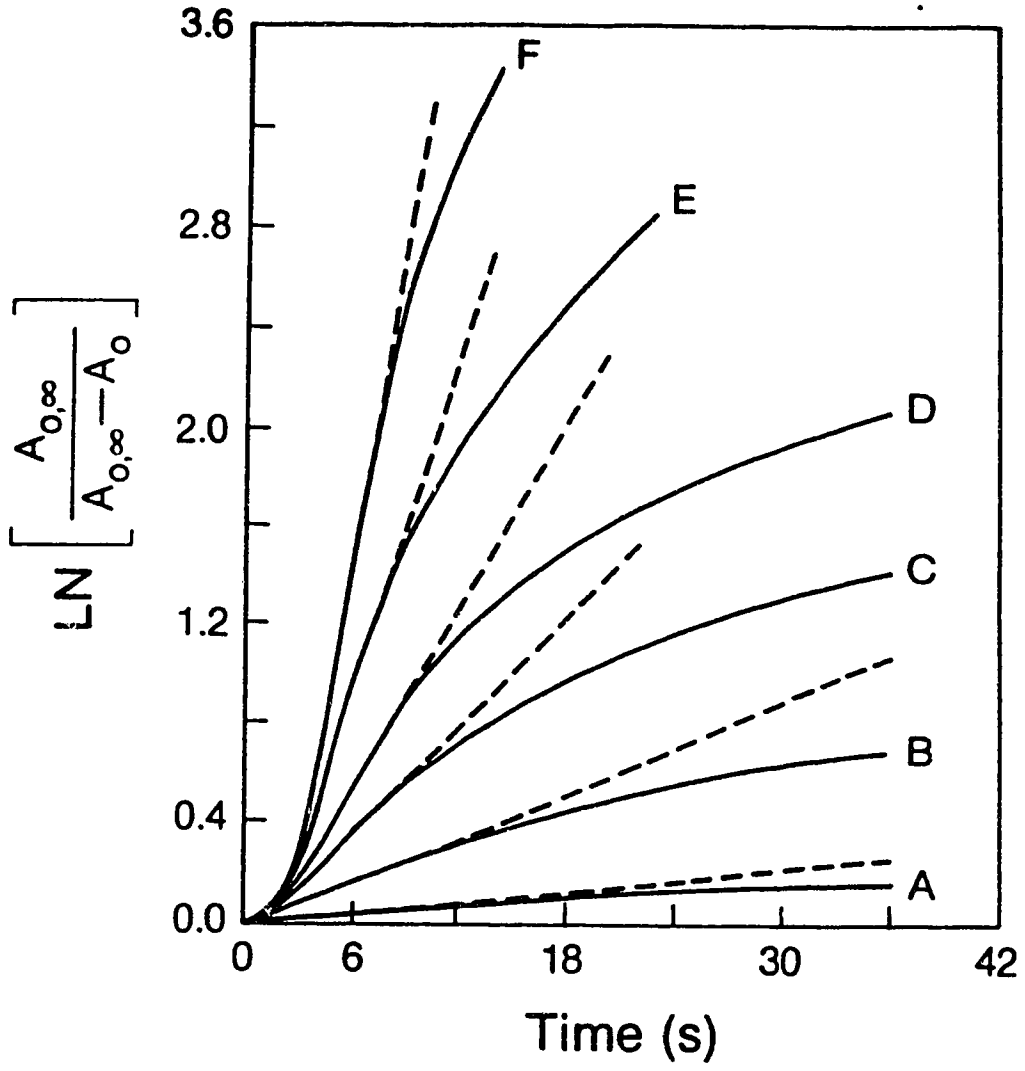

Figure 6.4 Integrated first order plots for the deconvolved extraction profiles in Figure 6.3. Pseudo first order rate constants (see Table 6.1) were obtained from the slopes of the dashed lines.

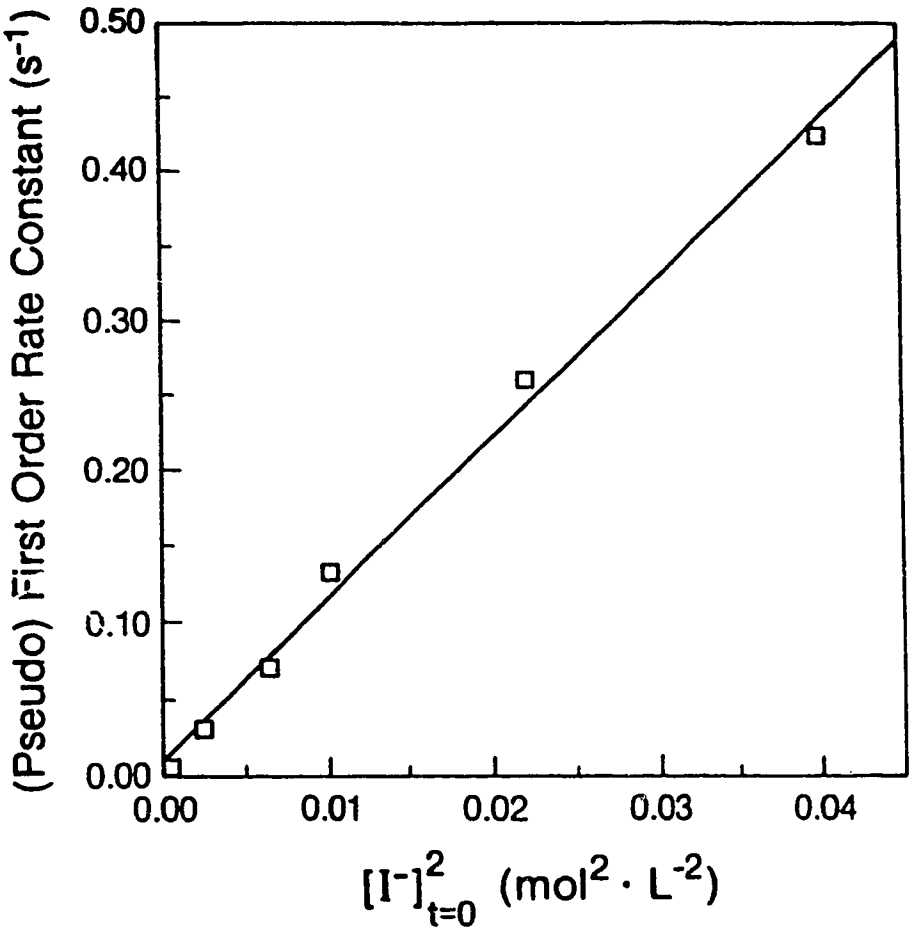

Figure 6.5 Plot of pseudo first order rate constants, k_{obs}, for the oxidation of iodide by ferric vs the square of iodide concentration. (see Equation 6.11).

Table 6.2: Third Order Rate Constants for the Reaction between Ferric and Iodide Ions

Technique	3rd order rate constant ($L^2mol^{-2}s^{-1}$)	Ionic strength (M)	$[H^+]$ (M)	Temperature (ºC)
Solvent Extraction	10.6 + 0.3[a]	0.30	0.05	20.0 +0.1
Back titration with thoisulfate	21.8[b]	0.067	0.01	19
Back titration with thiosulfate	7.4[b]	0.602	0.10	20

References: (a) present work; (b) [155].

6.3.3 EFFECT OF COMPLEXING ANIONS

It has been shown that anions such as chloride, sulfate and nitrate retard the rate of the oxidation reaction between iodide and Fe(III) [157]. In this work nitrate, which complexes Fe^{3+}, is present in all of the experiments at a fixed concentration ranging from 0.1 to 0.3 M. At ionic strength 0.3 the complex formation constant, K_{FeNO_3}, is about 0.7 [160], which means that in these experiments the fraction of Fe(III) present as the Fe^{3+}species is given by the following equation:

$$\alpha_{Fe^{3+}} = \frac{[Fe^{3+}]}{[Fe(III)]} = \frac{1}{1 + 0.7[NO_3^-]} \qquad (6.13)$$

Values of $\alpha_{Fe^{3+}}$ are shown in column 4 of Table 6.1, where it can be seen that between 84% and 93% of Fe(III) is present as Fe^{3+}. It is not known whether only the hydrated Fe^{3+} species can act as an oxidant for I^- or whether the nitrato-complex $FeNO_3^{2+}$ can also perform that role and if so, what the relative values of the rate constant k_1 would be for these two Fe(III) species [154, 157]. The discussion so far assumes that Fe^{3+} and $FeNO_3^{2+}$ behave, kinetically, in an identical manner. On the other hand, if $FeNO_3^{2+}$ is inactive as an oxidant for I^-, then Equation 6.11 can be modified by multiplying the numerator term by $\alpha_{Fe^{3+}}$. This makes the pseudo first order rate constant $k_1(\alpha_{Fe^{3+}})[I^-]^2$. When the plot of the pseudo first order rate constants from column 8 of Table 6.1 vs the quantity $\alpha_{Fe^{3+}}[I^-]^2$ is made, as shown in Figure 6.6, a straight line with an intercept = 0.034 ± 0.010 s.d, and a slope of 11.2 ± 0.5 s.d which corresponds to the third order rate constant k_1, is obtained. This is close to the value of 10.6 obtained when $FeNO_3^{2+}$ is assumed to be redox-active, as discussed above. Thus, whether $FeNO_3^{2+}$ is assumed to be redox-active or not, the calculated value of k_1 is little affected and, importantly, the agreement of the k_1 obtained by the solvent extraction method with the literature values

attests to the accuracy of this method of measuring homogeneous chemical reaction kinetics.

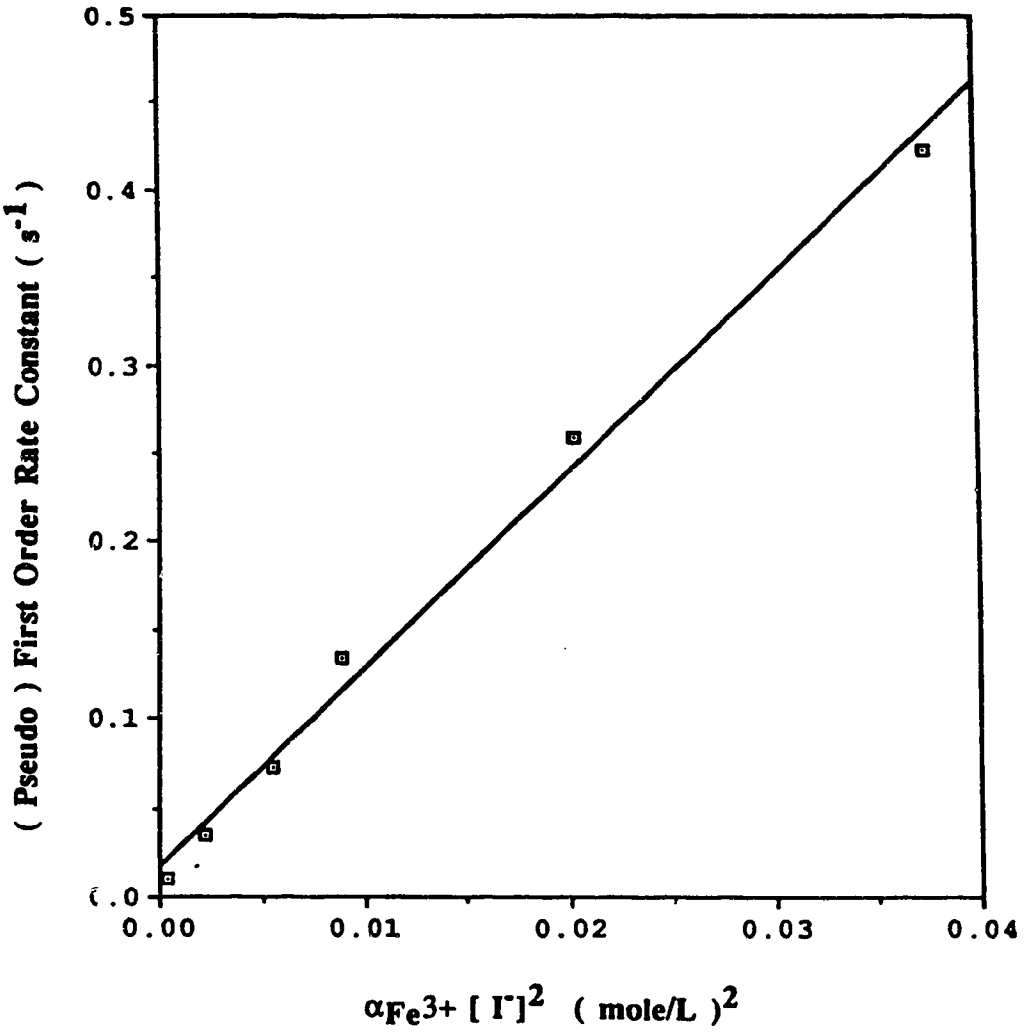

Figure 6.6 Plot of pseudo first order rate constants, k_{obs}, for the oxidation of iodide by ferric vs $\alpha_{Fe}{}^{3+}[I^-]^2$. (see Section 6.3.3. for details).

6.3.4 LIMITATION OF SOLVENT EXTRACTION FOR CHEMICAL REACTION KINETIC STUDUES

As indicated by Equation 3.3 the contribution of the chemical reaction is obtained only by removing the contributions of mass transfer and instrument bandbroadening. The fastest rate measured in the present study occured when [I^-] was 0.200 M. Under that condition the overall variance, σ_o^2, for the observed extraction profile was 19.8 s^2 , and the combined variance for mass transfer and instrument, ($\sigma_M^2 + \sigma_I^2$),was 6.6 s^2 so that the variance resulting from the chemical reaction, σ_R^2, was 13.2 s^2. As the chemical reaction rate gets faster the variance associated with it also becomes smaller and eventually the magnitude of the chemical reaction variance will become so small that it is lost in the uncertainty in the difference between σ_o^2 and ($\sigma_M^2 + \sigma_I^2$). The same conclusion can be drawn by comparing curves A and C in Figure 6.1. For faster reaction rates curve A would be closer to curve C. Eventually the difference between the two curves would be lost in the noise and deconvolution would be impossible. It is, of course, the uncertainty, or noise, rather than the absolute magnitudes of the experimental signal and the IRF that impose the limit on taking the difference of their variances or deconvolving them. The uncertainty (the percent relative standard deviation) in ($\sigma_M^2 + \sigma_I^2$) is about 13 % .

If the relative uncertainty in σ_I^2 is assumed to be independent of the absolute magnitude of σ_I^2 , then, since $\sigma_I^2 >> \sigma_M^2$ in this rapid stir instrument , reducing σ_I^2 would be the most effective way of making feasible the measurement of faster rates of chemical reaction. It was shown in the previous experiments using this apparatus (Chapter 4) that, for extractable compounds whose distribution ratio is very large so that they are quantitatively extracted, the value of σ_M^2 is on the order of 0.3 s^2. If the instrument bandbroadening could be eliminated completely then, since there should be no difficulty in accurately obtaining by deconvolution the A vs t profile associated with a chemical reaction for which the variance σ_R^2 is about equal to σ_M^2 , it should be possible to measure rates

of chemical reactions for which $\sigma_R^2 \geq 0.3\ s^2$. This corresponds to a pseudo first order rate constant of about 2 s^{-1} ($t_{1/2} \approx 0.4$ s). The likelihood of reducing the magnitude of σ_M^2 by more rapid stirring is not promising, both because drop diameter seems to reach a lower limit at high stirring rates, and because the thickness of the Nernst diffusion film is not readily reduced below about 0.002 cm in a rapid stir system [70].

The discussion, so far, is based only on reactions in which both reactants are present in the same (i.e. aqueous) phase and in which the chemical reaction is homogeneous and pseudo first order. In many metal-ligand extractions the metal ion is present in the aqueous phase and the ligand in the organic phase. When the ligand is essentially insoluble in the aqueous phase so that the metal ion reacts heterogeneously with ligand adsorbed at the liquid-liquid interface then the processes giving rise to σ_R^2 and σ_M^2 can still be treated as independent of one another and, when the ligand is present in large stoichiometric excess, pseudo first order reaction conditions prevail. Deconvolution can, in this case, still be used to measure the rate of a fast chemical reaction occurring in the presence of comparable fast mass transfer [36].

However, for reactions in which the ligand is present initially in the organic phase but has a reasonable solubility in the aqueous phase, and where the reaction takes place homogeneously, then mass transfer rate and chemical reaction rate are coupled and cannot be treated as independent. In this case σ_M^2 and σ_R^2 are not independent. A suitable impulse function for deconvolution cannot be obtained and the rate of a chemical reaction occuring in the presence of a comparably fast mass transfer cannot be obtained by deconvolution. In this mixed regime the chemical reaction rate is, in fact, difficult to measure in any way by solvent extraction alone [36].

In contrast to this variable situation regarding the role of mass transfer, the contribution of instrument bandbroadening will always be independent of both mass transfer and chemical reaction so that deconvolution with a suitable IRF [70] can be used to remove it. Of course, the success of deconvolution is subject to the limitations of signal noise discussed

above. This is, for practical purposes, encouraging since at the present stage of development of solvent extraction apparatus it is instrument bandbroadening, rather than mass transfer, which imposes a practical limit on the magnitude of chemical reaction rates that can be measured by rapid stir solvent extraction.

CHAPTER 7

INTERFACIAL ADSORPTION OF TETRAHEXYL AMMONIUM ION-PAIRS OF PICRATE AND BROMOTHYMOL BLUE AT THE CHLOROFORM/WATER INTERFACE

7.1 INTRODUCTION

Extraction rate laws for solutes that are not surface-active are accurately expressed as functions of bulk phase concentrations [5, 32, 77, 78, 80, 161-164]. However, as reported by England and Berg [165], analysis of mass transfer kinetic data for the transfer of surface active agents should take into account not only molecular diffusion in both liquid phases but also adsorptive accumulation at the interface and energy barriers to adsorption and / or desorption. It is important therefore that any interfacial mass transfer kinetic studies should be preceded by a thorough interfacial adsorption study.

Before the introduction of the microporous membrane phase separator, interfacial tension measurements were the most commonly used techniques for obtaining information about interfacial activity of solutes [166, 167] . Interfacial tension data alone are, however, inadequate for obtaining the total interfacial area created in a liquid-liquid dispersion. Other techniques which utilize the light-scattering properties of dispersions [118, 145] have also been applied for measuring the interfacial area of dispersions. However, these techniques have, as discussed by Calderbank [59], severe limitations and have therefore not been wildly applied.

With the microporous phase separator [63] it is possible to measure both interfacial area [64] and interfacial concentration of solute [64, 69, 146, 168-171] under rapid stirring conditions. During stirring there is preferential adsorption of surfactants at the greatly increased liquid-liquid interface. This is indicated by a reversible decrease in absorbance of the bulk liquid phase. At a constant interfacial area (constant stirring speed)

it is possible to obtain an adsorption isotherm for the solute by varying the bulk phase concentration.

In this chapter, the interfacial equilibria of tetrahexyl ammonium ion-pairs of picrate and bromothymol blue at the chloroform/water interface are examined under conditions encountered in rapid stir solvent extraction systems incorporating a microporous membrane phase separator.

7.2 EXPERIMENTAL

7.2.1 REAGENTS

Water was demineralized, distilled and finally distilled over alkaline permanganate. Reagent grade chloroform (Caledon Laboratory Ltd.) was washed with distilled water prior to use. Two 1.0 x 10^{-3} M solutions of tetrahexyl ammonium bromide (Eastman Kodak Co., Rochester, N.Y.) were prepared with chloroform and aqueous buffer as solvents respectively. Aqueous phosphate buffers at pH's 6.5 and 5.0 were prepared at an ionic strength of 0.05 M with sodium hydrogen and dihydrogen phosphates. Bromothymol blue (BDH Canada Ltd.) was purified by recrystallization from ethanol, and used to prepare 5.0 x 10^{-4} M aqueous solution in phosphate buffer pH 5.0. Picric acid, reagent grade (Matheson, Coleman and Bell Ltd.), was used as received to prepare 1.0 x10^{-3} M aqueous solution in phosphate buffer pH 6.5.

I <u>Preparation of sodium bromothymol blue (NaHB) stock solution</u>

Bromothymol blue, 0.0781gm, was weighed into a 100 mL beaker. 1.25 mL of 0.10 M NaOH solution was added and the mixture triturated until a consistent slurry was formed. The slurry was dissolved by applying gentle heat and then quantitatively transfered into a 250 mL volumetric flask with phosphate buffer pH 5.0 and made to volume.

II Preparation of tetrahexyl ammonium bromide (QBr) stock solution

Tetrahexyl ammonium bromide, 0.0435 gm, was weighed into a 100 mL beaker. 60.0 mL of phosphate buffer pH 5.0 was added and stirred while heating (below boiling temperature) on a hot plate until complete solution was achieved. The solution was then quantitatively transferred into a 100 mL volumetric flask and made to volume with buffer. Another stock solution was prepared with chloroform as solvent.

III Preparation of sodium picrate (NaP) stock solution

A quantity of picric acid, 0.0229 gm, was dissolved in 1.0 mL of 0.10 M NaOH and then made to volume in a 100 mL volumetric flask with phosphate buffer pH 6.5.

IV Preparation of stock chloroform solutions of tetrahexyl ammonium bromothymol blue (QHB)

An appropriate volume of aqueous solution of tetrahexyl ammonium bromide was pipetted into a separatory funnel containing about 60 mL of chloroform. An excess amount of NaHB ($\geq$ 5 times the moles of QBr taken) was added to the mixture and extracted by shaking for about 5 min. After allowing the phases to separate, the chloroform extract was separated into another separatory funnel containing about 20 mL of aqueous buffer. This second mixture was shaken gently (to rinse the chloroform extract) and again allowed to separate. The rinsed chloroform extract was quantitatively separated in a 100 mL volumetric flask and made to volume with chloroform. The initial volumes of tetrahexyl ammonium bromide taken were varied such that the final concentration of QHB in 100 mL of chloroform cover the range 2.0×10^{-6} to 2.0×10^{-4} M.

V Preparation of stock chloroform solutions of tetrahexyl ammonium picrate (QP)

Chloroform solutions of QP were made the same way as described for QHB,

except that excess NaP instead of NaHB was used. The concentrations of QP prapared ranged from 2.0×10^{-6} to 2×10^{-4} M.

7.2.2 APPARATUS

The rapid stir solvent extraction system incorporating the microporous membrane phase separator used in this work has been described in Chapter 4. Two different UV spectrophotometers were used as detector. The Varian UV-50 detector was used when continuous monitoring is possible. The HP photo diode array detector was used when continuous monitoring is not possible and samples have to be collected prior to detection. When chloroform was the phase being monitored, the phase separator membrane used consisted of two layers of Teflon sheet having 2-5 μm pore size and 0.0075 inch thick. On the other hand, when the aqueous phase was being monitored the phase separator membrane consisted of one layer of Whatman No. 2 filter paper. For all the experiments involving rapid stirring, 100.0 mL each of the organic and aqueous phase was used. The two phases were stirred at a constant speed of 2300 rpm and the flow rate of the phase being monitored was 1.0 mL/min.

Interfacial tensions were measured by means of the drop-volume method at $22^{o}C \pm 0.1$ [172], using a modified Gilmont micrometer buret (Scientific Apparatus, Arthur H. Thomas Co., Philadelphia, PA). The buret tip was made of a 0.3176 cm o.d. Teflon tube. In all the measurements, chloroform was the dropping phase while the second phase was 20 mL of aqueous solution which was previously equilibrated with chloroform.

7.2.3 MEASUREMENT OF TETRAHEXYL AMMONIUM ION ADSORPTION AT THE CHLOROFORM/WATER INTERFACE

A 100.0 mL volume of a solution of QBr in chloroform and 100.0 mL volume of aqueous buffer pH 6.5 were placed in the extraction cell. While stirring, 10.0 mL of the organic phase was sampled into a 125 mL separatory funnel by means of Teflon membrane

phase separator. The stirring was stopped and after allowing enough time for the phases to separate a second 10.0 mL portion of the organic phase was again taken. The amount of QBr present in each of these samples was measured by extraction as an ion-pair with 10.0 mL of 1.0 x 10^{-3} M solution of NaP followed by absorbance measurements at a wavelength of 372 nm. The amount of tetrahexyl ammonium ion, Q^+, that is adsorbed at the liquid-liquid interface when the mixture is being stirred corresponds to the difference between the amounts of QBr found in the two samples. The experiment was repeated over an initial QBr concentration in chloroform in the range of 5.0 x10^{-6} - 2.0 x 10^{-4} M.

7.2.4 MEASUREMENT OF SODIUM BROMOTHYMOL BLUE ADSORPTION AT THE CHLOROFORM/WATER INTERFACE

A 100.0 mL volume of chloroform and 100.0 mL of NaHB solution were measured into the extraction cell. While stirring, 10 ± 1 mL of the aqueous phase was separated by means of a filter paper membrane into a stoppered vial. The stirring was stopped and after allowing time for the phases to separate another 10 ± 1 mL of the aqueous phase was sampled into another vial. The absorbances of these samples were measured at 434 nm on a photo diode array UV spectrophotometer. The measured absorbances were converted to concentrations by dividing the absorbance values by the molar absorptivity (ε = 1.79 x10^4 L/(mole cm)) obtained from a linear A vs C calibration plot. The experiment was repeated for bromothymol blue concentrations ranging from 5.0 x 10^{-6} to 2.0 x 10^{-4} M

Another set of measurements was made to check the effect of the presence of tetrahexyl ammonium bromothymol blue ion-pair, QHB, in the chloroform phase on the adsorption of NaHB at the liquid-liquid interface. For these measurements the aqueous phase was a solution of NaHB while the chloroform phase contained 4.0 x 10^{-5} M of ion-pair.

7.2.5 MEASUREMENT OF TETRAHEXYL AMMONIUM BROMOTHYMOL BLUE ION-PAIR ADSORPTION AT THE CHLOROFORM/WATER INTERFACE

The procedure used is similar to that described for the adsorption of NaHB except that a Teflon membrane phase separator was used since it was the organic phase that was monitored. Also, absorbances were measured directly by pumping the chloroform phase through the flow cell of the Varian UV-50 spectrophotometer. The organic phase was 100.0 mL of chloroform solution of QHB while the aqueous phase was 100.0 mL of buffer pH 5.0 . The absorbance was monitored at a wavelength of 440 nm. Absorbances were converted to concentrations using $\varepsilon = 1.45 \times 10^4$ L mole^{-1} cm^{-1}, which was obtained from a linear A vs C calibration plot. The measurements were repeated over an initial QHB concentration range of 5.0×10^{-6} to 1.0×10^{-4} M. Four other sets of measurements were made to study the effect of the presence NaHB in the aqueous phase on the QHB adsorption. During these measurements the aqueous phase contained different concentrations 1.0, 2.0, 4.0 and 6.0×10^{-5} M, of NaHB.

7.2.6 MEASUREMENT OF TETRAHEXYL AMMONIUM PICRATE ION-PAIR ADSORPTION AT THE CHLOROFORM/WATER INTERFACE

The procedure used for the measurement of interfacial adsorption of tetrahexyl ammonium picrate ion-pair, QP, was similar to that described for the QHB except that the aqueous phase was phosphate buffer pH 6.5, while the organic phase was a chloroform solution of QP. Again the adsorption was studied over the initial concentration range of 2.0×10^{-6} to 1.0×10^{-4} M. Three sets of measurements were made. In the first set , a Teflon membrane was used to separate and monitor the bulk organic phase at a wavelength of 372 nm. Absorbances were converted to concentration by extrapolating from a non-linear A vs C calibration plot. Both the aqueous and the chloroform bulk phases used for this first set of measurements were kept for the second set of measurements. For the second set of measurements a Whatman No. 2 filter paper was used to separate and monitor the bulk

aqueous phase. About 10 mL samples of the aqueous phase were separated into stoppered vials for absorbance measurements at a wavelength of 362 nm. Absorbances were converted to concentrations using $\varepsilon = 1.5 \times 10^4$ L mole^{-1} cm^{-1}, which was obtained from a linear calibration A vs C plot. During the third set of measurements the aqueous phase was composed of 4.0×10^{-4} M of NaP while the chloroform phase was composed of QP in the range given above. The chloroform phase absorbance was monitored during this third set of measurements.

7.2.7 MEASUREMENT OF THE DISTRIBUTION COEFFICIENT OF TETRAHEXYL AMMONIUM BROMIDE BETWEEN CHLOROFORM AND WATER

The distribution coefficient of QBr between chloroform and phosphate buffer pH 6.5 was determined by the batch method followed by ion-pair extraction [173]. It was determined over an initial QBr concentration range of 5.0×10^{-6} - 1.0×10^{-4} M. Two versions of the method were used. The first version was used when the initial concentration of QBr in the organic phase was lower than 1.0×10^{-5} M. A 100.0 mL volume of a known concentration of QBr in chloroform was equilibrated by shaking in a separatory funnel with an equal volume of buffer. After the phases were allowed to separate 20.0 mL of the organic phase was pipetted and extracted with an equal volume of buffer containing an excess (x10) of NaP. The amount of QBr in the form of QP in the organic phase was determined spectrophotometrically on a photo diode array UV detector. Absorbances were converted to concentrations using $\varepsilon = 1.82 \times 10^4$ L mole^{-1}cm^{-1} , which was obtained from a linear A vs C calibration plot. A 50.0 mL volume of the original aqueous phase was analysed in a similar manner except that the ion-pair was extracted into a smaller volume (10.0 mL) of chloroform phase to enhance sensitivity of the absorbance measurement.

The second version of the method was used when the initial concentration of QBr in the chloroform was $\geq 1 \times 10^{-5}$ M. The experiment was performed in the rapid stir cell as described in section 7.2.3. The equilibrium concentration of QBr was determined in the

chloroform phase by the picrate method after the stirrer had been shut off and the phases allowed to coalesce. The equilibrium concentration in the aqueous phase was then calculated by difference using Equation 7.1A. This equation compensates for the change in phase ratio that was caused by removal of the 10.0 mL aliquot when the stirrer was still on (see section 7.2.3).

$$[QBr]_{a,ns} = \frac{1}{0.1}\left[[QBr]_o^* \times 0.1 - [QBr]_{o,s} \times 0.01 - [QBr]_{o,ns} \times 0.09\right] \quad (7.1A)$$

Values of $[QBr]_o$* are given in column 1 in Table 7.3.

7.3 RESULTS AND DISCUSSION

The choice of reagents used in this work was based on the ability to detect them in solution by spectrophotometric means. They must either be surface active or be capable of forming ion-pairs which have surface activity as well as high extraction constants from water into chloroform. Picric acid (2, 4, 6-trinitrophenol) was used in the form of the sodium salt (NaP). Bromothymol blue (3, 3'-dibromothymol sulphonephthalein), a diprotic acid ($pKa_1 = 1.4$, $pKa_2 = 7.4$ [177]), was used in the form of the monosodium salt (NaHB). Tetrahexyl ammonium bromide (QBr) forms colored ion-pairs with both of these salts.

7.3.1 INTERFACIAL TENSION MEASUREMENT

Surface (interfacial) tension, γ, is a physiochemical property that describes the energetics of the interface between two fluid phases. It is defined as the force which operates on a surface perpendicularly inward from the boundaries of the surface tending to decrease the area of the surface (units of Nm^{-1} or dynes cm^{-1}) [174]. The magnitude of

the interfacial tension between two immiscible liquids changes with changes in the properties of the liquid phases. Surface active solutes tend to decrease the interfacial tension while some inorganic solutes tend to increase the interfacial tension. For some ionic and amphiphatic surfactants, lowering of the interfacial tension continues until the critical micelle concentration, CMC. Beyond the CMC the interfacial tension becomes independent of the surfactant concentration [166, 174, 175]. The relationship between the interfacial tension (γ) and the amount of adsorbed surfactant (surface excess Γ, mole cm^{-2}) is given by the Gibb's adsorption equation [174] as follows;

$$\Gamma = \frac{-1}{RT}\left(\frac{d\gamma}{d\mathrm{Ln}\ C}\right) \qquad (7.1)$$

where R is the gas constant (8.314×10^7 ergs/mole K), T the absolute temperature and C is the bulk phase concentration of the surfactant (mole/L). There are several experimental techniques for measuring surface or interfacial tension. The most commonly used include the Wilhelmy plate, the Du Nouy ring and the Drop-weight-volume methods [176]. Among these methods the Drop-weight-volume is much simpler, rapid and more accurate [172, 176] especially for interfacial tension determinations.

DROP-WEIGHT-VOLUME METHOD

This technique involves measuring the mass or volume of a drop which detaches itself, under the influence of gravity alone, from the tip of a sharply cut and polished capillary of accurately known radius (o.d). Prior to detachment the weight of the drop is balanced by the surface tension of the liquid. Therefore at the point of detachment the surface tension is equal to the weight of the drop. Thus;

$$\gamma = \frac{mg\phi}{2\pi r} = \frac{V(\rho_1 - \rho_2)g}{r} F \qquad (7.2)$$

where m and V are the drop mass (g) and volume (mL) respectively, g is the local acceleration due to gravity (cm s^{-2}), r is the radius of the capillary (cm), $\rho_1 - \rho_2$ is the difference in densities of the two phases (g/mL), ϕ is an empirical correction factor and $F = \phi/2\pi$. It has been shown that the factor ϕ is independent of the nature of the liquid or the material of the capillary but depends only on the capillary constant, $r/V^{1/3}$. Tables of ϕ for $r/V^{1/3}$ ranging from 0.3 to 1.22 are available [172, 176].

Shown in Figure 7.1 are plots of the interfacial tension at the chloroform/aqueous buffer interface vs concentration for NaP, NaHB and QBr designated A, B and C respectively in the figure. It is clear that QBr and NaHB are highly surface active because they cause a decrease in the interfacial tension with increasing concentration. Although both QBr and NaHB have been found [177] to exist as micelles or aggregation complexes at high concentrations in solution, the interfacial tension data did not indicate the presence of any of these forms in the concentration range studied in this work. NaP on the other hand does not have any significant effect on the interfacial tension. Equation 7.1 suggests that a plot of γ vs Ln C should result in a curve on which the tangent at any point on the curve corresponds to the interfacial excess of the adsorbed solute. Such plots for the solutes studied are shown in Figure 7.2. The curve in each case is linear (constant slope) over the concentration range studied. The constant slope implies that at the concentrations used a saturated monolayer of adsorbed solute is present at the liquid-liquid interface. Prior to complete monolayer coverage of the interface by adsorbed solute the plots in Figure 7.2 are expected to be non-linear. However, because surface contamination at low surfactant concentrations becomes significant, the expected curvature is not observed. From the slopes the interfacial excess for QBr and NaHB are 5.6×10^{-11} and 2.0×10^{-10} moles/cm^2 respectively.

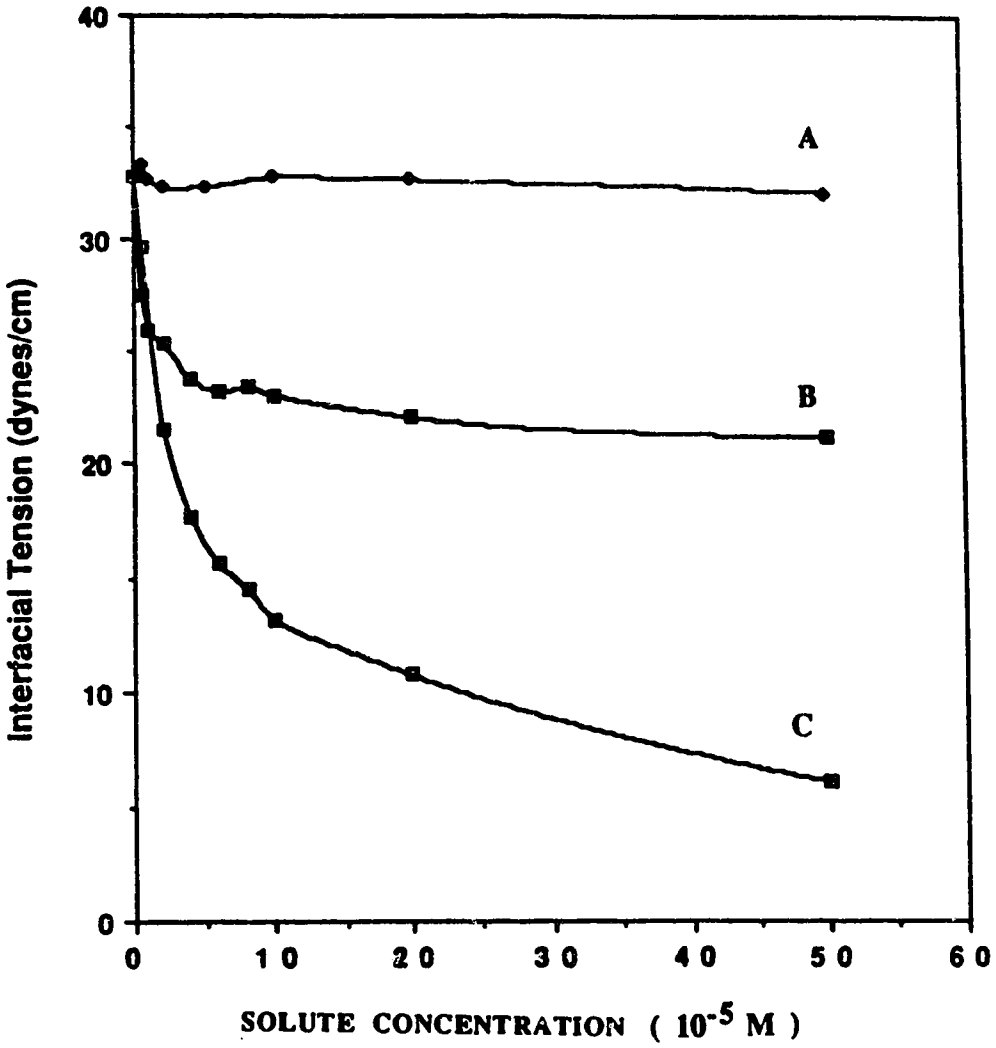

Figure 7.1 Plots of interfacial tension vs concentration of solute. Interfacial tension at the chloroform/water interface was measured by the drop-volume method. Solute: (A) NaP; (B) QBr; (C) NaHB.

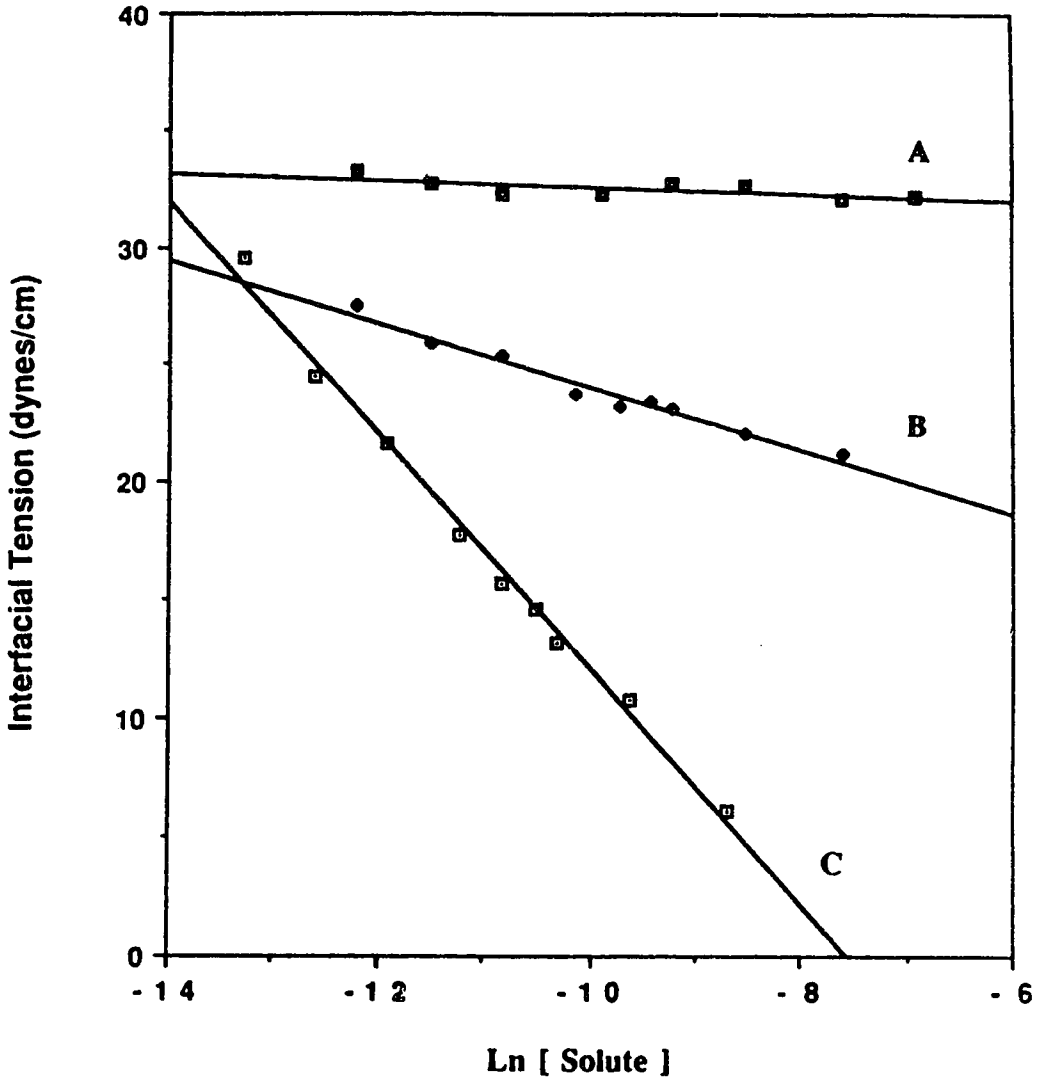

Figure 7.2 Plots of interfacial tension vs Ln [Solute] according to Equation 7.1 for the data in Figure 7.1. Solute: (A) NaP; (B) QBr; (C) NaHB.

7.3.2 MEASUREMENT OF AN ADSORPTION ISOTHERM AT THE LIQUID-LIQUID INTERFACE BY RAPID STIRRING AND MEMBRANE PHASE SEPARATION

It is possible with a microporous membrane phase separator (either Teflon or filter paper) to sample the bulk phase of one of the phases in a rapidly stirred two phase mixture. When the phase being monitored contains a surface active solute, there is a reversible and reproducible (<10% r.s.d) concentration change in the bulk phase between rapid stirring (large interfacial liquid-liquid area) and non-stirring (negligible interfacial area) conditions. The magnitude of the concentration change corresponds to the amount of solute that is adsorbed at the interface during rapid stirring. For a solute which has a significant solubility in both liquid phases the equilibrium distribution of the solute in the presence of a large liquid-liquid interfacial area can be described as follows;

$$i_o \rightleftharpoons i_I \rightleftharpoons i_a \qquad (7.3)$$

where i is the component of interest and the subscripts "o", "I" and "a" imply the organic phase, interface and the aqueous phase respectively. The distribution coefficient, K_D, of the solute between the two liquid phases is defined as;

$$K_D = \frac{C_o}{C_a} \qquad (7.4)$$

where C means concentration. Depending on the phase being monitored, the moles of surfactant that are adsorbed at the interface, n_{ads}, is given by the following expressions;

$$n_{ads} = C_{o,ns}\left[V_{o,ns} + \frac{V_{a,ns}}{K_{D,\,ns}} \right] - C_{o,s}\left[V_{o,s} + \frac{V_{a,s}}{K_{D,\,s}} \right] \qquad (7.5)$$

when the organic phase is the phase being monitored, and

$$n_{ads} = C_{a,ns}\left[V_{a,ns} + K_{D,\,ns}\,V_{o,s}\right] - C_{a,s}\left[V_{a,s} + K_{D,\,s}\,V_{o,s}\right] \qquad (7.6)$$

when it is the aqueous phase that is monitored. Here V is the volume of a liquid phase, and subscripts "ns" and "s" mean non-stirring and stirring, respectively. The adsorption isotherm is a plot of n_{ads} vs either $C_{o,\,s}$ or $C_{a,\,s}$.

If the adsorption of solute follows a Langmuir isotherm it will have the following characteristics. At low surfactant concentrations the value of n_{ads} will not be large enough to completely saturate the entire liquid-liquid interface with a monolayer of solute. By gradually increasing the concentration of the surfactant in the bulk phase n_{ads} will increase and eventually approach a constant value corresponding to the amount required to saturate the available interface with a monolayer.

By combining the data from the adsorption isotherm obtained by rapid stirring with interfacial tension data it is possible to estimate the total liquid-liquid interfacial area, A (units of cm^2), created during the dispersion of the two phases. The quantity n_{ads} is related to the interfacial excess by;

$$n_{ads} = \Gamma A \qquad (7.7)$$

Substituting for Γ from Equation 7.1 gives the expression;

$$n_{ads} = \frac{-1}{RT}\left(\frac{d\gamma}{d\mathrm{Ln}\,C}\right)A \qquad (7.8)$$

where the parenthetic term is the slope of the lines in Figure 7.2. From this equation, A can be calculated since n_{ads}, γ and C are known.

7.3.3 ADSORPTION OF NaHB AT THE CHLOROFORM/WATER INTERFACE

The interfacial adsorption of NaHB was measured by monitoring the change in concentration of NaHB in the aqueous phase. In order to evaluate the number of moles of NaHB adsorbed at the interface it is necessary to know the value of the liquid-liquid distribution coefficient, K_D , of NaHB between chloroform and aqueous buffer pH 5.0. To achieve this, K_D was calculated using the data shown in columns 2 and 3 of Table 7.1 which are the aqueous and organic phase concentrations of NaHB, respectively. At the pH, ionic strength and the concentration of NaHB used the solute, NaHB, exists in the chloroform phase as the acid, H_2B [177A]. The absence of NaHB in the chloroform phase is confirmed by the absence of absorbance at wavelengths greater than 290 nm. However, irrespective of the chemical form which the solute exists in the chloroform phase the total concentration of the solute in the chloroform phase will be designated as $[NaHB]_o$ hereafter. The concentration of NaHB in the aqueous phase, $[NaHB]_{a,ns}$, was obtained directly from the absorbance of the aqueous phase measured with the stirrer off, as described in section 7.2.4. The concentration of NaHB in the organic phase, $[NaHB]_{o,ns}$, was obtained by difference using Equation 7.8A. This equation, like Equation 7.1A, compensates for the change in phase ratio caused by removal of a 10.0 mL aliquot of aqueous phase while the stirrer was still on (see section 7.2.4).

$$[NaHB]_{o,ns} = \frac{1}{0.1}\left[[NaHB]_a^* \times 0.1 - [NaHB]_{a,s} \times 0.01 - [NaHB]_{a,ns} \times 0.09\right] \qquad (7.8A)$$

Values of $[NaHB]_a$* are given in column 1 in Table 7.1. A plot of $[NaHB]_{o,\,ns}$ vs $[NaHB]_{a,\,ns}$ should give a curve from which the distribution coefficient at any point can be calculated as the slope of a line drawn from the origin through the point. Figure 7.3 shows

that such a plot is linear (c.c.= 0.996) with zero ($0.08 \pm 0.26 \times 10^{-5}$ M) intercept, indicating that the distribution coefficient of NaHB between chloroform and aqueous buffer pH 5.0 is independent of concentration of NaHB over the range studied. The slope of the curve therefore corresponds to $K_D = 2.19 \pm 0.07$.

Substituting the value of K_D into Equation 7.6 allows the evaluation of the amount of NaHB that is adsorbed at the interface during rapid stirring. These values are given in column 4 of Table 7.1. A plot of the data in column 4 vs that in column 2 of this table is the interfacial adsorption isotherm, shown in Figure 7.4. To confirm whether the adsorption process follows the Langmuir behaviour, the data are also plotted according to the expression [174];

$$\frac{[NaHB]_{a,\,s}}{n_{ads}/V} = \frac{N_A\sigma^*}{A/V}[NaHB]_{a,\,s} + \frac{N_A\sigma^*}{K\ A/V} \qquad (7.9)$$

where N_A is Avogadro's number σ^* is the interfacial area occupied per molecule, A is the interfacial area, V is the volume of the aqueous phase, and K is the adsorption equilibrium constant (L $mole^{-1}$). For Langmuir adsorption behaviour a plot of $[NaHB]_{a,s}/(n_{ads}/V)$ vs $[NaHB]_{a,s}$ should be linear. Shown in Figure 7.5 is a plot of Equation 7.9 for the data in Table 7.1. The plot is linear with an intercept = 0.0147 ± 0.0105 and a slope = $0.1476 \pm 0.0062 \times 10^5$ L/mole. The linearity of the plot implies that adsorption of NaHB at the liquid-liquid interface is Langmuir in nature. The ratio of the slope to the intercept is equal to K, which for the adsorption of NaHB at the chloroform/aqueous buffer interface, is estimated to be $1.0 \pm 0.7 \times 10^6$ $Lmole^{-1}$.

Taking the amount of NaHB required to saturate the liquid-liquid interface to be 6.8 µmole (from the value of n_{ads} on the plateau of the curve in Figure 7.4) and taking ($d\gamma/dLn\ C$) to be 4.79 (from the slope of the line in Figure 7.2, curve C), the total interfacial area created during rapid stirring of 100.0 mL chloroform and 100.0 mL

aqueous buffer at 2300 rpm is estimated by Equation 7.8 to be 3.4 x 10^4 cm^2. From this value the average dispersed aqueous phase drop size is estimated to be 180 μm, which agrees with values reported in Chapter 4.

Also shown in Figure 7.4 is the plot of the amount of NaHB adsorbed when the organic phase contains a fixed added amount of QHB. It is expected that since both NaHB and QHB are surface active the amount of NaHB required to saturate the interface would be decreased. However, the similarity of the two plots indicates that there is no significant change in the interfacial concentration of NaHB resulting from the presence of the QHB. We can conclude therefore, that the chloroform/water interface is more selective for NaHB than for the QHB. Insofar as adsorption is due to polar influences, ionizable surfactants such as NaHB would be more surface active than neutral , less polarizable surfactants, i.e. QHB [178]. NaHB exists at the interface in the dissociated form with the HB^- anion adsorbed at the interface while sodium ions act as counterion in the diffused part of the double layer on the aqueous side of the interface [175]. The ion-pair, QHB, on the other hand, exists at the interface as a neutral species.

Table 7.1 NaHB Data for the Evaluation of Distribution Coefficient and the Liquid-Liquid Interfacial Adsorption Isotherm

$[NaHB]^*$ (10^{-5} M)	$[NaHB]_{a,ns}$ (10^{-5} M)	$[NaHB]_{o,ns}$ (10^{-5} M)	n_{ads} (10^{-6} mole)	$[NaHB]_{a,s}$ (10^{-5} M)
0.50	0.162	0.484	0.461	0.011
1.0	0.318	0.712	0.919	0.017
2.0	0.658	1.405	1.922	0.029
4.0	1.366	2.759	3.810	0.117
6.0	1.958	4.537	4.686	0.413
8.0	2.666	5.513	5.390	0.876
10.0	3.095	7.120	6.406	0.970
12.0	3.993	8.227	6.562	1.790
15.0	5.1[illegible]	10.08	7.622	2.605
20.0	6.308	13.91	6.261	4.127

(*) Concentration of NaHB in the aqueous phase prior to equilibration with chloroform.

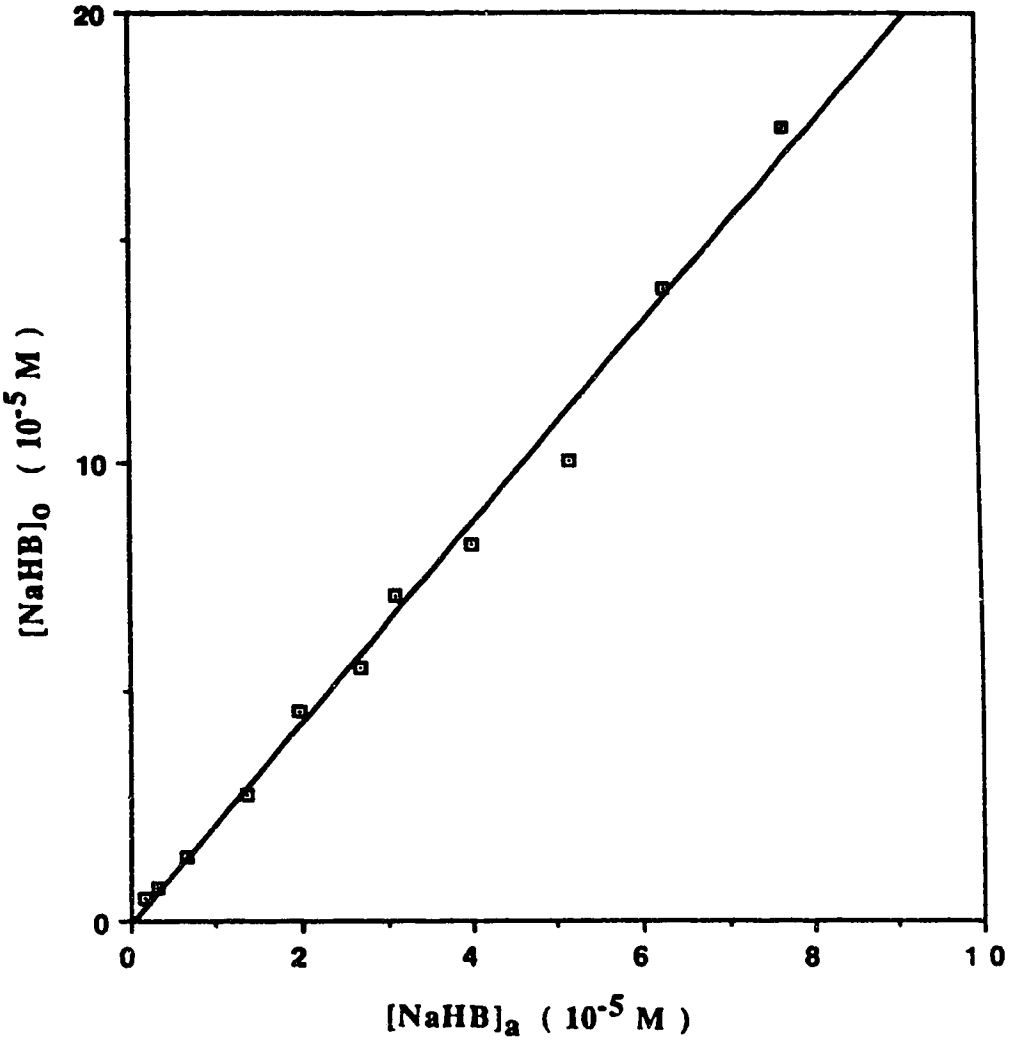

Figure 7.3 Plot of chloroform Phase concentration of NaHB *vs* aqueous phase concentration of NaHB after equilibration of equal volumes of the two phases. Aqueous phase absorbance (concentration) was measured on the HP doide array spectrophotometer and the organic phase concentration obtained by difference

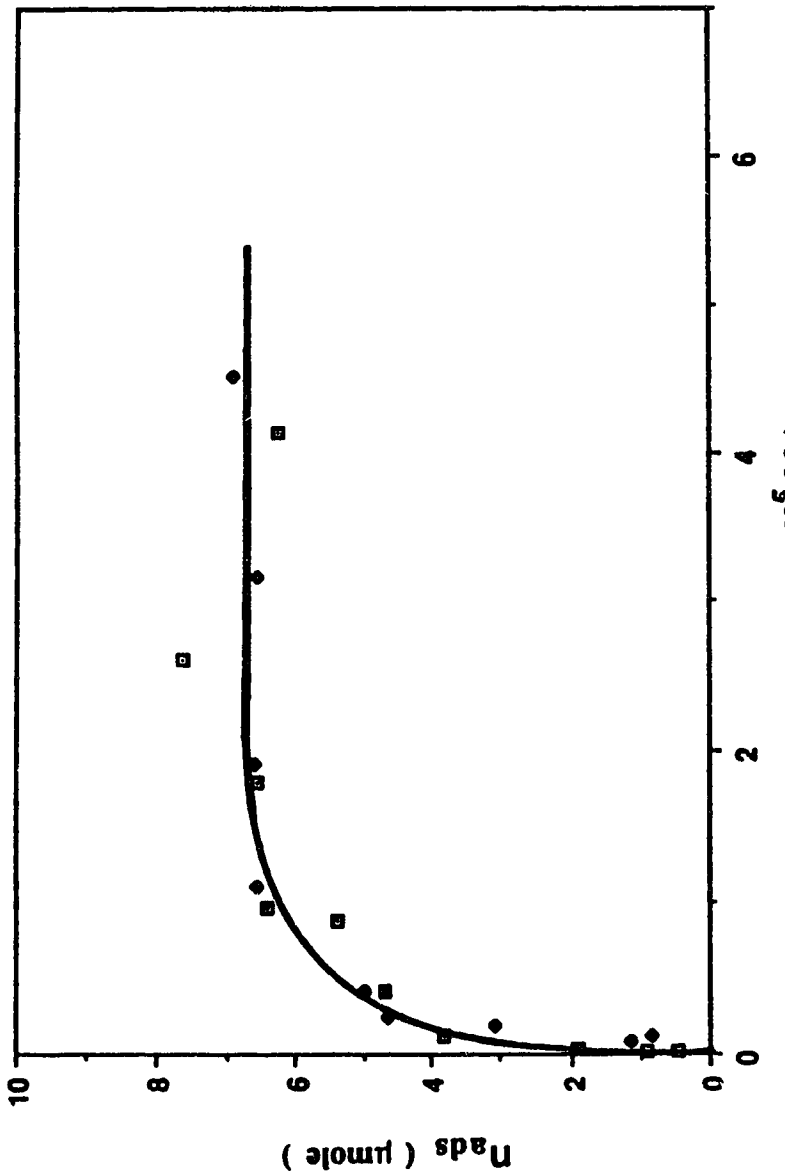

Figure 7.4 Adsorption isotherm for the adsorption of NaHB at the chloroform/water interface. Concentration of QHB in the chloroform phase: ⊡, 0.0; ◆, 4 x 10^{-5} M.

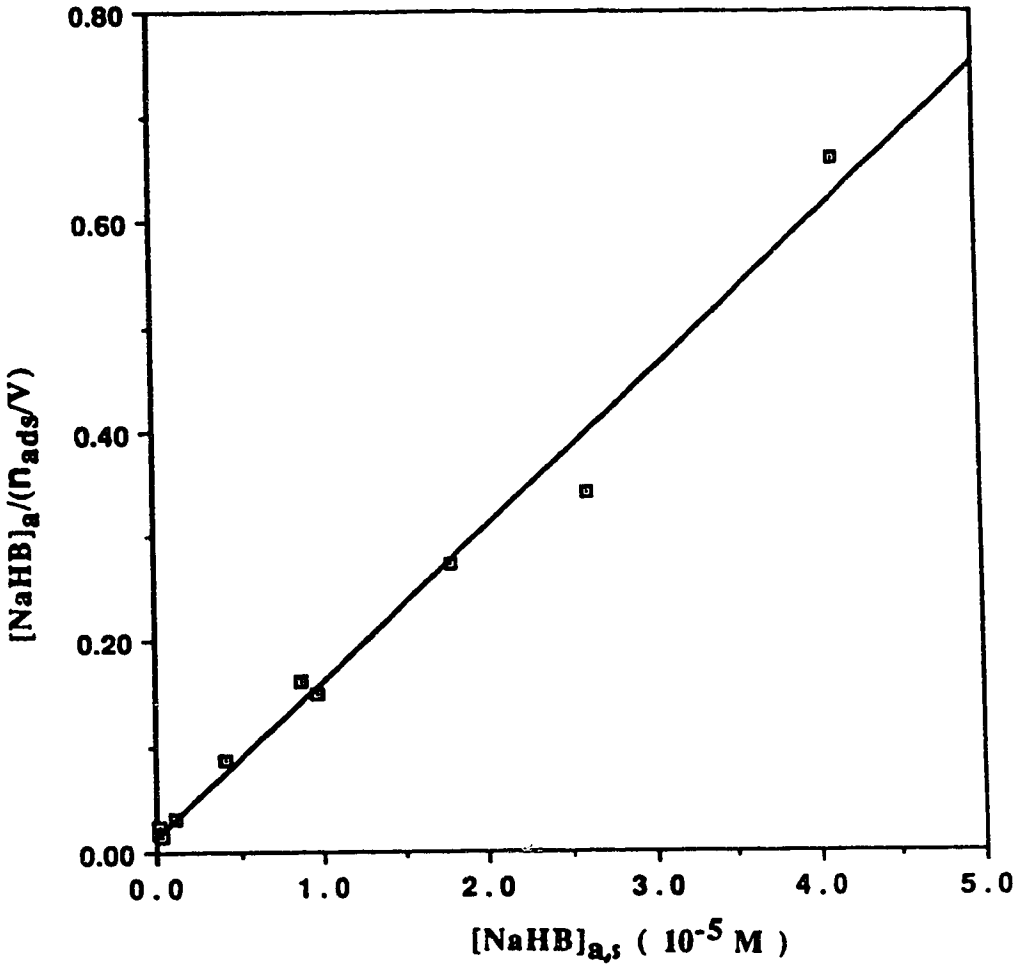

Figure 7.5 Langmuir plot for the adsorption of NaHB at the chloroform/water interface (see Equation 7.9).

7.3.4 ADSORPTION OF QHB AT THE CHLOROFORM/WATER INTERFACE

In order to measure the adsorption of QHB at the chloroform/water interface, it is necessary to first determine the liquid-liquid distribution coefficient for QHB. This was not done in this work. However, because QHB has a large extraction constant between chloroform and water ($\sim 10^{13}$) [179], and also because ion-pair formation in the aqueous phase is negligible [180], the distribution coefficient of QHB between chloroform and water is assumed to be large. Consequently, QHB is assumed to exist quantitatively in the chloroform phase.

The adsorption isotherm for QHB was measured by the rapid-stir with membrane phase separation method. The number of moles of QHB adsorbed (n_{ads}) at chloroform/ aqueous buffer interface during rapid stirring was estimated in a similar manner as described for NaHB. However, since it was the chloroform phase that was monitored for decrease in absorbance, ($\approx n_{ads}$) was calculated by Equation 7.5. Shown in Figure 7.6 is a series of adsorption isotherms for the adsorption of QHB at the chloroform/aqueous buffer interface during rapid stirring in the presence of various concentrations of NaHB. The isotherms do not exhibit the distinct plateau characteristic of monolayer adsorptions, especially in the presence of the lower concentrations of NaHB. The curves show the start of an upward curvature at higher concentrations of $[QHB]_o$. The increases in the amount of adsorbed solute after the plateau region may suggest a possible interaction between QHB molecules at the interface [181, 182]. Interaction between molecules at the interface is possible, especially for neutral solutes, since interfacial fluid properties such as viscosity, dielectric constant and density are entirely different from those of the bulk phases [164].

Quantitative Interpretation of the Effect of NaHB on the Adsorption of QHB

Application of Equation 7.9 to the isotherms in Figure 7.6 up to the points at which upward curvature becomes noticable indicates that up to this point all the isotherms

conform to Langmuir behaviour. The Langmuir plots are shown in Figure 7.7, while the slopes, intercepts and corresponding values of the interfacial adsorption constants, K, are given in Table 7.2. Since N_A and σ^* are constants for a given adsorbed species (for example, QHB), the slopes of the linear Langmuir plots are inversely proportional to A/V. Here, A is the interfacial area available for adsorption of QHB. In the presence of NaHB the value of A decreases with increasing concentration of NaHB because the interface is occupied by the more strongly adsorbed NaHB. Given in column 5 of Table 7.2 are the number of moles of QHB adsorbed on the plateau, $n_{ads,\ plateau}$, for each of the isotherms in Figure 7.6 and in column 6 the ratios of the values of $n_{ads,\ plateau}$ to the value of $n_{ads,\ plateau}$ (1.45×10^{-6} mole) corresponding to the isotherm obtained in the absence of NaHB. The corresponding fractions of the interface unoccupied by NaHB (1-Ø) are given in column 7. Here Ø is the fractional monolayer coverage of the interface by NaHB. A plot of the data in column 6 vs those in column 7 yields a straight line (see Figure 7.8) with an intercept = 0.10 ± 0.05 s.d. and a slope = 0.91 ± 0.06 s.d. The linearity of the curve indicates that the number of moles of QHB adsorbed is directly proportional to the interfacial area unoccupied by NaHB. Comparison of the number of moles (6.8×10^{-6} moles) of NaHB adsorbed on the plateau of the isotherm (Figure 7.4) with that for QHB adsorption (1.45×10^{-6} mole) from curve A in Figure 7.6 indicates that the interfacial area occupied per molecule of QHB is 4.7 times as large as that occupied by a molecule of NaHB. This value is in good agreement with the ratio of molecular areas of QHB to NaHB of about 5.0 which was estimated from the dimensions of models (CPK Models, Ealing Scientific Ltd., Quebec. Canada) of these molecules.

The values of the adsorption constants (column 4 in Table 7.2) indicate that the strength of QHB adsorption decreases with the number of moles of NaHB adsorbed at the interface. Shown in Figure 7.9 is a plot of Ln K vs Ø (values for Ø are in column 8 in Table 7.2). The plot is linear with an intercept = 11.81 ± 0.06 and a slope = $- 3.17 \pm 0.14$.

The linearity of the plot means that there is a linear dependence of the free energy of adsorption of QHB (i.e. $\Delta G = - RTLnK$) on the fractional coverage of the interface by NaHB. This implies that the chemical properties of the interface as an adsorbent are altered in a linear fashion with the extent of coverage by NaHB. Thus, the competitive adsorption between the strongly adsorbed NaHB and the weakly adsorbed QHB involve both a competition for space and a change in the chemical properties of the interface.

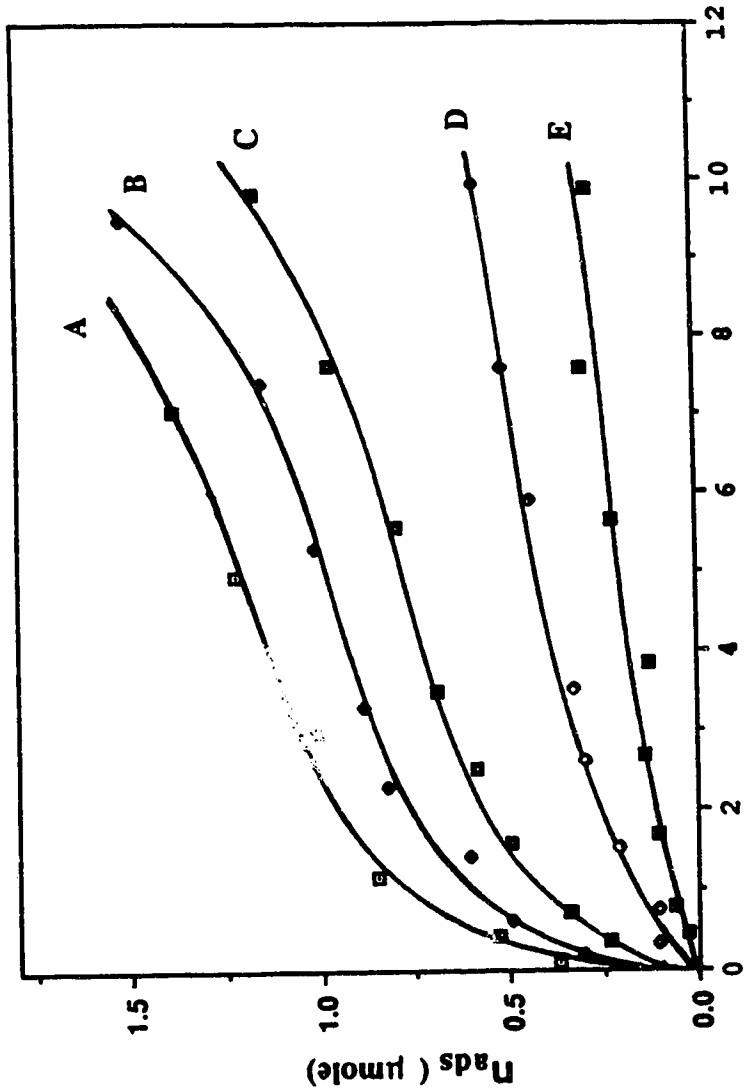

Figure 7.6 Adsorption isotherms for the adsorption of QHB at the chloroform/water interface. Concentration of NaHB in the aqueous phase is: (A) 0.0; (B) 1.0×10^{-5} M; (C) 2.0×10^{-5} M; (D) 4.0×10^{-5} M; (E) 6.0×10^{-5} M.

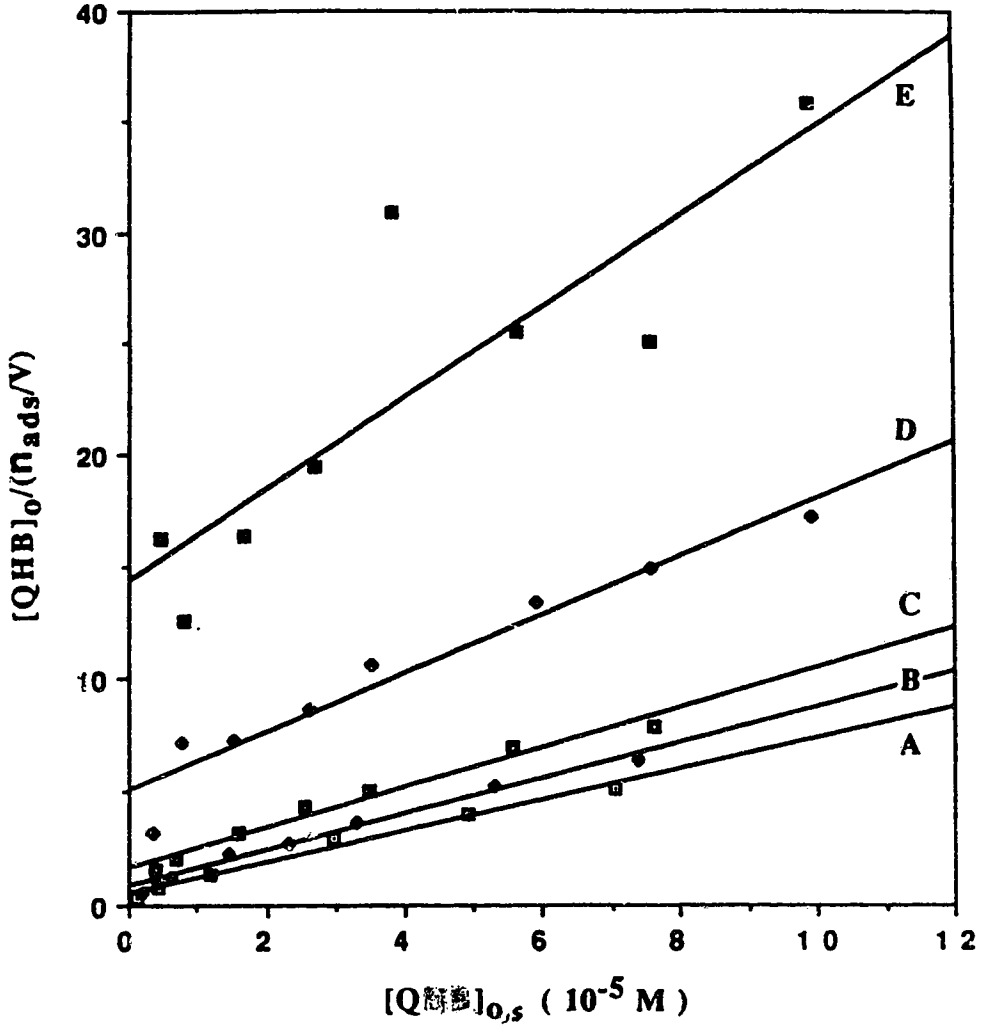

Figure 7.7 Langmuir plots for the adsorption of QHB at the chloroform/water interface. Concentration of NaHB in the aqueous phase is: (A) 0.0; (B) 1.0 x 10^{-5} M; (C) 2.0 x 10^{-5} M; (D) 4.0 x 10^{-5} M; (E) 6.0 x 10^{-5} M. (see Equation 7.9).

Table 7.2 Data for the adsorption of QHB in the presence of various concentrations of NaHB in the aqueous phase

[NaHB] (10^{-5} M)	Slope (10^{-5} M^{-1})	Intercept	K (10^{5} M^{-1})	$n_{ads, plateau}$	$\frac{n_{ads, plateau}}{n_{ads, plateau, max}}$	1-Ø	Ø
0.00	0.688±0.047	0.522±0.178	1.320±0.770	1.450	1.00	1.00	0.00
1.00	0.792±0.050	0.866±0.191	0.915±0.210	1.260	0.871	0.864	0.136
2.00	0.883±0.069	1.670±0.276	0.529±0.097	1.133	0.781	0.717	0.284
4.00	1.290±0.131	5.100±0.675	0.253±0.420	0.775	0.535	0.438	0.562
6.00	2.030±0.490	14.50±2.52	0.140±0.040	0.493	0.340	0.308	0.692

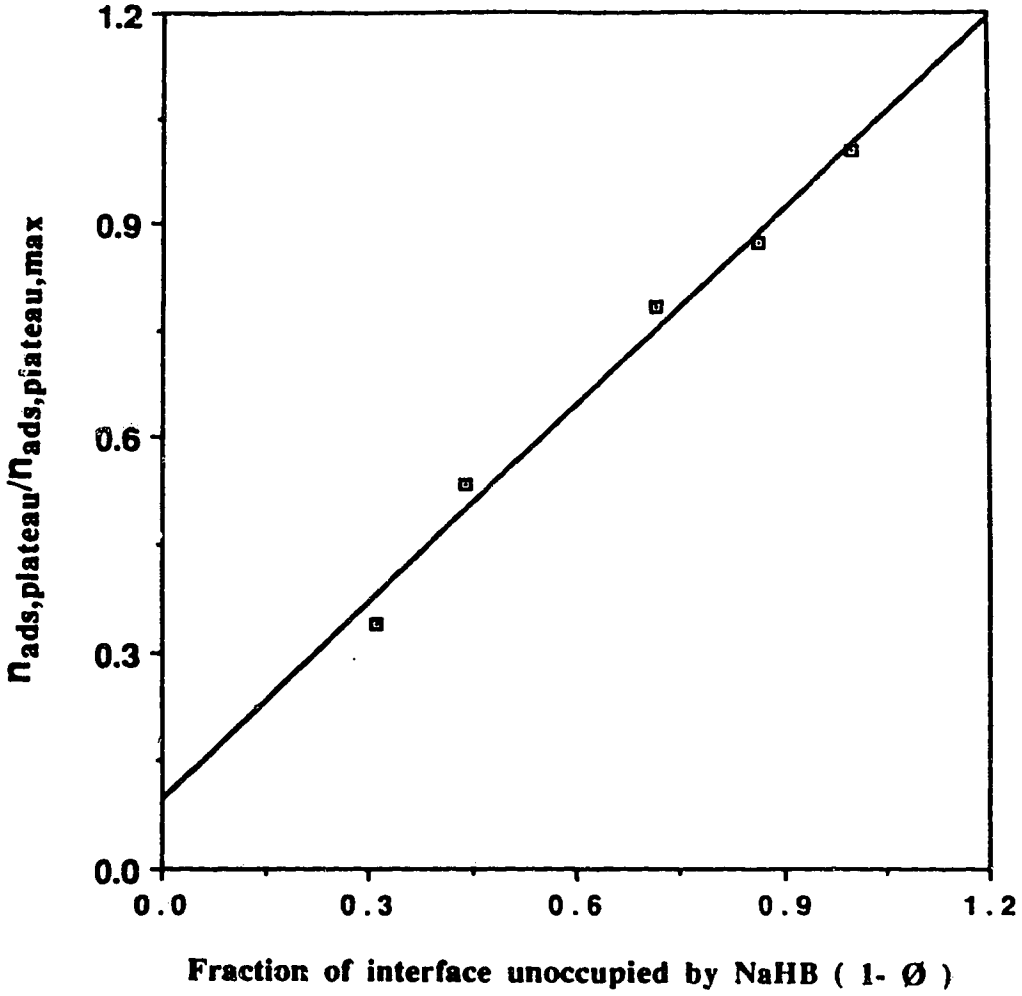

Figure 7.8 Plot of $n_{ads,\ plateau}/n_{ads,\ plateau,\ max}$ for the adsorption of QHB at the chloroform/water interface vs (1 - Ø). (1 - Ø) is the fraction of the interface unoccupied by NaHB. (see Table 7.2).

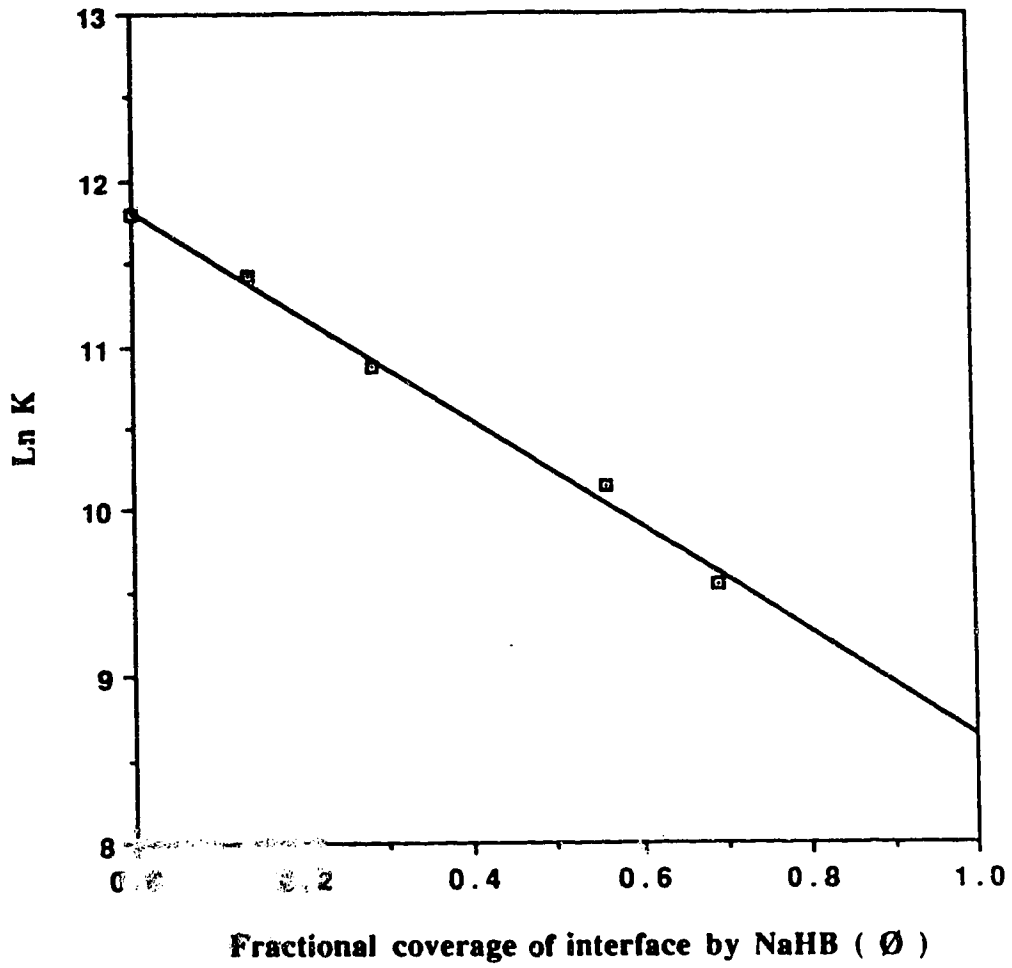

Figure 7.9 Plot of Ln K *vs* Ø. K is the adsorption constant for QHB and Ø is the fraction of the interface that is occupied by NaHB.

7.3.5 ADSORPTION OF TETRAHEXYL AMMONIUM BROMIDE AT THE CHLOROFORM/WATER INTERFACE

Owing to the fact that QBr exhibits significant solubility in both water and chloroform, the liquid-liquid distribution coefficient, K_D, between chloroform and aqueous buffer was measured prior to measuring the adsorption of QBr at the interface. Given in Table 7.3 are the initial concentrations of QBr in the chloroform phase and the corresponding concentrations found in both phases after equilibration with an equal volume of aqueous buffer pH 6.5. A plot of $[QBr]_o$ vs $[QBr]_a$ should produce a curve on which the tangent to the curve at any point corresponds K_D of QBr between the two phases. As shown in Figure 7.10, such a plot is nonlinear, implying that the distribution coefficient of QBr is concentration dependent. QBr exists in the aqueous phase in the dissociated form, while in the chloroform phase it exists as the ion-pair QBr. At equilibrium we have;

$$Q^+_a + Br^-_a \rightleftharpoons (QBr)_o \qquad (7.10)$$

from which the extraction constant, K_{ext}, is defined as;

$$K_{ext} = \frac{[QBr]_o}{[Q]_a[Br]_a} \qquad (7.11)$$

Since both $[Q^+]_a$ and $[QBr]_o$ are known quantitatively and also since $[Q^+]_a$ is equivalent to $[Br^-]_a$, a plot of $[QBr]_o$ vs the $[Q^+]_a^2$ should be linear with a slope corresponding to K_{ext}. In fact, the assumption that $[Q^+]_a$ is equal to $[Br^-]_a$ is valid since the buffer anion does not form extractable ion-pairs with Q^+ [176]. Shown in Figure 7.11 is the plot of $[QBr]_o$ vs $[Q^+]_a^2$. The plot is indeed linear (c.c. 0.985) with a slope of $2.1 \pm 0.2 \times 10^6$ M^{-1} and zero (0.75 ± 0.55) intercept.

The adsorption isotherm for QBr is shown in Figure 7.12. The number of moles, of QBr adsorbed at the interface during rapid stirring, n_{ads}, was calculated by Equation 7.5. The values of $K_{D,\,ns}$ and $K_{D,\,s}$ were obtained from Figure 7.8 as the tangent to the curve at corresponding concentrations of QBr. The value of n_{ads} on the plateau of the adsorption isotherm is 2.4×10^{-6} mole. Combining this data with the interfacial excess value of 5.6×10^{-11} mole/cm^2, the total liquid-liquid interfacial area created under the conditions of the experiment is 4.3×10^4 cm^2. From this value of the interfacial area, the dispersed aqueous phase drop size is estimated to be 140 μm. This value agrees with the value obtained when NaHB was the surfactant. Also, the value of the size of the dispersed aqueous drops agrees well with the value obtained in Chapter 4.

Table 7.3 Data for Estimating the Distribution Coefficient of QBr between Chloroform and Aqueous Buffer.

[QBr]* (10^{-5} M)	$[QBr]_a$ (10^{-5} M)	$[QBr]_o$ (10^{-5} M)	$[QBr]_a^2$ (10^{-10} M)
0.450	0.135	0.246	0.018
0.900	0.325	0.554	0.106
1.00	0.224	0.834	0.050
5.00	0.525	4.740	0.276
10.0	0.679	9.485	0.461

(*) Concentration of QBr in the chloroform phase prior to equilibration with aqueous buffer.

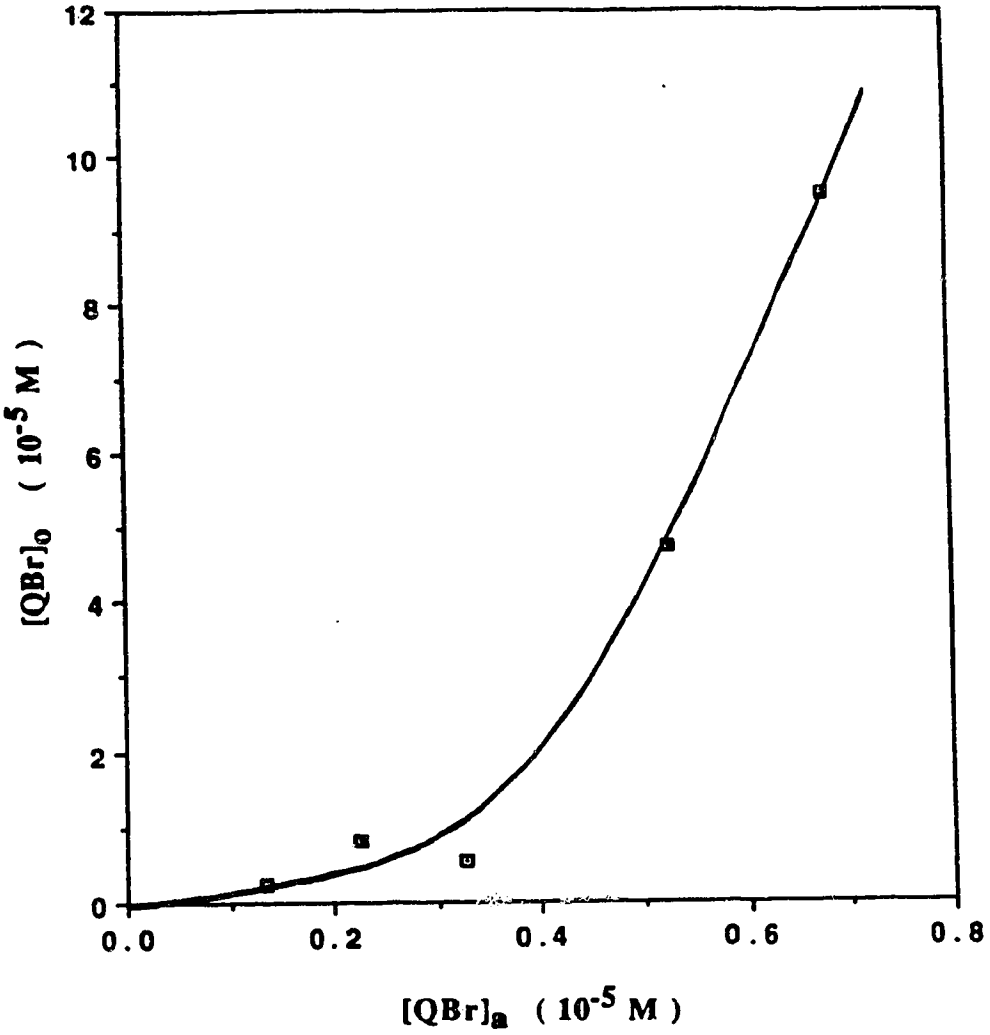

Figure 7.10 Plot of the chloroform phase concentration of QBr *vs* the aqueous phase concentration of QBr after equilibration of equal volumes of the two phases.

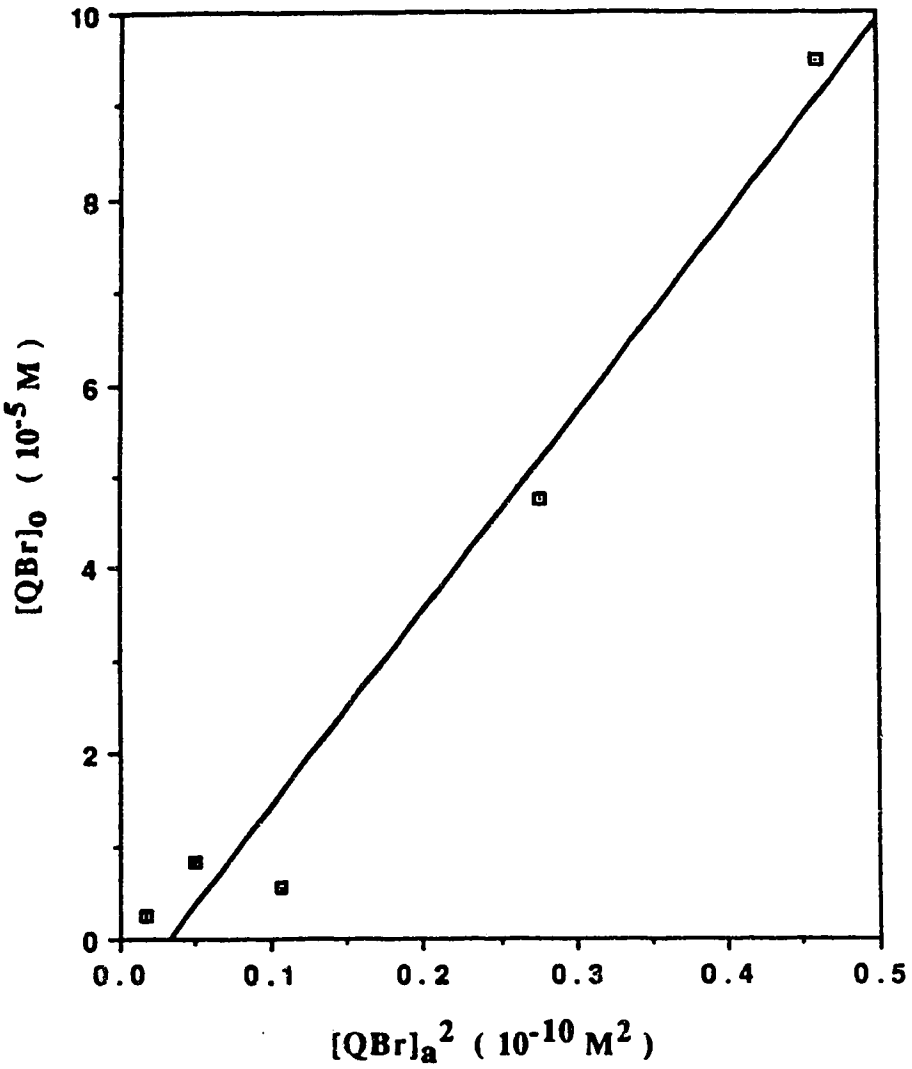

Figure 7.11 Plot of the chloroform phase concentration of QBr vs the square of the aqueous phase concentration after equilibration of equal volumes of the two phases. The slope of the line corresponds to K_{ext} in Equation 7.11.

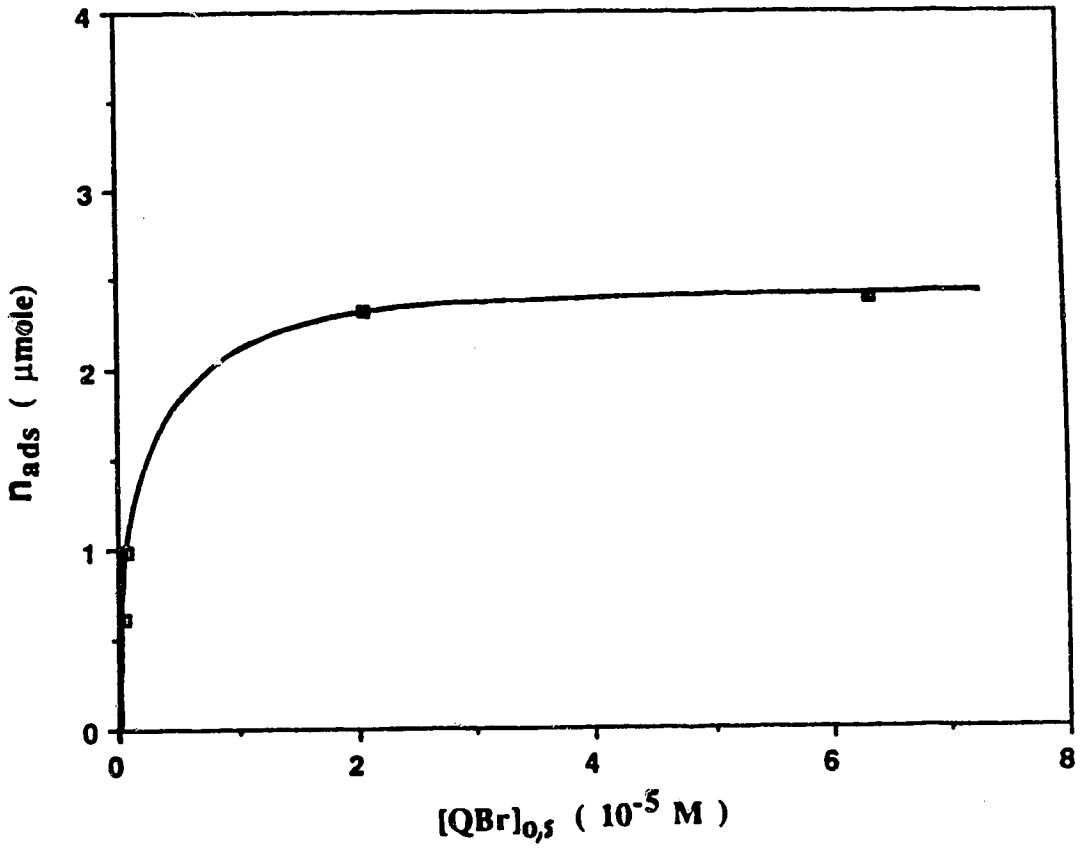

Figure 7.12 Adsorption isotherm for the adsorption of QBr at the chloroform/water interface. Measurement was made while stirring 100.0 mL each of chloroform and water at 38.3 rps.

7.3.6 ADSORPTION OF TETRAHEXYL AMMONIUM PICRATE AT THE CHLOROFORM/WATER INTERFACE

QBr and NaP react to form ion-pair, QP, which extracts from water into chloroform with an extraction constant of about $10^{10.6}$ [179]. In the presence of a large liquid-liquid interfacial area a significant amount of the ion-pair adsorbs at the interface, resulting in a decrease in the bulk chloroform phase concentration of the ion-pair. Shown in Figure 7.13 are the plots of the amount of QP adsorbed at the liquid-liquid interface during rapid stirring of 100.0 mL each of a chloroform solution of QP and an equal volume of aqueous buffer pH 6.5. Curve A is a plot of the number of moles, n_{ads}, of the solute adsorbed vs the concentration of the solute in the bulk chloroform phase when the original aqueous phase contained no NaP, while curve B is the plot of n_{ads} vs the concentration of QP in the bulk chloroform phase when the original aqueous phase contained an excess (4.0×10^{-4} M) of NaP. Application of Equation 7.9 to the data in curve A indicates that the adsorption behaviour at the interface does not follow the Langmuir model. It is interesting to note that although P^- does not exhibit any surface activity at the liquid-liquid interface, we still see a suppression of the number of moles of QP adsorbed when the original aqueous phase contains NaP.

To help explain this observed phenomenon another adsorption experiment was performed without NaP in the original aqueous phase. During this experiment the aqueous phase was monitored for P^-. Shown in curve B of Figure 7.14 is a plot of the concentration of NaP found in the aqueous phase vs the concentration of QP in the chloroform phase. Also shown by curve A in the same Figure is a plot of amount of QP adsorbed at the interface under the same conditions. It is important to remember that, because of the large extraction constant of QP, when a chloroform solution of QP is mixed with an aqueous phase in the presence of negligible interfacial area, no measurable amount of picrate anion exists in the aqueous phase at equilibrium. As indicated by curve B in Figure 7.14, during

rapid stirring (large interfacial area created) a significant concentration of picrate ion appears in the aqueous phase. The appearance of picrate in the aqueous phase is reversible. The picrate disappears from the aqueous phase once the interface is removed (stirrer off). It is clear therefore that the appearance of picrate in the aqueous phase is interfacially induced. Thus we have the equilibrium;

$$(QP)_o \rightleftharpoons (QP)_i \rightleftharpoons Q_i^+ + P_a^- \qquad (7.12)$$

where the subscripts "i", "o" and "a" mean interface, organic phase and aqueous phase respectively. The dissociation of QP occurs at the interface. However, because picrate ion is not surface active it enters the bulk aqueous phase rather than staying at the interface. The mass balance can therefore be expressed as;

$$n_{ads} = n_{QP,\,i} + n_{Q,\,i} \qquad (7.13)$$

At equilibrium the interface is occupied by the two species QP and Q^+. The ratio of QP to Q^+ at the interface is dependent, however, upon the concentration of picrate ion, P^-, in the aqueous phase.

Measurement of the Ion-Pair Formation Constant (K_{IP}) at the Interface

Although evidence for dissociation of ion-pairs in the organic phase exists [180], this was not studied in this work. The measured absorbance of the chloroform phase corresponds to the total concentration, C_O, of all forms of ion-pair components in the chloroform phase. Thus, whether or not dissociation of the ion-pair occurs in the chloroform phase, it is irrelevant in this work.

From Equation 7.12, the ion-pair formation constant at the interface is expressed as;

$$K_{IP} = \frac{[QP]_i}{[Q^+]_i\,[P^-]_a} \qquad (7.14)$$

Let the distribution constant for QP between the interface and the bulk chloroform phase be;

$$K_{ads} = \frac{[QP]_i}{C_o} \qquad (7.15)$$

and let K'_{ads} be the ratio of all forms of Q at the interface to C_o. Thus, K'_{ads} is expressed as;

$$K'_{ads} = \frac{n_{ads}}{A\,C_o} \qquad (7.16)$$

By substituting for $[Q^+]_i$ from Equation 7.14 into Equation 7.13, one obtains

$$n_{ads} = [QP]_i\,A + \frac{[QP]_i\,A}{K_{IP}[P^-]_a} \qquad (7.17)$$

As shown by Equation 7.17, n_{ads} decreases with increasing concentration of P^- and eventually approaches a limiting value $[QP]_iA$ at high concentrations (4.0×10^{-4} M) of P^-. The experimental data for n_{ads} obtained under this condition is plotted as curve B in Figure 7.13. Similarly, by substituting Equation 7.17 into Equation 7.16 it can be shown that

$$K'_{ads} = K_{ads} + \frac{[QP]_i}{C_o K_{IP}[P^-]_a} \qquad (7.18)$$

therefore at high concentrations of P^-, $K'_{ads} = K_{ads}$. Thus, the number of moles of QP adsorbed in the presence of high concentrations of picrate in the aqueous phase at a given

C_o is the same as the number of moles of solute at the interface in the form of QP that will be adsorbed at the same C_o when the original aqueous phase contains no picrate ion.

From Equation 7.12, when no other source of P^- is present other than QP, then n_Q is equal to n_P. Hence, Equation 7.14 can be expressed as;

$$K_{IP} = \frac{n_{QP} V_a}{n_P^2} \qquad (7.19)$$

or

$$n_P^2 = \frac{1}{K_{IP}} [n_{QP} V_a] \qquad (7.20)$$

where n_P is the number of moles of picrate ions in the aqueous phase of volume V_a.

A plot of n_P^2 vs ($n_{QP} V_a$) should be linear with zero intercept and a slope corresponding to $1/K_{IP}$. The experimental values for n_{QP} can be obtained in two ways.

hod 1. The values of n_{QP} at different values of C_o are taken as the differences between mber of moles plotted in curves A and B in Figure 7.14, while n_P is taken as the r of moles plotted in curve B of the same figure at corresponding C_o. Shown in .15 is a plot of Equation 7.20 for the data in Figure 7.14. The plot is indeed linear. The slope, intercept and the corresponding values of K_{IP} are given in Table 7.4. The average value for K_{IP} obtained by this method is $0.81 \pm 0.61 \times 10^5$ L/mole.

Method 2. As shown above, $n_{ads} = n_{QP}$ when the concentration of picrate in the aqueous phase is made large by addition of NaP (4.0×10^{-4} M). Therefore the values for n_{ads} were the data plotted in Curve B in Figure 7.13. The plot of Equation 7.20 using this method is shown in Figure 7.16. The values of the slope, intercept and K_{IP} are also given in Table 7.4.

The average value for K_{IP} obtained by this method is $1.43 \pm 0.03 \times 10^5$ L/mole. Using this value of K_{IP} the percentage dissociation of QP at the interface when the aqueous phase contains 4.0×10^{-4} M of NaP is only 1.5 % over the whole range of C_o studied. Therefore, the assumption of complete suppression of dissociation under this condition is justified.

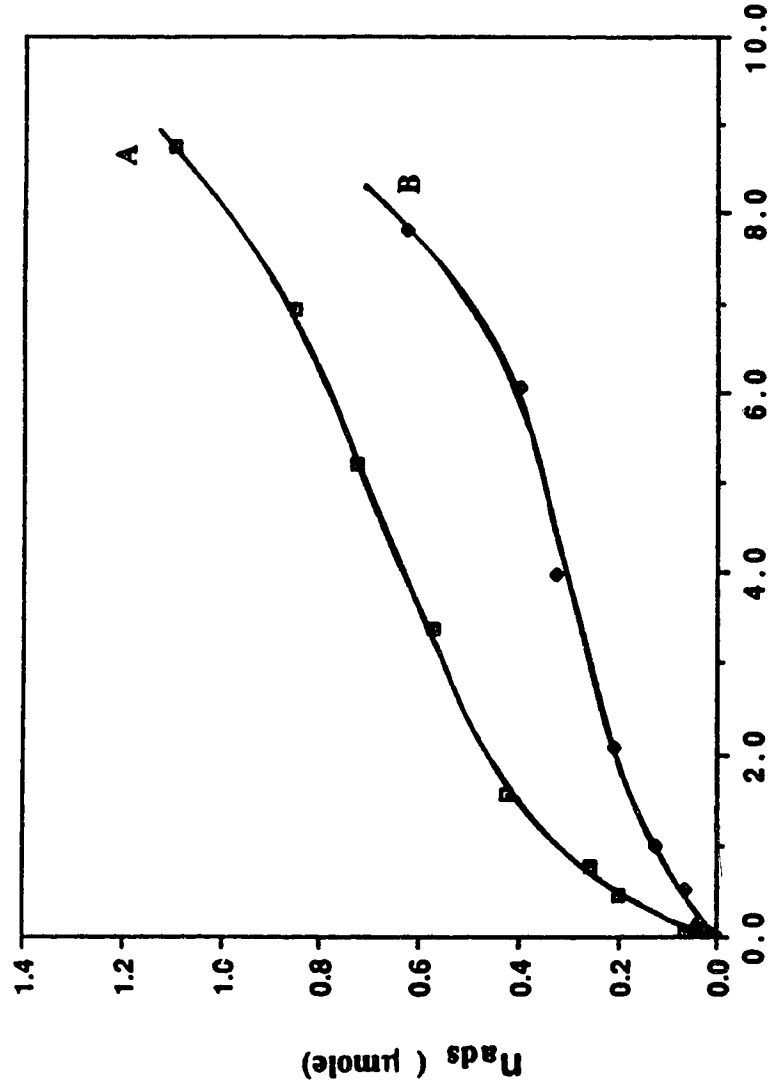

Figure 7.13 Adsorption isotherms for the adsorption of QP at the chloroform/water interface. Initial concentration of NaP in the water phase is: (A) 0.0 M; (B) 4.0×10^{-5} M.

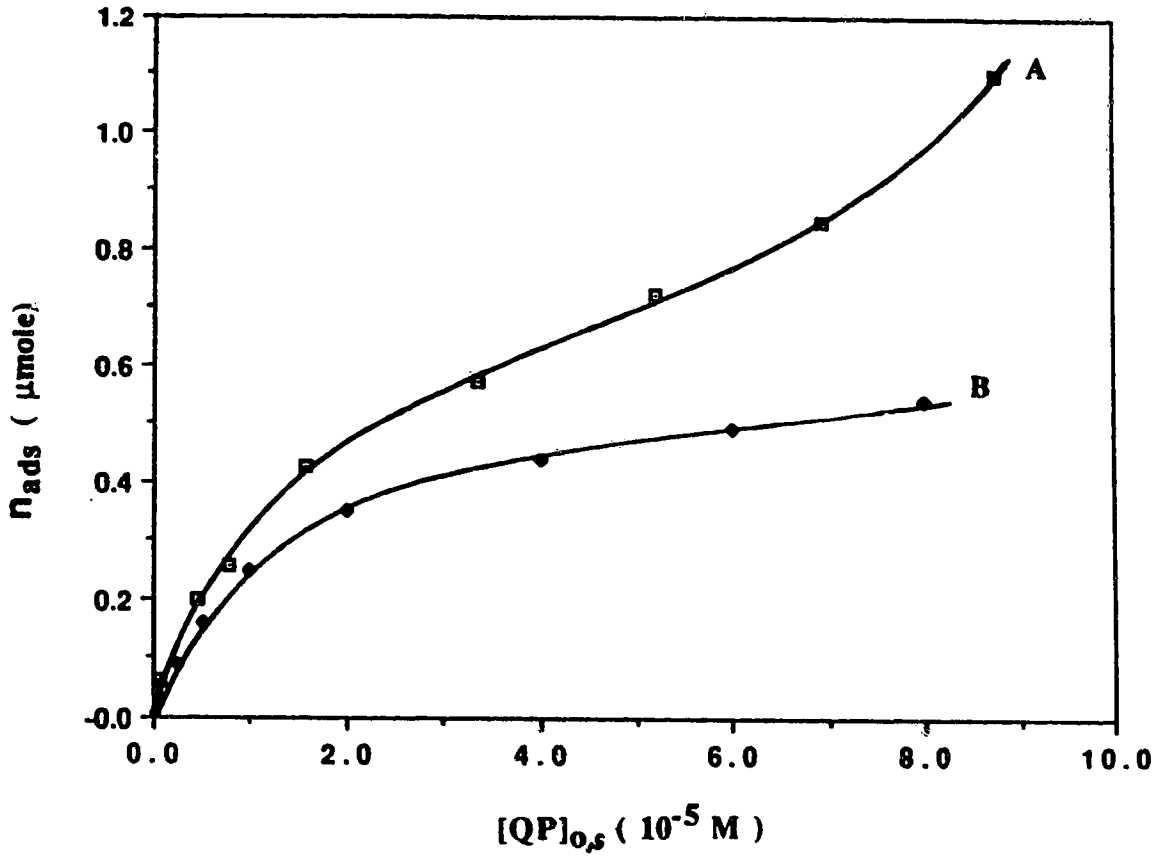

Figure 7.14 Curve (A); Adsorption isotherm for the adsorption of QP at the chloroform/water interface. (same as curve A in Figure 7.13)
Curve (B); Plot of the number of moles of NaP found in 100.0 mL of the aqueous phase during the adsorption studies in Curve A.

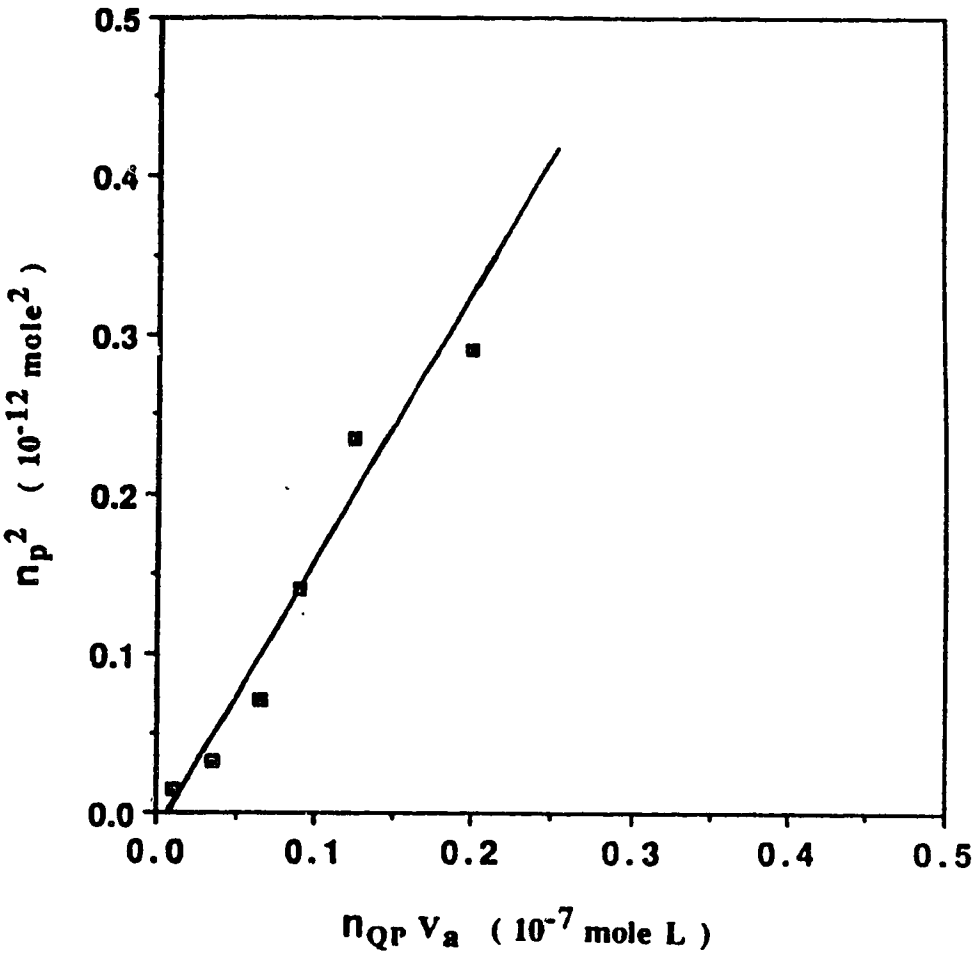

Figure 7.15 Plot of the square of the number of moles of NaP found in the aqueous phase vs the number of moles of QP adsorbed at the chloroform/water interface (see Equation 7.20). The moles of QP adsorbed were calculated as described in Method 1.

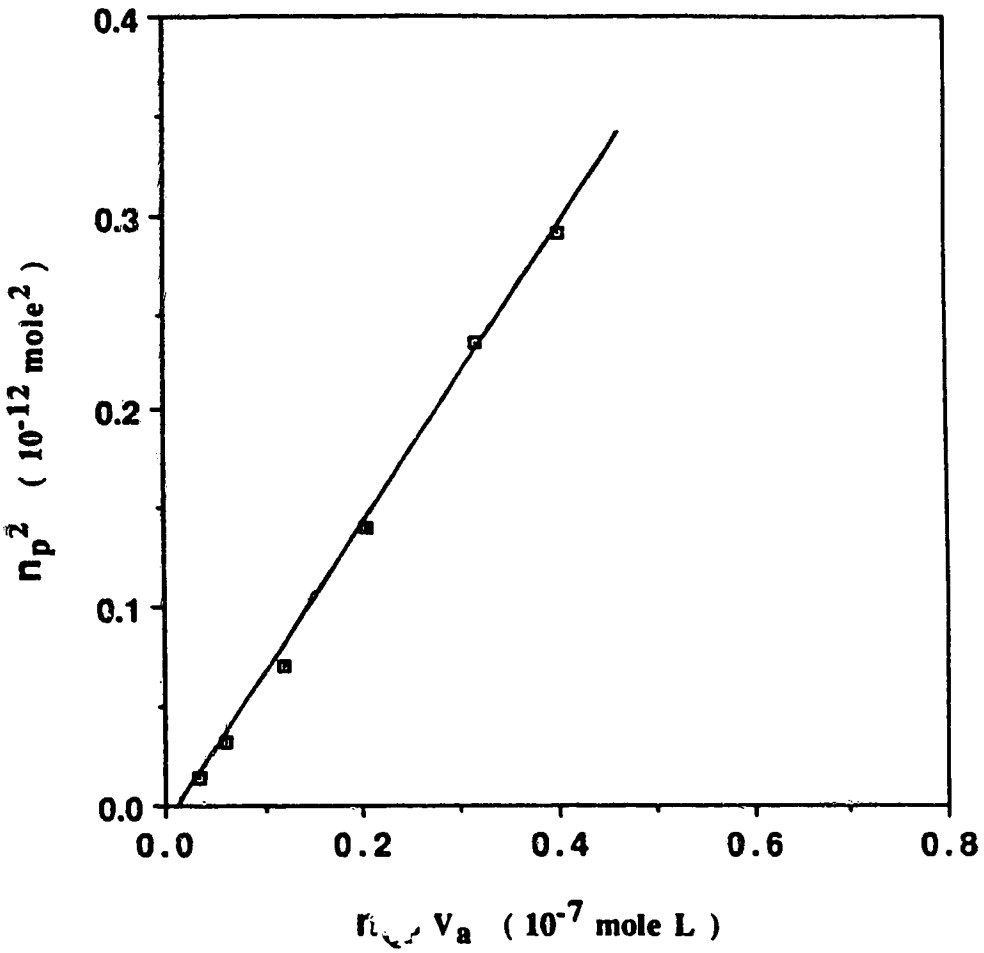

Figure 7.16 Plot of the square of the number of moles of NaP found in the aqueous phase vs the number of moles of QP adsorbed at the chloroform/water interface (see Equation 7.20). The moles of QP adsorbed were calculated as described in Method 2.

Table 7.4 Values of the Ion-pair Formation Constant at the Liquid-Liquid Interface for Tetrahexylammonium Picrate

n_{QP}	Intercept	Slope (10^{-5} mole/L)	K_{IP} (10^{5} L/mole)
Method 1	-0.0168 ± 0.0188	0.998 ± 0.123	1.00 ± 0.11
	-0.0102 ± 0.0200*	1.610 ± 0.186*	0.62 ± 0.06*
Method 2	-0.013 ± 0.002	0.644 ± 0.008	1.55 ± 0.00
	-0.015 ± 0.004*	0.765 ± 0.016*	1.31 ± 0.03*
(Double-	-0.0453 ± 0.0217	1.799 ± 0.219	0.563 ± 0.062
layer)	-0.0320 ± 0.0266*	2.816 ± 0.394*	0.355 ± 0.043*

(*) These data were obtained on a different day.

7.3.7 APPLICATION OF THE ELECTRICAL PROPERTIES OF THE INTERFACE TO THE ESTIMATION OF THE ION-PAIR FORMATION CONSTANT AT THE CHLOROFORM/WATER INTERFACE

The discussion presented in Section 7.3.6 did not take into consideration the effect of charge at the liquid-liquid interface on the evaluation of the concentration of picrate ions that will be in equilibrium with solutes (QP and Q) adsorbed at the interface. Owing to the positive charge on Q the interface will acquire an electrical potential (ψ_0) which can be described by the Gouy-Chapman Equation [174, 175, 183-185];

$$\text{Sinh}\left(\frac{ZF\psi_o}{2RT}\right) = (8.53 \times 10^4)\, I^{-1/2}\, \sigma \qquad (7.21)$$

where Z is the charge on Q, F is the Faraday constant, R is the ideal gas constant, T is the absolute temperature and I is the ionic strength of the aqueous phase. The surface charge density, σ (c/cm^2), can be calculated as follows;

$$\sigma = ZF\Gamma \qquad (7.22)$$

It might be assumed that it is only those picrate ions near to the interface that will be in equilibrium with the species at the interface but not those in the bulk aqueous phase as assumed in section 7.3.6. The concentration of picrate ion in the aqueous phase near the interface is given by the Boltzmann Equation [175, 183, 184];

$$C_{P,i} = C_{P,\,bulk} \exp\left(\frac{-ZF\psi_x}{RT}\right) \qquad (7.23)$$

where the value of Z is the charge on P (i.e., -1). ψ_x is the potential at a distance x cm away from the interface itself. The value of x is taken to be 10^{-7} cm , which corresponds to the thickness of the adsorbed layer. ψ_x is calculated as follows;

$$\psi_x = \frac{2kT}{ze} \mathrm{Ln}\left(\frac{1 + \chi\exp[-\kappa x]}{1 - \chi\exp[-\kappa x]}\right) \qquad (7.24)$$

where k is the Boltzmann constant, $1/\kappa$ is a measure of thickness of the double-layer, and χ is a complex ratio defined as follows [174, 175]:

$$\chi = \frac{\exp[ze\psi_o/2kT] - 1}{\exp[ze\psi_o/2kT] + 1} \qquad (7.24A)$$

Expressing the concentration of $C_{P,i}$ in terms of moles and substituting it into Equation 7.20 gives Equation 7.25.

$$n_{p,i}^2 = \frac{1}{K_{IP}}\left(\frac{n_{QP} V_a}{\exp(-ZF\psi_x/RT)}\right) \qquad (7.25)$$

Equation 7.25 predicts that a plot of $(n_{p,i})^2$ vs $(n_{QP} V_a / \exp(-ZF\psi_x/RT)$ should be linear with zero intercept and a slope corresponding to $1/K_{IP}$. The slopes and intercepts of the plots of Equation 7.25 are given in row 3 (double-layer) in Table 7.4 along with the values of K_{IP}. The average value of $K_{IP} = 0.459 \pm 0.075 \times 10^5$ L/mole, calculated from Equation 7.25, is about 50 % smaller than that calculated from Equation 7.20. This discrepancy could be due to the fact that, as pointed out by Cockbain [166], the double-layer theory does not exactly apply to an adsorbed film which is in a dynamic equilibrium with the bulk solution.

CHAPTER 8

KINETIC STUDIES ON THE EXTRACTION OF TETRAHEXYL AMMONIUM ION-PAIRS WITH BROMOTHYMOL BLUE AND PICRATE

8.1 INTRODUCTION

Although numerous reports on the kinetic aspects of ion-pair extraction have been published [32, 34, 76-81, 83, 186, 187], there is still no consensus on the mechanism [32,70, 77, 80,] of ion-pair formation and on the factors that affect the extraction rate [32, 76, 79, 81]. Higuchi et.al [32] have studied the extraction of dextromethorphan hydrobromide from water into chloroform under the slow stirring conditions of the Lewis cell, and concluded that the extraction rate was governed by diffusional mass tarnsfer. Their conclusion was later supported by Lippold et.al. [188]. The hydrodynamic conditions under which these studies were performed, however, preclude any observation of possible chemical reaction rate since the Lewis cell connot be operated in the "chemical kinetic" regime [77]. In other reports by Nordgren et.al. [77, 80, 81, 187] on studies on ion-pair extraction by the single drop technique, it was concluded that the rate of mass transfer was fast while subsequent ion-pair formation in the organic phase was the rate limiting step [77, 80].

More recently, Cantwell and Freiser [70] have disputed this claim. They have measured the rate of extraction of tetrabutyl ammonium picrate from water into chloroform using the rapid-stir technique and a porous Teflon membrane phase separator. With rapid stirring k_{mt} (Equation 2.12) can be made large because both the mass transfer coefficient, β_{mt} , and the specific surface area, A/V_1 , can be made large. A large value of k_{obs} increases the possibility of observing the rate of ion-pair formation as discussed in Section 2.5. It was concluded that $k_r >> k_{mt}$ because the first order extraction rate constants (0.4 s^{-1}) were found to be independent of the concentration of the ion pairing reagents and also

because the magnitude of the rate constant was similar to that obtained for the extraction of *o*-nitroaniline, a process which, undoubtedly, is mass transfer controlled. Thus, for ion-pair extraction the actual ion-pair formation reaction itself is fast and does not influence the ion-pair extraction rate.

In all of the work discussed above no attempt was made to study the effect of interfacial adsorption of reagents on the extraction rate despite the fact that Harada et.al. [189] and Nordgren et.al. [81] had noted decreases in extraction rates in the presence of interfacial adsorption of surfactants. In fact, studies on the extraction of copper with LIX reagents [84] and the extraction of nickel with 8-quinolinols [69] have indicated that adsorption at the liquid-liquid interface plays an important role on the mechanism of metal extraction. Also, a theoretical model [165] describing the transfer of surface-active agents across the liquid-liquid interface has suggested that the presence of an adsorption or desorption barrier can significantly affect the bulk concentration profile and decrease the mass transfer rate.

In this chapter, the effect of interfacial adsorption of ion-pair reagents and products on the extraction rates of ion-pairs of tetrahexyl ammonium bromothymol blue and tetrahexyl ammonium picrate will be presented.

8.2 EXPERIMENTAL

8.2.1 REAGENTS

Two stock solutions of *o*-nitroaniline (BDH Ltd. Poole, England) were prepared, both at a concentration of 1.00×10^{-1} M. One was prepared with aqueous phosphate buffer pH = 5.0 and ionic strength 0.05 as solvent and the other with chloroform as solvent. Other reagents used were as described in Section 7.2.1. These included, among others, two aqueous phosphate buffers, one at pH = 5.0 and the other at pH= 6.5, and both with ionic strength 0.05; aqueous 5.00×10^{-4} M NaHB in phosphate buffer (pH =5.0, ionic strength 0.05); aqueous 1.00×10^{-4} M QBr in phosphate buffer (pH = 5.0, ionic strength

0.05); and aqueous 1.00 x 10^{-3} M NaP in phosphate buffer (pH= 6.5, ionic strength 0.05).

8.2.2 APPARATUS

The rapid-stir apparatus used for this study has already been described in Chapter 4, while the experimental parameters were described in Section 7.2.2. Extraction data were acquired digitally at an acqusition rate of one point every 200 ms. Each A vs t extraction profile was defined by 512 data points.

8.2.3 EFFECT OF INTERFACIAL ADSORPTION OF BROMOTHYMOL BLUE ON THE EXTRACTION RATE OF *o*-NITROANILINE

Initially, 100.0 mL of chloroform and 99.0 mL of an aqueous buffer (pH = 5.0) were measured into the extraction cell. 1.00 mL of the aqueous stock solution of *o*-nitroaniline was pipetted into the injector before assembling it, as described in Chapter 4. Stirring of the two phases in the extraction cell was begun and, after allowing enough time for the phases to equilibrate, injection was made to start the extraction while the absorbance of the chloroform phase was being monitored with time at 396 nm. The extraction was repeated with various concentrations of NaHB (1.0 x 10^{-5} - 2.0 x 10^{-4} M) added to the aqueous phase. In another experiment, 1.00 mL of the stock chloroform solution of *o*-nitroaniline was injected into a mixture of 100.0 mL of aqueous buffer and 99.0 mL chloroform and the absorbance of the chloroform phase monitored with time. Data from this latter experiment was used to generate the IRF required for deconvolving to eliminate the distortions caused by instrument band broadening.

8.2.4 EFFECTS OF SODIUM PICRATE ON THE EXTRACTION RATE OF *o*-NITROANILINE

The experiments performed to study the effects of sodium picrate on the extraction rate of *o*-nitroaniline were similar to those described in Section 8.2.3 except that the aqueous phase consisted of different concentrations of NaP instead of NaHB.

8.2.5 MEASUREMENT OF THE EXTRACTION RATE OF TETRAHEXYL AMMONIUM BROMOTHYMOL BLUE

Initially, 100.0 mL of chloroform and 99.0 mL of NaHB solution (pH = 5.0) were measured into the extraction cell. An appropriate volume of a stock aqueous solution of QBr was pipetted into the injector before assembling it as described. The volume of QBr solution to be injected was such that the ratio of the equilibrium concentration of NaHB to that of QBr was always greater than or equal to unity. Stirring of the two bulk phases in the extraction cell was initiated and, after allowing enough time for the phases to equilibrate, injection was made to start the extraction while the absorbance of the chloroform phase was being monitored at 412 nm with time. The extraction was repeated at different concentrations (2.00×10^{-6} - 2.00×10^{-4} M) of NaHB in the aqueous phase while the concentration of QBr injected was maintained constant throughout a set. In all, the concentrations of QBr extracted were 0.20, 0.50, 1.00, 5.00and 7.50×10^{-5} M. In another experiment, 1.00 mL of a stock chloroform solution of tetrahexyl ammonium bromothymol blue, QHB, was injected into a mixture of 100.0 mL of aqueous buffer pH = 5.0 and 99.0 mL of chloroform and the absorbance of the aqueous phase was monitored with time. Data from this latter experiment was used to generate the IRF required for deconvolving to eliminate the distortions caused by instrument band broadening.

8.2.6 MEASUREMENT OF THE EXTRACTION RATE FOR TETRAHEXYL AMMONIUM PICRATE

The procedure used for this extraction was as described in section 8.2.5 except that the pH of the aqueous phase was 6.5, and the concentrations of NaP used varied from 1.00 x 10^{-5} to 2.00 x 10^{-4} M. Also, the wavelength at which the chloroform phase was monitored was 375 nm.

8.3 RESULTS AND DISCUSSION

All the kinetic data presented in this chapter were obtained from extraction A vs t profiles that had been corrected for instrument band broadening by deconvolution. Any interfacial concentration data that are used in this chapter were obtained as described in Chapter 7.

8.3.1 EFFECT OF SODIUM BROMOTHYMOL BLUE ON THE EXTRACTION RATE OF *o*-NITROANILINE

The extraction of *o*-nitroaniline from aqueous buffer into chloroform has already been discussed in Chapter 5. It was found that the rate of extraction was solely mass transfer controlled, with a first order extraction rate constant of about 1.0 s^{-1}. *o*-Nitroaniline is not adsorbed at the liquid-liquid interface. The effect of NaHB in the aqueous phase on the rate of extraction of *o*-nitroaniline is shown by curve B in Figure 8.1. There is a decrease of the extraction rate constant of this non-adsorbed compound towards a limiting value with increasing concentration of NaHB. As shown in Chapter 7, NaHB is highly surface active and adsorbs at the liquid-liquid interface; as a result the overall resistance to mass transfer, R_O, in Equation 2.6 increases.

Although the exact mechanism by which interfacial adsorption of a surface active agent increases the resistance to mass transfer for a non-adsorbed solute is not fully understood, two mechanisms have been propounded, the hydrodynamic and the barrier

mechanisms [39, 124, 163, 164, 190]. The hydrodynamic mechanism assumes that the presence of a film of surfactant at the liquid-liquid interface significantly changes the hydrodynamic properties, such as viscosity of the interface [39, 163]. This leads to a decrease in the transfer of momentum from one liquid phase to another liquid phase across the interface and, consequently, to reduced convection in the liquid phase. In terms of the two-film model, this means the thickness of the Nernst diffusion films increases. In Equation 2.6 this corresponds to increases in R_1 and R_2. According to the "hydrodynamic mechanism" the value of R_i is still essentially zero even when surfactant is adsorbed at the interface. The barrier mechanism, on the other hand, assumes that the surfactant molecules form a kind of a barrier to diffusing solute molecules [20]. This is represented in Equation 2.6 by giving R_i a non-zero value.

Irrespective of the mechanism by which adsorbed solutes decrease extraction rates, it is important that the extent of the suppresson of the rate constant be known so that the extraction rate in the absence of surfactant can be obtained. To do this, it is necessary to calculate a correction factor, F, which, when multiplied by an experimental rate constant obtained in the presence of a known concentration of surfactant, will give the corresponding rate constant in the absence of the surfactant. The correction factor can be calculated from the extraction rate data for a solute for which the extraction is purely mass transfer controlled. The equation for F is given by;

$$F = \frac{k_{mt}}{k_{mt,\ surf}} \qquad (8.1)$$

where k_{mt} and $k_{mt,\ surf}$ are the mass transfer rate constants for the solute in the absence of and in the presence of surfactant respectively. Because F is related to the concentration of surfactant at the interface it varies with the total concentration of surfactant . Shown in Figure 8.2 is a plot of F vs the total concentration of NaHB for the extraction of *o*-

nitroaniline. F was calculated from the data in Figure 8.1, Curve B. This plot can be used to correct for the suppression of the extraction rate constant caused by the adsorption of NaHB at the liquid-liquid interface for the extraction of a non-adsorbed solute whose extraction is purely mass transfer controlled.

8.3.2 EFFECT OF SODIUM PICRATE ON THE EXTRACTION RATE OF *o*-NITROANILINE

The presence of NaP in the aqueous phase during the extraction of *o*-nitroaniline has no measurable effect on the extraction rate constant for the non-adsorbed compound *o*-nitroaniline. This is illustrated by curve A in Figure 8.1. The fact that NaP shows no effect on the extraction rate constant for *o*-nitroaniline is consistent with the fact that NaP does not adsorb at the interface, as shown in Chapter 7.

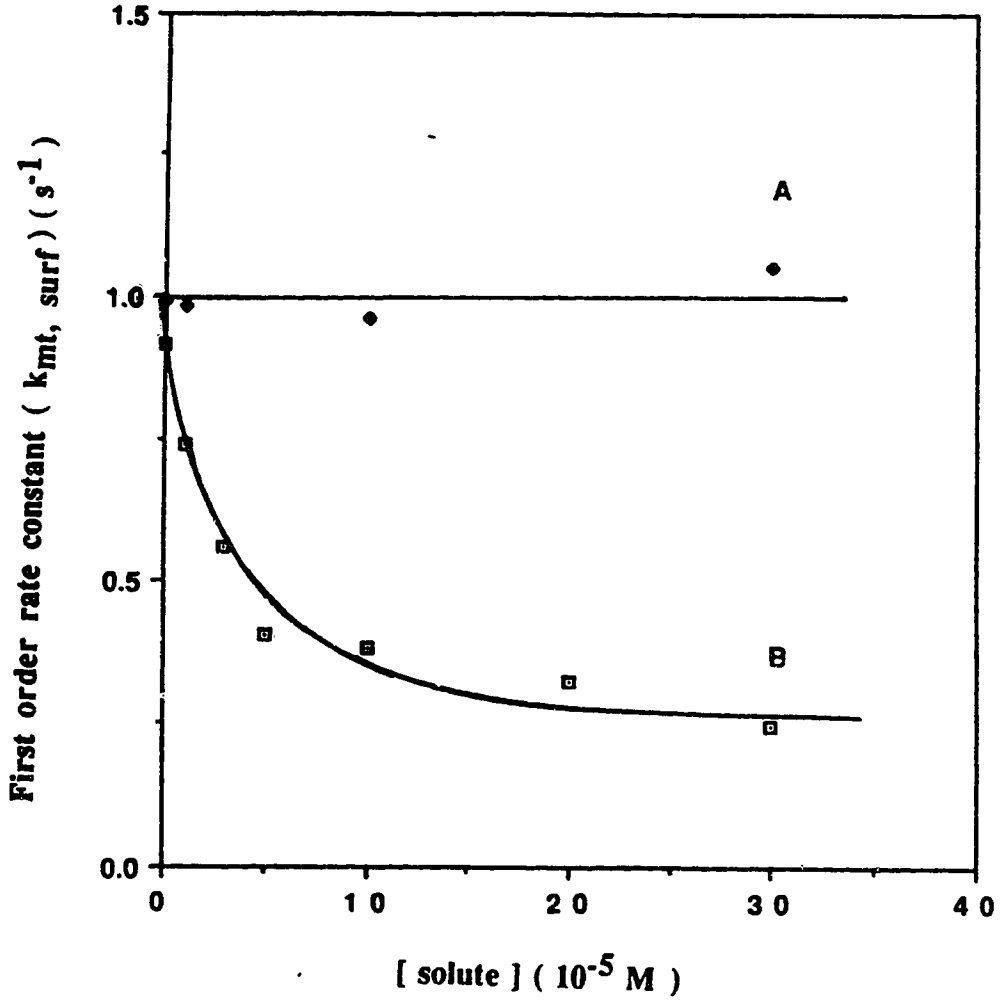

Figure 8.1 Plots of $k_{mt, surf}$ vs [solute] (i.e., NaP or NaHB) for the extraction of o-nitroaniline from water into chloroform. Solute: (A) NaP; (B) NaHB.

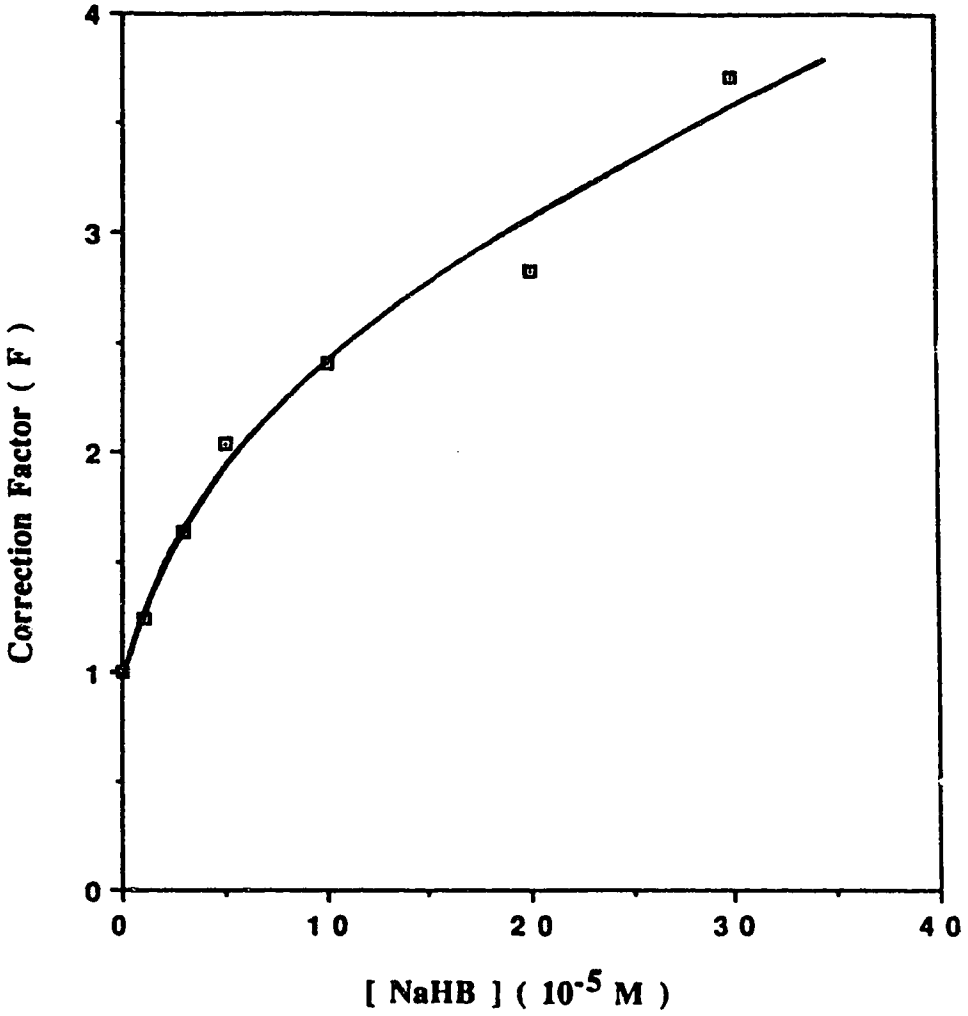

Figure 8.2 Plot of the correction factor, F, in Equation 8.1 vs [NaHB] in the aqueous phase. (see Section 8.3.1 for details).

8.3.3 EXTRACTION OF TETRAHEXYL AMMONIUM BROMOTHYMOL BLUE

The extraction of QHB as an ion-pair from aqueous buffer into chloroform was performed under conditions such that the ratio of initial [NaHB] to the initial [QBr] was always equal to or greater than unity. As shown in Chapter 7, both QHB and NaHB are surface active. Hence, the extraction can be described as involving the transfer of a surface active solute, QHB, in the presence of another surface active solute, NaHB. Shown in Figure 8.3 are the absorbance(not normalized) vs time profiles for a series of extractions of QHB from aqueous buffer into chloroform. The number of moles of QBr injected for each of these extractions was the same (1.00×10^{-5} M), while the concentration of NaHB in the aqueous phase prior to injection was different for each curve. The values of the absorbances on the equilibrium plateau of the profiles (at ratios $\leq$ 1:5, i.e., Figure 8.3A) indicate that, although the same amount of limiting reagent, QBr, was used, the equilibrium absorbance (concentration) of the ion-pair in the chloroform phase increases with increasing concentration of NaHB. For ratios > 1:5 the equilibrium absorbances approach the same limiting value (based on [QBr] injected). Also, for these higher ratios equilibrium is attained over much longer times (Figure 8.3B). A plot of the equilibrium absorbances vs the concentration of NaHB remaining in the aqueous phase after ion-pair formation is shown in Figure 8.4. The equilibrium absorbance increases to a maximum value after which it remains constant with further increase in NaHB concentration. This phenomenon can be explained by the fact that both QHB and NaHB are surface active and therefore adsorb at the liquid-liquid interface during rapid stirring of a mixture of chloroform and water. As shown in Chapter 7, NaHB is more selectively adsorbed than QHB. Therefore, as the concentration of NaHB remaining in the aqueous phase after the ion-pair formation ($[NaHB]_{excess} = [NaHB]_{added} - [QBr]_{injected}$) is increased, the amount of NaHB that will be adsorbed at the interface will also increase and therefore less

and less interface will be available for QHB to adsorb. Consequently, more and more of QHB will be displaced into the bulk chloroform phase.

To calculate the ion-pair extraction rate constant the extraction profiles in Figure 8.3 were normalized with respect to their equilibrium absorbance values to give the profiles shown in Figure 8.5. The normalized absorbance vs time profiles (see Figure 8.5A) indicate that the rate of ion-pair extraction increases with [$NaHB]_{excess}$ over the range 1.00×10^{-5} to 5.00×10^{-5} M. At values of $[NaHB]_{excess}$ greater than 5.00×10^{-5} M the extraction rate decreases with further increases in $[NaHB]_{excess}$ (see Figure 8.5B). The first order rate constant $k_{mt,surf}$ for each of the profiles in Figure 8.5 was calculated using the integrated first order rate equation (Equation 2.11) after deconvolving with the IRF to correct for instrument band broadening. Values of k_{mt} were then calculated from values of $k_{mt,surf}$ by multiplying by the appropriate values of F. Given in column 6 in Tables 8.1 to 8.5 are the resulting extraction rate constants, k_{mt}, for the extraction of QHB from aqueous buffer into chloroform. In Figure 8.6 are shown plots of k_{mt} (from column 6 in Tables 8.1 to 8.5) vs $[NaHB]_{excess}$ (from column 2 in the tables).

Two kinds of dependence on $[NaHB]_{excess}$ are evident from the curves in Figure 8.6, depending on the value of $[QBr]_{injected}$. At lower values of $[QBr]_{injected}$ ($\leq 0.50 \times 10^{-5}$ M) the value of k_{mt} increases with increasing $[NaHB]_{excess}$ and approaches a limiting plateau at higher $[NaHB]_{excess}$. At higher $[QBr]_{injected}$ the value of k_{mt} initially increases with increasing $[NaHB]_{excess}$ but, instead of leveling off, it then decreases with further increases in $[NaHB]_{excess}$. The reasons for these dependencies of k_{mt} on $[NaHB]_{excess}$ are explained separately in the following sections.

Table 8.1 Ion-Pair Extraction Data for the Extraction of QHB. Concentration of QBr injected = 0.20×10^{-5} M.

[NaHB] (10^{-5} M)	$[NaHB]_{excess}$ (10^{-5} M)	$(NaHB)_{ads}$ (10^{-6} mole)	$k_{mt,surf}$ (s^{-1})	F	k_{mt} (s^{-1})
0.60	0.40	0.62	0.122	1.10	0.132
0.80	0.60	0.85	0.130	1.14	0.148
1.20	1.00	1.25	0.174	1.24	0.216
2.00	1.80	2.05	0.200	1.41	0.282
4.00	3.80	3.67	0.270	1.80	0.486
8.00	7.80	5.75	0.340	2.26	0.768
10.0	9.80	6.25	0.350	2.40	0.840
15.0	14.8	6.70	0.425	2.62	1.110

Table 8.2 Ion-Pair Extraction Data for the Extraction of QHB. Concentration of QBr injected = 0.50×10^{-5} M.

[NaHB] (10^{-5} M)	$[NaHB]_{excess}$ (10^{-5} M)	$(NaHB)_{ads}$ (10^{-6} mole)	$k_{mt,surf}$ (s^{-1})	F	k_{mt} (s^{-1})
0.50	0.00	0.52	0.129	1.00	0.129
1.00	0.50	1.05	0.180	1.12	0.202
1.50	1.00	1.57	0.213	1.24	0.264
2.00	1.50	2.05	0.266	1.34	0.356
3.00	2.50	2.95	0.297	1.56	0.463
4.00	3.50	3.68	0.335	1.75	0.586
5.00	4.50	4.33	0.357	1.91	0.682
7.50	7.00	5.57	0.395	2.19	0.865
10.0	9.50	6.25	0.354	2.38	0.843
20.0	19.5	6.80	0.372	2.82	1.049

Table 8.3 Ion-Pair Extraction Data for the Extraction of QHB. Concentration of QBr injected = 1.00×10^{-5} M.

[NaHB] (10^{-5} M)	$[NaHB]_{excess}$ (10^{-5} M)	$(NaHB)_{ads}$ (10^{-6} mole)	$k_{mt,surf}$ (s^{-1})	F	k_{mt} (s^{-1})
1.00	0.00	1.05	0.192	1.0	0.129
2.00	1.00	2.05	0.340	1.24	0.422
3.00	2.00	2.95	0.420	1.45	0.609
4.00	3.00	3.67	0.480	1.65	0.792
5.00	4.00	4.23	0.460	1.83	0.842
8.00	7.00	5.75	0.463	1.19	1.014
10.0	9.00	6.25	0.390	2.35	0.917
15.0	14.0	6.70	0.351	2.62	0.920
20.0	19.0	6.80	0.300	2.80	0.840

Table 8.4 Ion-Pair Extraction Data for the Extraction of QHB. Concentration of QBr injected = 5.00×10^{-5} M.

[NaHB] (10^{-5} M)	$[NaHB]_{excess}$ (10^{-5} M)	$(NaHB)_{ads}$ (10^{-6} mole)	$k_{mt,surf}$ (s^{-1})	F	k_{mt} (s^{-1})
5.00	0.00	4.32	0.385	1.00	0.388
8.00	3.00	5.75	0.519	1.65	0.856
10.0	5.00	6.25	0.423	1.99	0.842
15.0	10.0	6.70	0.276	2.40	0.662
20.0	15.0	6.80	0.274	2.66	0.728
25.0	20.0	6.80	0.242	2.84	0.687

Table 8.5 Ion-Pair Extraction Data for the Extraction of QHB. Concentration of QBr injected = 7.50×10^{-5} M.

[NaHB] (10^{-5} M)	$[NaHB]_{excess}$ (10^{-5} M)	$(NaHB)_{ads}$ (10^{-6} mole)	$k_{mt,surf}$ (s^{-1})	F	k_{mt} (s^{-1})
7.50	0.00	5.57	0.533	1.00	0.533
10.0	2.50	6.25	0.490	1.57	0.769
12.5	5.00	6.55	0.387	1.99	0.779
15.0	7.50	6.70	0.316	2.23	0.705
20.0	12.50	6.80	0.221	2.54	0.561
25.0	17.50	6.80	0.188	2.78	0.522

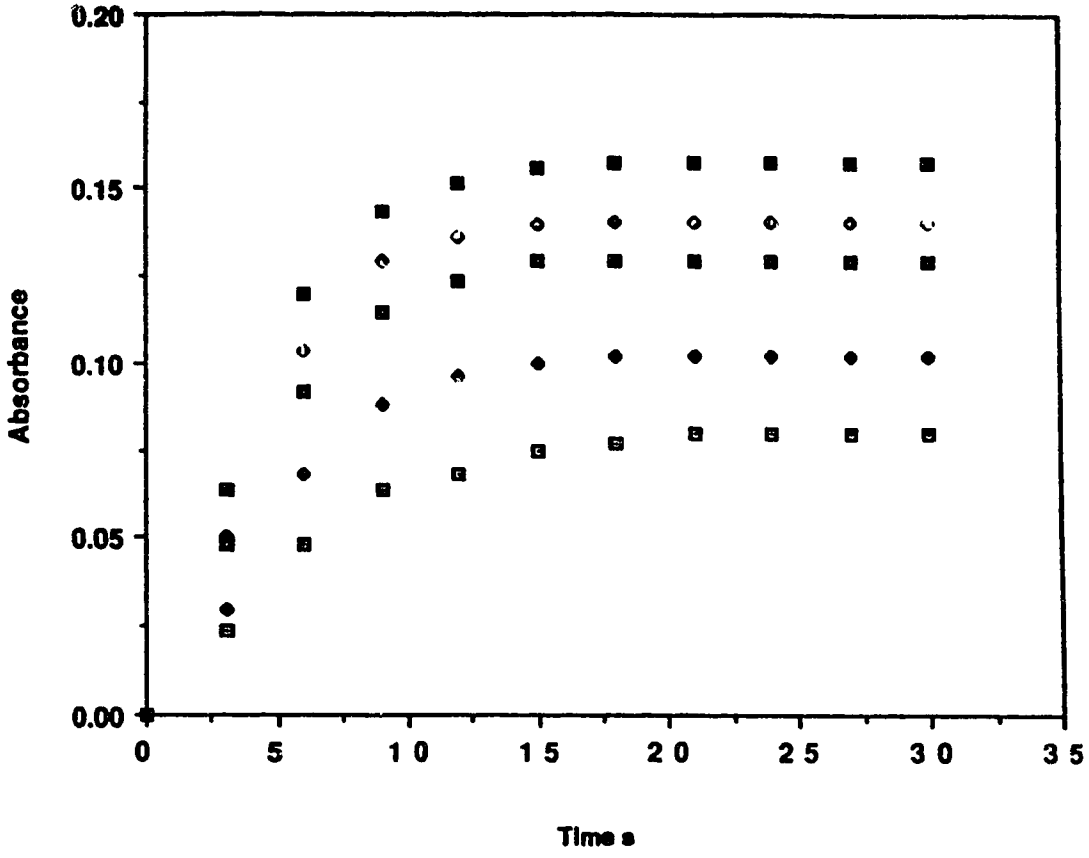

Figure 8.3A Plots of the chloroform phase absorbance vs time for the extraction of QHB from water into chloroform. Concentration of QBr injected was 1.0×10^{-5} M. Concentration of NaHB was: ⊡ , 1.0×10^{-5} M; ◆ , 2.0×10^{-5} M; ■ , 3.0×10^{-5} M; ◆ , 4.0×10^{-5} M; ■ , 5.0×10^{-5} M.

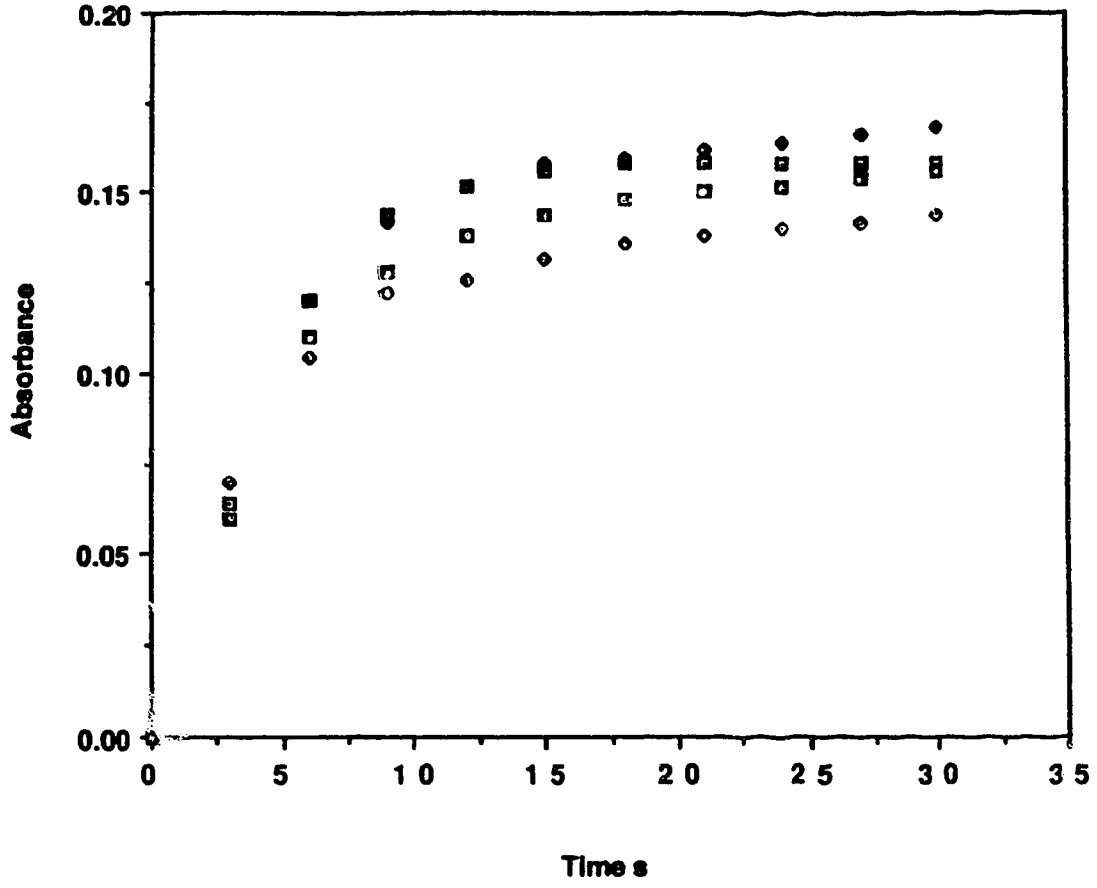

Figure 8.3B Plots of the chloroform phase absorbance vs time for the extraction of QHB from water into chloroform. Concentration of QBr injected was 1.0×10^{-5} M. Concentration of NaHB was: ▣ , 5.0×10^{-5} M; ◆ , 8.0×10^{-5} M; ■ , 1.0×10^{-4} M; ◆ , 2.0×10^{-4} M.

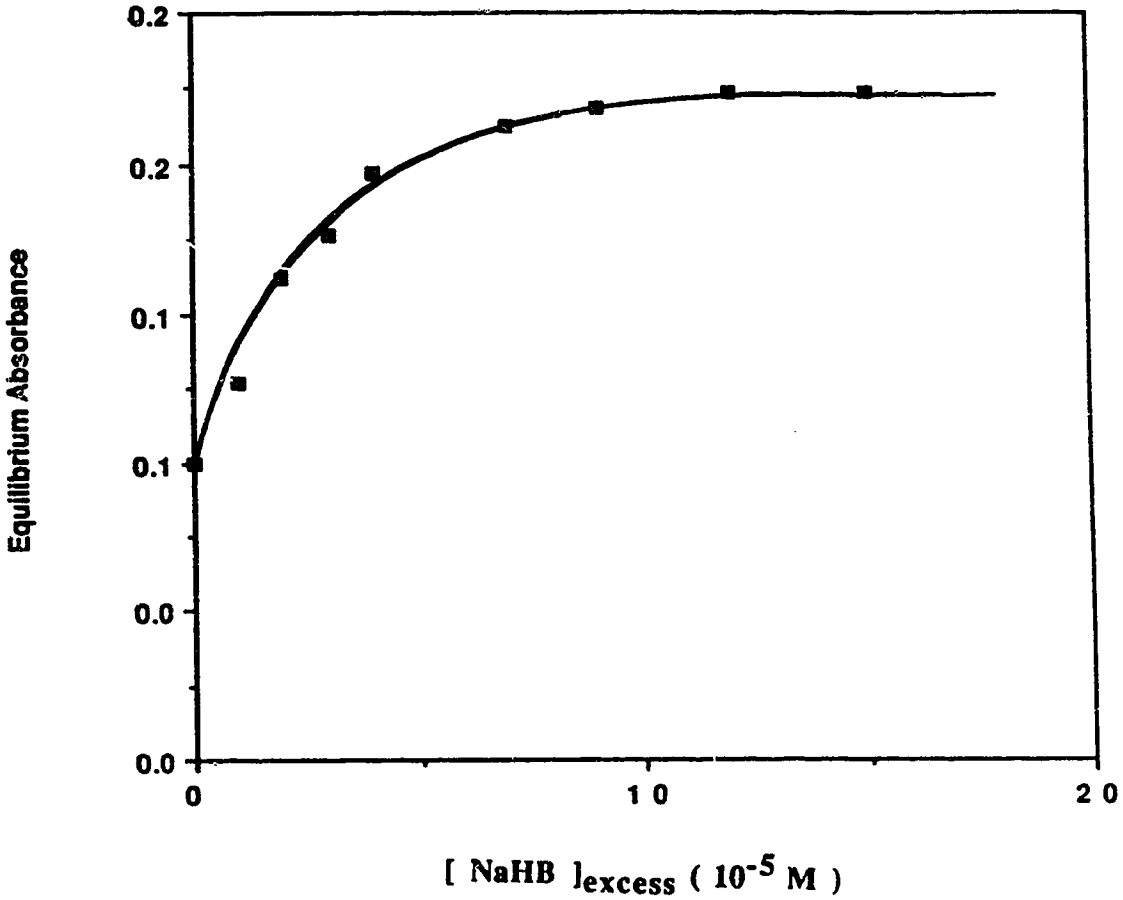

Figure 8.4 Plot of the equilibrium absorbances of the profiles in Figure 8.3 vs. $[NaHB]_{excess}$ in the aqueous phase.

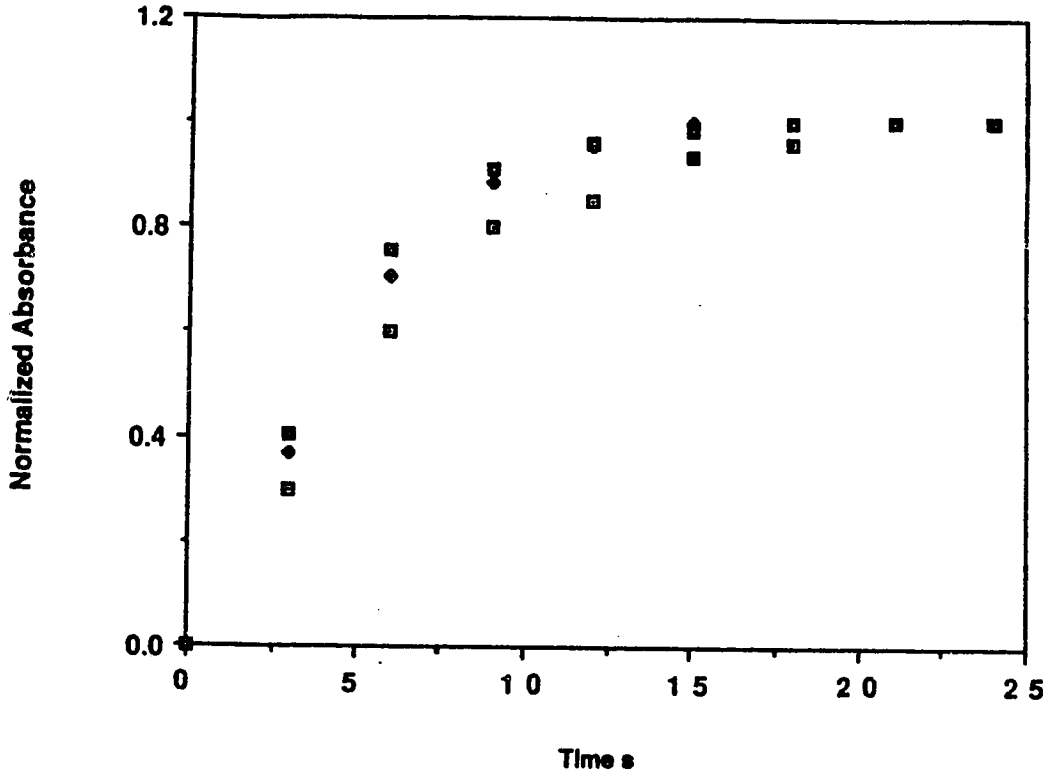

Figure 8.5A Plots of the normalized absorbance of the chloroform phase vs time for the extraction of QHB from water into chloroform. Concentration of QBr injected was 1.0×10^{-5} M. Concentration of NaHB was: ⊡, 1.0×10^{-5} M; ◆, 3.0×10^{-5} M; ■, 5.0×10^{-5} M.

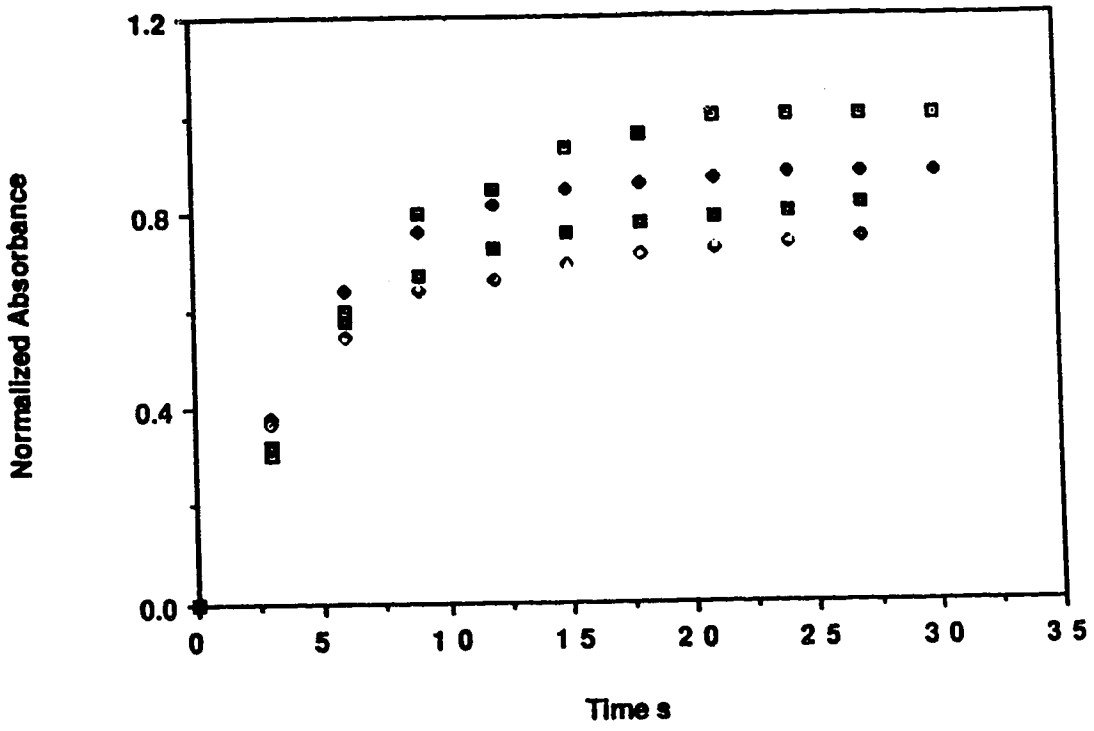

Figure 8.5B Plots of the normalized absorbance of the chloroform phase vs time for the extraction of QHB from water into chloroform. Concentration of QBr injected was 1.0×10^{-5} M. Concentration of NaHB was: ⊡, 1.0×10^{-5} M; ◆, 8.0×10^{-5} M; ■, 1.0×10^{-4} M; ◆, 2.0×10^{-4} M.

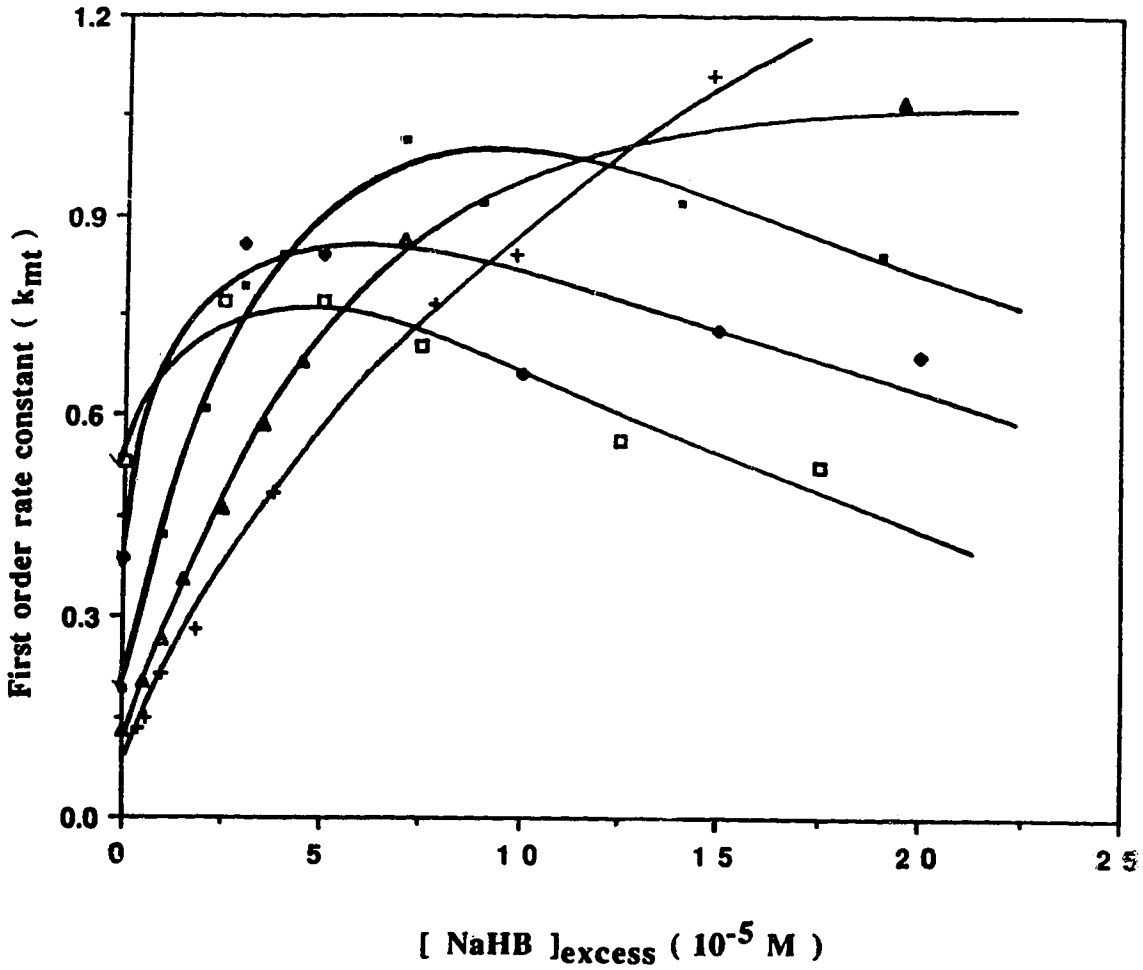

Figure 8.6 Plots of first order rate constants (k_{mt}) vs $[NaHB]_{excess}$ for the extraction of QHB from water into chloroform. Concentration of QHB was: (+), 0.2 x 10^{-5} M; (▵) , 0.5 x 10^{-5} M; (•) , 1.0 x 10^{-5} M; (♦), 5.0 x 10^{-5} M; (□) , 7.5 x 10^{-5} M.

8.3.4 EFFECT OF INTERFACIAL ADSORPTION ON THE EXTRACTION RATE CONSTANT OF SURFACE ACTIVE ION-PAIRS

In order to explain why adsorption of NaHB at the liquid-liquid interface causes the extraction rate constant of QHB to increase, it is important to clarify the extraction process involved. First, ion-pair formation can occur either in the bulk aqueous phase or at the liquid-liquid interface. Irrespective of where ion-pair formation occurs, once at the interface, transfer into the chloroform phase is determined by the magnitude of the equilibrium adsorption constant, K_{ads}, for the adsorption of QHB from chloroform into the interface since QHB is itself surface active. It has been shown [165, 190] that interfacial adsorption of a transfering solute during mass transfer of that solute can create large energy barriers to adsorption and/or desorption and thereby result in a decrease in the extraction rate. These barriers occur both between the aqueous phase and the interface and between the interface and the organic phase. However, owing to the large extraction constant for QHB from water into chloroform, the rate limiting equilibrium will be only that involving adsorption and desorption of QHB between the interface and the bulk chloroform phase. Thus, the desorption and adsorption equilibrium can be defined as;

$$(QHB)_i \quad \rightleftharpoons \quad (QHB)_o \qquad (8.2)$$

where k_{ads} (i.e., for o $\rightarrow$ i) and k_{des} (i.e., for i $\rightarrow$ o) are the adsorption and desorption rate constants respectively. For a linear adsorption isotherm, K_{ads} is related to these rate constants as follows [165];

$$K_{ads} = \frac{k_{ads} d K_D}{k_{des}} \qquad (8.3)$$

or

$$k_{des} = k_{ads}\left[\frac{d K_D}{K_{ads}}\right] \qquad (8.4)$$

where K_D is the liquid-liquid distribution coefficient for QHB between chloroform and water, Equation 1.2, and d is the thickness of the interfacial layer ($\sim 10^{-7}$ cm) [39, 146].

Equation 8.4 indicates that the larger K_{ads} gets, the the smaller k_{des} becomes, and consequently the lower the rate for desorption of solute from the interface into the Nernst film on the chloroform side of the interface. The effect of adsorption and desorption barriers during the transfer of a surface active solute is to give a non-zero value to R_i in Equation 2.6. If the resistance to mass transfer of QHB into the chloroform phase is a result of both mass transfer through the aqueous Nernst film and the resistance to desorption at the interface into the chloroform phase, then the overall extraction rate constant, k_{mt}, can be expressed as follows;

$$\frac{1}{k_{mt}} = \frac{1}{k_{mt,\,a}} + \frac{1}{k_{mt,\,i}} \qquad (8.5)$$

where $k_{mt,a}$ and $k_{mt,i}$ are the rate constants for the transfer through the aqueous Nernst film and for desorption at the interface respectively.
Substituting $k_{mt,i}$ in Equation 8.5 with k_{des} from Equation 8.4 gives;

$$\frac{1}{k_{mt}} = \frac{1}{k_{mt,\,a}} + \frac{K_{ads}}{d K_D k_{ads}} \qquad (8.6)$$

Equation 8.6 suggests that a plot of $1/k_{mt}$ vs K_{ads} should give a straight line with an intercept equal to $1/k_{mt,a}$.

8.3.5 EXTRACTION RATE OF QHB: ROLE OF COMPETING ADSORPTION

As shown in Chapter 7, the adsorption of NaHB at the interface decreases the extent of adsorption of QHB at the interface (see Figure 7.6) and consequently, K_{ads} for QHB adsorption also decreases in the presence NaHB. The values of K_{ads} for the adsorption of QHB in the presence of NaHB were calculated by taking the initial slopes of the QHB isotherms in Figure 7.6. The magnitude of K_{ads} decreases with increasing concentration of NaHB in the aqueous phase; a plot of K_{ads} vs $[NaHB]_a$ is shown in Figure 8.7. To check whether the extraction rate data agree with Equation 8.6, values of K_{ads} were obtained by interpolating from Figure 8.7 and plotting against $1/k_{mt}$ according to Equation 8.6. It was only possible to obtain values for K_{ads} under extraction conditions which involved the extractions of 2.0×10^{-6} and 5.0×10^{-6} M QBr. The plots are given in Figures 8.8 and 8.9 respectively. Indeed, both plots were linear with similar intercepts and slopes (see Table 8.6). The reciprocal of the intercepts is equal to $k_{mt,a} \approx 1.0\ s^{-1}$, which agrees well with values of k_{mt} obtained for extractions whose rates were limited only by mass transfer (see Chapter 5). Extractions of QBr concentrations greater than 5.0×10^{-6} M occur in the non-linear region of QHB isotherm, hence K_{ads} does not remain constant during the extraction. Therefore the rate constants could not be fitted to Equation 8.6.

8.3.6 EXTRACTION RATE OF QP: ROLE OF DISSOCIATION AT THE INTERFACE

As shown in Chapter 7, tetrahexyl ammonium picrate (QP) is surface active and adsorbs strongly at the chloroform/water interface. Extraction of QP from water into chloroform will therefore involve having to overcome energy barriers due to adsorption and/or desorption at the liquid-liquid interface. In consequence, the overall extraction rate constant, k_{mt}, can be defined by Equation 8.6. It was also shown in Chapter 7 that, because of dissociation of QP at the interface, the presence of NaP in the aqueous phase

suppresses the adsorption of QP at the interface and thus, K_{ads} for the adsorption of QP decreases with increasing concentration of NaP in the aqueous phase. As predicted by Equation 8.6, the rate constant for the extraction of QP from water into chloroform should increase with increasing concentration of NaP in the aqueous phase.

Shown in Figure 8.10 is a plot of experimental values of k_{mt} vs the concentration of NaP in the aqueous phase for the extraction of 1.0×10^{-5} M QP from water into chloroform. Indeed, as predicted, k_{mt} increases with increasing concentration of NaP up to concentrations of NaP of about 6.0×10^{-5} M NaP in the aqueous phase. Although k_{mt} initially increases with [NaP] in the aqueous phase, the extraction was performed at a QP concentration where K_{ads} does not remain constant during the extraction. Hence, the experimental values of k_{mt} could not be fitted to Equation 8.6. At concentrations greater than 6.0×10^{-5} M, due to effects that will be discussed in Section 8.3.7, k_{mt} decreases with further increases in the concentration of NaP.

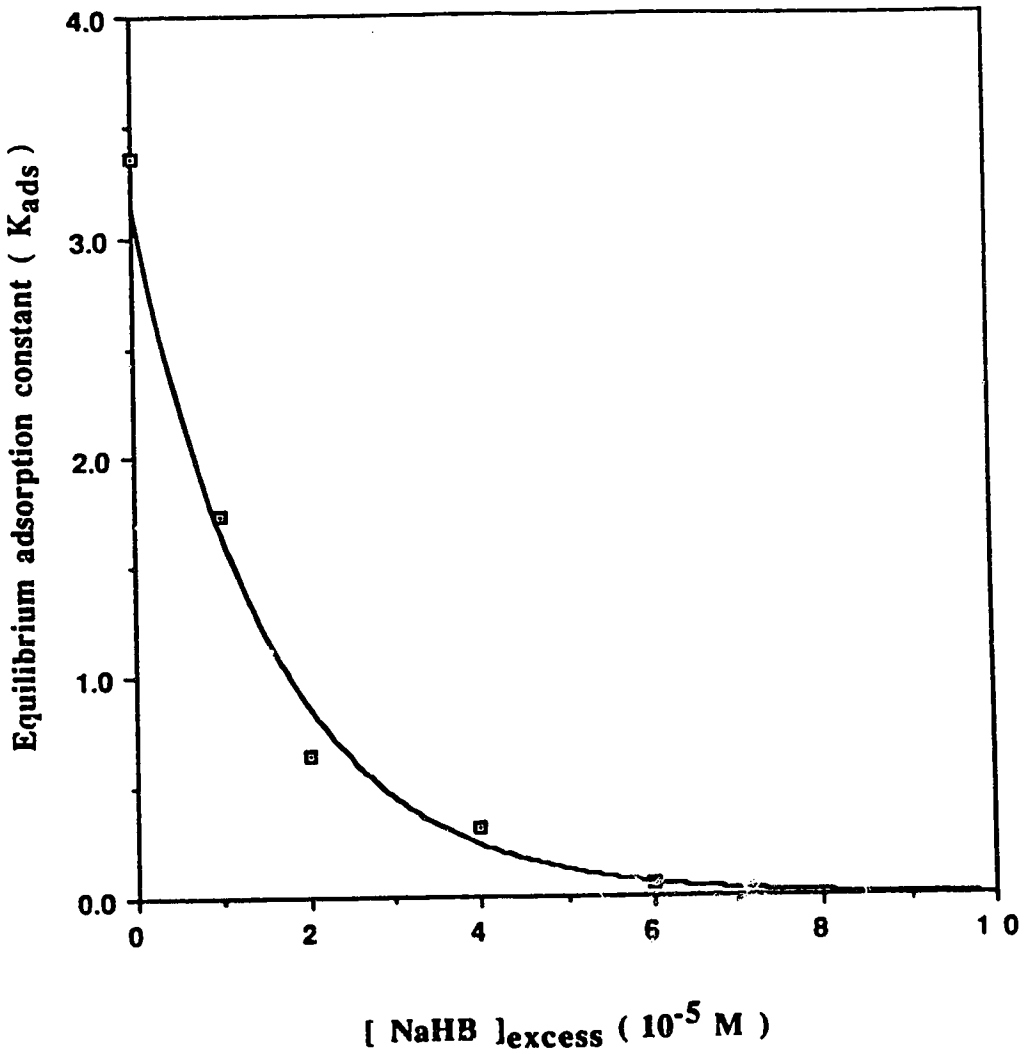

Figure 8.7 Plot of the equilibrium adsorption constant (K_{ads}) for QHB vs $[NaHB]_{excess}$ in the aqueous phase.

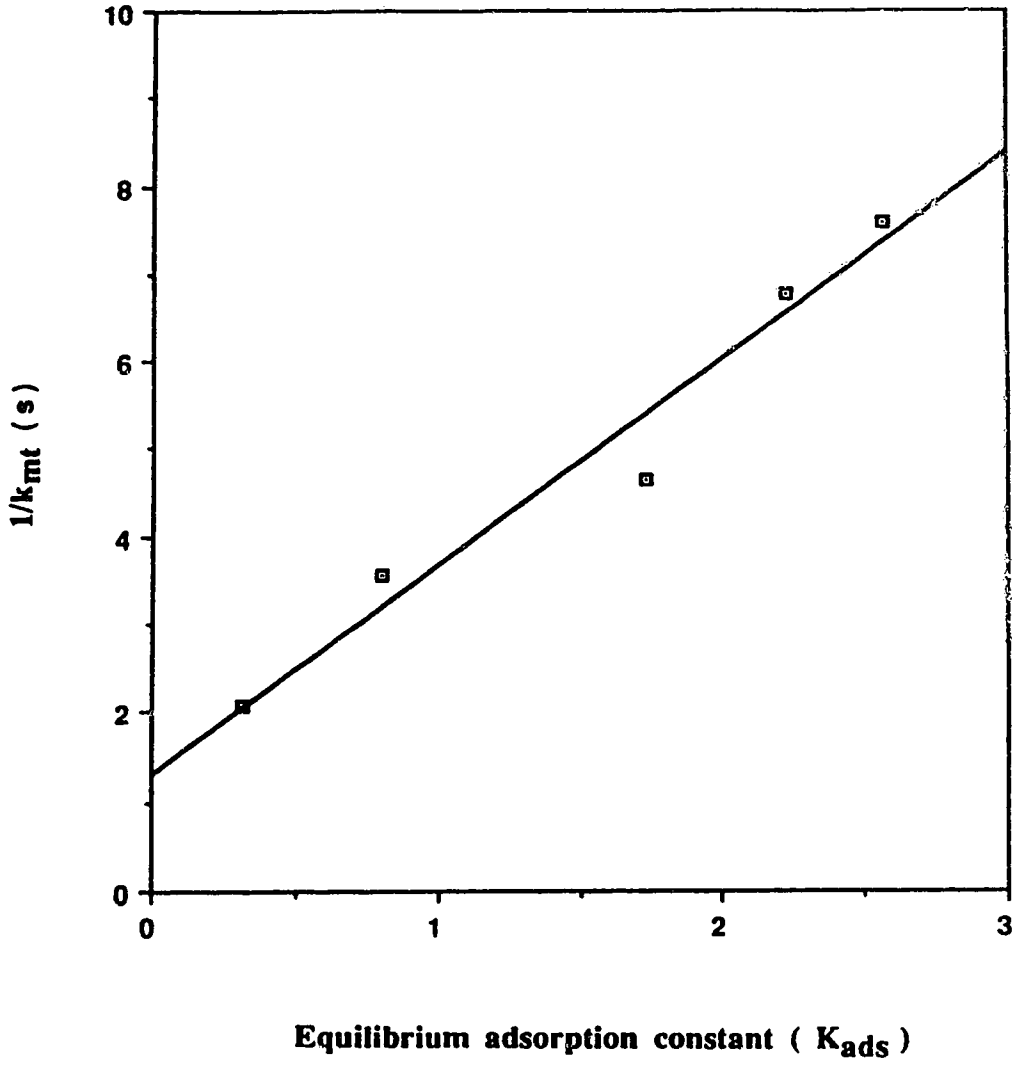

Figure 8.8 Plot of $1/k_{mt}$ vs the equilibrium adsorption constant (K_{ads}) for extraction of 0.02×10^{-5} M QHB according to Equation 8.6. k_{mt} is the first order rate constant whose the values are given in Table 8.1.

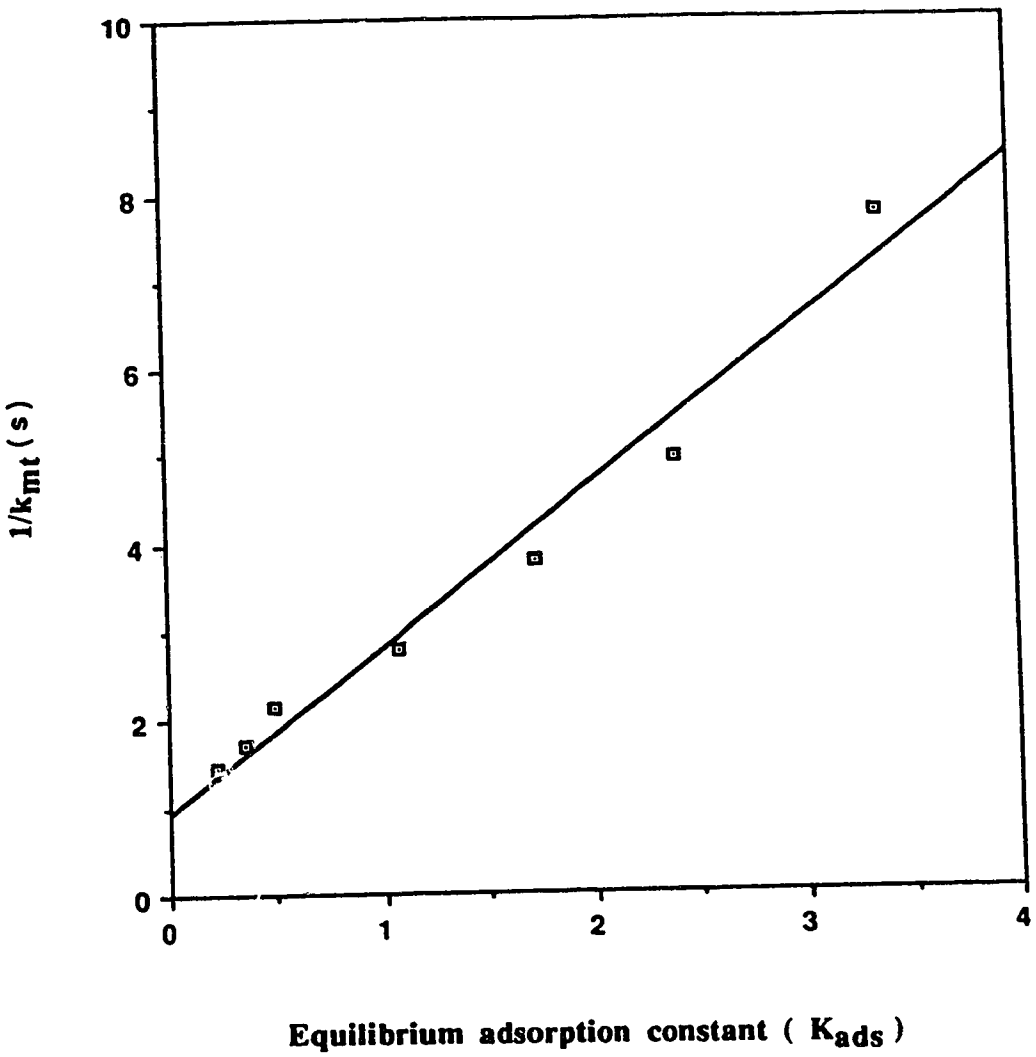

Figure 8.9 Plot of $1/k_{mt}$ vs the equilibrium adsorption constant (K_{ads}) for extraction of 0.05×10^{-5} M QHB according to Equation 8.6. k_{mt} is the first order rate constant whose the values are given in Table 8.2.

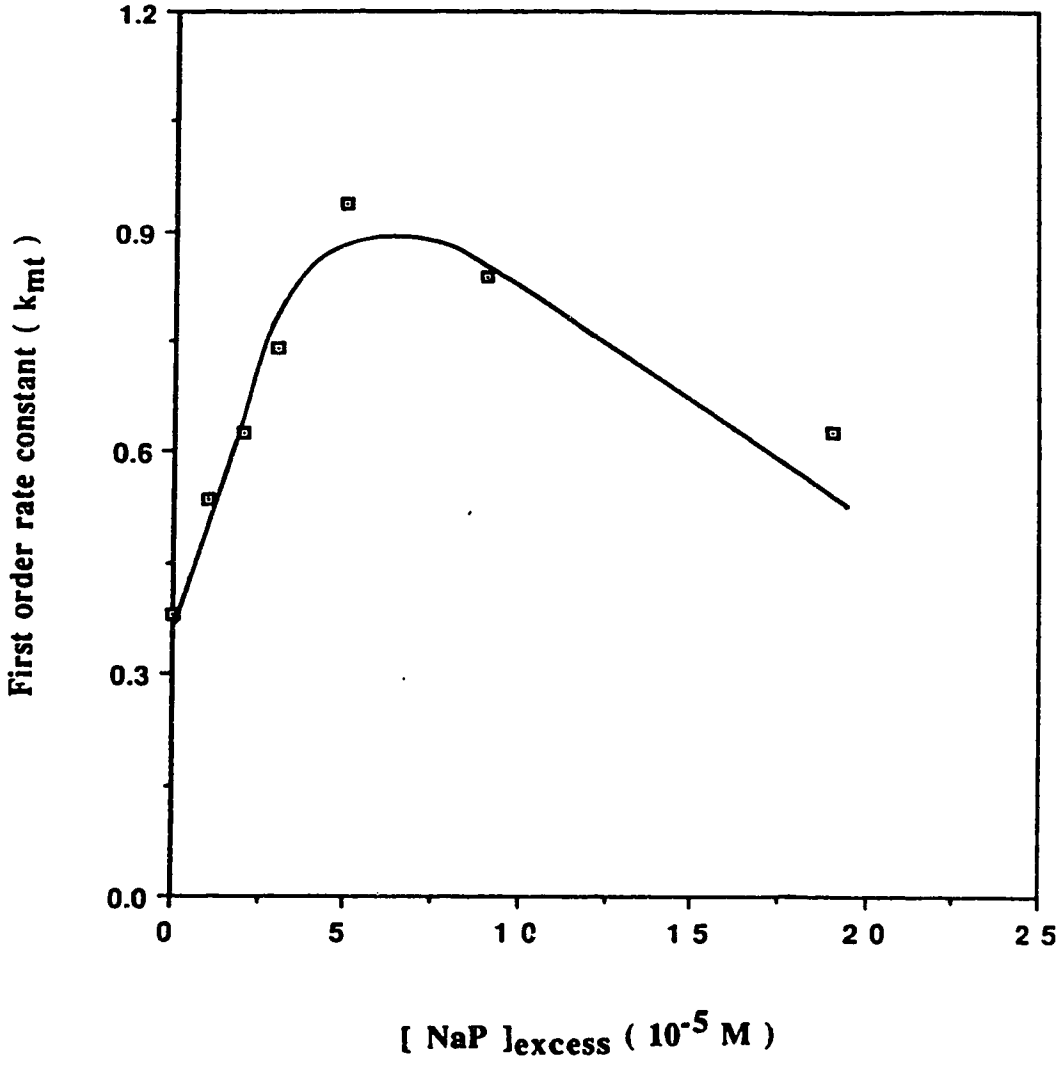

Figure 8.10 Plot of first order rate constant (k_{mt}) vs [NaP]$_{excess}$ for the extraction of 1.0 x 10^{-5} M QP from water into chloroform.

Table 8.6 Data from the plot of $1/k_{mt}$ vs K_{ads} for the extraction of QHB.

Uncertainties are one standard deviation.

[QBr] (10^{-5} M)	Intercept (s)	Slope (s cm^{-1})	$k_{mt,a}$ (s^{-1})
0.20	1.322 ± 0.478	2.35 ± 0.27	0.76 ± 0.43
0.50	0.942 ± 0.240	1.87 ± 0.14	1.06 ± 0.22

8.3.7 EFFECT OF COLLOID FORMATION ON THE EXTRACTION RATE CONSTANTS OF ION-PAIRS

As reported by Schill [180] there are various kinds of aggregation processes involving components of ion-pairs that can occur in the aqueous phase and as a result decrease ion-pair extraction. Some of these aggregation processes include dimerization, tetramerization, micellization and salt precipitation [177]. Although there are very few reports [180, 191, 192] on ion-pair formation between organic components in the aqueous phase, ion-pair formation in the aqueous phase prior to the start of extraction will lead to slower extraction rates. Most organic ion-pairs have very small solubilities in water, hence once they are formed they begin to aggregate into clusters which eventually precipitate out of solution as fine crystals. Depending on the solubility of the ion-pair and the presence of an excess electrolyte [174, 175] the ion-pairs may adsorb enough ions (potential determining ion) onto their surfaces to prevent further aggregation and precipitation [174, 175]. Such solutions can be described as colloidal dispersions when the size the the ion-pair clusters are in the range 1 nm to 1 μm. Shown in Table 8.7 are the characteristics of aqueous solutions containing mixtures of NaHB and QBr. The stabilities with respect to precipitation of QHB are found to increase with increasing ratio of NaHB to QBr. This is explained by the fact that adsorption of excess negatively charged HB ions onto the surface of QHB increases with increasing concentration of NaHB in solution. The electrostatic repulsion between adjacent moleclues of QHB therefore increases with increasing concentration of NaHB. Formation of a colloidal dispersion during extraction of ion-pairs decreases the extraction rate because often the liquid-liquid interface acquires the same charge as that on the ion-pairs and consequently the ion-pairs are repelled from the interface through which they must cross in order for transfer to occur. The overall ion-pair extraction process in the presence of colloidal dispersions is given schematically in Figure 8.11. Retardation of extraction rates resulting from colloid formation in the aqueous phase

become significant only at much higher concentrations of ion-pair components. This is especially true when at least one of the ion-pair components is surface active. This explains why, for the extraction of QHB, retardation of rate constants (see Figure 8.6) was not apparent until at concentrations of NaHB which are more than enough to saturate the available interface with a monolayer of solute.

Table 8.7 Characteristics of Aqueous Solutions Containing Mixtures of NaHB and QBr

[NaHB]/[QBr]	Observation after 1 min.	Observation after 5 days
1	Turbid solution	Precipitate + clear solution
4	Slightly turbid solution	Precipitate + turbid solution
7	Almost clear solution	Precipitate + turbid solution
10	Clear solution	Gelatinous precipitate + solution

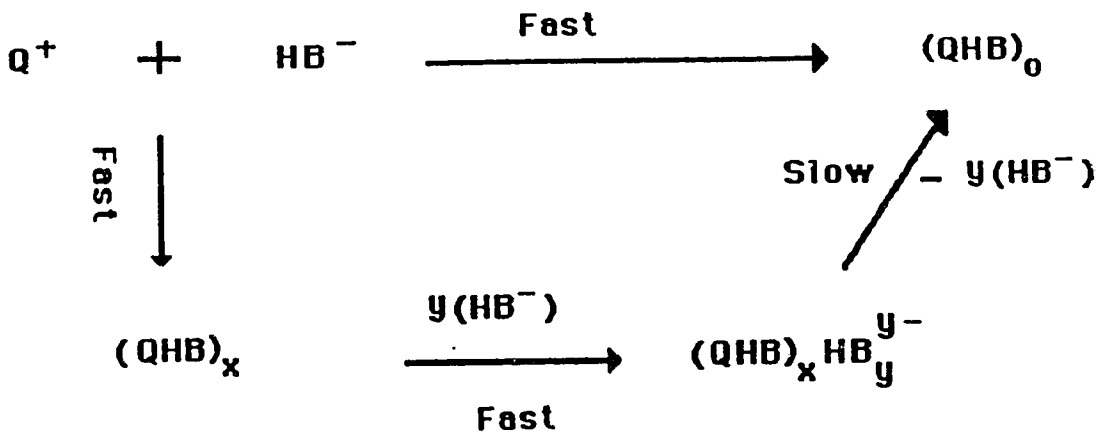

Figure 8.11 Model for extraction of an ion-pair (QHB) from water into chloroform showing colloid formation in the aqueous phase. The neutral colloidal particle (QHB)$_X$ is made up of X "molecules" of QHB. It rapidly adsorbs excess HB^- to become a negatively charged colloid which slows down its extraction into the chloroform as ion-pair (QHB)$_O$.

CHAPTER 9

FUTURE STUDIES

The work presented in this thesis has given insight into some aspects of mass transfer in solvent extraction. In this chapter two areas are identified which would benefit from extension of this work.

9.1 FIBER OPTIC PROBE FOR SOLVENT EXTRACTION KINETIC STUDIES

The new rapid-stir instrument design reduces instrument band broadening. Nevertheless, instrument band broadening still makes a much greater contribution to signal variance than does mass transfer (see Table 4.2). While deconvolution can, to a point, successfully remove effects of instrument band broadening, it is evident that future efforts to improve the instrument for making measurements of either mass transfer rates or the rates of fast chemical reactions should concentrate on decreasing band broadening by improved design.

In this chapter, a new design of the sampling and monitoring components of the rapid-stir instrument is proposed. The new design incorporates a fiber optic probe which has been modified to provide in situ sampling and monitoring of the liquid phase of interest. That is, the detector cell is located right inside the extraction cell so as to eliminate the distortion caused by the filter-probe and connecting tubing used to transport the sample to the detector cell for absorbance measurement.

The design of the rapid-stir extraction cell will be similar to that described in Chapter 4, except that the filter will be replaced by a fiber optic probe [193, 194], F. In order to achieve phase separation prior to absorbance measurement, the tip of the probe will have to be modified to incorporate a membrane phase separator. Shown in Figure 9.1 is a schematic diagram of the proposed extraction apparatus. The fiber optic probe is connected by a wave-guide, WG, to a UV-VIS spectrophotometer, D. Pumping of the separated

phase through the cell in the probe is provided by nitrogen pressure as described in Chapter 4. The peristaltic pump, P, is used to limit the flow rate of the separated phase.

9.2 INTERFACIAL ADSORPTION STUDIES

The liquid-liquid interfacial adsorption studies discussed in this thesis have demonstrated that it is possible to measure both thermodynamics and kinetics (i.e. mass transfer) of interfacial adsorption by means of rapid stirring and membrane phase separation. The effect of interfacial adsorption at the liquid-liquid interface on the extraction rate of metal-ligand complexes could also be studied. Although the role of interfacial adsorption has been studied for metal-ligand complexes in the chemical kinetic regime, the approach used in the present work could make it possible to study the effect of interfacial adsorption of ligand and/or complex on fast complexation reactions taking place in the mass transfer controlled regime.

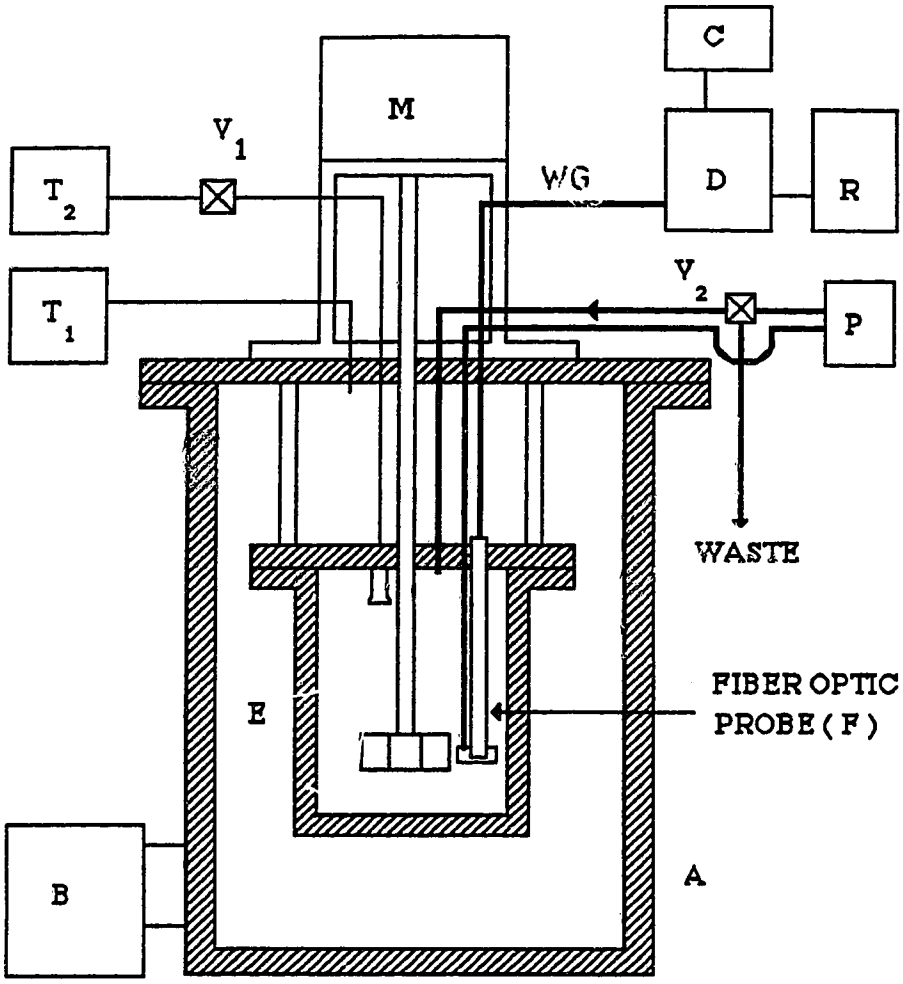

Figure 9.1 Diagram of the rapid-stir apparatus incorporating a Fiber optic probe, F; A, Alunimum pressure cylinder; E, stainless steel extraction cell; M high-speed motor; B, circulating constant temperature bath; T_1 and T_2 , tanks of pressurized nitrogen; WG, connecting wave-guide; D, UV-VIS spectrophotometer; C, microcomputer; R, strip chart recorder; P, peristaltic pump; V_1 solenoid valve; V_2, manual valve.

REFERENCES

1 Berthelot, M. and Jungfleisch, J. Ann. Chim. Phys., 26, 396, **1872**

2 Nernst, W. Z. Phys. Chem., (Leipzig), 8, 110, **1891**

3 Sekine, T. and Hasegawa, Y. " Solvent Extraction Chemistry", Marcel Dekker, New York, **1977**, Chapter 3.

4 Irving, H. and Williams, R. J. P. " Treatise on Analytical Chemistry", Part 1C, Kolthoff, I. M. and Elving, P. J. (Ed.), **1961**, Chapter 31.

5 Lo, T. C., Baird, M. H. I. and Hanson. C. " Handbook of Solvent Extraction", John Wiley and Sons., New York. **1983**

6 Derry, R. Warren Spring Larboratories, UK. Mineral Dressing Information Note No. 7, **1972**

7 Marcus, Y. and Kertes, A. S. "Ion Exchange and Solvent Extraction of Metal Complexes", Wiley- Interscience, London, **1969**

8 Anonymous, World Mining, 32(2), 48, **1979**

9 Cadman, T. W. and Dellinger, R. W. Chem. Eng., 8, 79, **1974**

10 Flett, D. S. and Spink, D. R. Hydrometallurgy, 1, 207, **1976**

11 Kiezyk, P. R. and Mackay, D. Can. J. Chem. Eng., 49. 747, **1971**

12 Earhart, J. P., Won, K. W., King, C. J. and Prausnitz, M. M. " Extraction of Chemical Waste Pollutants from Industrial Waste Waters with Volatile Solvents", USEPA-600/2-76-220, Dec., **1976**

13 British Patents 995,471 and 1,055,532 **1964**

14 German Patent 2,161,525 **1973**

15 Batchelor, F. R., Doyle, F. P., Naylor, J. H. C. and Rolinson, G. N. Nature, 183, 257, **1959**

16 Souders, M., Pierotti, G. J. and Dunn, C. L., " History of Penicillin Production", Chem. Eng. Prog., Symposium Series Volume 66 (100), Chapter 5, **1970**

17 Beecham Group Ltd., British Patent 1,565,656 **1975**

18 Weber, W. P. and Gokel, G. W., " Phase Transfer Catalysis ", Springer-Verlag, New York, **1977**

19 General Food Corporation, US Patent 2309092 **1943**

20 German Federal Republic Patent Application 2721765 to Soc des Prodiuts Nestle SA, **1977**

21 German Federal Republic Patent Application 2357590 to HAG AG, **1975**

22 Langmuir, A. C. J. Amer. Chem. Soc., 22, 102, **1900**

23 Stary, J. " The Solvent Extraction of Metal Chelates" Pergamon, Oxford, **1964**

24 Craig, L. C. Anal. Chem., 21, 85, **1949**

25 Morrison, G. H. and Freiser, H. " Solvent Extraction In Analytical Chemistry" Wiley, New York, **1957**

26 Zolotov, A. Y. " Extraction of Chelate Compounds" Ann-Arbour-Humprey Science Publication, Ann-Arbor, **1970**

27 Freiser, H. Anal. Chem., 38, 131R, **1966**

28 Honaker, C. B. and Freiser, H. J. Phys. Chem., 66, 127, **1962**

29 Irving, H., Andrew, G. and Ridson, E. J. J. Chem. Soc., 541, **1949**

30 Gieger, R. W. Ph.D. thesis, University of Minnesota, **1951**

31 Yamada, K., Nakagawa, K., Haraguchi, K. and Ito, S. Nippon Kagaku Kaishi, 1431, **1975**

32 Higuchi, T. and Michaelis, A. F. Anal, Chem., 40, 1925, **1968**

33 Nanda, K. and Sharma, R. Chem. Eng. Sci., 22, 769, **1967**

34 McClellan, B. E. and Freiser, H. Anal. Chem., 36, 2262, **1964**

35 Schlichting, H. "Boundary-Layer Theory" McGraw-Hill Book Company, Sixth Ed., New, York, **1968**, Chapter 2

36 Danesi, P. R. and Chiarizia, R. CRC Critical Rev. Anal. Chem., 10, 1, **1980**

37 Hanna, G.J. and Noble, R. D. Chem. Rev., 85, 585, **1985**

38 Tavlarides, L. L. Chem. Eng. Commun., 8, 133, **1981**

39 Davies, J. T. and Redeal, E. K. " Interfacial Phenomena " Academic Press, New York, **1961**,, Chapter 7

40 Tarasov, V. V. and Yagodin, G.A. in " Ion Exchange and Solvent Extraction" Marinski, J. A. and Marcus, Y. (Eds.), Marcell Dekker Inc., New York, **1988**, Volume 10, Chapter 4

41 Nernst, W. Z. Phys. Chim., 47, 52, **1904**

42 Sherwood, T. K., Pigford, R. L. and Wilke, C. R. " Mass Transfer " McGraw-Hill, New York, **1975**, Chapters 5 and 8

43 Higbie, R. Trans. AIChE. J., 31, 365, **1935**

44 Dankwerts, P.V. Ind. Eng. Chem., 43, 1460, **1951**

45 Cussler, E. L. " Diffusion: Mass Transfer in Fluid systems" Cambridge University Press, Cambridge, **1986**, Chapter 11

46 Whitman, G. W. Chem. Metallurg. Eng., 29, 147, **1923**

47 Whitman, G. W. and Davis, D. S. Ind. Eng. Chem., 16, 1233, **1924**

48 Meares, P. Faraday Discuss. Chem. Soc., 77, 7, **1984**

49 Amankwa, L. and Cantwell, F. F. Anal. Chem., 61. 1063, **1989**

50 Lewis, B. Chem. Eng. Sci., 3, 218, **1959**

51 Nitsch, N. and Hillekamp, K. Chem. Ztg., 96, 254, **1972**

52 Danesi, P. R., Cianetti, C., Horowitz, E. P. and Diamond, H. Sep. Sci. Technol., 17(7), 961, **1982**

53 Byron, P. R., Guest, R. T. and Notari, R. E. J. Pharm. Sci., 70(11), 1265, **1981**

54 Asai, S., Hatanaka, J. and Uekawa, Y. J. Chem. Eng. Jpn., 16(6), 463, **1983**

55 Bhaduri, M., Hanson, C., Hughes, M. A. and Whewell, R. J. Int. Solv. Extr. Conf. [Proc]. 293, **1983**

56 Perry's Handbook of Chemical Engineering, Perry, R. H. and Green, D. W. (Eds.), McGraw-Hill Book Company, New York, **1984**, Chapters, 5, 19 and 21

57 Hanson, C. " Recent Advances in Solvent Extraction" Pergamon, New York, **1971**, Chapter 14

58 Laddha, G. S. and Degaleesan, T. E. " Transport Phenomena in Solvent Extraction" McGraw-Hill, New Delhi, **1976**, Chapter 6

59 Uhl, V. W. and Gray, J. B. " Mixing" Academic Press Inc., New York, **1967**, Volume 2, Chapter 6

60 Shinner, R. J. Fluid Mech., 10, 259, **1961**

61 Rydberg, J., Rienhardt, H. and Liljenzin, J. O. Ion Exch. Solv. Extr., 3, 111, **1973**

62 Carter, S. P. anf Freiser, H. Anal. chem., 51, 1100, **1979**

63 Watarai, H., Cunningham, L. and Freiser, H. Anal. chem., 54, 23900, **1982**

64 Aprahamian Jr., E. A., Cantwell, F. F. and Freiser, H. Langmuir, 1, 79, **1985**

65 Danesi, P. R., Chiarizia, R. abd Vandegrift, G. F. J. Phys. Chem., 84, 3455, **1980**

66 Haraguchi, K. and Freiser, H. Inorg. Chem., 22, 1187, **1983**

67 Watarai, H. and Freiser, H. J. Amer. Chem Soc., 105, 189, **1983**

68 Freiser, H. Act. Chem. Res., 17, 126, **1984**

69 Aprahamian Jr., E. A. and Freiser, H. Sep. Sci. Technol., 22, 233, **1987**

70 Cantwell, F. F. and Freiser, H. Anal. Chem., 60, 226, **1988**

71 Whewell, R. J., Hughes, M. A. and Hanson, C. J. Inorg. Nucl. Chem., 37, 2303, **1975**

72 Garner, F. H. Trans. Inst. Chem. Engrs., 88, **1950**

73 Handlos, A. E. and Baron, T. AIChE. J., 3(1), 127, **1957**

74 Johns Jr., L. E. and Beckmann, R. B. AIChE. J., 12(1), 10, **1966**

75 Kronig, R. and Brink, J. C. Appl. Sci. Res., (A2), 142, **1950**

76 Brodin, A. and Nilsson, M. Acta. Pharm. Suec., 10, 187, **1973**

77 Nordgren, T. and Kolstad, A. K. Acta. Pharm. Suec., 16, 125, **1979**

78 Jansson, S. O., Nordgren, T. and Schill, G. Acta, Pharm. Suec., 14, 435, **1977**

79 Brodin, A. and Agren, A. Acta. Pharm. Suec., 8, 609, **1971**

80 Nordgren, T. and SJoden, E. K. Acta. Pharm. Suec., 15, 241, **1978**

81 Nordgren, T. and Hackzell, L. Acta Pharm. Suec., 16, 135, **1979**

82 Nordgren, T. Acta. Pharm. Suec., 16, 215, **1979**

83 Kolstad, A. K. and Nordgren, T. Acta. Pharm. Suec., 17, 327, **1980**

84 Albery, W. J., Cooper, M. A., Hadgraft, J. and Ryan, C. C. J. Chem. Soc. Faraday Trans. (1), 70, 1124, **1974**

85 Albery, W. J., Burk, J. F., Leffler, E. B. and Hadgraft, J. J. Chem. Soc. Faraday Trans. (1), 72, 1618, **1976**

86 Levich, V. G. "Physicochemical Hydrodynamics" Prentice Hall, Englewood Cliffs, NJ, **1962**

87 Guy, R. H. and Fleming, R. International J. Pharm., 3, 143, **1979**

88 Guy, R. H. and Fleming, R. J. Colloid and Interface Sci., 83, 130, **1981**

89 Fleming, R., Guy, R. H. and Hadgraft, J. J. Pharm. Sci., 72, 142, **1983**

90 Guy, R. H., Hinz, R. S. and Amantea, M. Faraday Discuss. Chem Soc., 77, 127, **1984**

91 Guy, R. H., Honda, D. H. and Aquino III, T. R. J. Colloid and Interface Sci., 87, 107, **1982**

92 Sagert, N. H., Quinn, M. J. and Dixon, R. S. Can. J. Chem., 59, 1096, **1981**

93 Albery, W. J. and Fisk. P. R. Hydrometallurgy, 81 Soc. Chem. Ind. Symp., FS1-FS15, **1981**

94 Albery, W. J., Riaz, A. C. and Fisk, P. R. Faraday Discuss. Chem. Soc., No. 77, P77/5, **1981**

95 Freeman, R. W. and Tavlarides, L. L. Chem. Eng. Sci., 35, 559, **1980**

96 Freeman, R. W. and Tavlarides, L. L. Chem. Eng. Sci., 37, 1547, **1982**

97 Karlberg, B. and Thelander, S. Anal. Chim. Acta., 98, 1, **1978**

98 Bergamin, F. H., Medeiros, J. X., Reis. B. F. and Zagatto, E. A. G. Anal. Chim. Acta., 101, 9, **1978**

99 Nord, L., Backstrom, K., Danielson, L. G., Ingman, F. and Karlberg, B. Anal. Chim. Acta., 194, 221, **1987**

100 Lucy, A. C. Ph.D. Thesis, University of Alberta, **1988**

101 Ruzicka, J. and Hansen, E. H. " Flow Injection Analysis in Chemical Analysis" Second Ed., Wiley, New York, **1988**, Volume 62

102 Nord, L. and Karlberg, B. Anal. Chim. Acta., 164, 233, **1984**

103 Prothero, J. and Burton, A. C. Biophysical. J., 1, 565, **1961**

104 Kharkats, Y. I., Volkov, A. G. and Boguslavsky, L. I. J. Theor. Boi., 65, 379, **1977**

105 Koryta, J. J. Electrochim. Acta., 24, 293, **1979**

106 Wang, Z. and Pang, Z. J. Electroanal. Chem., 189, 1, **1985**

107 Yoshida, Z. and Freiser, H. J. Electroanal. Chem., 162, 307, **1984**

108 Vanysek, P. and Buck, R. P. J. Electroanal. Chem., 163, 1, **1984**

109 Koryta, J., Du, G., Ruth, W. and Vanysek, P. Faraday Discuss. Chem Soc., 77, 209, **1984**

110 Trouve, G., Malher, E., Colinart, P. aand Renon, H. Chem. Eng. Sci., 37(8), 1225, **1982**

111 Watarai, H. and Suzuki, N. Inorg. Nucl. Chem. Lett., 10, 431, **1974**

112 Langlois, G. E., Gulberg, J. E. and Vermeulen, T. Rev. Sci. Instr., 25, 360, **1954**

113 Madden, A. J. and McCoy, B. J. Chem Eng. Sci., 19, 506, **1964**

114 Smith, T. N. Chem. Eng. Sci., 29, 583, **1974**

115 Chen, H. T. and Middleman, S. AIChE. J., 13, 989, **1967**

116 Sprow, F. B. AIChE. J., 13, 995, **1967**

117 Sprow, F. B. Chem. Eng. Sci., 22, 435, **1967**

118 Vermeulen, T., William, G. M. and Langlois, G. E. Chem. Eng. Progr., 51, 85F, **1955**

119 Boyadzhiev, L. and Elenkov, D. Chem Eng. Sci., 21, 955, **1966**

120 Uhl, V. W. and Gray, J. B. " Mixing" Academic Press, New York, **1966**, Volume 1, Chapter 4

121 Nanda, A. K. and Sharma, M. M. Chem. Eng. Sci., 21, 707, **1966**

122 Sharma, M. M. and Danckwerts, P.V. British Chem. Eng., 15, 206, **1970**

123 Calderbank, P. H. Trans. Inst. Chem. Engrs. (London). 36, 443, **1958**

124 Laddha, G. S. and Degaleesan, T. E. " Transport Phenomena in Solvent Extraction " McGraw-Hill, New Delhi, **1976**, Chapter 7

125 Horlick, G. and Hieftje, G. M. In " Comtemporary Topics in Analytical and Clinical Chemistry" Hercules, D. M., Hieftje, G. M., Snyder, L. R. and Evans, M. A. (Eds.), Plenum Press, New York, **1978**, Volume 3, Chapter 4

126 Sternberg, J. C. In " Advances in Chromatography " Giddings, J. C. and Keller, R. A. (Eds.), Marcell Dekker, New York, **1966**,Volume 2

127 Snyder, L.R. and Kirkland, J. J." Introduction to Modern Liquid Chromatography " John Wiley and Sons, New York, **1974**, Chapter 5

128 Dykes, J.T. and Fernando, Q. Talanta, 32(8B), 807, **1985**

129 Korn, G. A. and Korn. T. M. " Mathematical Handbook for Scientists and Engineers" McGraw-Hill Book Company, New York, **1968**

130 Grushka, E., Myers. M. N., Schetller, P.D. and Giddings, J. C. Anal. Chem., 41, 889, **1969**

131 Said, A.S., Al-Ali, H. and Hamad, E. J. High Res. Chrom. Chrom. Commun., 5, 306, **1982**

132 Bidlingmeyer, B. A. and Warren Jr., F. V. Anal. Chem. 56, 1583A, **1984**

133 Chesler, S. N. and Gram, S. P. Anal. Chem., 43, 1922, **1971**

134 Petitclerc, T. and Guichon, G. J. Chromatogr. Sci., 14, 531, **1976**

135 Anderson, D. J. and Walter, R. R. J. Chromatogr. Sci., 22, 353, **1984**

136 Kirkland, J. J., Yau, W. W., Stokloso, H. J., and Dilks, C. H. J. Chromatogr. Sci., 15, 303, **1977**

137 Rony, P. R. and Funk, J. E. J. Chromatogr, Sci, 9, 215, **1971**

138 Lam, R. B., Wiebeldt, R. C. and Isenhour, T. L. Anal. Chem., 53, 889A, **1981**

139 Wright, R. A., Villalanti, D. C. and Burk, M. F. Anal. Chem., 54. 1735, **1982**

140 Cooyey, J. W. and Tukey J. W. Math. Comput., 19, 297, **1965**

141 Perrin, D. D. " Dissociation Constants of Organic Bases in Aqueous Solutions " Butterworth, London, **1965** pg. 90

142 Sendell, Naturwissenschaften, 53, 330, **1966**

143 Uhl, V. W. and Gray, J. B. " Mixing" Acedemic Press, New York, **1967**, Volume 2, Chapter 9

144 Uhl, V. W. and Gray, J. B. " Mixing" Acedemic Press, New York, **1967**, Volume 1, Chapter 3

145 Roger, W. A., Trice, V. G. and Rushton, J. H. Chem. Eng. Progr., 52, 515, **1956**

146 Persaud, G., Tian, X-M. and Cantwell, F. F. Anal. Chem. 59, 2, **1987**

147 Laity, D. S. and Treybal, R. E. AIChE. J., 3, 176, **1957**

148 Cantwell, F. F. and Mohammed, H. Y. Anal. Chem., 51, 218, **1979**

149 Fossey, L. Ph.D. Thesis, University of Alberta, **1985**

150 Boyadzhiev, L., Elenko, D. and Kyuchukov, G. Can. J. Chem. Eng., 47, 42, **1969**

151 IUPAC Ionization Constants of Organic Acids in Aqueous Solutions. Serjeant, E. P. and Dempsey, B. (Eds), Pergamon Press, Oxford, UK. **1979**

152 Leo, A., Hansch, L. C. and Elkins, D. " Partition Coefficients: Their Uses" Chem. Rev., 71, 525, **1971**

153 Awtrey, A. D. and Connick, P.E. J. Amer. Chem. Soc., 17, 1842, **1951**

154 Fudge, A. J. and Sykes, K. W. J. Chem. Soc., 119, **1952**

155 Laurence, G. S. and Ellis, K. J. J. Chem. Soc. (Dalton), 2229, **1972**

156 Hershey, A. V. and Bray, W. C. J. Amer. Chem. Soc., 58, 1760, **1936**

157 Sykes, K. W. J. Chem. Soc., 124, **1952**

158 Perrin, D. D. and Dempsey, B. " Buffer for pH and Metal ion Control" Chapman and Hall, London, **1974**

159 " Stability Constants" J. Chem. Soc., Special Publication. No. 17, 344, **1964**

160 Smith, R. M. and Martell, A. E. " Critical Stability Constants" Plenum Press, New York, **1976**, Volume 4

161 Thorsen, G. and Terjesen, S. G. Chem. Eng. Sci., 17, 137, **1962**

162 Whewell, R. J., Hughes, M. A. and Hanson, C. J. Inorg. Nucl. Chem., 37, 2303, **1975**

163 Brown, A. H. British, Chem. Eng., 10, 622, **1965**

164 Borwankar, R. P. and Wasan, D. T. Ind. Chem. Fundam., 25, 662, **1986**

165 England, D. C. and Berg, J. C. AIChE. J., 17, 313, **1971**

166 Cockbain, E. G. Trans. Faraday Soc., 50, 874, **1954**

167 Scibana, G., Danes , P. R., Conte, A. and Scuppa, B. J. Colloid and Interface Sci., 35, 631, **1971**

168 Watarai, H. Talanta, 32, 817, **1985**

169 Watarai, H. J. Phys. Chem., 89, 384, **1985**

170 Dietz, M. L. and Freiser, H. Langmuir, 3, 467, **1987**

171 Chamupathi, V. G. and Freiser, H. Langmuir, 4, 49, **1988**

172 Lando, J. L. and Oakley, H. T. J. Colloid and Interface Sci., 25, 526, **1967**

173 Mohammed, H. Y. and Cantwell. F. F. Anal. Chem., 52, 553, **1980**

174 Hiemenz, P. C. " Principles of Colloid and Interface Chemistry " Marcell Dekker Inc., New York, Second Ed., **1986**

175 Shaw, D. J. " Introduction to Colloid and Surface Chemistry " Butterworth, London, Third Ed., **1980**

176 Harkins, W. D. and Brown, F. E. J. Amer. Chem. Soc., 41, 499, **1919**

177 Schill, G. Acta. Pharm. Suec., 1, 101, **1964**

177A Schill, G. Acta. Pharm. Suec., 1, 169, **1964**

178 Gibby, C. W. and Addison, C. C. J. Chem Soc., 119, **1936**

179 Modin, R. and Schill, G. Acta. Pharm Suec., 4, 301, **1967**

180 Schill, G. " Ion Exchange ans Solvent Extraction " Marinsky, J. A. and Marcus, Y. (Eds.), Marcell Dekker Inc., New York, **1974**, Volume 6, Chapter 1

181 Rosen, J. M. " Surfactants and Interfacial Phenomena" John Wiley and Sons, New York, **1978**, Chapter 1

182 Giles, C. H., D'Silva, A. P. and Easton, I. A. J. Colloid and Interface Sci., 47, 766, **1974**

183 Haely, T.W. and White, L. R. Adv. Colloid and Interface Sci., 9, 303, **1978**

184 Kolstad, A. K., Chow, P, Y. T. and Cantwell, F. F. Anal. Chem., 60, 1565, **1988**

185 Scibona, G., Danesi, P. R. and Fabiani, C. " Ion Exchange and Solvent Extraction" Marinsky, J. A. and Marcus, Y. (Eds.), Marcell Dekker Inc., New York, **1981**, Volume 8, chapter 2

186 Doyle, T. D. and Levin, J. Anal Chem., 39, 1282, **1967**

187 Nordgren, T. Acta. Pharm. Suec., 16, 215, **1979**

188 Lippold, B. C. and Schneider, G. F. Arzneim. Forsch., 25, 843, **1975**

189 Harada, M., Imamura, T., Fujiyoshi, K. and Eguchi, W. J. Chem. Eng, Jpn., 8, 233, **1975**

190 Shimbashi, T. Bull. Chem. Soc. Jpn., 48, 626, **1975**

191 Divatia, G. J. and Biles, J. A. J. Pharm. Sci., 50, 916, **1961**

192 Borg, K. O. and Schill, G. Acta. Pharm. Suec., 5, 323, **1968**

193 Fitch. P. and Gargus, A. G. Amer. Lab., Dec., **1985**

194 Guided Wave, Inc., El Dorado Hills, CA. 95630

195 Klee, A. J. and Treybal, R. E. AIChE. J., 2, 444, **1956**

196 Hu, S. and Kintner, R. C. AIChE. J., 1, 42, **1955**

197 Garner, F. H. and Skelland, A. H. P. Chem. Eng. Sci., 4, 149, **1955**

APPENDIX A

BEHAVIOUR OF SINGLE DROPS

The following treatment pertains directly to the ascending/descending single drop experiment in which single drops rise or fall through a non-flowing continuous phase. It should also serve as a starting point for understanding the behaviour in the drop-dispersions encountered in rapid stir systems which are more complicated due, for example, to coalescence and re-dispersion in the droplet swarm.

A.I MASS TRANSFER COEFFICIENTS WITH LIQUID DROPS

As discussed by Laddha et.al. [124], different correlations for estimating mass transfer coefficients with liquid drops have been proposed. The appropriate correlation to use depends upon the drop hydrodynamics (e.g. stagnant, partial circulation, etc.) and the phase being considered (i.e. dispersed phase coefficient, $\beta_{mt,\,d}$, or continuous phase coefficient, $\beta_{mt,\,c}$). For turbulent eddy motion inside drops with fully developed internal circulation, Handlos and Baron [73] have proposed the following relationship for $\beta_{mt,\,d}$.

$$\beta_{mt,\,d} = \frac{0.00375 v_t}{1 + \left(\frac{\mu_d}{\mu_c}\right)} \qquad (A.1)$$

where v_t is the terminal velocity of the drop, and μ_d and μ_c are the viscosities of the drop and the surrounding fluid respectively. The corresponding correlation for $\beta_{mt,\,c}$ is given as:

$$\beta_{mt,\,c} = 2\left(\frac{D_c\, v_t}{\pi\, d_p}\right)^{1/2} \qquad (A.2)$$

where D_c is the solute diffusion coefficient in the continuous phase and d_p is the drop diameter.

A.II TERMINAL VELOCITY OF LIQUID DROPS

Whenever relative motion exists between a drop and a surrounding immiscible fluid, the fluid will exert a drag upon the moving drop. The drag force, F, on the drop is defined as [56];

$$F = \frac{C\ A_p\ \rho\ V_t^2}{2\ g_c} \qquad (A.3)$$

where C is the drag coefficient. C is dimensionless and is a function of the Reynolds number and drop shape [195, 196]. A_p is the projected area of the drop in the direction of motion, ρ is the density of the surrounding fluid and g_c is a constant related to the acceleration due to gravity.

A drop falling under gravity will accelerate until the drag force just balances the gravitational force, after which it will continue to fall at a constant velocity known as the terminal velocity. For a spherical drop v_t is defined by [56];

$$V_t = \sqrt{\frac{4\ g\ d_p\ (\rho_d - \rho)}{3\ \rho\ C}} \qquad (A.4)$$

where g is the local acceleration due to gravity and ρ and ρ_d are the densities of the surrounding fluid and the drop respectively. For some systems the drop terminal velocity passes through a maximum with increasing drop diameter while, for others, it levels off at

some ultimately high value [195, 196]. Evidently, the appearance of a maximum in the velocity-diameter curve depends upon the development of oscillations in the drop [197].

Shown in Figure A1 are the V_t vs d_p plots for water drops in chloroform and for chloroform drops in water. Values of C used for the calculation of V_t were calculated by the method described by Hu and Kintner [196]. For both systems the maximum in the plots occurs at a drop diameter of about 0.5 cm. Plots of the mass transfer coefficients vs drop diameter for the extraction of solute from aqueous drops into chloroform and for the extraction from water into chloroform drops are shown in Figure A2.

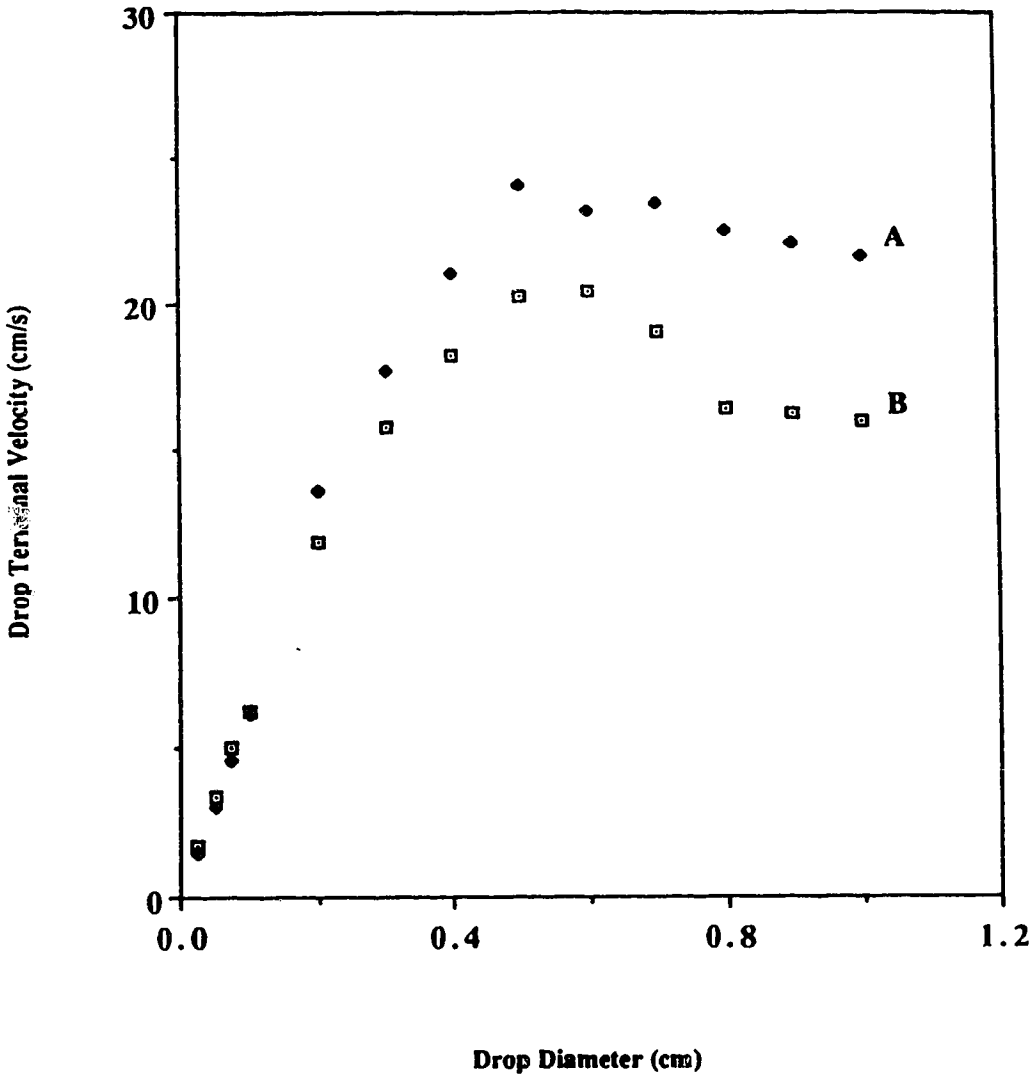

Figure A1 Plots of terminal velocity of falling drops predicted from Equation A.4 vs the diameter of the drops. (A) for chloroform drops moving through water; (B) for water drops moving through chloroform.

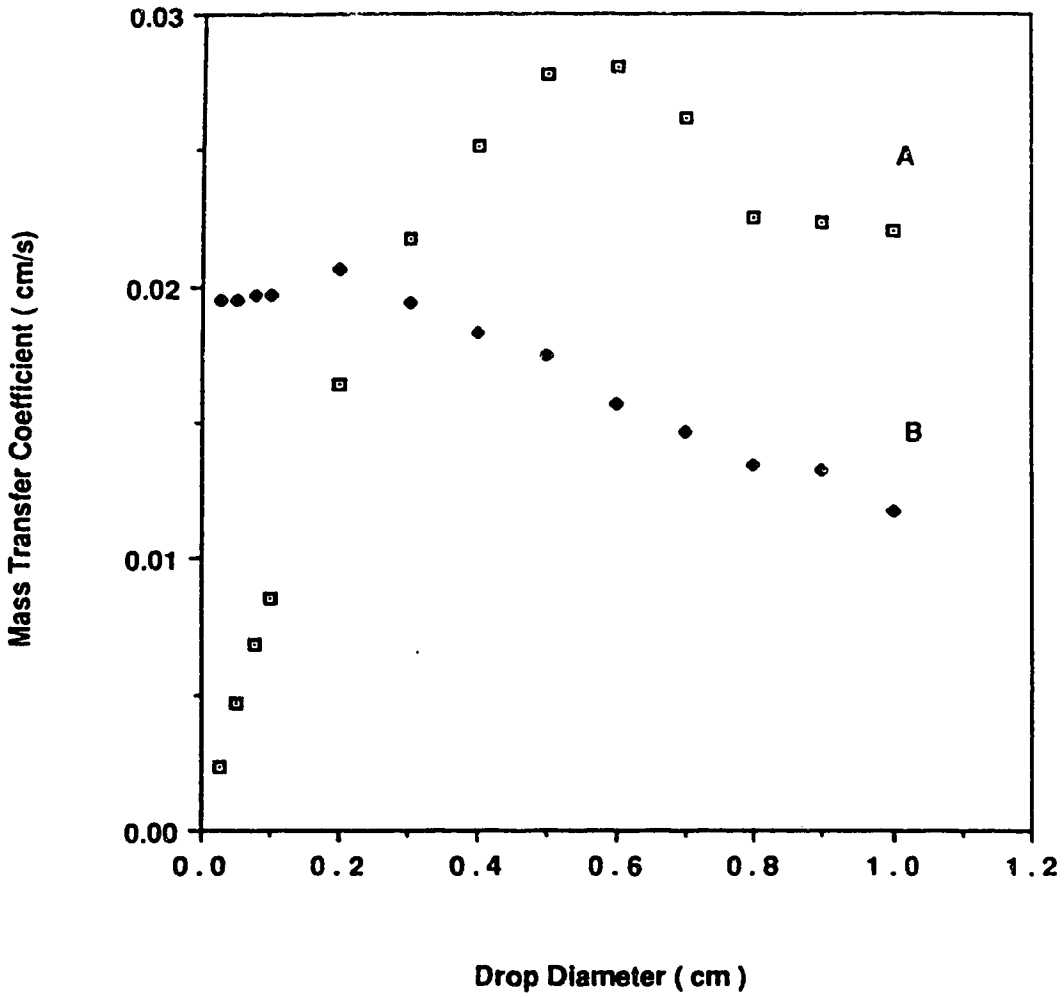

Figure A2 Plots of mass transfer coefficient for the extraction of fron and into falling drops vs the diameter of the drops. (A) for the extraction from water drops into chloroform, from Equation A.1; (B) for the extraction from water into chloroform drops, from Equation A.2.

Appendix B

Moment Analysis Program

```
\ PEAK MOMENT ANALYSIS PROGRAM

\ Program name: MOMENTS.ASY  (ASYST Version 2.0)
\ Directory:  ASYST2
\ Updated by: C. Lucy, 18 September 1987
\       ( This program is based on XYDPP.DMO shown in the ASYST
\         Module 1 manual, pg. I-20-16 to I-20-23. )

\     The program is designed to calculate the moments of data entered manually or
\  recalled from previously written files. Graphical displays are provided to aid the
\  operator. Various operations - smoothing, baseline set, derivatives - are available
\  for use.

\-------------------------------------- ----------------------------------------------------

\ Program Structure

\     The program is designed to be menu driven. The menus are two-tiered. The upper
\  most menu is Main Menu, from which either the Plot Menu or Summary menu can be
\  accessed.

\ Main Menu

\  F1) Quit - exits operation from the moments program and from Asyst.

\  F2) Plot - plots the data on the screen along with its baseline. Accesses the Plot Menu
\            where data massaging options are available.

\  F3) Enter data - sets up the input array for manual entry of data.

\  F4) Read file - scrolls all files with the extension .DAT on the screen, and then reads
\                  the file requested.

\  F5) Save file - stores the current data file. The filename should include the extension
\                  ".DAT".

\  F6) Edit data - displays the current data array on the screen and allows editing of the
\                  data. Three columns appear; the retention time, the signal, and the
\                  baseline.

\  F7) Moments - calculates the first five moments for the current data, i.e. the
\                  unnormalized peak area, the center-of-gravity, and the variance, and
\                  from the third and fourth moments the skew and excess are calculated.
\                  The asymmetry factor (10%) is also calculated.

\  F8) Summary - accesses the Summary Menu. Purpose is to produce a hard copy of
\                  the moments.
```

```
\ Plot Menu

\   F1) Exit - will return operation to the Main Menu.

\   F2) Plot - plots the signal on the screen.

\   F3) Plot baseline - plots the baseline onto the signal plot.

\   F4) Change symbols - allows selection of the symbol to be used for the signal and
\                baseline data. Default values are "." for signal and "." for baseline.

\   F5) Lin. Reg. Baseline - sets baseline by performing linear regression on the data
\                            before and after the peak. The before/after limits are set using
\                            manually controlled cursors.

\   F6) Derivative - calculates the derivative of the signal and automatically sets the baseline
\                    by drawing a straight line between the first and last data points.

\   F7) Smooth - applies a low pass filter to the data to remove noise.

\   F9) (hidden function) - stalls the computer until the baseline limits for F5 have been set.


\ Summary Menu

\   F1) Exit - returns operation to the Main menu.

\   F2) Print summary - prints out the data file specifications and the calculated moments.

\   F3) Print data - prints out the data file specifications and the data.

\   F4) Plot summary - prints out a copy of the data plot along with the file identification
\                      specifications, and the calculated moments.

\-------------------------------------------------------------------------------------------

\ Overlay check

ECHO.OFF
: OLOAD?
      CR BELL
      ." Are the overlays AR-EDIT.SOV, DATAFILE.SOV, MATFIT.SOV and
        WAVEOPS.SOV"
      CR ." in the system (Y/N) ? "
      KEY DUP EMIT
      DUP 90 > IF 32 - THEN 89 = NOT
      IF
          CR CR ." Please use the Configuration menu <F2> to load the Array Editor,"
          CR    ." Data File, Matrix manipulation and Waveform analysis overlays"
          CR    ." permanently in the system before continuing."
          CR    ." The last two overlays are located in Analysis overlays." CR CR
          57 ERROR
      THEN
;
```

```
OLOAD?
ECHO.ON

\----------------------------------------------------------------------------------------------------

\ Variable declarations

  INTEGER SCALAR MAXSETS
     SCALAR MAX.IN.SET
     SCALAR #SETS
     SCALAR COL#
     SCALAR LIN.END          \ End of baseline before peak
     SCALAR LIN.REG.#        \ No. of data points defining baseline.
     SCALAR FIRST#           \ First data point of the peak.
     SCALAR LAST#            \ Last data point of the peak.
     SCALAR #.IN.PEAK        \ No. of data points defining peak.
     SCALAR ARRAY.SIZE

  2000 MAXSETS   :=          \ Either of these lines may be changed
    3  MAX.IN.SET :=         \ to allow larger data sets to be used.

     DIM[ 2 ] ARRAY HOLDIT   \ Output buffer for #SETS & MAX.IN.SETS

REAL SCALAR DELTA.T          \ Interval between successive data points.
     SCALAR PEAK.LIMITS      \ % of max that defines the peak edges
     SCALAR PEAK.AREA        \          - zeroth moment
     SCALAR PEAK.CENTER      \ Moments variables - first moment
     SCALAR PEAK.VAR         \          - second moment
     SCALAR PEAK.SKEW        \          - from 3rd moment
     SCALAR PEAK.EXCESS      \          - from 4th moment
     SCALAR ASYM.FACTOR      \ Asymmetry factor at 10% maximum
     SCALAR W(1/2)           \ Width at half height
     SCALAR %MAX

     0.1 PEAK.LIMITS :=

     DIM[ MAXSETS , MAX.IN.SET ] ARRAY PEAK.DATA    \ Create the peak.data
                                                    \ set(s) buffer.
     DIM[ MAXSETS ] ARRAY CONC.i          \ Net peak intensities
     DIM[ 4 ] ARRAY BASELINE.LIMITS       \ Coordinates of markers.
     DIM[ MAXSETS ] ARRAY LIN.REG.X       \ x values of baseline
     DIM[ MAXSETS ] ARRAY LIN.REG.Y       \ y values of baseline
     DIM[ 2 ] ARRAY PEAK.MAX              \ location & mag of max

  25  STRING OP.NAME          \ Operator's name.
  25  STRING TITLE            \ Experiment title.
  25  STRING EXP#             \ Experiment number.
  25  STRING XLBL             \ X-axis label
  10  STRING YLBL             \ Y-axis label
   1  STRING DATA.SYM.S       \ Data symbol for signal
   1  STRING DATA.SYM.B       \ Data symbol for baseline
  14  STRING FILENAME
```

```
\----------------------------------------------------------------------------------------------------

\ Window definitions

\ Divides screen into small windows which are used to present plots, menus and specs.

  0 0   0 79   WINDOW (TOPLINE)      \ Top banner line across screen.
  1 0   6 19   WINDOW (SPECS)        \ Top left window for experiment specs.
  8 0  17 19   WINDOW (SPEC.MOM)     \ Mid left window for moments.
 19 0  19 79   WINDOW (SPLIT1)       \ Middle window for menu banners.
 20 0  21 79   WINDOW (SPLIT2)       \ Middle window for menus.
 24 0  24 79   WINDOW (BOTLINE)      \ Bottom line of screen for prompt.
  1 0  24 79   WINDOW (DEF-1)        \ Excludes top banner line.

\----------------------------------------------------------------------------------------------------

: DATA.VU   \ Defines plotting parameters for graph.

     .270 .300  VUPORT.ORIG                    \ Defines the position and
     .730 .650  VUPORT.SIZE                    \  size of the plot window.
     HORIZONTAL AXIS.FIT.OFF GRID.OFF          \ Removes the grids from
     VERTICAL   AXIS.FIT.OFF GRID.OFF          \  the graph.
     .180 .210  AXIS.ORIG                      \ Sets the graph position and
     .800 .740  AXIS.SIZE                      \  size with the window.
     .025 .008  TICK.SIZE
     .5   .8    TICK.JUST
;

\----------------------------------------------------------------------------------------------------

\ Screen Messages


: BANNER          \ Program banner
     (TOPLINE) SCREEN.CLEAR
     25 SPACES ." Peak Moment Analysis Program"
;


: PROMPT          \ Prompt on bottom line while menu is displayed.
     (BOTLINE) SCREEN.CLEAR ."     Your choice please "
;


: WAIT            \ Message signifying that the computer is performing calculations.
     (BOTLINE) SCREEN.CLEAR ."     Please wait "
;

\----------------------------------------------------------------------------------------------------
```

```
\ Screen Menus

: MAIN.MENU
    {SPLIT2} HOME SCREEN.CLEAR
    13 SPACES ." F1) Quit      F2) Plot      F3) Enter data  F4) Read file"
    CR 13 SPACES ." F5) Save file  F6) Edit data  F7) Moments F8) Summary"
    {SPLIT1} HOME SCREEN.CLEAR 32 SPACES ." ** Main Menu **"
    PROMPT
    CURSOR.OFF
;


: PLOT.MENU
    {SPLIT1} SCREEN.CLEAR
    32 SPACES ." **  Plotting menu  **"
    {SPLIT2} SCREEN.CLEAR
    8 SPACES
    ." F1) Exit  F2) Plot  F3) Plot baseline  F4) Change symbols  "
    CR 8 SPACES ." F5) Lin. reg. baseline  F6) Derivative  F7) Smooth "
;


: SUMMARY.MENU
    {SPLIT2} HOME SCREEN.CLEAR
    10 SPACES ." F1) Exit  F2) Print summary  F3) Print data  F4) Plot summary"
    {SPLIT1} SCREEN.CLEAR
    27 SPACES ." ** Summary Menu **"
    {BOTLINE} SCREEN.CLEAR
;

\-----------------------------------------------------------------------------------------------

\ Data Plotting functions


: DATA.VU.SET          \ Word to setup data viewport axis area
    PEAK.DATA XSECT[ 2 ] SUB[ 1 , #SETS ]    \ Sets the origin of the graph
    []MIN/MAX                                \ Offsets the baseline from the
    SWAP                                     \ horizontal axis. The offset is
    DUP                                      \ calculated by the expression
    ROT                                      \ []min - ( []max - []min ) / 5
    -
    5. /
    + DUP
    PEAK.DATA XSECT[ 2 ] SUB[ 1 , #SETS ]
    []MAX
    WORLD.COORDS
    VERTICAL WORLD.SET
    PEAK.DATA XSECT[ 1 ] SUB[ 1 , #SETS ] DUP
    []MIN/MAX HORIZONTAL WORLD.SET
    []MIN SWAP WORLD.COORDS AXIS.POINT
;
```

```
: SHOW.SPECS          \Displays experimental identification specs on screen.
    (SPECS)  SCREEN.CLEAR
    ." Date: " .DATE CR
    ." Operator: "      OP.NAME "TYPE CR
    ." Exp. title: " CR   TITLE "TYPE CR
    ." Exp. number: "     EXP# "TYPE
;

: SHOW.MOMENTS      \Displays the peak moments on the left side of screen.
    (SPEC.MOM)  SCREEN.CLEAR
    ." Area=" 4 SPACES    PEAK.AREA . CR
    ." Center=" 2 SPACES PEAK.CENTER . CR
    ." Variance="         PEAK.VAR . CR
    ." Skew=" 4 SPACES    PEAK.SKEW . CR
    ." Excess=" 2 SPACES PEAK.EXCESS . CR
    ." B/A (10%)= "     ASYM.FACTOR . CR
    ." W(1/2)     "       W(1/2) .
;

: LABEL.PLOT          \Positions the x and y labels for the plot axes.
    NORMAL.COORDS
    .0250 .75 POSITION 270 LABEL.DIR      \Positioning the y label
    YLBL LABEL                            \Writing the y label
    XLBL "LEN 2. /                        \1/2 the number of XLBL sets
    .0175 * .5 SWAP -                     \ the position of the y-label
    .05 POSITION  0 LABEL.DIR
    LABEL                                 \Writing the x label
    CURSOR.OFF
;

: PLOT.DATA           \ Command which plots signal data on the screen.
    DATA.VU                               \
    VUPORT.CLEAR                          \Setting up the axes of the
    DATA.VU.SET                           \ graph based on the range
    XY.AXIS.PLOT                          \ of the data.
    DATA.SYM.S SYMBOL
    PEAK.DATA XSECT[ 1 ] SUB[ 1 , #SETS ]  \
    PEAK.DATA XSECT[ 2 ] SUB[ 1 , #SETS ]  \Plotting the signal data
    XY.DATA.PLOT                          \
    LABEL.PLOT
    OUTLINE
    SHOW.SPECS
;

\-----------------------------------------------------------------------------------------
```

```
\ Plotting Options

: PLOT.BASELINE              \Overlays the baseline on the signal plot.
    WAIT
    DATA.VU
    DATA.VU.SET
    DATA.SYM.B SYMBOL
    PEAK.DATA XSECT[ 1 ] SUB[ 1 , #SETS ]      \Plotting the baseline
    PEAK.DATA XSECT[ 3 ] SUB[ 1 , #SETS ]      \ using the axes established
    XY.DATA.PLOT                               \ for the signal data.
    PROMPT
;

: CHANGE.SYMBOL              \Changing the plotting symbol for data plots.
    {SPLIT2} SCREEN.CLEAR ." Change " DATA.SYM.S "TYPE
        ." to (enter character <cr>)"          \
    "INPUT DATA.SYM.S ":=                      \Changing the signal
    DATA.SYM.S " " "= IF MYSELF THEN           \ plotting symbol
    PLOT.MENU
    SCREEN.CLEAR ." Change " DATA.SYM.B "TYPE
        ." to (enter character <cr>)"          \
    "INPUT DATA.SYM.B "=                       \Changing the baseline
    DATA.SYM.B " " "= IF MYSELF THEN           \ plotting symbol
    PLOT.MENU
;

: SET.BASELINE               \Allows operate to declare the start and end of peak
    0 BASELINE.LIMITS :=
    BASELINE.LIMITS
    READOUT>ARRAY
    ARRAY.READOUT    \Activates the cursor controls for setting the baseline limits
    {SPLIT2} HOME SCREEN.CLEAR
        ." Use cursor controls to position markers at"
        ." the baseline limits (left first)"
        CR ." Review ARRAY.READOUT for listing of key functions."
    {BOTLINE} SCREEN.CLEAR
        ." Press F9 when done"    \Purpose of F9 is to get the computer to wait for the
                                  \ operator to declare the peak limits.
;

: LIN.REG.BASELINE           \Calculates the best fit line through the
    {BOTLINE} SCREEN.CLEAR   \ baseline declared using SET.BASLINE.
    0 LIN.REG.# :=
    #SETS 1 + 1 DO
        PEAK.DATA [ I , 1 ] DUP
        BASELINE.LIMITS [ 1 ] =
        IF
            I LIN.END :=
        THEN
        DUP BASELINE.LIMITS [ 1 ] <=
        BASELINE.LIMITS [ 3 ] >=
```

```
        OR
        IF
            LIN.REG.#  1  +  LIN.REG.# :=
            PEAK.DATA [ I , 1 ]  LIN.REG.X [ LIN.REG.# ] :=
            PEAK.DATA [ I , 2 ]  LIN.REG.Y [ LIN.REG.# ] :=
        THEN
    LOOP
    LIN.REG.X SUB[ 1 , LIN.REG.# ]
    LIN.REG.Y SUB[ 1 , LIN.REG.# ]
    1 LEASTSQ.POLY.FIT                          \First order polynomial least squares
    DUP                                         \  i.e. linear least squares.
    [ 1 ]
    PEAK.DATA XSECT[ 1 ] SUB[ 1 , #SETS ]  *
    SWAP [ 2 ]  +
    PEAK.DATA XSECT[ 3 ] SUB[ 1 , #SETS ] :=
    PLOT.MENU
;


: DERIVATIVE     \Calculates the derivative of the signal data using the
                 \  equation:  f'(x) =[f(x + dx) - f(x)] / dt
        (Written by L. Amankwa for his research.  Not used in C. Lucy research.)
    #SETS 1 -
    #SETS :=
    PEAK.DATA XSECT[ 2 ] SUB[ 2 , #SETS ]     \Calculating change in response
    PEAK.DATA XSECT[ 2 ] SUB[ 1 , #SETS ]        \ for a dt change in time
    -
    PEAK.DATA XSECT[ 1 ] [ 2 ]                  \Calculating dt
    PEAK.DATA XSECT[ 1 ] [ 1 ]                  \
    -
    /                                           \change in response / dt
    PEAK.DATA XSECT[ 2 ] SUB[ 1 , #SETS ] :=
    PEAK.DATA XSECT[ 2 ] SUB[ 1 , #SETS ] [ 1 ] DUP      \
    PEAK.DATA XSECT[ 2 ] SUB[ 1 , #SETS ] [ #SETS ]      \Calculating the
    SWAP - #SETS 1. - /                                  \baseline - setting
    PEAK.DATA XSECT[ 3 ] SUB[ 1 , #SETS ] []RAMP         \a straight line
    PEAK.DATA XSECT[ 3 ] SUB[ 1 , #SETS ] 1. -           \between the first &
    * + PEAK.DATA XSECT[ 3 ] SUB[ 1 , #SETS ] :=         \last points
;


: PEAK.SMOOTH     \Smoothing of data by convolution with weights from a low
                  \  pass BLACKMAN window frequency response (l p filter)
        (Written by L. Amankwa for his research.  Not used in C. Lucy research.)
    PEAK.DATA XSECT[ 2 ] SUB[ 1 , #SETS ]
    SMOOTH
    PEAK.DATA XSECT[ 2 ] SUB[ 1 , #SETS ] :=
;

\----------------------------------------------------------------------------------------
```

```
\Summary options

: PRINT.SUMMARY      \Prints out experimental specs and moments.
     {SPLIT2} SCREEN.CLEAR
     ." <cr> when printer is ready..." BELL
     ." (Any other key aborts)"
     PCKEY ?DROP 13 <>
     IF
          SUMMARY.MENU
     ELSE
          {DEF-1} SCREEN.CLEAR OUT>PRINTER CR CR CR
          4 SPACES ." Date: " .DATE 5 SPACES ." Time: " .TIME
          8 SPACES ." Operator: "     OP.NAME "TYPE CR CR
          4 SPACES ." Experiment name: " TITLE "TYPE CR
          4 SPACES ." Experiment number: " EXP# "TYPE CR CR
          4 SPACES ." AREA:     "   PEAK.AREA .    CR
          4 SPACES ." CENTER    " PEAK.CENTER .    CR
          4 SPACES ." VARIANCE  "   PEAK.VAR .    CR
          4 SPACES ." SKEW      "   PEAK.SKEW .    CR
          4 SPACES ." EXCESS    " PEAK.EXCESS .    CR
          4 SPACES ." B/A (10%) " ASYM.FACTOR .    CR
          4 SPACES ." W(1/2)    "     W(1/2) .    CR CR
          CONSOLE
          CR ." Press any key to continue."
          PCKEY ?DROP DROP
          {DEF-1} SCREEN.CLEAR
          SUMMARY.MENU
     THEN
;


: PRINT.DATA          \Prints out a full listing of the data
     {SPLIT2} SCREEN.CLEAR
     ." <cr> when printer is ready..." BELL
     ." (Any other key aborts)"
     PCKEY ?DROP 13 <>
     IF
          SUMMARY.MENU
     ELSE
          {DEF-1} SCREEN.CLEAR OUT>PRINTER CR CR CR
          4 SPACES ." Date: " .DATE 5 SPACES ." Time: " .TIME
          8 SPACES ." Operator: "     OP.NAME "TYPE CR CR
          4 SPACES ." Experiment name: " TITLE "TYPE CR
          4 SPACES ." Experiment number: " EXP# "TYPE CR CR

          ." X-values       Signal       Baseline"
          CR CR
          #SETS 1 + 1 DO
               PEAK.DATA [ I , 3 ]
               PEAK.DATA [ I , 2 ]
               PEAK.DATA [ I , 1 ]
               . 18 ?COL - SPACES . 36 ?COL - SPACES . CR
          LOOP
          CONSOLE
```

```
        CR ." Press any key to continue."
        PCKEY ?DROP DROP
        {DEF-1} SCREEN.CLEAR
        SUMMARY.MENU
    THEN
;

: PLOT.SUMMARY              \Prints out a plot of the data with the moments
    SCREEN.CLEAR
    PLOT.DATA
    SHOW.MOMENTS
    {SPLIT1} SCREEN.CLEAR
    {SPLIT2} SCREEN.CLEAR
    ." <cr> when printer is ready . . ." BELL
    ." (Any other key aborts) "
    PCKEY ?DROP 13 <>
    IF
        SUMMARY.MENU
    ELSE
        {SPLIT2} SCREEN.CLEAR
        SCREEN.PRINT
        CONSOLE
        CR ." Press any key to continue. "
        PCKEY ?DROP DROP
        {DEF-1} SCREEN.CLEAR
        SUMMARY.MENU
    THEN
;

\-------------------------------------------------------------------------------

\Saving the data in memory.

: WRITE.FILE                \Default drive for data storage is C (Hard Drive).
    FILE.TEMPLATE
      5 COMMENTS                        \
      INTEGER DIM[ 2 ] SUBFILE          \Defines the format of
      REAL DIM[ #SETS ] SUBFILE         \ the data file.
      REAL DIM[ #SETS ] SUBFILE         \
      REAL DIM[ #SETS ] SUBFILE         \
    END

    HOME
    ." Opening file " FILENAME "TYPE
    13 EMIT FILENAME DEFER> FILE.CREATE
    ." Writing file " FILENAME "TYPE
    13 EMIT FILENAME DEFER> FILE.OPEN

    TITLE    1 >COMMENT                 \
    OP.NAME  2 >COMMENT                 \Outputs the variables to the
    EXP#     3 >COMMENT                 \ appropriate positions in
    XLBL     4 >COMMENT                 \ the data file.
    YLBL     5 >COMMENT                 \
```

```
    #SETS HOLDIT [ 1 ] :=
    MAX.IN.SET HOLDIT [ 2 ] :=
    1 SUBFILE HOLDIT    ARRAY>FILE
    2 SUBFILE PEAK.DATA XSECT[ 1 ] SUB[ 1 , #SETS ]  ARRAY>FILE
    3 SUBFILE PEAK.DATA XSECT[ 2 ] SUB[ 1 , #SETS ]  ARRAY>FILE
    4 SUBFILE PEAK.DATA XSECT[ 3 ] SUB[ 1 , #SETS ]  ARRAY>FILE
    FILE.CLOSE

    ONERR:                                  \Error trap.
        ." Can't open file for writing. "
        ." Type any key to continue."  BELL PCKEY ?DROP DROP
        ?FILE.OPEN IF FILE.CLOSE THEN
;


: GET.FILENAME                          \Requests name for data file.
    ." filename please ?  " "INPUT
    FILENAME ":=
    SCREEN.CLEAR
;


: OUTPUT.DATA.FILE                      \Invokes the words above to save the data.
    #SETS 0 >
    IF
        SCREEN.CLEAR
        {SPLIT2} SCREEN.CLEAR  ." Output "
        GET.FILENAME
        WRITE.FILE
        MAIN.MENU
    THEN
;

\-----------------------------------------------------------------------------------------------

\Data input  - either from memory (READ.FILE) or from the keyboard (ENTER.DATA)

: READ.FILE       \Must be in format used by DATACQ, MOMENTS & SEGMENT
    {SPLIT2} SCREEN.CLEAR
    ." Reading " FILENAME DEFER> FILE.OPEN
    FILENAME 'TYPE 13 EMIT
    1 COMMENT> TITLE ":=                    \
    2 COMMENT> OP.NAME ":=                  \
    3 COMMENT> EXP# ":=                     \
    4 COMMENT> XLBL ":=                     \ Assign values from the
    5 COMMENT> YLBL ":=                     \  data file to the
    1 SUBFILE HOLDIT FILE>ARRAY             \  various variables.
    HOLDIT [ 1 ] #SETS :=                   \
    HOLDIT [ 2 ] MAX.IN.SET :=              \
    2 SUBFILE PEAK.DATA XSECT[ 1 ] SUB[ 1 , #SETS ]  FILE>ARRAY
    3 SUBFILE PEAK.DATA XSECT[ 2 ] SUB[ 1 , #SETS ]  FILE>ARRAY
    4 SUBFILE PEAK.DATA XSECT[ 3 ] SUB[ 1 , #SETS ]  FILE>ARRAY
    FILE.CLOSE
```

```
    ONERR:                                  \Error trap.
        ." Can't open file for writing. "                                    244
            ." Type any key to continue." BELL PCKEY ?DROP DROP
     ?FILE.OPEN IF FILE.CLOSE THEN
;

: INPUT.DATA.FILE          \Prints out a list of files available & requests choice
    {DEF-1} SCREEN.CLEAR
    DIR *.DAT
    CR CR ." Input "
     GET.FILENAME
    READ.FILE
    MAIN.MENU
;

: ED.DATA                  \Word allows editing of the data array.
    #SETS 0 >
    IF
        PEAK.DATA SUB[ 1 , #SETS ; COL# , MAX.IN.SET ] ARRAY.EDIT
        INTEN.ON BELL
        ." Use the cursor keys to move cursor."
        CR CR
        ." Press <cr> to exit back to main menu"
        ARRAY.EDIT.WORDS                \Sets up array for editing
        INSERT                          \
        GRAPHICS.DISPLAY
        BANNER                          \Returns to main menu when done
        MAIN.MENU                       \  editing file.
    THEN
;

: ENTER.DATA               \Word allows manual entry of data.
    {DEF-1} SCREEN.CLEAR
    ." New data set:" CR CR
    ." Your name (or initials) please? " "INPUT OP.NAME ":= CR CR
    ." Title of experiment? (name for data set) " "INPUT TITLE ":= CR CR
    ." Experiment identification number? " "INPUT EXP# ":= CR CR
    ." X-axis label? (15 chars. or less) " "INPUT XLBL ":= CR
    ." Y-axis label? (10 chars. or less) " "INPUT YLBL ":= CR CR
    BEGIN
        ." Number of data sets in this experiment ? " #INPUT CR CR
        IF #SETS :=
        ELSE GRAPHICS.DISPLAY {SPLIT1} HOME ." Press F1" EXIT
        THEN
        #SETS MAXSETS >
        IF ." Maximum #sets allowable is " MAXSETS
            -1 0 FIX.FORMAT MAXSETS .
            -1 4 SCI.FORMAT FALSE
        ELSE TRUE
        THEN
    UNTIL
```

```
    2 COL# :=
    1 MAX.IN.SET :=                                          \
    PEAK.DATA XSECT[ 1 ] SUB[ 1 , #SETS ] []RAMP             \
    PEAK.DATA XSECT[ 1 ] SUB[ 1 , #SETS ] 1. -               \Filling in the
    ." The first x-value is: " #INPUT CR                     \retention values
    SWAP                                                     \into the data array
    ." The interval between points is: " #INPUT              \
    * + PEAK.DATA XSECT[ 1 ] SUB[ 1 , #SETS ] :=             \
    ED.DATA
    1 COL# :=
    3 MAX.IN.SET :=
    PEAK.DATA XSECT[ 2 ] SUB[ 1 , #SETS ] [ 1 ] DUP          \
    PEAK.DATA XSECT[ 2 ] SUB[ 1 , #SETS ] [ #SETS ]          \Calculating the
    SWAP - #SETS 1. - /                                      \baseline - setting
    PEAK.DATA XSECT[ 3 ] SUB[ 1 , #SETS ] []RAMP             \a straight line
    PEAK.DATA XSECT[ 3 ] SUB[ 1 , #SETS ] 1. -               \between the first &
    * + PEAK.DATA XSECT[ 3 ] SUB[ 1 , #SETS ] :=             \last points
;

\-------------------------------------------------------------------------------------------------

: LOCATE.PEAK.MAX  \Locates the maximum value in a data set. Stores the
                   \array index and the intensity of this maximum in the
                   \two-element array PEAK.MAX
    \Stack in : array containing peak
    \Stack out: empty
    0 PEAK.MAX [ 1 ] :=
    0 PEAK.MAX [ 2 ] :=
    #SETS 1 DO
        DUP
        [ I ]  PEAK.MAX [ 2 ] >
        IF
            DUP [ I ]  PEAK.MAX [ 2 ] :=
            I      PEAK.MAX [ 1 ] :=
        THEN
    LOOP
    DROP
;


: FIND.?.%MAX      \Locates the array index of the point along the front
                   \and tail of a peak which have an intensity of __% of the
                   \maximum. Stores these positions in the variables
                   \FIRST# AND LAST#
    \Stack in : array size
    \       % of maximum to be found
    \       array containing peak
    \Stack out: empty
    ARRAY.SIZE :=                \The top number on the stack denotes the array size
    1  FIRST# :=                 \Set variables to their default settings
    PEAK.MAX [ 1 ] LAST# :=      \  - i.e. the extremes of the array.
    100. /                       \The second number on the stack is the percentage
    PEAK.MAX [ 2 ] *             \  of the peak height. This % is converted to its
    %MAX :=                      \  numerical counterpart and stored in %MAX.
```

```
    PEAK.MAX [ 1 ]  1  DO
        DUP [ I ]  %MAX  <
        IF
            I  FIRST# :=
        THEN
    LOOP
    ARRAY.SIZE   PEAK.MAX [ 1 ]  DO
        DUP [ I ]  %MAX >
        I LAST# -  3    < AND
        IF
            I  LAST# :=
        THEN
    LOOP
    DROP
    LAST# FIRST# - 1 + #.IN.PEAK :=
;


: PEAK.MOMENTS              \ Calculation of the moments of the peak.
    WAIT
    PEAK.DATA XSECT[ 1 ] [ 2 ]
    PEAK.DATA XSECT[ 1 ] [ 1 ] -
    DELTA.T :=
    PEAK.DATA XSECT[ 2 ] SUB[ 1 , #SETS ]
    PEAK.DATA XSECT[ 3 ] SUB[ 1 , #SETS ] -
    DUP DUP
    CONC.I SUB[ 1 , #SETS ] :=
    LOCATE.PEAK.MAX
    PEAK.LIMITS
    #SETS
    FIND.?.%MAX

 \ The zeroth moment = unnormalized peak area
 \ Zeroth moment = summation( Ci * dt )
 \      Stack in: empty
 \      Stack out: (Ci * dt)
    CONC.I SUB[ FIRST# , LAST# ]  DELTA.T  *
    DUP                                    \ approx integration
    INTEGRATE.DATA [ #.IN.PEAK ]           \  with 1/3 Simpson's
    PEAK.AREA  :=                          \  rule and store.

 \ The first moment = peak center
 \ First moment = 1/area * integration( t * Ci * dt )
 \      Stack in: (Ci * dt)
 \      Stack out: empty
    PEAK.DATA XSECT[ 1 ] SUB[ FIRST# , LAST# ] *      \ t = time or volume
                                                      \     along the x axis
    INTEGRATE.DATA  [ #.IN.PEAK ]                     \ approx. integration
    PEAK.AREA /                                       \ divide by area.
    PEAK.CENTER :=                                    \ and store.
```

```
\ The second moment = peak variance
\ Second moment = 1/area * [ integration( (t-tr)2 * Ci * dt ) ]
\       Stack in: empty
\       Stack out: (t-tr)
      PEAK.DATA XSECT[ 1 ] SUB[ FIRST# , LAST# ]
      PEAK.CENTER -  DUP                          \ save t-tr on stack
      DUP *                                       \ calc (t-tr)2
      CONC.I SUB[ FIRST# , LAST# ]  *             \ and mult by Ci
      DELTA.T *                                   \ and mult by dt
      INTEGRATE.DATA [ #.IN.PEAK ]                \ and integrate
      PEAK.AREA /                                 \ and normalize.
      ABS
      PEAK.VAR :=                                 \ and store.

\ Third moment = 1/area * [ integration( (t-tr)3 * Ci * dt ) ]
\ Peak skew = third moment / variance3/2
\       Stack in: (t-tr)
\       Stack out: (t-tr)
      DUP                                         \ save extra t-tr
      3 **                                        \ calc (t-tr)3
      CONC.I SUB[ FIRST# , LAST# ]  *             \ and mult. by Ci
      DELTA.T *                                   \ and mult. by dt
      INTEGRATE.DATA [ #.IN.PEAK ]                \ and integrate
      PEAK.AREA /                                 \ and normalize
      PEAK.VAR 1.5 ** /                           \ and convert to the
      PEAK.SKEW :=                                \ skew and store.

\ Fourth moment = 1/area * [ integration( (t-tr)4 * Ci * dt )]
\ Peak excess = fourth moment / variance2 - 3
\       Stack in: (t-tr)
\       Stack out: empty
      4 **                                        \ calc (t-tr)4
      CONC.I SUB[ FIRST# , LAST# ] *              \ and mult. by Ci
      DELTA.T *                                   \ and mult. by dt
      INTEGRATE.DATA [ #.IN.PEAK ]                \ and integrate
      PEAK.AREA /                                 \ and normalize
      PEAK.VAR DUP * /                            \ and convert to the
      3. -                                        \ excess
      PEAK.EXCESS :=                              \ and store.
;

: ASYM.MEAS                   \ Asymmetry factor (B/A) at 10% of the peak max.
      CONC.I SUB[ 1 , #SETS ]
      10 #SETS
      FIND.?.%MAX             \ Locates the points at 10% of the peak max
      LAST# PEAK.MAX [ 1 ] -
      PEAK.MAX [ 1 ] FIRST# -
      / ASYM.FACTOR :=
;
```

```
: WIDTH.AT.HALF.HEIGHT          \Calculates the width at half height
    CONC.I SUB[ 1 , #SETS ]
    50 #SETS
    FIND.?.%MAX
    LAST# FIRST# -
    DELTA.T *
    W(1/2) :=
;

: MOMENTS                       \Primary word for initiating calculation of the moments.
    PEAK.MOMENTS
    ASYM.MEAS
    WIDTH.AT.HALF.HEIGHT
    SHOW.MOMENTS
    PROMPT
;

\-----------------------------------------------------------------------------------------

: SUMMARY.KEYS                  \Redefines the keys to the summary options.
    F1 FUNCTION.KEY.DOES ESCAPE
    F2 FUNCTION.KEY.DOES PRINT.SUMMARY
    F3 FUNCTION.KEY.DOES PRINT.DATA
    F4 FUNCTION.KEY.DOES PLOT.SUMMARY
    F5 FUNCTION.KEY.DOES NOP
    F6 FUNCTION.KEY.DOES NOP
    F7 FUNCTION.KEY.DOES NOP
    F8 FUNCTION.KEY.DOES NOP
    F9 FUNCTION.KEY.DOES NOP
;

: MAIN.SUMMARY
    SCREEN.CLEAR
    STORE.FUNCTION.KEYS
    SUMMARY.KEYS
    SUMMARY.MENU
    INTERPRET.KEYS
     0. PEAK.AREA   :=
    0. PEAK.CENTER :=
    0. PEAK.VAR    :=
    0. PEAK.SKEW   :=
    0. PEAK.EXCESS :=

    ONESCAPE: RESTORE.FUNCTION.KEYS MAIN.MENU
;

\-----------------------------------------------------------------------------------------
```

```
: PLOT.KEYS              \Redefines the function key to the plotting options
     F1 FUNCTION.KEY.DOES ESCAPE
     F2 FUNCTION.KEY.DOES PLOT.DATA
     F3 FUNCTION.KEY.DOES PLOT.BASELINE
     F4 FUNCTION.KEY.DOES CHANGE.SYMBOL
     F5 FUNCTION.KEY.DOES SET.BASELINE
     F6 FUNCTION.KEY.DOES DERIVATIVE
     F7 FUNCTION.KEY.DOES PEAK.SMOOTH
     F8 FUNCTION.KEY.DOES NOP
     F9 FUNCTION.KEY.DOES LIN.REG.BASELINE
;

: MAIN.PLOT.DATA
     #SETS 0 >
     IF
          SCREEN.CLEAR
          STORE.FUNCTION.KEYS          \
          PLOT.KEYS                    \
          PLOT.MENU                    \Sets up the plotting
          PLOT.DATA                    \ screen and plots
          PLOT.MENU                    \ the data.
          INTERPRET.KEYS               \
     THEN

     ONESCAPE: RESTORE.FUNCTION.KEYS MAIN.MENU
;

\-------------------------------------------------------------------------------------------

: PEAK.QUIT                   \Word to quit application of this program.
     SCREEN.CLEAR \Clears prompt
     (SPLIT2) SCREEN.CLEAR BELL ." Quit ?"
     PCKEY ?DROP 89 = IF BYE THEN
     MAIN.MENU
;

: MAIN.KEYS                   \Sets up function keys for MAIN.PROGRAM.
     F1 FUNCTION.KEY.DOES PEAK.QUIT
     F2 FUNCTION.KEY.DOES MAIN.PLOT.DATA
     F3 FUNCTION.KEY.DOES ENTER.DATA
     F4 FUNCTION.KEY.DOES INPUT.DATA.FILE
     F5 FUNCTION.KEY.DOES OUTPUT.DATA.FILE
     F6 FUNCTION.KEY.DOES ED.DATA
     F7 FUNCTION.KEY.DOES MOMENTS
     F8 FUNCTION.KEY.DOES MAIN.SUMMARY
     F9 FUNCTION.KEY.DOES NOP
;
```

```
: MAIN.PROGRAM
      MAIN.KEYS                        \Defines the function keys.
      MAIN.MENU                        \Displays the selection menu.
      INTERPRET.KEYS
;

\-------------------------------------------------------------------------------------------

: INIT                           \Starts the program once it has been loaded
      CLEAR.FUNCTION.KEYS
      GRAPHICS.DISPLAY
      BANNER
      " ." DATA.SYM.S  ":=               \Default values for
      " ." DATA.SYM.B  ":=               \ plotting symbols.
      -1 3 SCI.FORMAT
      MAIN.PROGRAM
;
```

Appendix C

Data Acquisition Program

```
\ DATA ACQUISITION PROGRAM
\
\ Program name: DATACQ.ASY  (ASYST Version 2.0)
\ Directory:    ASYST2
\
\     The program is menu driven for ease of use and assumes nothing of the
\  operator. The maximum number of data sets allowed in the present
\  version is 2000. This may be changed by editing the program and changing
\  MAXSETS to whatever value is desired.

\     Data acquisition is with a Tecmar LAB MASTER, configured as described
\  in Module 3 of the ASYST manuals with one exception - the data is unipolar.

\  Written by C. Lucy, 15 July 1985

\-------------------------------------------------------------------------------

\ Program Structure

\     This program is designed to be menu driven and utilizes a
\  two-tiered structure. The upper most tier is Main Menu from which
\  the Summary Menu can be accessed. Most primary functions are
\  available in the Main Menu

\ Main Menu

\  F1) Quit - exits operation from the acquisition program and from ASYST.

\  F2) Data Acquisition - will request information about the data to be acquired and then
\                         on manual initiation will collect data in the fore-ground mode.

\  F3) Repeat Acq. - will perform acquisition using the last stored acquisition
\                    parameters. Only the experiment identification number will be
\                    requested.

\  F4) Plot - plots the data on the screen. Y-axis goes from 0 to 4096 to indicate how
\             much of the ADC's dynamic range is being utilized.

\  F5) Save Data - stores the collected data. The filename should include the extension
\                  ".DAT".

\  F6) Summary - accesses the Summary Menu for creation of a hard copy of the data.
```

```
\Summary Menu

\    F1) Exit - returns operation to the Main Menu.

\    F2) Print Summary - prints out the data file specifications and acquisition settings.

\    F3) Print Data - prints out a table of the data points collected.

\    F4) Plot Summary - prints out a copy of the data plot along with the file specs and
                        the acquisition parameters.

\----------------------------------------------------------------------------------------

\Overlay check

\       Some functions used in this program are not available in the base ASYST system,
\    so it is necessary to install the extra overlays into the system.  These required
\    overlays are already installed in the system ASYST  in Directory ASYST2.

  ECHO.OFF
: OLOAD?
      CR BELL
      ." Are overlays DATAFILE.SOV, ACQUIS.SOV and ACQLM.SOV in the
      system (Y/N) ?"
      KEY DUP EMIT
      DUP 90 > IF 32 - THEN 89 = NOT
      IF
          CR CR ." Please use the Configuration menu <F2> to load the ,"
          CR    ." Data files, Data acquisition and Lab Master overlays in the"
          CR    ." system before continuing." CR CR
          57 ERROR
      THEN
;
  OLOAD?
  ECHO.ON

\----------------------------------------------------------------------------------------

\Variable declarations

  INTEGER
     SCALAR MAXSETS
     SCALAR MAX.IN.SET
     SCALAR #SETS
     SCALAR COL#
     SCALAR ACQ.RATE          \Time between successive data points (msec)
     SCALAR ACQ.GAIN          \Programmable gain setting for Lab Master

  2048 MAXSETS     :=         \Either of these lines may be changed
   3  MAX.IN.SET   :=         \to allow larger data sets to be used.

     DIM[ 2 ] ARRAY HOLDIT     \Output buffer for #SETS & MAX.IN.SETS
     DIM[ MAXSETS ] ARRAY ACQ.BUF  \Integer buffer for acquisition data
     DIM[ 4 ]  ARRAY CAP.REQ       \Capacitances required for gains used.
```

```
REAL
   DIM[ MAXSETS , MAX.IN.SET ] ARRAY PEAK.DATA \Peak data buffer

 25  STRING OP.NAME                \Operator's name.
 25  STRING TITLE                  \Experiment title.
 25  STRING EXP#                   \Experiment number.
 25  STRING XLBL                   \X-axis label
 10  STRING YLBL                   \Y-axis label
 14  STRING FILENAME

\----------------------------------------------------------------------------------------

\Data acquisition structure

\Defining A/D template for input on channel 0 of the acquisition board.

     LAB.MASTER
     0 0 A/D.TEMPLATE CHAN.0       \Sets channel 0 as the input channel.
     ACQ.BUF TEMPLATE.BUFFER       \Data will be temp. saved in ACQ.BUF

\----------------------------------------------------------------------------------------

\Window definitions

\ Divides screen into small windows in which plots, menus and specs will be presented.

   0  0   0 79  WINDOW {TOPLINE}   \Top banner line across screen.
   1  0   6 19  WINDOW {SPEC1}     \Top left window for experiment specs.
   8  0  10 19  WINDOW {SPEC2 ACQ} \Lower left window for acquisition specs.
  12  0  12 20  WINDOW {SPEC.SAVE} \Window to record saving of file
  19  0  19 79  WINDOW {SPLIT1}    \Middle window for menu banners.
  20  0  21 79  WINDOW {SPLIT2}    \Middle window for menus.
  24  0  24 79  WINDOW {BOTTOMLINE} \Bottom line of screen for prompt.
   1  0  24 79  WINDOW {DEF-1}     \Excludes top banner line.

\----------------------------------------------------------------------------------------

: DATA.VU   \ Defines plotting parameters for graph.
     .270 .300  VUPORT.ORIG                \Defines the position and
     .730 .650  VUPORT.SIZE                \ size of the plot window.
     HORIZONTAL AXIS.FIT.OFF GRID.OFF      \Removes the grids from
     VERTICAL   AXIS.FIT.OFF GRID.OFF      \ the graph.
     .180 .210  AXIS.ORIG                  \Sets the graph position &
     .800 .740  AXIS.SIZE                  \ size within the window.
     .025 .008  TICK.SIZE
     .5   .8    TICK.JUST
     VERTICAL LABEL.SCALE.OFF              \Inhibits automatic printing
     HORIZONTAL LABEL.SCALE.OFF            \ of the scaling factor
;

\----------------------------------------------------------------------------------------
```

```
\Screen Messages

: BANNER          \Program banner
     {TOPLINE} SCREEN.CLEAR
     25 SPACES ." Data Acquisition Program"
;

: PROMPT          \Prompt on bottom line while menu is displayed.
     {BOTLINE} SCREEN.CLEAR ."     Your choice please "
;

: WAIT            \Wait-message on bottom line while program is being executed.
     {BOTLINE} SCREEN.CLEAR ."     Please wait "
;

\-----------------------------------------------------------------------------------------

\Screen Menus


: MAIN.MENU
     {SPLIT2} HOME SCREEN.CLEAR
     ." F1) Quit  F2) Data Acq. F3) Repeat Acq.  F4) Plot "
     ."  F5) Save Data   F6) Summary "
     {SPLIT1} HOME SCREEN.CLEAR 30 SPACES ." ** Main Menu **"
     PROMPT
     CURSOR.OFF
;


: SUMMARY.MENU          \Presents & performs the summary options.
     {SPLIT2} HOME SCREEN.CLEAR
     10 SPACES ." F1) Exit  F2) Print summary  F3) Print data  F4) Plot summary"
     {SPLIT1} SCREEN.CLEAR
     32 SPACES ." **  Summary Menu  **"
     {BOTLINE} SCREEN.CLEAR
     ."   For more than 50 data points, F2 or F4 are recommended. "
;

\-----------------------------------------------------------------------------------------

\Data Plotting functions


: DATA.VU.SET          \Word to setup data viewport axis area
     WORLD.COORDS
     0. 4095.     VERTICAL  WORLD.SET          \Vertical axis: 0 to 4095
     PEAK.DATA XSECT[ 1 ] SUB[ 1 , #SETS ]
     DUP                                       \Horizontal axis: length
     []MIN/MAX    HORIZONTAL WORLD.SET         \ set by x-value limits.
     []MIN 0.  WORLD.COORDS AXIS.POINT         \Values at which axes meet.
;
```

```
: SHOW.SPECS          \Displays experimental specifications on screen
    {SPECS} SCREEN.CLEAR
    ." Date: " .DATE CR
    ." Operator: "      OP.NAME "TYPE CR
    ." Exp. title: " CR   TITLE "TYPE CR
    ." Exp. number: "      EXP# "TYPE
;

: SHOW.ACQ            \Shows settings for data acquisition on screen.
    {SPEC.ACQ} SCREEN.CLEAR
    ." Acq Rate="  ACQ.RATE . CR
    ." # Points="  #SETS   . CR
    ." Gain=   "  ACQ.GAIN .
;

: SHOW.SAVE           \Indicates on screen that the data has been saved.
    {SPEC.SAVE} SCREEN.CLEAR
    FILENAME "TYPE
    ."  saved"
;

: LABEL.PLOT          \Positions the x and y labels on the graph.
    NORMAL.COORDS
    .0250 .75 POSITION 270 LABEL.DIR      \Positioning the y-label
    YLBL LABEL                            \Writing the y-label.
    XLBL "LEN 2. /                        \1/2 the letters of XLBL sets
        .0175 * .5 SWAP -                 \ the position of the x-label
        .05 POSITION  0 LABEL.DIR
        LABEL                             \Writing the x-label
    CURSOR.OFF
;

: PLOT.DATA           \Routine to draw labelled graph on screen.
    DATA.VU                               \
    VUPORT.CLEAR                          \Setting up the
    DATA.VU.SET                           \axes of the graph.
    XY.AXIS.PLOT                          \
    PEAK.DATA XSECT[ 1 ] SUB[ 1 , #SETS ] \
    PEAK.DATA XSECT[ 2 ] SUB[ 1 , #SETS ] \Plotting the signal data
    XY.DATA.PLOT                          \
    LABEL.PLOT
    OUTLINE
    SHOW.SPECS
    SHOW.ACQ
    MAIN.MENU
;
```

```
: MAIN.PLOT.DATA            \Checks data before plotting
    #SETS 0 >
    IF
        SCREEN.CLEAR                    \Clears prompt and
        PLOT.DATA                       \ plots the data and
        INTERPRET.KEYS                  \ specs.
    THEN

    ONESCAPE: RESTORE.FUNCTION.KEYS MAIN.MENU
;

\-----------------------------------------------------------------------------------------

\Summary options

: PRINT.SUMMARY             \Prints out the file and acquisition specs.
    {SPLIT2} SCREEN.CLEAR
    ." <cr> when printer is ready..." BELL
    ." (Any other key aborts)"
    KEY 13 <>
    IF
        SUMMARY.MENU
    ELSE
        {DEF-1} SCREEN.CLEAR OUT>PRINTER CR CR CR
        4 SPACES ." Date: " .DATE 5 SPACES ." Time: " .TIME
        8 SPACES ." Operator: "     OP.NAME "TYPE CR CR
        4 SPACES ." Experiment name: " TITLE "TYPE CR
        4 SPACES ." Experiment number: " EXP# "TYPE CR CR
        4 SPACES ." Acq. Rate: "    ACQ.RATE    . CR
        4 SPACES ." No. data points:" #SETS     . CR
        4 SPACES ." Gain: "         ACQ.GAIN    . CR CR
        CONSOLE
        CR ." Press any key to continue."
        KEY DROP
        {DEF-1} SCREEN.CLEAR
        SUMMARY.MENU
    THEN
;


: PRINT.DATA                \Prints out the collected data.
    {SPLIT2} SCREEN.CLEAR
    ." <cr> when printer is ready..." BELL
    ." (Any other key aborts)"
    KEY 13 <>
    IF
        SUMMARY.MENU
    ELSE
        {DEF-1} SCREEN.CLEAR OUT>PRINTER CR CR CR
        4 SPACES ." Date: " .DATE 5 SPACES ." Time: " .TIME
        8 SPACES ." Operator: "     OP.NAME "TYPE CR CR
        4 SPACES ." Experiment name: " TITLE "TYPE CR
        4 SPACES ." Experiment number: " EXP# "TYPE CR CR
```

```
        ." X-values        Signal "
        CR CR
        #SETS 1 + 1 DO
              PEAK.DATA [ I , 2 ]
              PEAK.DATA [ I , 1 ]
              . 18 ?COL - SPACES . CR
        LOOP
        CONSOLE
        CR ." Press any key to continue."
        KEY DROP
        (DEF-1) SCREEN.CLEAR
        SUMMARY.MENU
      THEN
;

: PLOT.SUMMARY                \ Prints out plot of data, with all relevant specs.
      SCREEN.CLEAR
      PLOT.DATA
      SHOW.ACQ
      (SPLIT1) SCREEN.CLEAR
      (SPLIT2) SCREEN.CLEAR
      (BOTLINE) SCREEN.CLEAR
      ." <cr> when printer is ready . . ." BELL
      ." (Any other key aborts) "
      KEY 13 <>
      IF
         SUMMARY.MENU
      ELSE
         (SPLIT2) SCREEN.CLEAR
         SCREEN.PRINT
         CONSOLE
         CR ." Press any key to continue. "
         KEY DROP
         (DEF-1) SCREEN.CLEAR
         SUMMARY.MENU
      THEN
;

\-------------------------------------------------------------------------------

\ Saving the data in memory.

: WRITE.FILE                  \ Default drive for data storage is C (Hard Drive)
      FILE.TEMPLATE
         5 COMMENTS                          \
         INTEGER DIM[ 2 ] SUBFILE            \ Defines the format of
         REAL DIM[ #SETS ] SUBFILE           \ the data file.
         REAL DIM[ #SETS ] SUBFILE           \
         REAL DIM[ #SETS ] SUBFILE           \
      END
```

```
      HOME
      ." Opening file " FILENAME "TYPE
      13 EMIT FILENAME DEFER> FILE.CREATE
      ." Writing file " FILENAME "TYPE
      13 EMIT FILENAME DEFER> FILE.OPEN

      TITLE     1   >COMMENT              \
      OP.NAME   2   >COMMENT              \Outputs the variables to the
      EXP#      3   >COMMENT              \ appropriate positions in
      XLBL      4   >COMMENT              \ the data file.
      YLBL      5   >COMMENT              \
      #SETS HOLDIT [ 1 ] :=
      MAX.IN.SET HOLDIT [ 2 ] :=
      1 SUBFILE HOLDIT    ARRAY>FILE
      2 SUBFILE PEAK.DATA XSECT[ 1 ] SUB[ 1 , #SETS ]  ARRAY>FILE
      3 SUBFILE PEAK.DATA XSECT[ 2 ] SUB[ 1 , #SETS ]  ARRAY>FILE
      4 SUBFILE PEAK.DATA XSECT[ 3 ] SUB[ 1 , #SETS ]  ARRAY>FILE
      FILE.CLOSE

      ONERR:                \Error trap
         ." Can't open file for writing. "
         ." Type any key to continue."  BELL KEY DROP
         ?FILE.OPEN IF FILE.CLOSE THEN
;


: GET.FILENAME                    \Requests name for the data file.
      ." Filename please ?  " "INPUT
      FILENAME ":=
      SCREEN.CLEAR
;


: OUTPUT.DATA.FILE                \Invokes the words above to save the data.
      #SETS 0 >
      IF
         SCREEN.CLEAR
         {SPLIT2} SCREEN.CLEAR ." Output "
         GET.FILENAME
         WRITE.FILE
         SHOW.SAVE
         MAIN.MENU
      THEN
;

\-------------------------------------------------------------------------------------------
```

```
\ Performing the data acquisition.

: DATA.ACQ              \Performs data acquisition using the Lab Master ADC.
    CHAN.0 A/D.INIT                          \Initiating the data
    {DEF-1} SCREEN.CLEAR                     \acquisition board.
    {BOTLINE} SCREEN.CLEAR
    CR ." <cr> to start data acquisition . . ." BELL
    ." (Any other key aborts) "
    KEY 13 <>
    IF
       MAIN.MENU
    ELSE
       WAIT
       ACQ.RATE SYNC.PERIOD
       #SETS 1 + 1 DO                        \
            SYNCHRONIZE                      \Collects data at the rate
            A/D.IN>ARRAY                     \ specified by ACQ.RATE
       LOOP                                  \
       ACQ.BUF SUB[ 1 , #SETS ]                    \Stores the acquired
       PEAK.DATA XSECT[ 2 ] SUB[ 1 , #SETS ] :=  \ data.
       BANNER
       MAIN.MENU
       PEAK.DATA XSECT[ 2 ] SUB[ 1 , #SETS ] []MAX
       4095 = IF
            {BOTLINE} SCREEN.CLEAR
            ." WARNING: The inputted signal has saturated the ADC."
            BELL
       ELSE
            PROMPT
       THEN
    THEN
;


: ACQ.PARAMETERS        \Prompts operator for acquisition settings.
    {DEF-1} SCREEN.CLEAR
    ." New data set:" CR CR
    ." Your name (or initials) please? " "INPUT OP.NAME ":= CR CR
    ." Title of experiment? (name for data set) " "INPUT TITLE ":= CR CR
    ." Experiment ident. number? " "INPUT EXP# ":= CR CR
    BEGIN
       ." Number of data sets in this experiment ? " #INPUT CR CR
       IF #SETS :=
       ELSE GRAPHICS.DISPLAY {SPLIT1} HOME ." Press F1" EXIT
       THEN
       #SETS MAXSETS >
       IF ." Maximum #sets allowable is " MAXSETS
            -1 0 FIX.FORMAT MAXSETS .
            -1 4 SCI.FORMAT FALSE
       ELSE TRUE
       THEN
    UNTIL
```

```
      ." Data acquisition rate (msec) ?"                    \ Input acquisition      260
      #INPUT  ACQ.RATE :=                                   \  rate.
      PEAK.DATA XSECT[ 1 ] SUB[ 1 , #SETS ] []RAMP          \
      PEAK.DATA XSECT[ 1 ] SUB[ 1 , #SETS ] 1. -            \Filling in the
      ACQ.RATE FLOAT                                        \retention values in
      1000 /                                                \sec into the data file
      *
      PEAK.DATA XSECT[ 1 ] SUB[ 1 , #SETS ] :=
      CR CR  ." Connect input leads to Channel 0 and Ground. "
      CR ." Type any key to continue. " KEY DROP
      CR CR  ." Gain required ?"                            \Input & store the
      CR  ." 1 = 1X  2 = 10X  3 = 100X  4 = 500X  "         \ programmable
      #INPUT  ACQ.GAIN :=                                   \ gain.
      CR CR ." Require a " CAP.REQ [ ACQ.GAIN ] . .         \ Setting low pass
      ."  " pico-farad capacitor on the daughter board ."   \  filter on the ADC
      ACQ.GAIN 1 -  A/D.GAIN
      CR ." Type any key when the capacitor is set. "  KEY DROP
      DATA.ACQ
;

: REPEAT.ACQ     \Repeats data acquisition using the last set of conditions stored
      {DEF-1} SCREEN.CLEAR
      CR CR ." REPEAT ACQUISITION "
      CR CR ." New experiment ident. number? " "INPUT EXP# ":=
      DATA.ACQ
;

\-----------------------------------------------------------------------------------------------

: SUMMARY.KEYS          \Redefines the function keys to the summary options.
      F1 FUNCTION.KEY.DOES ESCAPE
      F2 FUNCTION.KEY.DOES PRINT.SUMMARY
      F3 FUNCTION.KEY.DOES PRINT.DATA
      F4 FUNCTION.KEY.DOES PLOT.SUMMARY
      F5 FUNCTION.KEY.DOES NOP
      F6 FUNCTION.KEY.DOES NOP
;


: SUMMARY
      {DEF-1} SCREEN.CLEAR
      STORE.FUNCTION.KEYS
      SUMMARY.KEYS
      SUMMARY.MENU
      INTERPRET.KEYS

      ONESCAPE: RESTORE.FUNCTION.KEYS MAIN.MENU
;

\-----------------------------------------------------------------------------------------------
```

```
: ACQ.QUIT                    \Word to quit application of this program.
     SCREEN.CLEAR \Clears prompt
     {SPLIT2} SCREEN.CLEAR BELL ." Quit (y/n)?"
     KEY DUP EMIT
     DUP 90 > IF 32 - THEN 89 =          \Checks if response is "y" or "Y"
     IF BYE THEN
     MAIN.MENU
;

: MAIN.KEYS                   \Sets up function keys for MAIN.PROGRAM.
     F1 FUNCTION.KEY.DOES ACQ.QUIT
     F2 FUNCTION.KEY.DOES ACQ.PARAMETERS
     F3 FUNCTION.KEY.DOES REPEAT.ACQ
     F4 FUNCTION.KEY.DOES MAIN.PLOT.DATA
     F5 FUNCTION.KEY.DOES OUTPUT.DATA.FILE
     F6 FUNCTION.KEY.DOES SUMMARY
;

: MAIN.PROGRAM
     MAIN.KEYS                        \Defines the function keys.
     MAIN.MENU                        \Displays the selection menu.
     INTERPRET.KEYS
;

\-------------------------------------------------------------------------------------------

: ACQUIRE.DATA                \Starts the program once it has been loaded.
     CLEAR.FUNCTION.KEYS
     GRAPHICS.DISPLAY
     BANNER
     " TIME (sec) " XLBL ":=
     " COUNTS "    YLBL ":=
     CAP.REQ @[ 1 ] ENTER[ 0 , 0 , 1500 , 8200 ]
     7 2 FIX.FORMAT
     MAIN.PROGRAM
;
```